# Analysis of nanoparticulate coatings with relevance to dentine sensitivity


Thesis submitted in accordance with the
Requirements of the University of Liverpool for the
degree of Doctor of Philosophy

by

Joanne Marie Convery

May 2008

Joanne Marie Convery

**Analysis of nanoparticulate coatings with relevance to dentine sensitivity**

## Abstract

Dentine sensitivity is a common dental complaint. It is caused by the exposure of root dentine to the oral environment. A popular method of overcoming dentine sensitivity is the occlusion of the dentinal tubules. In this thesis the use of nanoparticulate silica sols, of sizes 7, 14 and 21nm diameter for the treatment of dentine sensitivity, as occluding agents was explored.

Previous work at the University of Liverpool has identified a simple two step method for coating surfaces in silica nanoparticles. This process required the use of a poly cationic polymer (Zetag™ 7689). TEM and QCM-D were used to observe the creation of nanoparticulate coatings, in the absence and following manipulation of the polymer binding layer. It was demonstrated that on gold, carbon and hydroxyapatite surfaces a polymer binding layer was required. However, using the QCM-D and XPS it was identified that on dentine surfaces a polymer binding layer was unnecessary.

To investigate the potential of the nanoparticulate sols to be used as a desensitizing treatment, the ability of the nanoparticles to reduce dentine permeability was assessed. Using the hydraulic conductance method it was demonstrated that treatment of the dentine with nanoparticulate silica resulted in a decrease in dentine permeability. This would suggest that the silica nanoparticles would be a suitable occluding agent in the treatment of dentine sensitivity.

The ability of the nanoparticulate coatings to endure some of the stresses of the oral environment was also investigated. It was demonstrated that the coatings were able to withstand gentle flow conditions and it was identified that the nanoparticulate coatings did not hinder the adsorption of salivary components. This is significant as the creation of a salivary pellicle has been shown to aid the remineralisation of the dentine and offer protection from acid challenge. It was demonstrated that the nanoparticulate silica coating remained intact on dentine surfaces following acid challenge. Therefore, offering some protection to the underlying exposed dentine from the periodic decreases in pH that are endured in the oral environment.

In conclusion, it is possible to affect the overall density of a nanoparticulate coating by altering the underlying polymer layer. A polymer layer however, is not required to adhere the silica nanoparticles to dentine surfaces. Treatment of dentine with nanoparticulate silica resulted in a reduction in dentine permeability, therefore enforcing its abilities as an occluding agent for treatment of dentine sensitivity. The results demonstrated that the colloidal silica could protect the dentine from further demineralisation due to acid attack. However, it would appear that nanoparticulate silica was unable to offer any remineralising benefits to the dentine.

This thesis is dedicated to the loving memory of my
grandparents
Nana and Taid Convery
and Granddad Gemmell

## Acknowledgements

I would like to thank all my supervisors at the University of Liverpool, Rachel Williams, Mike Garvey and Patrick Doherty for all their enthusiasm, support and patience throughout this project. I would also like to thank my industrial supervisors, Gareth Rees and Charles Parkinson, their input, assistance and support has been invaluable. Special thanks are due to Nic Martin, for providing assistance with the dental aspect of the project. Also to the BBSRC and GalxoSmithKline for funding the project

I would like to express my thanks to; Graham Beamson of the STFC Daresbury for all training me on the XPS and for his continued assistance and input to the project, I shall always be grateful; Cornelia Munke of the EM unit at the University of Liverpool, for training me on the use of the TEM; Tim Rudd and Amy Schofield for their Knowledge and assistance on the use of the "little blue box"; to Shirley Rawlings for being there with a cup of coffee and an open ear, and for putting up with my inability to fill in forms; also Sandra Fawcett, Jude Curran, Lisa Baldwin and Fanrong Pu who have always been present with wise words and encouragement. A special thank you goes to Victoria for tutoring me in the use of SPSS. Thanks must also be given to Jill Bullock for getting her red pen out of retirement for me.

Thanks must be offered to all my friends. To those from the department Evi Kavatzikidou, Katie Smith, Victoria Kearns, Katie Nickson, Nick Bryan (and Jo), Sandra Cachinho, Dan Jones and Ste Thompson for putting up with me daily, they have shared the daily trials and tribulations of the project and provided support and the occasional bitter shandy when required. To my friends from home "the boys", Brez, James Will and Simon Slinn I want to say thank you for everything. You have all been never more than a phone call away and always encouraging and supporting. Chris, Susannah and Carla - thank you for always being there with sound advice and a gig guide to distract me. Also to Martin for just being you.

Finally I would like to thank my family and Chris my TV husband for being able to live with me for the last few years. For listening to me rant and supplying me with wine, your friendship has been invaluable. Thanks also to the Jones family for smoothing the way with chocolate and encouragement. I would like to thank my Mum and Dad for their inexhaustible support and their love and their encouragement in everything I do. Nana Gemmell thank you for your love and enthusiasm (and the comedic interludes). Thanks to James and Caroline for being so caring, and reminding me of the light at the end of the tunnel. Finally I would like to thank Mark for all that he has done. His patience, care and love has helped keep me focused and grounded, I shall always be grateful.

# Contents

## List of Figures

## List of Tables

## List of Abbreviations

| | |
|---|---|
| AFM | Atomic Force Microscopy (AFM) |
| $E_B$ | binding energy |
| C* | overlap concentration |
| *r* | decay time |
| DEJ | dentine enamel junction |
| $dH_2O$ | deionised water |
| *d* | dissipation |
| $\Delta d$ | dissipation shift |
| hν | energy |
| $\Delta H_R$ | enthalpy |
| $\Delta S_R$ | entropy |
| *f* | frequency |
| $\Delta f$ | frequency shift |
| $\Delta G_R$ | Gibbs Free energy |
| Lp | hydraulic conductance |
| HA | hydroxyapatite |
| $E_K$ | kinetic energy |
| MRSA | Methicillin Resistant *Staphylococcus aureus* |
| PVP | polyvinylpyrrolidine |
| PDJ | pulpo-dentinal junction |
| QCM-D | quartz crystal microbalance with dissipation monitoring |
| SEM | Scanning Electron Microscopy |
| TEM | Transmission electron microscopy |
| XPS | X-ray Photoelectron Spectroscopy |

# Chapter 1

# Introduction

## 1.1 The tooth

Teeth are comprised of three mineralized tissues enamel, dentine and cementum, which surround an inner core of loose connective tissue the dental pulp (Berkovitz, Holland et al. 2005) (figure1.1).

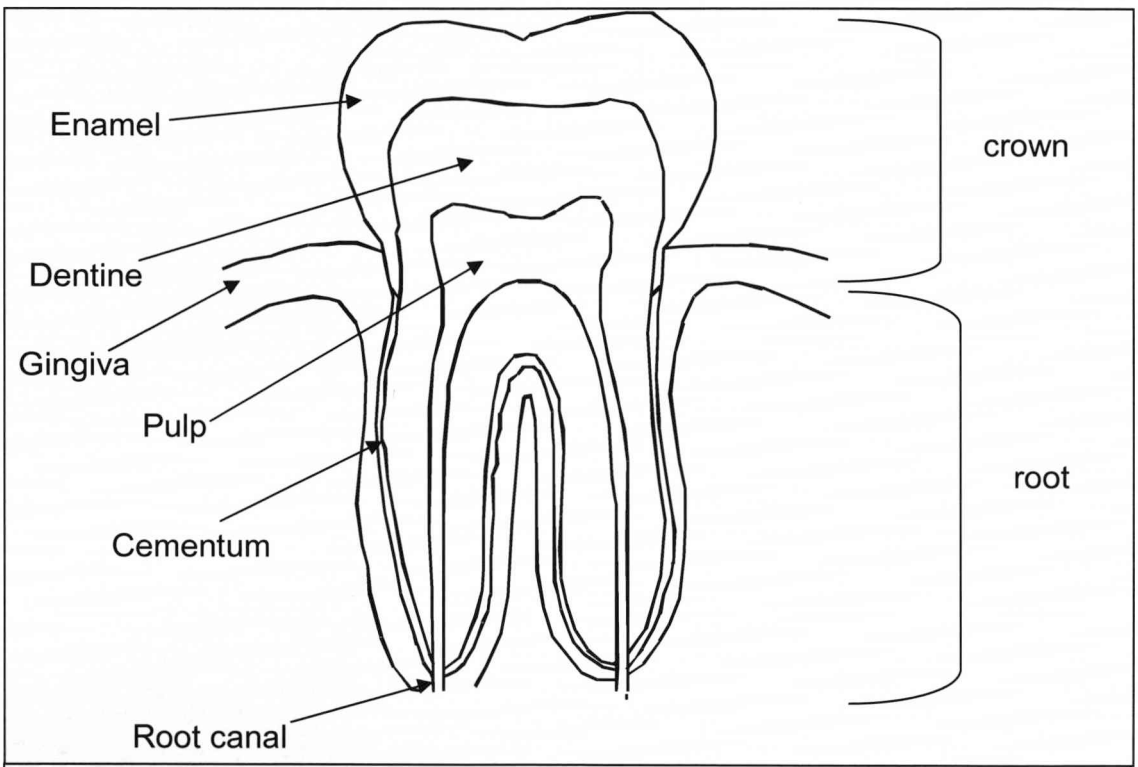


**Figure 1.1** Diagram of the anatomy of the tooth. Adapted from (Berkowitz, Holland et al. 2005)

### 1.1.1 Dental pulp

The dental pulp is contained within the pulp chamber and canals of the tooth (Berkovitz, Holland et al. 2005). It is a specialized connective tissue and has a specific anatomical arrangement. The odontoblasts are the cells responsible for deposition of the dentine which surrounds the pulp and lie at the periphery of the tissue (Ten Cate and Nanci

2003). Within the odontoblast layer there is a network of capillaries termed the terminal capillary network, and also nerve fibres, that pass between the odontoblasts as free nerve endings. Surrounding these structures is the inter-odontoblastic fibrous structure, which consists of collagen fibrils, proteoglycans and fibronectin. Subjacent to the odontoblast layer an area relatively free of cells is observed, it has a rich network of unmyelinated nerve fibres and blood capillaries. Underlying this is the cell-rich zone which contains a high density of fibroblasts, undifferentiated mesenchymal cells, macrophages and lymphocytes (Pashley 2002; Nanci 2003).

### 1.1.2 Enamel

Enamel has evolved as an epithelially derived protective covering for the anatomical crown of the tooth (Nanci 2003). Mature enamel is highly mineralized consisting of approximately 96% mineral and 4% organic material and water (Berkovitz, Holland et al. 1992). Due to its high mineral content enamel is extremely hard, enabling it to withstand the mechanical forces applied during tooth functioning. The inorganic or mineral content of enamel is a calcium phosphate in the form of, hydroxyapatite crystals substituted with carbonate ions (Ten Cate and Nanci 2003). The hydroxyapatite crystals are between 60 and 70 nm wide and 25 - 30 nm thick, it is thought the length of the crystal spans the entire thickness of the enamel layer (Nanci 2003). These crystals are then packed into a long thin rod, 5 - 6$\mu$m in diameter (Berkovitz, Holland et al. 2005). Surrounding the rods are interred regions where the crystals are orientated in a direction different, from those making up the rod. This results in an increased micro-porosity surrounding the prism boundary, accommodating slightly more organic material (Nanci 2003; Berkovitz, Holland et al. 2005). However, despite being very hard without the support of underlying tissue enamel can be very brittle.

### 1.1.3 Cementum

Cementum is a hard avascular connective tissue that covers the roots of teeth. Cementum is approximately 45% to 50% hydroxyapatite, (inorganic) and 50% collagen and non collagenous matrix proteins (organic) (Ten Cate and Nanci 2003). Cementum is contiguous with the periodontal ligament on its outer surface, and firmly adherent to

dentine on its deep surface. The prime function of cementum is to give an attachment to collagen fibres of the periodontal ligament and is therefore a highly responsive mineralized tissue helping to maintain the tooth in its functional position in the mouth (Berkovitz, Holland et al. 2005). Cementum is softer than dentine. This relative softness of cementum, combined with its thinness cervically, means that its readily removed by abrasion, when gingival recession exposes the root. Loss of cementum in such cases will result in the exposure of the dentine.

### 1.1.4 Dentine

Dentine is the third mineralized tissue of the tooth. It underlies the enamel at the crown of the tooth and the cementum at the root and surrounds the dental pulp. It is the mineralized tissue that forms the bulk of the tooth (Berkovitz, Holland et al. 1992). Dentine possesses an elastic quality that is important for the proper functioning of the tooth, because the elasticity provides flexibility, preventing fracture of the overlaying brittle enamel (Nanci 2003). Dentine is often described as a heterogeneous composite material, with mature dentine composed by weight of 70% inorganic material, 20% organic material and 10% water (Pashley 1996; Nanci 2003). It can be regarded as a porous biological composite, composed of apatite crystal filler particles, within a collagen rich matrix (Pashley 2002). The mineralised matrix of dentine is produced developmentally prior to eruption, by the odontoblasts.

There are three types of dentine: primary, secondary and tertiary. Primary dentine is the original tubular dentine largely formed prior to eruption (Pashley 2002). Secondary dentine develops after root formation has been completed, and represents the continuing but slower deposition of dentine by odontoblasts. Since the same odontoblasts form both primary and secondary dentine, the tubules remain continuous (Pashley 2002; Ten Cate and Nanci 2003). Tertiary dentine is also known as reactive or reparative dentine, and is produced in reaction to various stimuli, including attrition, caries or a restorative dental procedure. It may or may not have tubules that are continuous with those of secondary dentine or no tubules at all (Nanci 2003).

The odontoblasts begin secreting collagen at the dentine enamel junction (DEJ) and continue inwards, while trailing odontobalst process (Pashley 2002). It is the presence of these processes that result in the tubular nature of primary and secondary dentine (figure 1.2) (Pashley 1996).

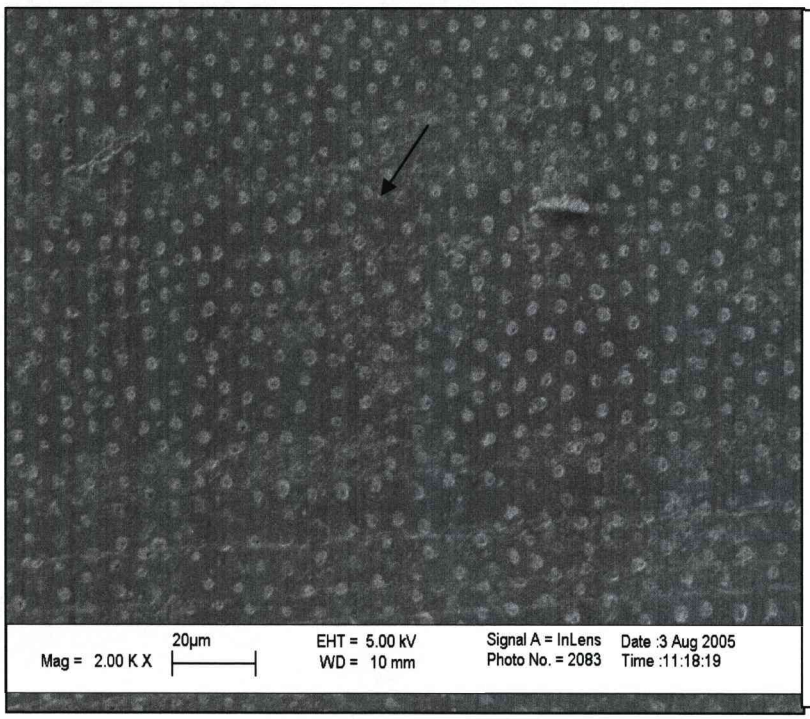


**Figure 1.2.** SEM image of a dentine disc following treatment with 6% (w/v) citric acid to remove the smear layer and expose the dentinal tubules highlighted by the arrow.

Due to the circumference of the most peripheral part of the tooth at the crown or root being greater, than the circumference of the final pulp chamber or root canal, the odontoblasts are forced closer together as they continue to lay down dentine (Couve 1986; Pashley 2002). As such the tubules are more widely separated at their peripheries, with 2.5% of the cross sectional area at the DEJ being composed of tubules, while at the pulp this increases to 20% (Berkovitz, Holland et al. 2005). The tubules extend the full thickness of the dentine, and taper from the pulp outwards, therefore, appearing as an upturned cone (Orchardson and Gillam 2006). Originally each tubule has a diameter of around 3$\mu$m, and the walls of the tubules are composed of mineralised type I collagen. However, with maturation another type of dentine is deposited on the walls of the tubules, narrowing the lumen to between 0.6 and 0.8$\mu$m. This is known as peritubular dentine, and unlike intertubular dentine, it lacks a collagen fibrous matrix. The width of

peritubular dentine is greatest at the DEJ, and decreases as tubules are followed toward the pulp (Blake 1968; Garberoglio and Brannstrom 1976).

The dentinal tubules are filled with a fluid resembling the composition of plasma (Coffey, Ingram et al. 1970). Although the complete composition of the dentinal fluid is unknown, it is thought to contain calcium and phosphate ions and is derived from the pulpal extracellular fluid (Orchardson and Cadden 2001). It is thought that the dentinal fluid aids, the deposition of minerals, within the dentinal tubules (Mjor 1985).

**1.2 Dentine Sensitivity**

A unique characteristic of dentine is that exposure can, but does not always, result in sensitivity (Berkovitz, Holland et al. 2005). Dentine hypersensitivity or "sensitive teeth" is a common dental complaint (Mac Carthy 2004). It is defined as a short, sharp pain arising from exposed dentine in response to stimuli typically thermal, cold, evaporative, tactile, osmotic or chemical and which cannot be ascribed, to any other form of dental defect or pathology (Holand, Narhi et al. 1997). Dentine sensitivity can affect a diverse age range of patients, from early teens to late seventies, with the peak incidence between 20-40 years of age (Graf and Glasse 1977; Flynn, Galloway et al. 1985; Fischer, Fischer et al. 1992). The prevalence of dentine sensitivity varies greatly, with reported values ranging from 8-57% of the adult population (Addy 1990; Irwin and Mc Cusker 1997).

It is caused by the exposure of the dentine, to the oral environment. Exposure of the dentine results from one of two processes, either removal of the enamel covering the crown of the tooth or denudation of the root surface by loss of cementum and overlying periodontal tissues (Dowell and Addy 1983). The enamel or cementum which normally covers the dentine surface may be removed or denuded as a result of attrition abrasion or erosion (Bartold 2006). The enamel may also be removed due to toothbrush abrasion, and dietary erosion or a combination of these factors. As previously discussed, cementum is readily removed by abrasion, following exposure of the root surface to the oral environment. Exposure of the cementum is multi factorial but gingival recession,

chronic periodontal disease, certain forms of periodontal surgery, incorrect tooth brushing and chronic trauma have all been implicated (Dowell and Addy 1983).

Clinical experience has demonstrated that not all exposed dentine on vital teeth is sensitive (Addy 1990). It has been shown that, in order for dentine to be sensitive not only must it be exposed to the oral environment, but the dentinal tubules have to be patent to the surface (Absi, Addy et al. 1987). It has been suggested the production of reparative tertiary dentine, and the creation of a smear layer through attrition, e.g. brushing, may occlude the tubules, preventing them being fully patent. It has also been noted that, the number and diameter of the tubules at the exposed surface are greater for sensitive dentine, than non sensitive dentine (Absi, Addy et al. 1987; Addy and Urquhart 1992). Tubules can become patent by removal of the smear layer, as a result of dietary acids (such as citric acids found in fruit juices). The tubules can then become enlarged, due to the dissolution of the peritubular dentine on the surface (Gwinnett 1984).

### 1.3 Theories of dentine sensitivity

There have been several theories regarding the mechanism by which thermal, tactile, chemical or electrical stimuli are transmitted through dentine, resulting in the sensation of pain. These include, the innervation of dentine, the dental receptor mechanism and the hydrodynamic mechanism (Dowell and Addy 1983).

#### 1.3.1 Innervation of the dentine.

It has been suggested that due to its sensitivity, the dentinal tubules are innervated with nerve fibres. The innervation of dentine has been the subject of much controversy, with contradicting studies both supporting, and denouncing the penetration of the dentinal tubules with a limited number of nerve fibres (Seltzer 1971). However, there has been little solid evidence to support the concept that the thermal or mechanical stimuli directly affect the nerve endings within the dentinal tubules. Silver salts have traditionally been used to disclose the distribution of nerve fibres, due to the affinity of nerve tissue for silver. However, it has been suggested that the demonstration of nerves within the dentine by staining with silver salts, may be artifactual, as blackened

collagen fibres can be mistaken for nerves (Rapp, Avery et al. 1959; Hildebrand, Fried et al. 1995).

### 1.3.2 The dental receptor mechanism

The dentinal receptor mechanism postulates that, the odontoblast has a specialised sensory function. It has been observed that, the odontoblasts that line the pulpal cavity at the pulpo-dentinal junction (PDJ) have long cytoplasmic processes (odontoblastic processes), that extend into the dentinal tubules (Pashley 1996; Pashley 2002). It has been hypothesised that, the interpenetration of the odontoblast layer within the pulp, with nerve fibres allows the odontoblastic processes to function as excitary synapses (Seltzer 1971). It has been hypothesised that, the odontoblasts transform the action potential into a chemical message, e.g the release of acetylcholine, which plays an essential role in the transmission of nerve impulses. However, this theory has also been widely debated, with several studies dismissing this method of pain transduction, due to the lack of cholinergic activity close to the odontoblastic layer (Winter, Bishop et al. 1963; Ten Cate and Shelton 1966; Polito and Antila 1968).

### 1.3.3. The hydrodynamic theory

A popular and widely accepted theory is that of Brännström, the hydrodynamic theory (Dowell and Addy 1983). The hydrodynamic theory states that, the transmission of pain stimuli is mediated by hydrodynamic factors, including the flow and displacement of the tubule contents (Brannstrom 1966; Brannstrom and Astrom 1972). It was proposed that the rapid displacement of the tubular contents at the pulp-dentine border, as opposed to the slow outward fluid flow which appears to occur normally, results in the induction of pain (Brannstrom 1966; Brannstrom and Astrom 1972; Dowell and Addy 1983). It was suggested that, the pulp fluid expands and contracts in response to the hydrostatic pressure elicited by fluid flow, therefore activating pressure sensors (baroreceptors) within the pulp (Mumford and Newton 1969). Rapid flow in the pulpal part of the dentinal tubule can be expected to result in deformation, not only of the cellular processes but also of nerve fibres which are present in the adjacent pulp (Brannstrom and Johnson 1978).

It has been demonstrated that an outward flow of fluid caused by cold, air blasts and probing results in an immediate sharp pain. However, the application of heat results in an inward flow of fluid. It has been observed that the pain elicited from heat takes longer to develop, than the pain elicited from cold. It has been suggested that, a larger volume of dentine must be heated, before a sufficiently pronounced dislocation of fluid content is produced (Brannstrom and Astrom 1972). For the purpose of this study this will be the favoured theory.

### 1.4. Current treatments for dentine sensitivity

There are a large number of treatments available for dentine sensitivity. These treatments can be divided into two categories, those administered in a dental office (in house) by a dental health professional, and patient applied home therapy or over the counter treatments (Mac Carthy 2004). Over the counter or self applied treatments are generally in the form of, a toothpaste or mouthwash or rinse, while in house treatments can vary greatly, from the application of a sealant or resin, to oral surgery or laser treatment. In general desensitizing agents attempt either to cover or occlude the exposed dentinal tubules, preventing fluid flow, or desensitize the nerve, resulting in the nerve becoming less responsive to stimulation (Jacobsen and Bruce 2001)

#### 1.4.1 Nerve desensitization

A number of studies have reported the efficacy of potassium nitrate for the management of dentine hypersensitivity (Gillam, Bullman et al. 1996; Pamir, Ozyazici et al. 2005). It has been demonstrated that, potassium nitrate at a concentration of 5% in a low abrasive toothpaste was able to desensitize dentine, for up to four weeks (Bartold 2006). Although the mechanism for desensitization using potassium nitrate is not fully understood, it has been proposed; that the mode of action is due to the depolarization of the nerve. It has been suggested, that the potassium ions are the active component, and due to the depolarizing activity of the potassium ions, treatment results in a reduction in dentinal sensory nerve activity (Jackson 2000). Recently, the possibility of the use of lasers in the prevention of dentine sensitivity have also been explored (Kimura, Wilder-

Smity et al. 2000). Although the exact mechanism is not fully understood, it has been suggested that low energy laser irradiation desensitized the nerve, blocking the depolarisation of nerve fibres (Wakabayashi, Hamba et al. 1993).

### 1.4.2 Covering or occluding of dentinal tubules

Based on the hydrodynamic theory of dentine sensitivity the occlusion or covering of the exposed dentinal tubules to prevent fluid movement, would be a logical treatment for dentine sensitivity. In house or professional treatments include the use of resins, sealants and bioceramics (Savarino, Breschi et al. 2004). It has been suggested that, the enhanced adhesion properties of these materials, would offer improved and longer lasting desensitization, in comparison to topically applied agents (Orchardson and Gillam 2006). Other professional methods of covering the dentinal tubules include, periodontal surgery to bring the tissue over the surface of the exposed dentine (Bartold 2006).

An alternative mechanism is to occlude or plug the inside of the dentinal tubule, this may be achieved by enhancing the natural occlusion of the tubules, or through intervention with an occluding substance (Jacobsen and Bruce 2001). In house methods of occluding the dentinal tubules includes the use of medium output lasers to induce the occlusion or narrowing of the dentinal tubules(Lan and Liu 1995; Lan and Liu 1996). Another proposed treatment that is based on the occlusion of the dentinal tubules, is the use of gluteraldehyde or formaldehyde. Both these agents are able to precipitate salivary proteins in the dentinal tubules. Gluteraldehyde reacts with serum albumin found in the dentinal fluid resulting in the coagulation of the fluid therefore, occluding the dentinal tubules (Zappa 1994; Duran, Sengun et al. 2005; de Assis, Antoniazzi et al. 2006)

Agents which enhance the natural occlusion of the tubules are thought to enhance the mineralization of the tubules, creating a calcified barrier blocking the tubule opening on the dentine surface. It has also been suggested even a reduction in tubule diameter, through the enhanced precipitation of mineralised components upon the tubule walls, is capable to reducing sensitivity. This is the suggested mode of action of dental

preparations containing calcium hydroxide, sodium fluoride, stannous fluoride and sodium monofluorophosphate (Addy and Urquhart 1992; Mac Carthy 2004; Bartold 2006). Occlusion of the dentinal tubules has also been achieved through the use of oxalates, such as potassium oxalate and ferric oxalate, to reduce the permeability of dentine (Collaert and Fischer 1991). It has been suggested that the oxalate treatments occlude the tubules, through the creation of crystals both within the tubules and upon the surface of the dentine (Zappa 1994; Ling, Gillam et al. 1997; Zhang, Agee et al. 1998; Orchardson and Gillam 2006). However, the use of crystalline materials to reduce permeability has also been demonstrated to be a short term solution, as they are slowly dissolved by oral fluid, over time (Zhang, Agee et al. 1998).

Over the counter sensitivity treatments are generally toothpastes or dentifrices. Studies have shown that in some instances, it may not be the reported active ingredient within the dentifrice or toothpaste that results in a reduction in permeability, but the abrasives that are present. Silica is a common abrasive agent found in toothpastes, and chemical analysis of the dentinal tubules following treatment with a silica containing toothpaste, has identified the presence of silica within the tubules. It has therefore, been suggested that in some instances the reductions in permeability, may not be due to the suggested desensitizing agent, but the presence of abrasive silica particles contained within the toothpaste, occluding the tubules (Ling, Gillam et al. 1997). As such, the possibility of using nanoparticulate silica which is also known as colloidal silica as a desensitizing agent was investigated in this project. The possible use of nanoparticulates in the prevention of dentine sensitivity has also been previously investigated, and it was observed that gold nanoparticles of 30nm in diameter were able to enter and occlude the dentinal tubules (Liu, Chan et al. 2007). It was proposed that the nanoparticulate silica would also be able to enter the dentinal tubules occluding the dentine. It was proposed that the smaller dimensions of the nanoparticulate silica will facilitate the possibility of penetration and therefore, the occlusion of the dentinal tubules with silica.

**1.5 Introduction to silica**

Silicon dioxide or as it is more commonly known silica is the oxide of silicon having the chemical formula $SiO_2$. The word silica includes silicon dioxide in all its crystalline, amorphous, soluble or chemically combined forms in which the silicon atom is surrounded by four or six oxygen atoms (Helms 1988; Bergna 1994). It however, does not include any orgnao silicon compounds, which are man made and have carbon atoms linked directly to the silicon atoms, these are commonly known as Silicones and they do not occur in nature (Bergna 1994).

Compounds of silicon occur in all natural waters and may be present either in solution or as suspended solids(Macdonald 1983). The abundance of silica containing compounds in nature, is due to the weathering of rocks which have an abundance of silica crystals present (Iler 1979a; Macdonald 1983). This is hardly surprising when you realise that silica is the main component of the earth's crust, the most commonest crystalline form of which is quartz (common sand) (Iler 1979a). In solution silica containing compounds are fairly abundant, but their concentrations are controlled by processes such as precipitation, bio removal and recycling (Macdonald 1983).

Living organisms such as diatoms, algae, bacteria and sponges require silica for growth. Silica is the main constituent of the skeletal structure of diatoms, and in the open water they are the dominant biological organisms which remove silicon from solution (Spencer 1983). Diatoms are photosynthetic unicellular organisms, with a unique double shell that is composed of opaline silica (Raven and Johnson 1999) Diatoms absorb soluble silica in the form of silicic acids, rather than colloidal particles, even at low concentrations, they then metabolize and deposit it as an external skeleton (Iler 1979e)

The silica particles present in natural water can be in a colloidal or polymeric state, as well as monosilicic acids or silicate ions.

$$SiO_2 + 2H_2O \longrightarrow Si(OH)_4$$

Monosilicic Acid

The most common form of silicon present in natural solutions, is the silicate anion, ($SiO_4^{4-}$) (Macdonald 1983). The $SiO_4^{4-}$ anion, is derived from the weathering reactions of silicate and aluminosilicate minerals, the products of such weathering, is a solid clay mineral and silicic acid in solution (Macdonald 1983). Un dissociated silicic acid is the stable form of the silicate species at pH values below 9, above this some dissociation does occur, however, this is unlikely in most natural waters as their pH is maintained below 9 (Macdonald 1983).

Monosilicic acid is present in this form only in dilute solutions. An increase in silicic acid concentration leads to the formation of dimeric or trimeric poly silicic acid species, leading to oligomer and eventually polymeric species, that are recognizable as colloidal particles (Iler 1979a). The polymerisation of silicic acid is via a condensation reaction that, involves the nucleophilic substitution of a Si-OH oxygen atom on another silicon atom, which leads to the formation of a Si-O- Si siloxane bond, and the departure of water.

$$Si(OH)_4 + H\underline{O}\text{-}Si(OH)_3 \longrightarrow (OH)_3Si\text{-}\underline{O}\text{-}Si(OH)_3 + H_2O$$

(Coradin and Lopez 2003)

Supersaturated solutions of silicic acid in pure water are thermodynamically unstable, because condensation and polymerization through dehydration takes place (Iler 1979a). This reaction is slow between two neutral species, but in the presence of a nucleophilic oxygen atom in the charged species $Si\text{-}O^-$ the reaction is accelerated (Coradin and Lopez 2003). Thus, formation of larger chain silicic acids, trimers, tetramers (cyclic), and oligomers proceeds likewise. However, with each substitution of a Si-OH group for a siloxane linkage, there is an increase in the electron charge of the silicon atom, which become more electrophilic and constitute preferential sites for further monomer addition (Coradin and Lopez 2003). Condensed rather than chained oligomers are formed, which lead to the formation of a sol of colloidal particles (Coradin and Lopez 2003) Figure 2.1

### 1.6 Colloidal silica

The International Union of Pure and Applied Chemistry (IUPAC) suggest that a colloidal dispersion should be defined as, a system in which particles of colloidal size

(1-1000nm) of any nature (solid, liquid or gas) are dispersed in a continuous phase of a different composition or state (Bergna 1994). A stable dispersion of solid colloidal particles in a liquid is called a sol, the particles do not settle or agglomerate at a significant rate (Bergna 1994). Colloidal silica is a stable dispersion or sol of discrete particles of amorphous silica, however, it excludes solutions to poly-silicic acid, in which the polymer molecules or particles are so small that they are not stable (Iler 1979c).

The formation of colloidal silica particles is a result of the polymerisation of monosilicic acid. When a solution is highly supersaturated and there are insufficient solid silica surfaces available to permit rapid deposition of soluble silica, new small cyclic (tetramer) particles are formed, by inter-condensation of monomer and low chain length silicic acids (Iler 1979a). The ring like tetrameric structures can link together, to form larger three dimensional structures that condense internally to the most compact state, with SiOH groups remaining on the outside (Iler 1979a).

These 3 dimensional spheres are in effect nuclei that can develop into larger particles, (a process known as Ostwald ripening) or they may begin linking together to form branched chains, that become networks that stretch throughout the liquid medium thickening it, until a gel is formed (Iler 1979b) (Figure1.3). What happens to the nuclei if they become larger particles or interlink to become a gel network, in the absence of a salt or other additive, is dictated by the pH of the solution (Coradin and Lopez 2003). Below pH 7 the particles are able to aggregate to form a network and thus a gel, because there are only weak electrostatic repulsion, and Brownian motion renders interparticle collisions possible (Iler 1979b; Coradin and Lopez 2003). If the contact time is long enough siloxane bonds can be formed thus irreversibly binding the particles together (Bergna 1994). Due to steric and electrostatic considerations further particles additions can then take place at the end of the elongating chains forming fibrillar assemblies (Coradin and Lopez 2003). As the fibrils grow there is the addition of side chains and a three dimensional network of branched chains is formed in which the liquid is retained by capillary action (Iler 1979c; Coradin and Lopez 2003).

However, when the pH is above 7 the rate of aggregation is reduced, because there are fewer collisions between particles, due to the increased charge on the particles(Iler 1979c). Therefore, primary particles increase in size and decrease in number, as a result of the Ostwald ripening process. Ostwald ripening or coarsening as it is also known is a phase transformation process, that has been observed when particles with various sizes are dispersed in a matrix (Baldan 2002). The driving force of this process is the decrease in total surface free energy. In poly disperse sols the smaller particles have a greater solubility than the larger particles and so will tend to grow at their expense (Shaw 1992). The rate of growth is dependent on the distribution of particle sizes since the growth occurs by the more soluble smaller particles dissolving and the silica being deposited upon the larger particles (Iler 1979b)

At ambient room temperature and above pH 7 where the rate of dissolution and deposition of silica is high, growth continues until particles are between 5 and 10nm in diameter, after which growth is negligible; by increasing the temperature it is possible to continue particle growth (Iler 1979b). Below pH 7 where the rate of polymerisation and de polymerisation is slower, particle growth becomes negligible after a size of 2-4nm (Iler 1979b). As mentioned above, due to the presence of a strong negative charge at pH's above 7 the particles do not collide, so particle growth will continue without aggregation (Iler 1979b; Coradin and Lopez 2003)

It is this ionic charge on the particles in the presence of alkali that is the chief mechanism of stabilisation in commercial sols, e.g. Ludox® (Iler 1979c). The basic stabilisation mechanism is due to the overlap of the electron double layers of two particles as they approach one another (Iler 1979c). This is often referred to as the Deryagin- Landau and Verwey – Overbeek (DLVO) theory in which the stability of a sol is treated in terms of the energy changes which take place when particles approach one another (Shaw 1992) The DLVO theory involves an estimation of the energy due to the overlap of double layers (usually repulsion) and the London – van der Waals energy (usually attraction) in terms of interparticle distance (Shaw 1992). In the case of a stable

silica sol the attractive energy is not great enough to overcome the energy hurdle of overlapping two highly charged double layers, therefore, the particles repel each other.

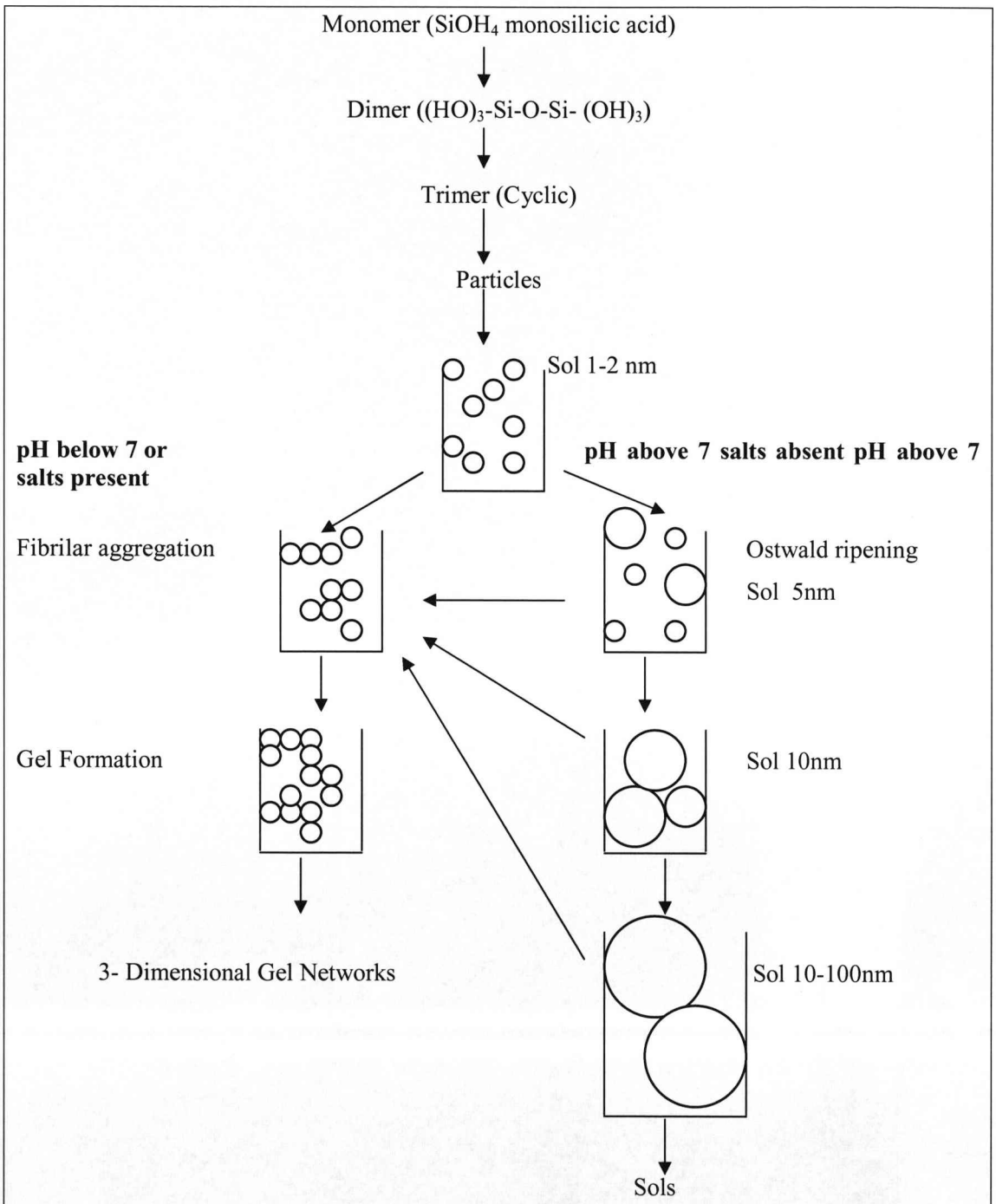


**Figure 1.3** A depiction of the polymerisation of silica: in an alkali solution absent from salts (right) where the particles increase in size with a decrease in number; and in either an acidic or alkali solution in the presence of salts (left) whereby particles aggregate and form bonds eventually forming a three dimensional gel network this schematic has been adapted from (Iler 1979b; Bergna 1994; Coradin and Lopez 2003).

Commercial colloidal sols can contain particles between 5 and 50 nm in diameter, with between 30-50% by weight silica (Iler 1979c) In most cases the sols are stabilized by alkali either sodium or ammonium hydroxide, and have a pH between 8 and 10 (Iler 1979c). In some commercial sols a small amount of salt is added, as this will lower the viscosity of a highly concentrated sol by making a minor reduction to the thickness of the electron double layer (Iler 1979c). This is of utmost importance in commercial sols where there is a requirement for a high silica concentration, but also stability. Commercial colloidal silica sols have many varied uses. These include, as a stiffening and binding agent, a soil retardant in carpet shampoos, silicon wafer polish, photographic coatings, anti slip floor polishes, a reactant for molecular science and in creation of gel moulds ( Ludox literature). These are just some of the varied uses of commercial sols.

**1.7 Nanoparticulate silica coatings.**

Recent research at the University of Liverpool has investigated the uses of commercially available colloidal silica sols as a coating for medical devices (Cousins, Doherty et al. 2004; Cousins 2005). Nanoparticulate silica was selected for this purpose as silica is often found within the body in small amounts and as such is thought to offer biocompatibility. It was shown that adherence of the silica nanoparticles onto a surface affected the adhesion, morphology and proliferation of fibroblasts (Cousins, Doherty et al. 2004). The nanoparticulate silica was shown to have influenced the cellular behaviour over a prolonged time with no detrimental effect on cell viability. It has since been shown that creation of a nanoparticulate coating on a surface can also alter cell attachment of the yeast *Candida albicans* (Cousins, Allison et al. 2007).

The creation of modified surfaces that minimise bacterium and yeast cellular attachment and growth is of great importance to the health care industry, particularly with the widely reported increase in nosocomial infections and the rise of the "super bugs" such as Methicillin Resistant *Staphylococcus aureus* (MRSA). However, creation of coated surfaces that minimise bacterial attachment is also of interest to the dental care industry, as a mechanism to prevent plaque formation. The method of altering the surface

topography of a substrate employed by Cousins et al. was a simple two step dipping process. The test substrate was first dipped into a polycationic polymer Zetag™ (Ciba Speciality Chemicals Ltd) which adhered through ionic attraction, producing a positively charged surface. This was subsequently dipped into the silica sol, resulting in the adhesion of the negatively charged silica nanoparticles to the polymer binding layer, creating a nanoparticle coating (Cousins, Doherty et al. 2004). This two step coating method is not commercially favourable. Therefore in this project the necessity of the polymer binding layer and the manipulation of the coating process, to create a more commercially viable method was explored.

From this discussion it can be seen that the colloidal silica could have the potential to provide both an anti-plaque and sensitivity treatment. To be able to realise these objectives it is necessary to investigate and understand the interaction of colloidal silica with the dentine surface. This project concentrated on developing different methodologies for studying the interaction of the silica nanoparticles, with particular relevance to its use as a treatment for hypersensitivity.

## 1.8 Aims and Objectives

### 1.8.1 Aim

The aim of this project is to investigate the use of nanoparticulate silica to occlude the dentinal tubules.

### 1.8.2 Objectives

1. To investigate the creation of the nanoparticulate coatings, the effect of altering the underlying polymer layer and the possibility of creating a commercially favourable "one-step" process.
2. To investigate the ability of the nanoparticulate coatings to reduce the permeability of dentine and, therefore, act as a desensitizing agent.
3. To investigate the ability of the coatings to aid remineralisation through the adsorption of salivary components and to withstand acid challenge.

To achieve theses objectives several different techniques were employed transmission electron microscopy (TEM), quartz crystal microbalance with dissipation monitoring (QCM-D), hydraulic conductance and X-ray photoelectron spectroscopy (XPS). The following chapters shall contain a brief introduction to the technique, the materials and methods used, and the results obtained with each technique and a discussion.

Chapter 2 TEM

TEM was used to gain a visual representation of the nanoparticulate coatings. It was used to ascertain the effect of altering the polymer concentration and chemistry on the overall density and appearance of the coating.

Chapter 3 QCM-D

QCM-D was used to monitor the formation of the coatings in-situ. It was possible to test a number of different surfaces using QCM-D including gold, hydroxyapatite (HA) and dentine. It was also possible to investigate the ability of the coatings to withstand flow conditions, and the adsorption of artificial saliva components onto both nanoparticulate coated and un coated surface, to explore the creation of a salivary pellicle.

Chapter 4 hydraulic conductance

Hydraulic conductance is a good indication of the ability of a potential desensitising agent to occlude the dentinal tubules. It is a standard industry test for any potential desensitizing agents. As such, to investigate the ability of the nanoparticulate coatings to reduce dentine permeability and, therefore, their potential as a desensitizing agent, hydraulic conductance measurements were used.

Chapter 5 XPS

XPS was used to monitor the chemical composition of both etched and non etched dentine. It was used to identify the presence of both nanoparticulate silica and NaF on the dentine surfaces following treatment. An attempt was made to assess the penetration depth of the treatments using an argon ion gun, to remove surface layers. XPS was also

used to monitor the remineralisation of the dentine following artificial salvia treatment, as increases in the inorganic phase associated peaks. The ability of the nanoparticulate coating to offer protection to the underlying dentine from acid attack was also explored.

# Chapter 2

# Investigation of the morphology of silica nanoparticulate coated surfaces with Transmission Electron Microscopy.

*This chapter explains the basic procedure for coating surfaces with commercially available colloidal silica for Transmission Electron Microscopy (TEM) analysis. Recent research at the University of Liverpool has identified a procedure for coating surfaces in nanoparticulate silica. This procedure required the use of a polymer binding layer, to which the nanoparticles can attach to form a stable coating. In this study, the use of different molecular weight polymers and the lowering of the concentration of the polymers were investigated to see if this would affect the density of the nanoparticulate coating. The possibility of creating a one step process for coating surfaces with nanoparticulate silica was also investigated. In this chapter, TEM has been used to study the size, arrangement and density of the various nanoparticulate coatings on the test surfaces.*

## 2.1 Introduction

As discussed in chapter 1 recent work at the university of Liverpool investigated the creation of nanoparticulate coated surfaces (Cousins, Doherty et al. 2004; Cousins, Allison et al. 2007). Cousins et al. investigated the creation of these nanoparticulate coated surface using both Atomic Force Microscopy (AFM) and Scanning Electron Microscopy (SEM) (Cousins 2005). Both these methods are effective techniques for assessing the surface morphology of a substrate. However, neither technique evaluated the thickness of the coating. Although AFM is able to take readings in three dimensions (x, y and z) with a single scan, (Goodhew, Humphreys et al. 2001) it is still unable to provide information from the internal structure of a sample. The lack of information regarding the internal structure of the coating is frustrating as it prevents a full understanding. Some of the questions that still needed to be answered after AFM and SEM analysis included:-

1. Is a monolayer of nanoparticulates being adsorbed onto the surface?
2. What effect would altering the underlying polymer have on the overall density of the coating?

Therefore, in this study, Transmission Electron Microscopy (TEM) was used in an attempt to answer some of these outstanding questions.

### 2.1.2 TEM for morphological analysis of nanoparticulate silica coated surfaces.

TEM uses a fine beam of electrons to image a surface and enables the exploration of the internal structure of a thin specimen (Chescoe and Goodhew 1990). TEM has already proven useful when investigating colloidal silica for the purpose of investigating particle size of a given sol (Iler 1979c) .

In TEM electrons are transmitted through a sample in a vacuum. Upon interaction of the beam with the specimen, there are a number of possible fates for each electron. The three most significant of these are:

a) It is undeflected – transmitted without interacting with any atom.
b) It is deflected but loses no energy - elastically scattered
c) It loses a significant amount of energy and is probably deflected – non elastic scattering, so as a result secondary electrons and even x-rays may be excited. (Amelincx, Van Dyck et al. 1997)

If all these types of electrons were able to continue down the microscope column, then they would all contribute to the image and there would be no difference between areas of different thickness or composition (Chescoe and Goodhew 1990). To create contrast in the image, the scattered electrons must be separated from the nonscattered electrons. This is achieved using an objective lens aperture.

The objective lens aperture prevents high angle diffracted electrons from continuing down the microscope column and contributing to the image enhancing the contrast (Goodhew, Humphreys et al. 2001). However, if the aperture is centred about the optical axis and in the absence of a specimen, a bright background can be seen. This is known as bright field imaging (Goodhew, Humphreys et al. 2001). When a specimen is placed within the electron beam, regions that are thicker or of a higher density will scatter more strongly and will appear darker in the image created on the underlying phosphorous screen (Chescoe and Goodhew 1990; Goodhew, Humphreys et al. 2001).

TEM is therefore able to produce high resolution, high magnification images, but it also identifies alterations in the density of coatings at a nanometre scale. It is for these reasons it was decided to use TEM to investigate the coating of surfaces with nanoparticulate silica. Unlike the techniques previously utilised, it should allow identification of density of layers, as well as a visual representation of the surface coverage. TEM has, therefore, been used in this instance to investigate the effect of the underlying polymer on the surface coverage of the nanoparticulate silica, both by altering the concentration and by using different polymers with varying chain lengths. It was also important to investigate the creation of a "one-step process" for coating surfaces with nanoparticulates, as this would be a more commercially viable method. Using the TEM, it was possible to obtain images that gave information regarding the surface morphology, as well as gaining an appreciation of the density of coverage.

## 2.2 Materials

Carbon coated copper TEM grids purchased from Agar Scientific were used as received. As with the previous work at the University of Liverpool (Cousins 2005) aqueous colloidal silica sols were donated by W.R. Grace & Co. USA. Three sols were selected for these experiments: Ludox® SM-30 (7nm particle diameter), Ludox® HS-40 (14nm particle diameter) and Ludox® TM-50 (21nm particle diameter). The polycationic polymers Zetag™ 7689 and 7109 were donated by Ciba Speciality Chemicals Ltd. Zetag™ 7689 is a polycationic polymer comprised of a co-polymer of acrylamide and quaternised dimethylaminoethylacrylate. Zetag™ 7689 polymer is 80% cationic and has a molecular weight in the region of $10^8$Da, whereas Zetag™ 7109 polymer is 100% cationic and has a molecular weight in the region of $10^6$Da. A third polymer was also tested, UCARE™ polymer JR-125 (Amerchol Cooperation). It is a lower molecular weight polymer than either Zetag™ polymers of around $10^5$Da. UCARE™ polymers are polymeric, quarternary ammonium salts of hydroxyethylcellulose reacted with trimethyl ammonium substituted epoxide. The quaternization of the hydroxyethylcellulose results in the creation of multiple cationic sites to which anionic groups can attach (figure 2.1). The UCARE™ polymers are commonly found within hair care products such as conditioners, due to their unique ability to deposit on a surface as a flat coherent

layer. For this reason UCARE™ polymer JR -125 is very attractive for use as a polymer binding layer.

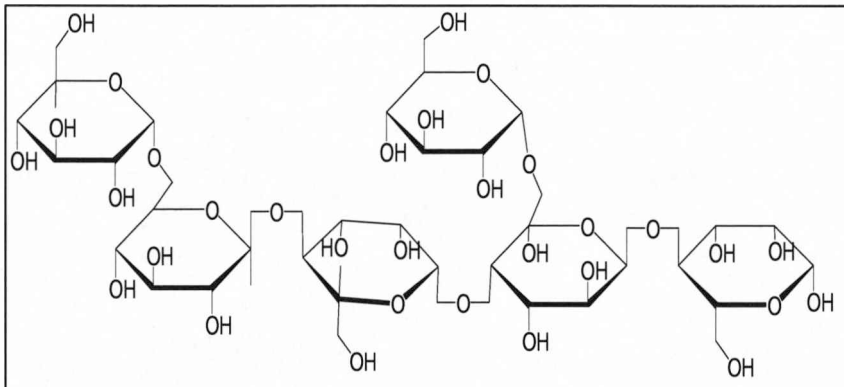

**Figure 2.1.** The chemical configuration of UCARE™ Polymers

Although a two step procedure for creating a nanoparticulate coated surface has been shown to work (Cousins 2005), the production of a "one step" method of coating the surface would be of commercial interest. For this purpose, two commercially available nanoparticulate silica products were investigated. The first was Ludox® CL (W.R. Grace & Co. USA). Ludox® CL is a commercial silica sol, in which the silica nanoparticles have been modified with the addition of an alumina coat to the surface so that they are now positively charged (Figure 2.2.), unlike the Ludox® grades already tested which have a negative surface charge. The Ludox® CL grade silica also has a much larger variation in particle size, with particles varying between 14 and 30 nm in diameter.

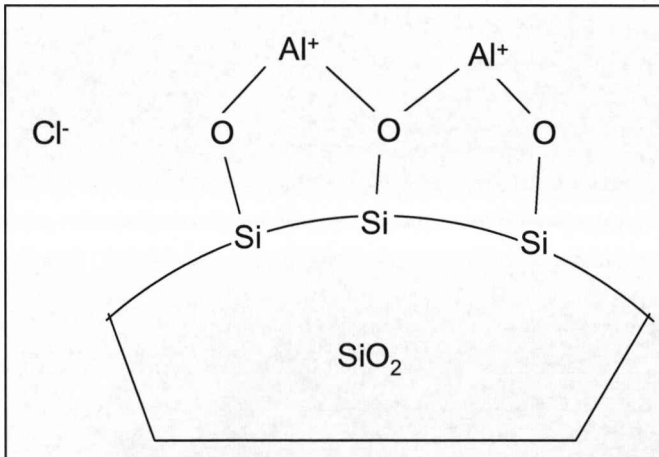


**Figure 2.2** Schematic representation of Ludox® CL surface, showing the binding of an Alumina "coat" to the silica nanoparticles.

The second was the use of the commercially available silica containing product Percoll™. Percoll™ is a poly disperse colloidal silica containing sol, in which the silica particles are coated in polyvinylpyrrolidine (PVP) (figure 2.3). The silica particles in Percoll™ vary in diameter between 15 and 30nm (Pertoft 2000). Percoll™ is often used for the separation of cells, sub cellular particles and viruses. The importance of Percoll™ in this project was that the addition of the PVP coating to the silica nanoparticles rendered them attractive to a negative surface, due to the strong dipole of the pyrrolidone structure of the polymer.

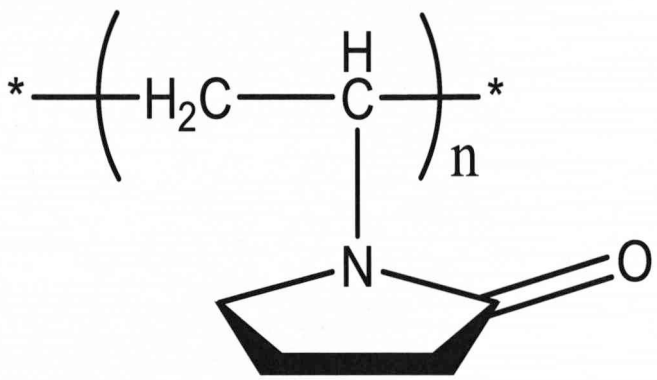


**Figure 2.3.** Schematic representation of the repeating unit of polyvinylpyrrolidone (PVP).

## 2.3 Methods

### 2.3.1 Deposition of colloidal silica onto the surface of a TEM grid in the absence of a polymer binding layer

To assess the requirement for a polymer binding layer, carbon coated TEM grids were modified with nanoparticulate silica, using the following method:

1. The TEM grids were held with forceps so only the non-carbon coated side was touching the surface of 10ml of the 40%(W/V) Ludox® silica sol for 1 minute.
2. The samples were gently rinsed in copious amounts of $dH_2O$ for 3 minutes.
3. The substrate was allowed to dry at room temperature for 5 minutes
4. The coated TEM grids were then stored in a grid case at room temperature overnight, prior to their analysis with TEM.

a. Influence of silica sols

Three different silica sols were used in step 1: Ludox® SM-30 (7nm particle diameter), Ludox® HS-40 (14nm particle diameter) and Ludox® TM-50 (21nm particle diameter).

### 2.3.2 Deposition of colloidal silica onto the surface of TEM grids using the two step process.

The carbon coated copper TEM grids were modified, following the procedures described in previous work at the University of Liverpool (Cousins, Doherty et al. 2004; Cousins 2005; Cousins, Allison et al. 2007) to assess the effect of a polymer binding layer. However, it was very important for TEM that only one side of the TEM grid was coated. If both sides were coated, as would happen using the traditional dipping method (Cousins 2005), then the coating would have been not only too thick to visualise with TEM but would also have resulted in an inaccurate analysis of the density of the coating. The following coating method was used to produce nanoparticulate coated TEM grids:

1. The TEM grids were held with forceps so only the non-carbon coated side was touching the surface of 10ml of the polymer solution for 1 minute.

2. The polymer coated TEM grid was gently rinsed in copious amounts of $dH_2O$ for 3 minutes.
3. The substrates were allowed to dry at room temperature for 5 minutes.
4. The grid was held with the forceps with the polymer coated surface touching the 40% (W/V) Ludox® silica sol.
5. The samples were rinsed in copious amounts of $dH_2O$ for 3 minutes.
6. The substrate was allowed to dry at room temperature for 5 minutes.
7. The coated TEM grids were stored in a grid case at room temperature overnight, prior to their analysis with TEM.

a) Influence of polymer molecular weight

   The polymer solution in step 1 above was either Zetag™ 7689, with a molecular weight of $10^8$Da, or the shorter chain Zetag™ 7109, with a molecular weight of $10^6$Da

b) Influence of polymer concentration

   The polymer solutions in step 1 were made up to two concentrations of 3.2g/l and 0.3g/l to evaluate whether or not the uniformity of the polymer binding layer could be enhanced.

c) Influence of different polymer chemistry

   UCARE™ polymer JR-125 was selected for this purpose. Samples were created, where the concentration of UCARE™ polymer JR-125 at step 1 was both 3.0g/l and 0.3g/l.

d) Influence of silica sols

   Three different silica sols were used in step 4: Ludox® SM-30 (7nm particle diameter), Ludox® HS-40 (14nm particle diameter) and Ludox® TM-50 (21nm particle diameter).

### 2.3.3 Creation of a "one step" process

Although the two step process of using Zetag™ to create a polymer binding layer, to which the silica nanoparticles can adhere, has been shown to be a viable method for obtaining nanoparticulate coated substrates (Cousins, Doherty et al. 2004), a process that required only one dipping step could be more desirable in a commercial context. Two different methods of creating a one-step process were investigated:

Method 1: Direct mixing of the 14nm silica particles (Ludox® HS-4O) with UCARE™ polymer JR-125.

1. 500ml of 0.3g/l UCARE™ polymer JR-125 was mixed, using high shear mixing.
2. Ludox® HS-40 was diluted with $dH_2O$ to 10% (w/v).
3. 500ml of the diluted HS-40 was slowly (roughly 10 ml per minute) added to the UCARE™ polymer, under continuous mixing.
4. The mixture was allowed to settle overnight prior to the coating of TEM grids

a) High shear homogeniser (LIGHTNIN, LabMaster mixer): The probe was set to a constant output of 200,000rpm. This created a vortex within the polymer solution. The UCARE™ polymer was continuously mixed during the addition of the diluted HS-40. The Homogeniser remained on for a further 10 minutes, after the addition of all the Ludox® sol.

b) Ultrasonic probe (Microson™ Ultrasonic cell disruptor XL misonix):
The probe was set to an output of 131 watts and run, continuously, for the duration of the addition of the Ludox® sol. After all the silica sol had been added to the UCARE™ solution, the mix was sonicated intermittently for one minute at a time, for a further 10 mins in an attempt to break up any possible aggregates that had formed.

TEM grids were coated in the same manner as in the two step process, starting from step 4:

Method 2: Commercially available surface coated silica products.
The two products selected were Ludox® CL and Percoll™. The method for coating the TEM girds remained the same as that described above.

### 2.3.4 Topographical surface analysis with TEM

The TEM (FEI 120KV Tenai G2 Spirit BioTwin) was used at 100KV high tension, with the filament set to 32° and at spot size 3.

1. Holding the TEM grid of interest with forceps, the grid was placed in the specimen holder, with the coated surface the uppermost surface.
2. The grid was clamped into place.

3. The specimen holder was slowly inserted into the microscope column.
4. Once the vacuum pump had finished, it was possible to twist and slowly insert the holder fully into the microscope column.
5. The microscope underwent several alignment steps (including the condenser lens, condenser aperture and alignment of the electron gun) by following instructions set out from the user manual (Munke 2005).
6. Images were taken digitally at a range of magnifications (ranging from 8,200x and 160,000x) and at a variety of different, randomly chosen, positions across the grid.

Table 2.1 lists all the different surface coatings investigated with TEM.

| **Silica** / **Polymer** | Ludox® SM (7nm) | Ludox® HS-4O (14nm) | Ludox® TM-50 (21nm) | Ludox® CL | Percoll ™ |
|---|---|---|---|---|---|
| None | • | • | • | • | • |
| Zetag™ 7689 3.2g/l | • | • | • | | |
| Zetag™ 7689 0.3g/l | • | • | • | | |
| Zetag™ 7109 3.2g/l | • | • | • | | |
| Zetag™ 7109 0.3g/l | • | • | • | | |
| JR-125 3.2g/l | • | • | • | | |
| JR-125 0.3g/l | • | • | • | | |
| JR-125 0.3g/l shear mixed with | | • | | | |
| JR-125 0.3g/l sonic mixed with | | • | | | |

**Table 2.1** Table of different coatings investigated using TEM. A • indicates that there are TEM images of the combination of polymer binding layer and nanoparticulate silica.

## 2.4 Results

### 2.4.1 TEM analysis of the nanoparticle silica coating without the polymer binding layer

When the nanoparticle coated grids without a polymer binding layer (method 2.3.1) were viewed using the TEM, the particles were attached intermittently in small clusters across the surface (Figure 2.4). It was clear that there was poor nanoparticle attachment for all the particle sizes, although a few more particles were observed on the 14 and 21nm coated surfaces than on the 7nm coated surface.

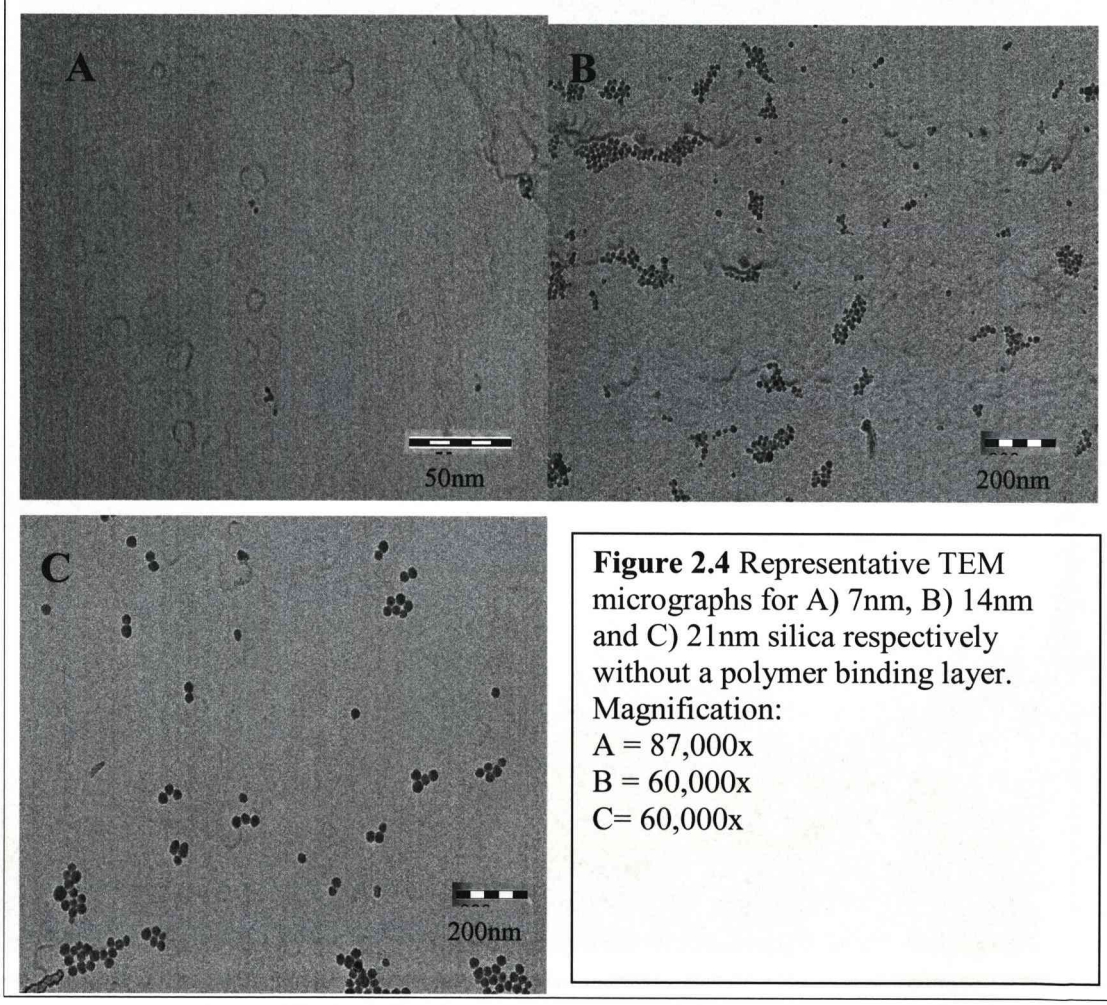


**Figure 2.4** Representative TEM micrographs for A) 7nm, B) 14nm and C) 21nm silica respectively without a polymer binding layer. Magnification:
A = 87,000x
B = 60,000x
C= 60,000x

### 2.4.2 TEM analysis of nanoparticle silica coating with the polymer binding layer

Influence of molecular weight: All samples were prepared following method 2.3.2.

a) Zetag$^{TM}$ 7689 :

Using Zetag™ 7689 at the concentration of 3.2g/l, increased the number of silica nanoparticles attached to the substrate, in comparison with no polymer binding layer (Figure 2.5). This was particularly evident when the two smallest and largest size nanoparticles were used. The coating, however, was uneven, with some darker areas apparent, demonstrating alterations in the density of the coating. This was more apparent when the grids were viewed as a whole and, particularly, when the 14nm particles were used, as there were some large areas, which lacked any coverage in close proximity to areas consisting of dense coverage.

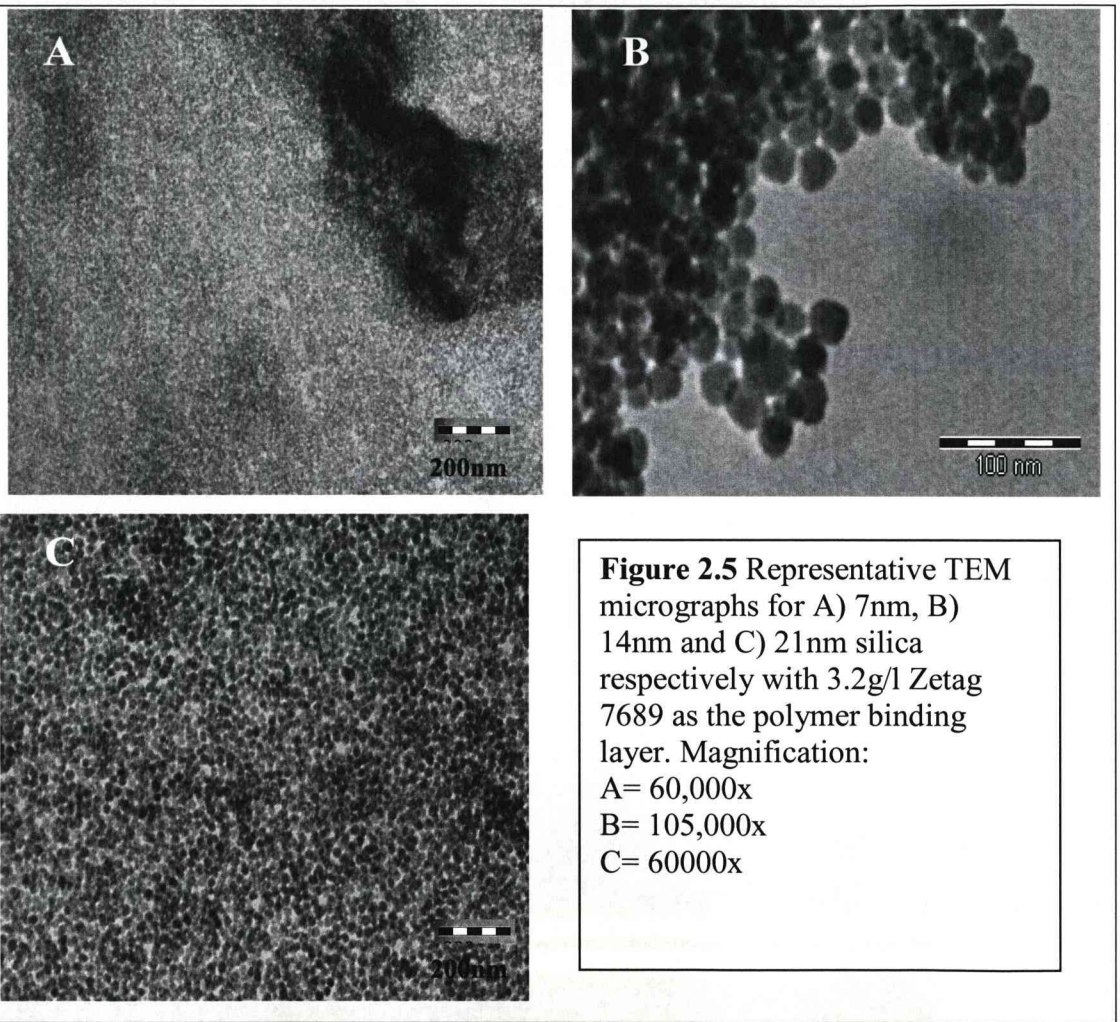


**Figure 2.5** Representative TEM micrographs for A) 7nm, B) 14nm and C) 21nm silica respectively with 3.2g/l Zetag 7689 as the polymer binding layer. Magnification:
A= 60,000x
B= 105,000x
C= 60000x

b) Zetag™ 7109 :

Using Zetag™ 7109 at a concentration of 3.2g/l as the polymer binding layer, produced a continuous layer of nanoparticles but there were still areas with greater density, suggesting that the layer was non-uniform (Figure 2.6). In

this instance, when the entire grid was viewed at a lower magnification, the areas of non coverage seen when Zetag™ 7689 was used, were absent. There also appeared to be fewer areas of high density.

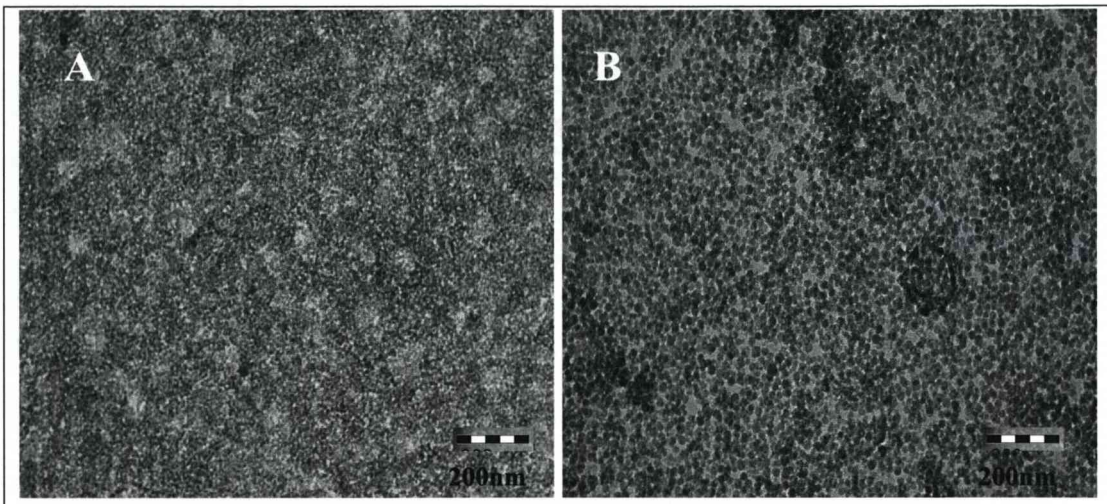


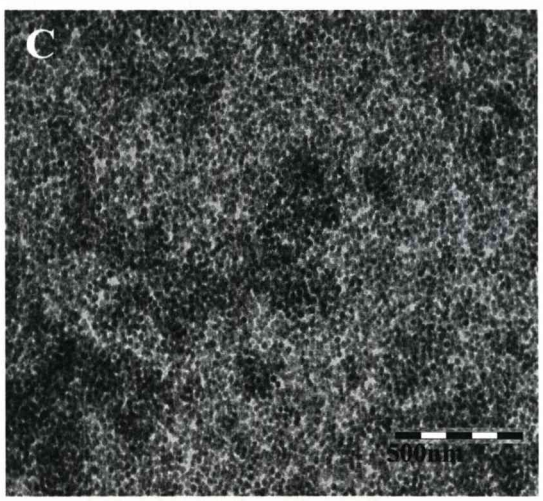


**Figure 2.6** Representative TEM micrographs for A) 7nm, B) 14nm and C) 21nm silica respectively with 3.2g/l Zetag 7109 as the polymer binding layer. Magnification:
A= 60,000x
B= 60,000x
C= 43,000x

c) Influence of concentration:

Lowering the concentration of the Zetag™ 7689 polymer to 0.3g/l allowed a more uniform coating of nanoparticles to be achieved (figure 2.7) than when the higher concentration polymer was used.

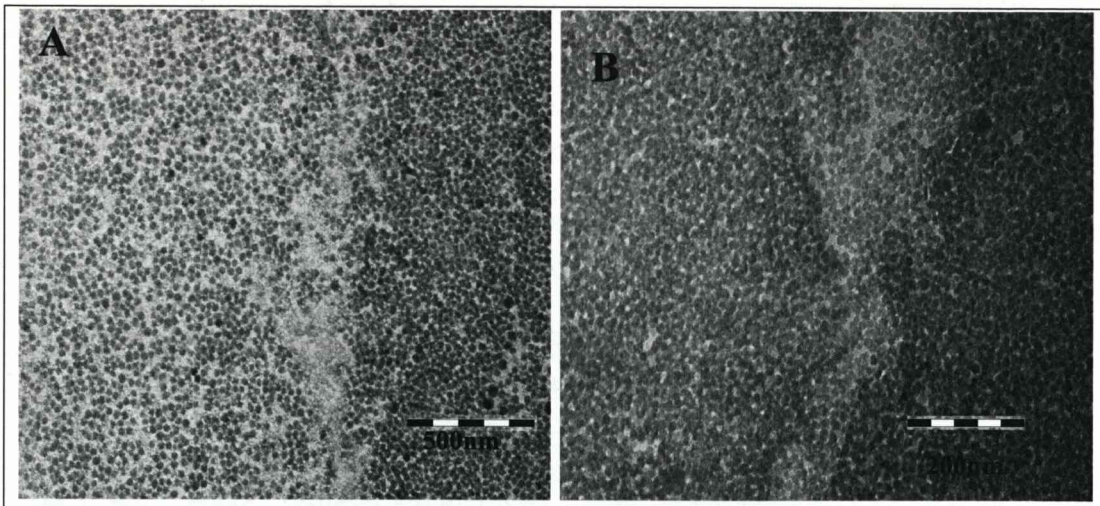


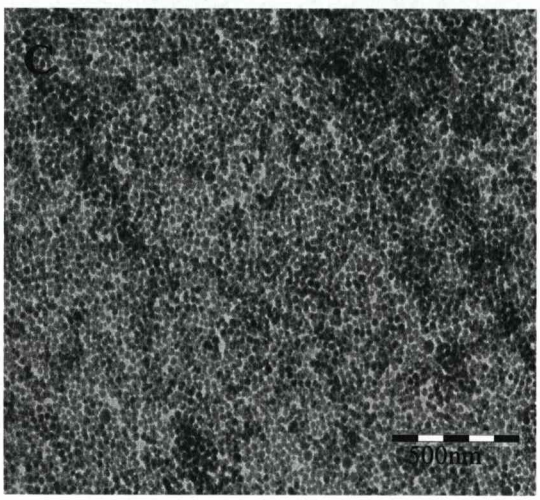


**Figure 2.7** Representative TEM micrographs for A) 7nm, B) 14nm and C) 21nm silica respectively with 0.3g/l Zetag 7689 as the polymer binding layer.
Magnification:
A= 43,000x
B= 105,000x
C= 43,000x

Similarly, lowering the concentration of Zetag™ 7109 polymer (Figure 2.8) created a uniform nanoparticulate coating.

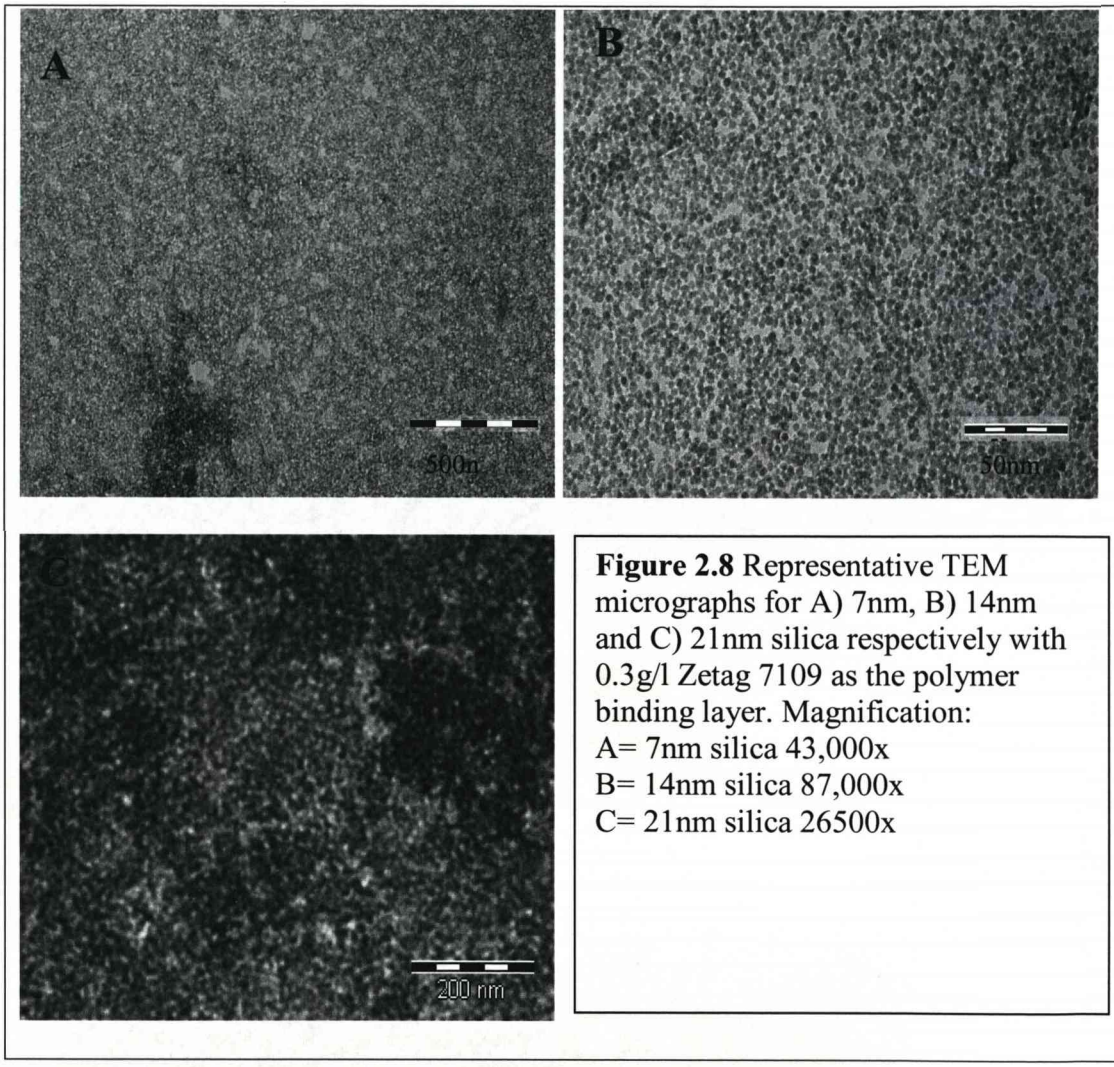


**Figure 2.8** Representative TEM micrographs for A) 7nm, B) 14nm and C) 21nm silica respectively with 0.3g/l Zetag 7109 as the polymer binding layer. Magnification:
A= 7nm silica 43,000x
B= 14nm silica 87,000x
C= 21nm silica 26500x

d) Influence of polymer chemistry:

As demonstrated in Figure 2.9, using the UCARE™ polymer at 3.2g/l resulted in the production of a coherently coated surface with few areas of variation. This showed that the UCARE™ polymer could be used as an effective alternative to the Zetag™ polymers to create a polymer binding layer to attach the silica nanoparticles.

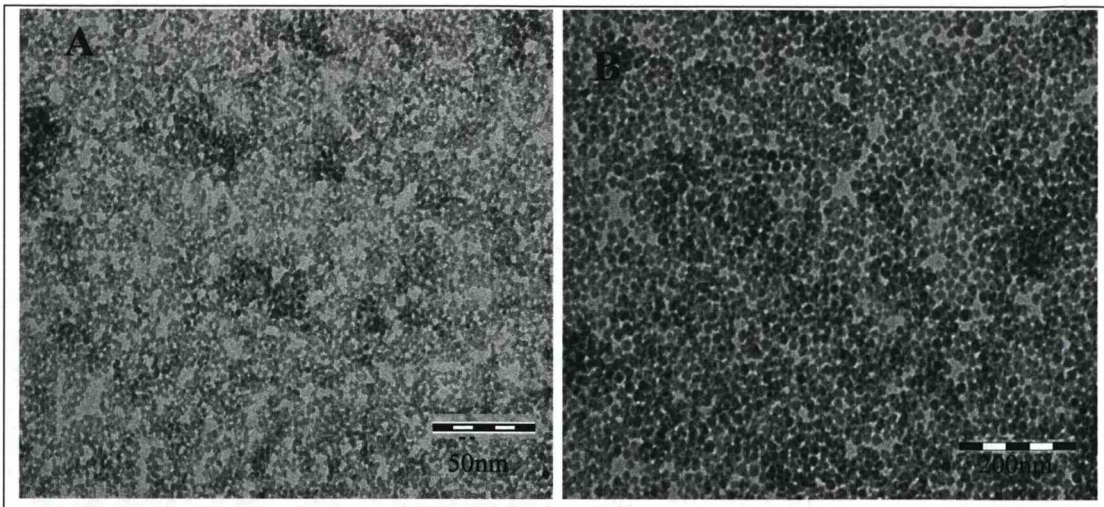


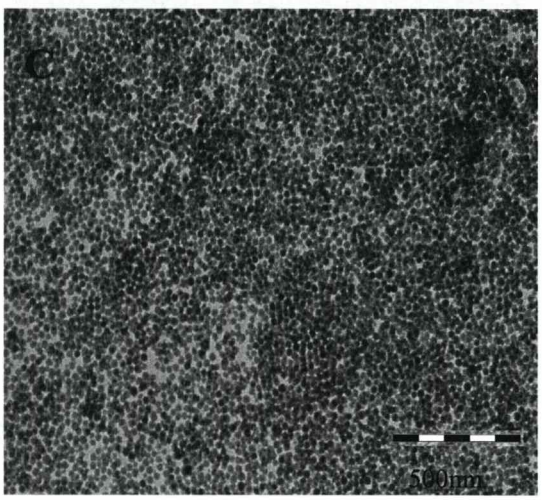


**Figure 2.9** Representative TEM micrographs for A) 7nm, B) 14nm and C) 21nm silica respectively with 3.2g/l UCARE™ JR 125 as the polymer binding layer. Magnification:
A=87,000x
B=105,000x
C=43,000x.

Figure 2.10 demonstrates that lowering the concentration of UCARE™ Polymer JR-125 to 0.3g/l still resulted in the production of a uniform nanoparticulate coated surface, although it was apparent on the 14nm silica coated surface (figure 2.10b) that there was some spacing between the nanoparticles.

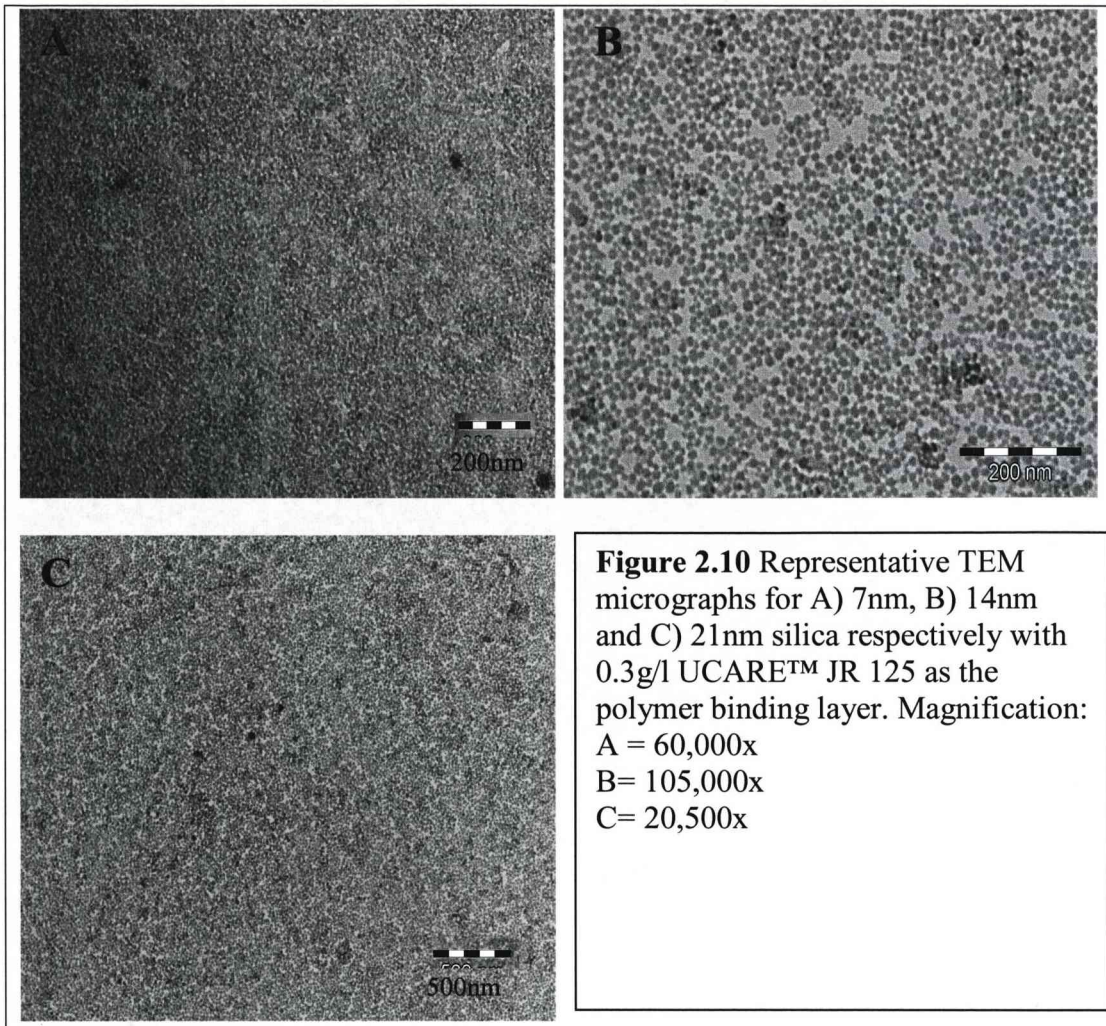


**Figure 2.10** Representative TEM micrographs for A) 7nm, B) 14nm and C) 21nm silica respectively with 0.3g/l UCARE™ JR 125 as the polymer binding layer. Magnification:
A = 60,000x
B= 105,000x
C= 20,500x

### 2.4.3 TEM analysis of the nanoparticle coated surfaces using a one step coating process

Method One:

a) High shear homogeniser:

TEM images of the nanoparticle coated grids produced, when 14nm silica particles were mixed with the UCARE™ polymer JR-125, were difficult to achieve. Many areas of the surface were too thick to allow penetration of the electron beam (Figure 2.11).

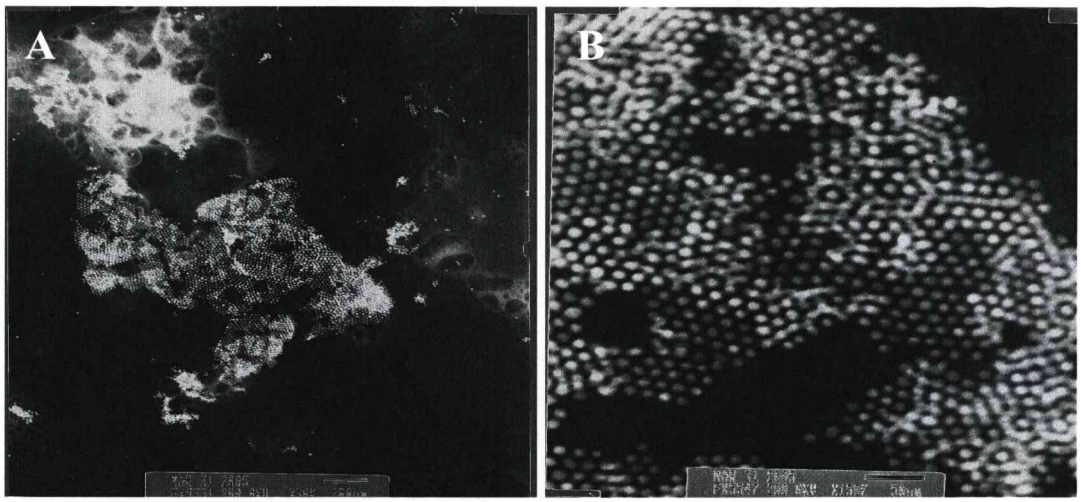


**Figure 2.11** Representative TEM micrograph of 14nm silica particles coated with 0.3g/l UCARE polymer Jr-125 using a high shear homogeniser
A= 30,000x
B= 150,000x

This is highlighted in Figure 2.11a, at the lower magnification. However, when the magnification of the central area of the surface was increased to 150,000x (figure 2.11b), it was possible to identify discrete particles of roughly 14nm in diameter that were periodically spaced, forming an ordered honeycomb-like structure on the surface. This ordered surface patterning was not observed on any of the surfaces coated using the two step process.

b) Ultrasonic probe mixing

The ultrasonic probe mixing was used to disrupt the aggregates that formed when the high shear homogeniser was used. It was demonstrated that the ultrasonic probe was successful at reducing the clumping of the particles (Figure 2.12). However, only discrete patches of nanoparticles were observed attached to the surface and, within the patches, the particles were closely associated, unlike the even spacing observed in Figure 2.11.

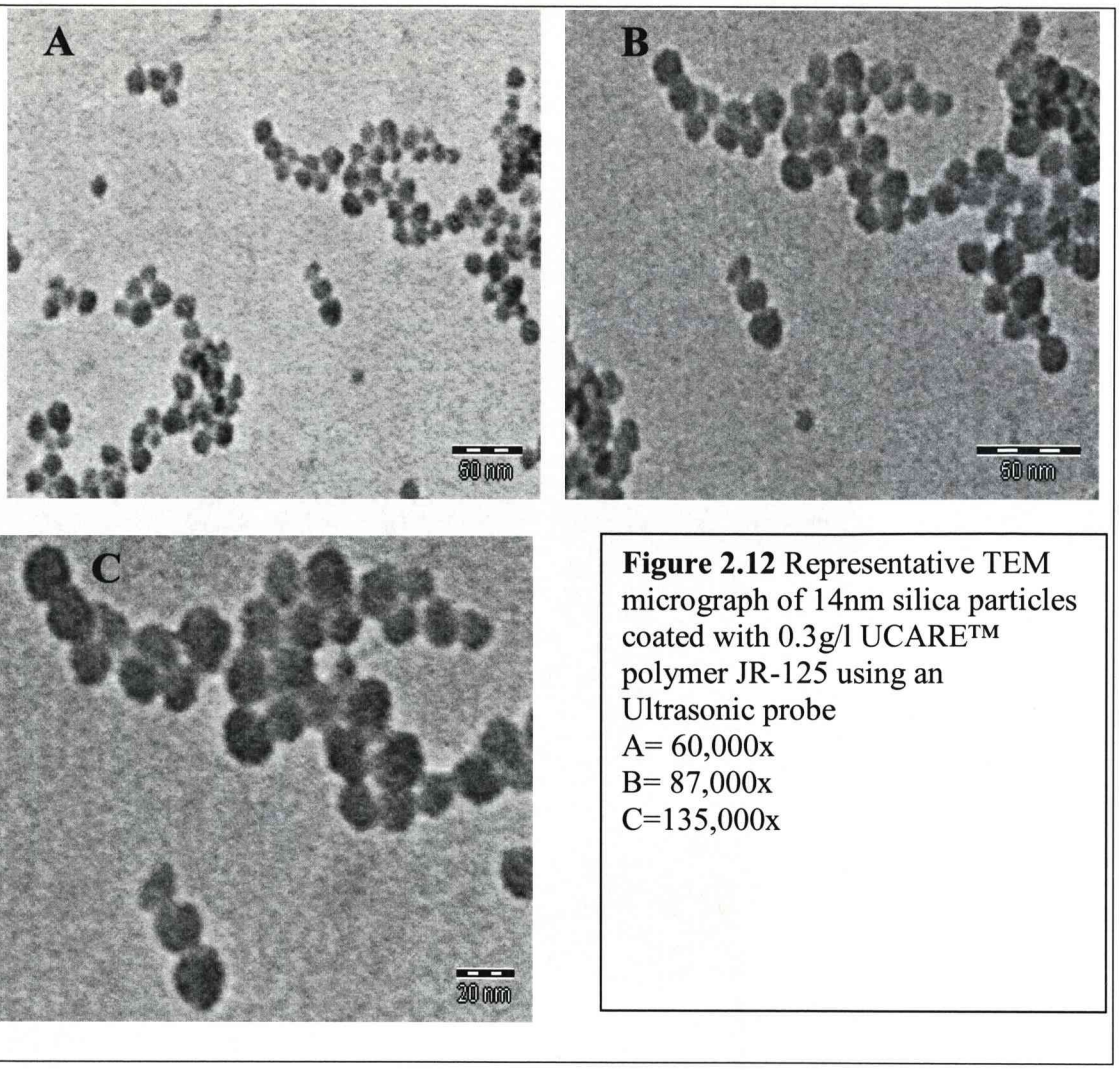


**Figure 2.12** Representative TEM micrograph of 14nm silica particles coated with 0.3g/l UCARE™ polymer JR-125 using an Ultrasonic probe
A= 60,000x
B= 87,000x
C=135,000x

Method 2:

a) Ludox® CL™:

Ludox® CL™ consists of silica nanoparticles, chemically modified with an alumina coating such that the particles have a positive surface charge. TEM analysis (Figure 2.13) showed that, although a nanoparticulate coating was observed on the grid, there were cracks present in the layer. When the magnification was increased to 160,000x (figure 2.13c), it was possible to identify discrete nanoparticles bound to the surface in small clusters with spacing between the particle clusters, which may be due to interparticle repulsion.

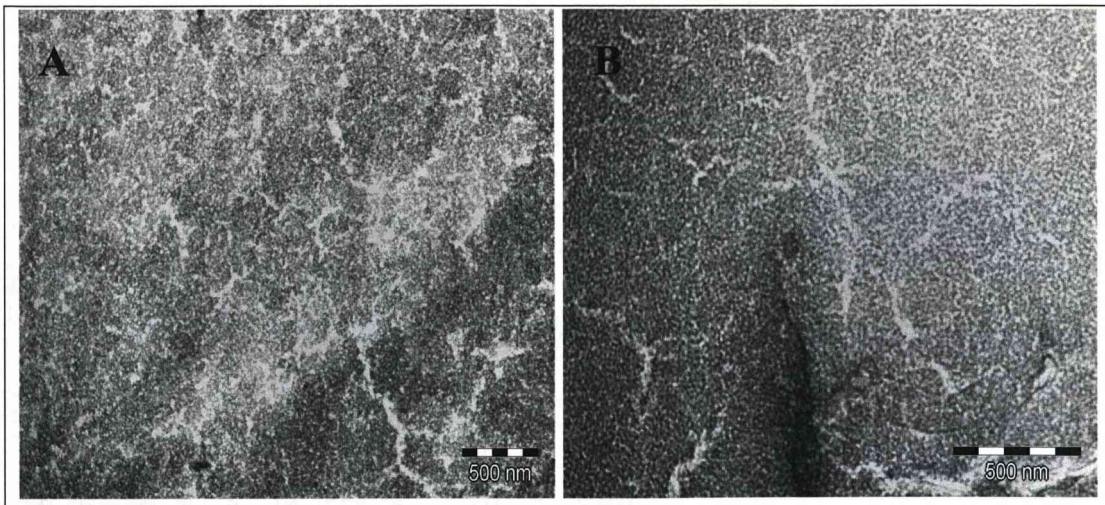


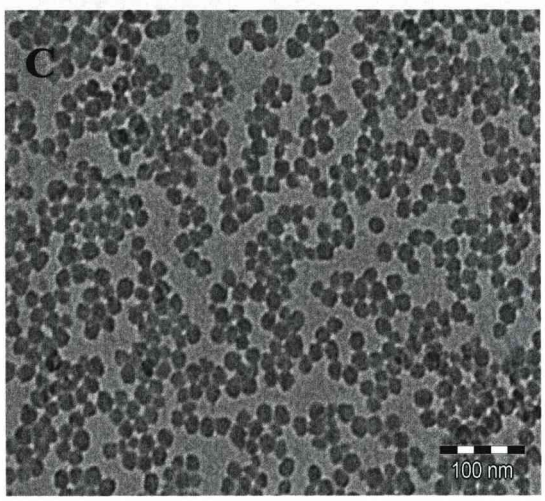


**Figure 2.13** Representative TEM micrograph of Ludox® CL™ attached directly to the grid
A= 26,500x
B= 43,000x
C= 160,000x

b) Percoll™:

In this instance, the silica nanoparticles had been commercially coated in polyvinylpyrrolidine (PVP). TEM analysis demonstrated that these particles only adhered to the surface in a few patches and, within these areas, the coating did not attach uniformly to the surface (Figure 2.14).

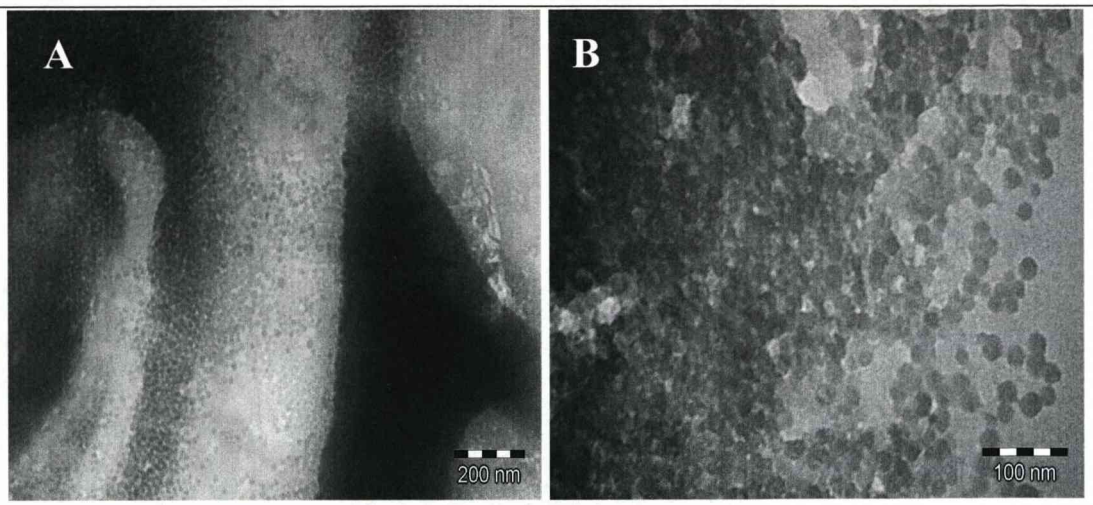


**Figure 2.14** Representative TEM micrograph of Percoll$^{TM}$ attached directly to the grid
A= 60,000x B= 160,000x

## 2.5 Discussion

The surface analysis of a coating with particles in the size range of less than 100nm poses some practical problems. The purpose of using the TEM, as opposed to other surface analysis techniques, was that it would provide information on the density of the coating on the test substrates, as well as surface arrangement of the nanoparticles. The TEM proved very useful in this respect, as it identified variations in the surface densities and arrangements of the different coatings.

To identify conclusively that a polymer binding layer was required, the adsorption of the nanoparticles in its absence was assessed. As hypothesised, in the absence of a polymer binding layer, there were very few nanoparticles present on the surface, most likely due to the repulsion of the negatively charged silica nanoparticles from the negatively charged surface. The larger size particles demonstrated some increased binding to the surface compared to the smallest (7nm) particles. This could be linked to the increased ability of larger particle to form van der Waals attractions with the surface.

In physical adsorption ( physisorption), an adsorbed molecule is bound to the surface via a weak van der Waals attraction (Prutton 1998). This involves no charge transfer from the substrate to the adatom (atom to be adsorbed onto the surface) or vice versa. Rather the attraction is formed by the instantaneous dipole moments between the adatom and its neighbour (Prutton 1998). This is based on the assumption that the distribution of electronic charge around an atom changes with time. At any instant, the charge distribution is not perfectly symmetrical. If a second atom is in close proximity (3 to 4 Å apart), the position of the electronic charge in the second atom will be correlated to that in the first atom. The presence of these instantaneous dipoles in the two atoms is such that attraction ensues. (Napper 1970; Stryer 1999). As demonstrated in Figure 2.15, even if the electronic charge in the first atom moves to a new position, the second atom's charge will also move so the polarity of the instantaneous dipoles is reversed and attraction still occurs (Napper 1970).

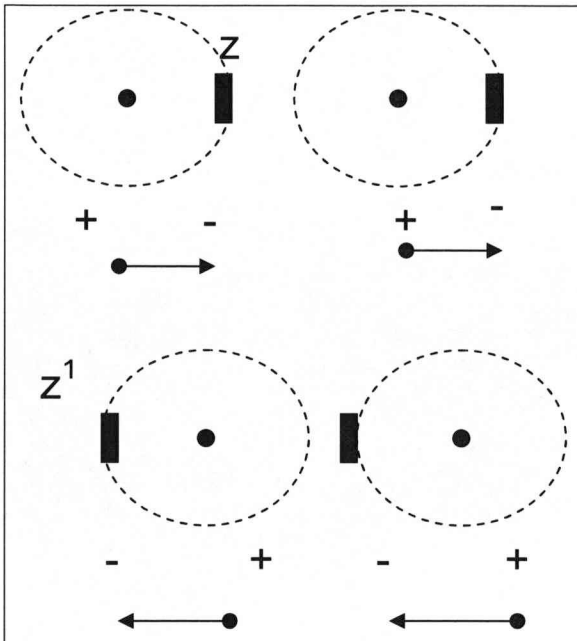


**Figure 2.15** Schematic representation of origin of dispersion forces. Z is the area of electron charge. $Z^1$ is if the electron charge moves to a new position. This diagram was adapted from (Napper 1970)

In colloidal particles, the attractive forces created due to these momentary dipoles is increased because every atom or molecule in one colloidal particle attracts every atom or molecule in another. Therefore, in colloidal particles, the attractive forces due to van der Waals interactions are increased and, depending on the size of the particle, can have a relatively long range effect. This could explain why, when the larger size nanoparticles were used, there was a slight increase in adsorption to the surface. The fact the particles adsorb in clusters may be due to the fact that the particles are stabilised from desorption from the surface in clusters. An individually bound particle has only one interaction with the surface so it could be easily desorbed from the surface. However, when particles adhere in a cluster, there are several interactions involved, not only between each particle and the surface, but also due to the combined effect of bonding between the particles neighbours. Thus the energy required for desorption from the surface increases.

In previous studies, a cationic polymer was used to alter the surface charge and increase adsorption of the nanoparticles. The polymer used in these studies was the 80% cationic polymer Zetag™ 7689 (Cousins, Doherty et al. 2004). It was used at a concentration of 3.2g/l. These data formed the basis of starting with this concentration and polymer. It was witnessed that the use of this polymer resulted in an effective coating of nanoparticles across the test surface. However, the coating

appeared uneven when viewed with the TEM. The TEM identified areas of variation in the density of the coating, relating to large dark areas on the surface and some areas of little or no coverage (figure 2.5).

To investigate the effect of the underlying polymer on the nanoparticulate coating a second polymer was used. The Zetag™ 7109 polymer is 100% cationic and has a lower molecular weight in the region of $10^6$ Da, $10^2$ Da less than Zetag™ 7689. When this polymer was used at the same concentration (3.2g/l) there was a decrease in the variability of the density of the surface coating. There were very few areas of increased density and no areas without nanoparticles adhered. This could lead to the hypothesis that the polymer layer is adhering in clumps on the surface when the larger molecular weight Zetag™ 7689 polymer was used. When the lower molecular weight Zetag™ 7109 polymer was used, the polymer may adopt a flatter configuration on the surface. This could be due to the ability of the polymer to uncoil in solution. If the polymer is unable to fully uncoil in solution, the coiled polymer chain adheres to the surface, rather than a flat uncoiled chain. The benefit of having a fully uncoiled polymer chain adhered to the surface is that, theoretically, there will be more positions available for the adhesion of the nanoparticles to the surface. As a result a more uniform and closely packed coating should be obtained. There will also be a flatter polymer layer to which the particles may adhere, minimising the possibility of the creation of micron scale, topographical features. This may be potentially advantageous when assessing the cellular response to the nanoparticles, as the scale of the surface topography will be constant.

A polymeric solution can be thought of as consisting of two parts, a suitable solvent and the polymeric molecules (Young 1981). The properties of solution depends on both the size of the polymer chain and the interactions between the polymer chain and the solvent molecule (Young 1981). If an appropriate solvent molecule is selected, there is an affinity between the two types of molecule and the polymer coil is expanded. However, if an inappropriate solute has been selected, there is less affinity between the polymer and the solute molecules and the polymer is more tightly coiled. (Young 1981) This is true of dilute polymeric solutions.

There are two factors that could affect the coiling of a polymer in solution: concentration and charge. In concentrated solutions, it may not be possible for the polymer to fully uncoil. Theoretically, each linear polymer chain will occupy a space e.g a sphere (Teraoka 2002). At low concentration, these spheres are separated from each other, but, as the concentration increases, they become congested and eventually touch one another (figure 2.16). At the overlap concentration (C*), the solution is packed with these spheres.

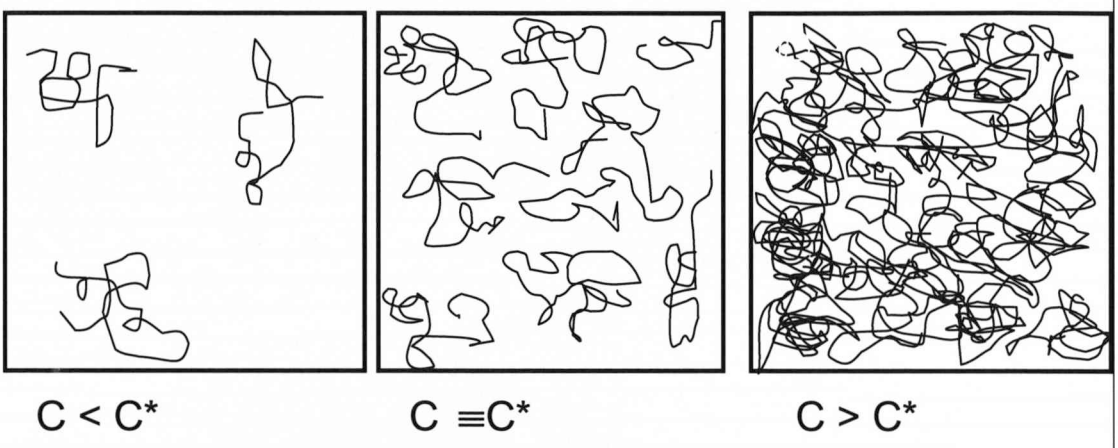


**Figure 2.16** concentration regimes for solutions of linear flexible polymers:
dilute solution C < C*
Solution at the overlap concentration C ≡C*
Semi-dilute solution C > C*
Adapted from (Teraoka 2002)

When C is below C*, as in a dilute mixture, the polymer chains are separated from each other and are free to uncoil. However, when the concentration is above C*, it is a concentrated regime and the polymer chains overlap and become entangled. It is under these conditions that the chains are unable to fully uncoil. This could explain why the use of a lower molecular weight polymer (Zetag™ 7109) at the same concentration resulted in fewer inconsistencies with the surface density of the coating. As fully uncoiled chains should provide more positions for binding nanoparticles, the increased molecular weight of the Zetag™ 7689 polymer at this concentration may have meant it was unable to uncoil and therefore bound to the surface in a coiled configuration masking some of the nanoparticulate binding positions.

The other factor that could prevent the polymer chain from fully uncoiling would be its charge. The Zetag™ 7989 polymer is 80% cationic, whereas the Zetag™ 7109 is 100% cationic. With an 80% cationic polymer chain, there will be more opportunities for coiling. However, with a 100% cationic polymer chain, there would be less coiling, due to charge repulsion within each polymer chain. Therefore, the Zetag™ 7109 polymer chain would be less likely to coil than Zetag™ 7689.

The increased density of the coating observed when Zetag™ 7689 was used, could be due to the combined effect of a concentration that is not conducive to uncoiling and the decreased % charge compared to the lower molecular weight 100% cationic Zetag™ 7109 polymer. Both could minimise the uncoiling and result in an uneven coating of the polymer. To maximise the opportunity for the polymer to uncoil, the concentration was reduced 10 fold. At the lower concentration of 0.3g/l, there were minimal areas of increased density and, unlike at the higher concentration, there were no areas on the grid that were uncoated with nanoparticles. It could be hypothesised that lowering the concentration allowed the polymer to uncoil more effectively. Therefore, the polymer is adhered to the surface in a flatter manner, creating a more uniform surface, on which the nanoparticles adhered (figure 2.17). When the concentration of the lower molecular weight polymer (Zetag™ 7109) was also reduced 10-fold, a continuous coating of nanoparticles was created.

A third polymer, UCARE™ polymer JR-125, was also assessed at the two concentrations. UCARE™ polymers are often used in hair care products, particularly in conditioning treatments mainly due to the fact that the polymer adheres to the coating surface smoothly. This is an ideal property for the polymer layer in the nanoparticulate coating.

The UCARE™ polymer JR-125 was demonstrated to be an excellent polymer for this coating process. At both the highest (3.2g/l) and lowest (0.3g/l) concentrations (figures 2.9 and 2.10) it was seen that continuous uniform coatings were produced. There was close random packing of the particles on the surface and minimal areas of density variation.

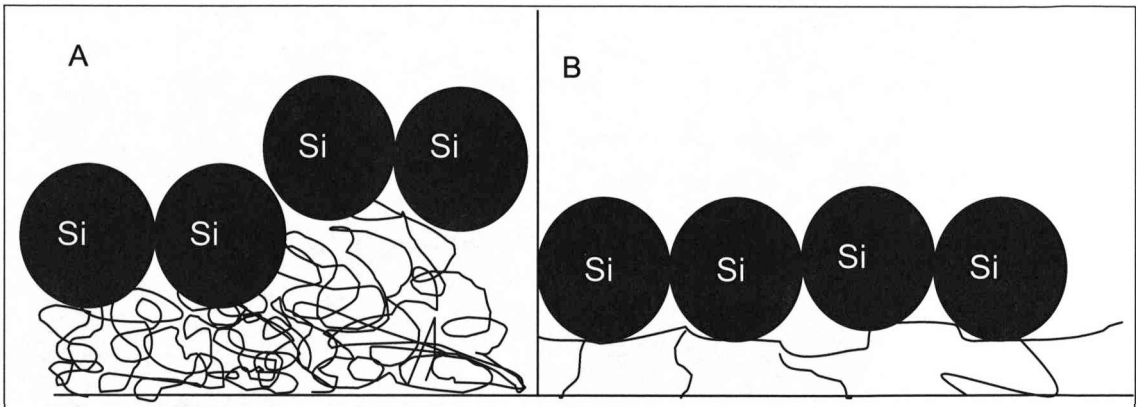


**Figure 2.17.** Schematic representation of the polymer layer beneath a silica nanoparticulate layer.
A: higher concentration high molecular weight polymer prevents uncoiling thus the polymer from uncoiling and adheres to the surface in clumps.
B: using either the lower molecular weight polymer or lowering the concentration of the high molecular weight polymer increases the opportunity for uncoiling in solution so the polymer adheres to the surface in a flat uncoiled manner creating an even surface for the particles to attach.

With these results in mind, it would be interesting to see if there is a minimum concentration of polymer for coating the surfaces. Identifying a minimum and even a maximum concentration could allow for creation of an optimally covered surface, with all the polymer chains associating closely and smoothly with the surface. This would result in a surface coating of minimal thickness, which could be advantageous in some clinical settings where a thinner coating layer, even by a few nanometres, may be advantageous. One example of this is a coating on an intravenous catheter, where the diameter of the lumen needs to be maintained, despite the presence of a coating.

When identifying a commercial product, ease of use is paramount to a product's success. A one step application process would result in a more commercially viable product. The possibility of directly altering the surface charge of the silica nanoparticles was, therefore, investigated so that there would no longer be a requirement for a polymer binding layer and the nanoparticles could adhere directly to the surface. Two commercially available silica containing products were identified. These are Percoll™ and Ludox® CL. Both these nanoparticulate silica containing products have had their surface charge altered to render them positive.

Therefore both of these products should theoretically coat a surface without the requirement of a polymer binding layer.

In the case of Percoll™, there was minimal coating of the test substrate. There were some areas of the grid that were coated in clusters of nanoparticles and large areas of sparse coating, this level of coating was far from satisfactory. The lack of coating when Percoll™ was used, could be due to high amounts of free PVP in the solution. Percoll™ is a silica containing sol, in which the silica particles have been commercially coated in PVP. If, however, there was an excess of PVP in the solution, which preferentially bound to the test surface, the PVP coated silica particles would be repelled from the surface due to steric repulsion.

The other product investigated was Ludox® CL, where the silica nanoparticles are rendered positive as a result of an alumina coat. In this instance, the particles were able to adhere to the surface in a continuous and relatively uniform manner. Unlike on the two-step coated surfaces, Ludox® CL resulted in defined spacing of the particles on the surface (figure 2.13C). This could be due to interparticle repulsion. However, despite the continuously coated surface, this coating dried very quickly. When a glass coverslip was coated in Ludox® CL, the coating dried out so quickly that crystalline like flakes could be seen by eye on the surface. These were easily removed by touch. Therefore, Ludox ® CL coating was far from ideal.

The second possible method was to individually coat the silica nanoparticles in a poly cationic polymer, rendering them positive and able to adhere directly to substrate. The lowest molecular weight polymer UCARE™ polymer JR-125 was selected for use, with the 14nm diameter silica nanoparticles. Non-ionic polymers adsorb particularly well at an adsorption level of $1mg{\cdot}m^2$. Based on this, a 10 fold reduced estimation of adsorption level of $0.1mg{\cdot}m^2$ was selected, in order to minimize the possibility of free unbound polymer in solution. This would minimize the possibility of competitive binding between the free polymer and the polymer coated nanoparticle that was seen with Percoll™. Combining the estimated level of adsorption of $0.1mg{\cdot}m^2$ and a supplied surface area of Ludox® HS-40 (14nm) particles of $240m^2g^{-1}$ , a polymer to nanoparticulate silica ratio of 0.3 : 10 was used (Garvey 2004).

To obtain a coating of polymer on each silica particle, a high shear mixer was required. When used to coat a TEM grid, it was clear the surface coating was very dense, with large areas of the surface too dense to image. However, there was a small area of monolayer coating, where individual nanoparticles with a hexagonal close packing arrangement could be seen (figure 2.11). Unlike on the two step UCARE™ polymer JR-125 (0.3g/l) and Ludox® HS-40 coated grids (figure2.10B), there was defined spacing between the particles. This would indicate that these particles have been coated in the polymer and are now sterically stabilised.

Steric stabilisation of the nanoparticles could lead to the periodic and uniform separation of the nanoparticles on the surface. When the adsorbed layers of two particles interpenetrate, there will be a local increase in the concentration of polymer segments, which could lead to repulsion (Shaw 1992). This is best explained thermodynamically, using Gibbs Free energy ($\Delta G_R$). $\Delta G_R$ may assume values which are zero, positive or negative. Flocculation will occur if the $\Delta G_R$ is negative or zero. However, if $\Delta G_R$ is positive, stabilisation can occur (Napper 1970). Steric stabilisation can be the result of a positive enthalpy ($\Delta H_R$) and/or a negative entropy ($\Delta S_R$) (Napper 1970; Shaw 1992). A positive $\Delta H_R$ would relate to the release of bound solvent from the polymer chains as they interpenetrate and a negative $\Delta S_R$ would reflect loss of configurational freedom as the polymer chains interpenetrate (Shaw 1992). In both cases, this would result in an increase in free energy and stability will be enhanced by an elastic repulsion effect.

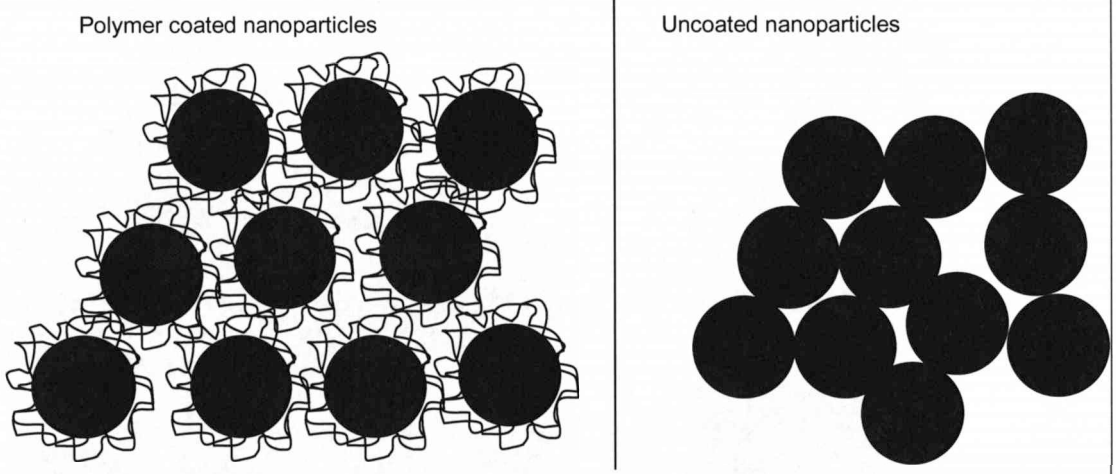


**Figure 2.18.** Schematic representation of how the presence of a polymer layer can alter the packing arrangement of nanoparticles on a surface. On the uncoated sample, the particles can make intimate contacts with each other. However, on the polymer coated nanoparticles, the particles are unable to form close contacts, due to interpenetration of the polymer layer leading to steric stabilisation.

This could explain the highly ordered surface coating observed, when a high shear mixer was used (figure 2.11). Due to the steric stabilisation of the nanoparticles, the polymer coatings surrounding them are unable to inter penetrate, leading to the highly ordered and uniformly spaced conformation seen, which was absent when the two step coating procedure was employed (figure 2.18).

However, the addition of a polymer to a solution of nanoparticles can also result in aggregation / flocculation. Flocculation may occur by two different mechanisms:

1. Particle bridging: where the polymer bridges more than one particle, which would lead to flocc formation,(Napper 1970).
2. Charge neutralisation: where polymer adsorption onto a particle surface can decrease interparticle electrostatic repulsion, inducing coagulation (Coradin and Lopez 2003).

The large dense areas of coverage witnessed were probably due to the aggregation of the nanoparticles during mixing. In an attempt to prevent any aggregates forming during mixing, an ultra sonic probe was used instead of a high shear mixer.

Sonication of the mixing polymer and nanoparticles could break up any aggregates and minimise aggregate formation at this stage. By minimising aggregate formation,

it was hoped that the resulting coating would be comprised of individually coated nanoparticles and the large dense areas observed when the high shear mixer was used, would be prevented. However, as evident in figure 2.12, the particles still adhered to the surface in aggregates. There were now some areas of no coverage, so this system will need to be modified further.

The creation of a one step coating process is of great benefit to the commercial viability of the project and would also be of great interest. If more time was available, it would have been of interest to look at this in more detail, possibly altering the polymer, as well as assessing different concentration ratios of polymer to particles. It would also have been interesting to identify alternative mixing techniques that would minimise aggregate formation but not be so overly aggressive as to modify the polymer in solution. This may be what was happening, when the sonic probe was used. As sonication is often used to lyse cells, it is possible that the use of the sonic probe is altering and breaking the polymer chain, which is leading to the intermittent coating and aggregate formation.

The TEM allowed analysis of the pre-coated surfaces. It would be of great interest and benefit to be able to monitor the coating process in situ. Therefore the next stage of the study was to investigate the in-situ monitoring of the creation of the nanoparticulate coatings on several surfaces.

# Chapter 3

## In-situ monitoring of the production of nanoparticulate silica coatings with a Quartz Crystal Microbalance with dissipation monitoring.

*This chapter explains the procedure for creating nanoparticulate silica coatings so that they can be monitored in situ with QCM-D. The coatings were created on three different surfaces; gold, hydroxyapatite (HA) and human dentine adhered to a gold crystal. In this study the use of different molecular weight and concentrations of binding polymers was investigated. The longevity of the coatings under flow condition was also investigated with the use of a peristaltic pump. The effect of a continuous flow of artificial saliva was used to assess the films under physiologically relevant conditions. The QCM-D was used to monitor coating production and stability by using the fluctuations in frequency as an indication of mass on the surface.*

### 3.1 Introduction

The QCM can be thought of as an ultra sensitive weighing device. It consists of a thin disk of single crystal quartz, with metal electrodes deposited on each side of the disk. By applying an alternating electric field across the quartz through metal electrodes, a mechanical oscillation of characteristic frequency $f$ is produced in the crystal (Marx 2003). Binding of a substance onto the resonating quartz surface causes this oscillating frequency to decrease (Rodahl, Hook et al. 1995; Marx 2003).

The frequency shift ($\Delta f$) has been shown to be related to the mass change using the Sauerbrey equation (eq.1):

$$\Delta f = \frac{-2 f_0^2 \Delta m}{A \sqrt{\rho_q \mu_q}}$$

$f_0$ = the fundamental resonant frequency of the crystal

A = the piezoelectrically active area defined by the electrode

$\rho_q$ = the density of the quartz ($2.648 gcm^{-3}$)

$\mu_q$ = the shear modulus ($2.47 \times 10^{11}$ $dyncm^{-2}$) (Atashbar, Bejcek et al. 2005)

(Equation 1.)

Using equation 1 it is possible to quantify precisely with nanogram (ng) sensitivity the quantity of elastic mass added to the surface (Marx 2003). The Sauerbrey equation is derived from uniform ultra thin films with material properties indistinguishable from those of quartz (Chitpan, Wang et al. 2007). Consequently, the Sauerbrey equation can only calculate the surface bound mass from the $\Delta f$ when the mass is evenly distributed, does not slip on the sensor surface and is sufficiently rigid and/or thin to have negligible internal friction (Berglin, Olsson et al. 2008). The interaction of the piezoelectric sensor with a viscoelastic film (such as protein) that does not satisfy the above criteria causes dampening of $f$ (Fogel, Mashazi et al. 2007). This is because the film does not fully couple to the oscillation of the quartz crystal (Chitpan, Wang et al. 2007). This can result in an over estimation of the mass of the attached layer using the Sauerbrey equation (Fogel, Mashazi et al. 2007).

In dissipation measurements, the decay time ($r$) of the sensor crystal is measured and is used to calculate the dissipation ($d$) (dimensionless units $x10^{-6}$) (Berglin, Olsson et al. 2008). $d$ provides data regarding the viscoelasticity of the attached layer and gives information about the strength of attachment and the structure of the adlayer (Fogel, Mashazi et al. 2007). A rigid bound layer will have an increased decay time and consequently, low dissipation. Vice versa addition of a viscoelastic material will result in fast dampening of the sensor crystal i.e. a short decay time and therefore a higher dissipation (Berglin, Olsson et al. 2008). Simultaneously measuring $d$ while measuring $f$ at multiple frequencies, as with the Q-Sense QCM-D used in this study, combined with a viscoelastic model (The Voight model) it is possible to make more accurate assumptions of thickness, viscoelasticity, and elasticity even for soft films (Voinova, Rodahl et al. 1999). However, several assumptions still have to be made (Chitpan, Wang et al. 2007).

The use of the QCM has become widespread and varied in recent years. The technique was traditionally used in vacuum deposition systems but is now commonly used out of vacuum in an abundance of different areas including surface adsorption studies, cell attachment, etching studies and many more. In this study the QCM-D was used to monitor nanoparticulate film formation and the decrease and/ or increase in $f$ is used as

an indication of mass on the surface. However, it is not used to calculate the mass as many of the assumptions that have to be made using the viscoelastic model require that the surface be continuous and when making thickness measurements assumes a uniform layer. In this instance the coating although continuous is comprised of spheres and the voight model would ignore the nanoscale variations in the surface topography resulting in discrepancies. Therefore to minimize the number of assumptions required and prevent over-analysis, $\Delta f$ is used to indicate mass while the $\Delta d$ can be used to indicate alterations to the viscosity of the coatings.

### 3.2 Materials

Gold coated (QSX301) and Hydroxyapatite coated TiOx (QSX327) quartz crystals were purchased from Scientific and Medical Products, and were used as received. Selected gold crystals were modified by adhesion of a bovine dentine disc using XP BOND™ (Dentsply donated by Dr N. Martin at Sheffield University).

Two polymers; Zetag™ 7109 (Ciba Scientific) and UCARE™ polymer JR 125 were used, to create coatings with a variety of Ludox® silica sols with average particle size 7,14, and 21nm (section 2.2).

### 3.3 Methods

#### 3.3.1 Creating the Dentine adhered Crystals.

As discussed in section 3.2, three different surfaces were investigated using QCM-D. Two were used as received ( gold and HA coated), the third was created using a dentine slice bound to a gold coated quartz crystal purchased from Scientific and Medical Products. The dentine was taken from bovine teeth donated by GlaxoSmithKline, Weybridge.

1. Dentine discs were prepared by sectioning the bovine teeth in a plane longitudinal to the long axis of the tooth between the enamel dentinal junction and the pulp. A slow speed saw (Isomet, Buehler, UK) with a diamond edged wafering blade (Buehler LT 11-44254, Buehler, UK.) was used to create dentine sections that were 0.5mm thick.
2. The dentine discs were polished using 4,000 grit silicon carbide paper, so that they were 0.01mm thick and had a diameter of roughly 2.6mm.
3. The discs were sonicated in $dH_2O$ for 5 minutes to remove any wear debris from polishing.
4. Conditioner 36 (Dentsply) was added to the dentine surface to be adhered to the gold crystal.
5. After 30 seconds the disc was rinsed in copious amounts of $dH_2O$.
6. Excess $dH_2O$ was removed by blotting with tissue

7. XP BOND™ (Dentsply) and Dentsply self cure activator (Dentsply) was dispensed in equal amounts into a small clix dish (supplied by Dentsply in the XP BOND™ kit).
8. Using an applicator the XP bond and self cure activator were mixed
9. Using the applicator brush the XP bond and self cure activator mix was applied to the conditioned dentine surface and left for 20 seconds.
10. The coated dentine surface was placed on a clean unused gold coated QCM crystals upper surface.
11. The sample was left for 1 minute.
12. The sample was light cured using a UV light curer for 20 seconds.
13. The sample was stored at room temperature within a desicator for 7 days prior to use.

### 3.3.2 QCM-D set- up

A QCM-D D300 (Q-sense AB, Sweden) was run at 19°C ± 0.1°C. The QCM-D takes measurements of frequency (*f*) and dissipation (*d*) at three different overtures, 14, 24 and 34 MHz. The QCM-D was setup following the user guide instructions. For the three different crystals (HA, gold and gold with dentine adhered) the frequency (*f*) and dissipation (*d*) readings were taken and automatically fitted.

### 3.3.3 Static Experiments

For the static experiments the QCM-D was set up with a simple reservoir system (figure 3.1).

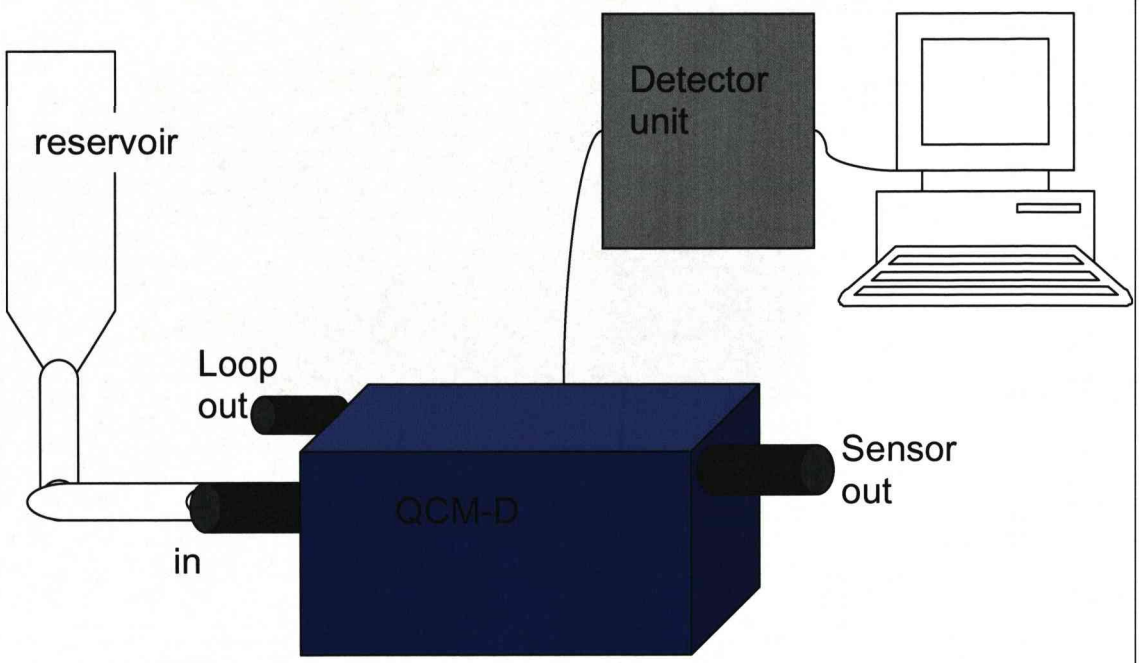


**Figure 3.1**Schematic drawing of the QCM-D Set up for static experiments. When the reservoir is run to loop the sensor remains unaffected. Running the reservoir to the sensor will result in a spike on the *f* and *d* readings in relation to the flow of liquid across the crystal surface.

The QCM-D set up in this manner was used to investigate the requirement for a polymer coating prior to addition of the nanoparticulates and the effect of altering the polymer layer through variation of the molecular weight and concentration of the polymer used. The two methods used to study this are described below

**Method 1**

Nanoparticulate coating in the absence of a polymer binding layer

1. 5ml of NaOH $10^{-5}$ M was added to the reservoir.
2. 1ml of NaOH was run to loop.
3. 80$\mu$l NaOH was run to the cell (a wash)
4. Step 3 was repeated until it was possible to wash the surface with NaOH resulting in a spike in the *f* and *d* readings but both then return to the same pre wash levels. Once achieved the excess NaOH was removed from the reservoir.

5. 450$\mu$l of Ludox® silica sol (diluted to 4% w/v with NaOH $10^{-5}$M) was added to the reservoir and run to loop.
6. 350$\mu$l was added to the reservoir and run to loop
7. A further 350$\mu$l was added to the reservoir and was run to the cell.
8. 5ml of NaOH $10^{-5}$M was added to the reservoir.
9. While the frequency and dissipation stabilized 2ml of NaOH was run to loop.
10. The cell was then washed by running 80$\mu$l of NaOH to the cell.
11. The *f* and *d* was allowed to settle
12. Steps 10 and 11 were repeated until a NaOH wash could be achieved whereby the *f* and *d* readings spike but would then return to the same pre wash level.

a) Influence of silica sols:
   Three different silica sols were used in step 5: Ludox® SM-30 (7nm particle diameter), Ludox® HS-40 (14nm particle diameter), and Ludox® TM-50 (21nm particle diameter)
b) Influence of QCM-D crystal surface:
   Three different surfaces were tested gold, HA and dentine adhered to a gold crystal the coatings tested on each surface are listed in table 3.1.

**Method 2**

Polymer and Nanoparticle coatings

1. 5ml of NaOH $10^{-5}$M was added to the reservoir.
2. 1ml of NaOH was run to loop.
3. 80$\mu$l of NaOH was run to the sensor (a wash).
4. Step 3 was repeated until it was possible to wash the surface with NaOH and resulting in a spike in the *f* and *d* readings but both returning to the same pre wash level. Once achieved the excess NaOH was removed from the reservoir.
5. 450$\mu$l of polymer solution was added to the reservoir and run to loop.
6. 350$\mu$l of NaOH $10^{-5}$M was added to the reservoir and run to lop

7. A further 350$\mu$l of NaOH $10^{-5}$M was added to the reservoir and run to the sensor.
8. 5ml of $10^{-5}$M NaOH was added to the reservoir.
9. While the *f* and *d* readings stabilized 2ml of NaOH was run to loop.
10. Once *f* and *d* had stabilized the surface was washed by running 80$\mu$l of NaOH to the sensor.
11. The *f* and *d* reading were allowed to settle.
12. Steps 10 and 11 were repeated until NaOH could be washed across the surface with the *f* and *d* readings spiking but then returning to the same pre-wash levels.
13. Any excess NaOH was then removed from the reservoir
14. 450$\mu$l of Ludox® silica sol (diluted to 4%w/v with NaOH $10^{-5}$M) was then added to the reservoir and run to loop.
15. 350$\mu$l of NaOH $10^{-5}$M was added to the reservoir and run to loop.
16. A further 350$\mu$l of NaOH $10^{-5}$M was added to the reservoir and run to the sensor.
17. 5ml of NaOH $10^{-5}$M was added to the reservoir.
18. While the *f* and *d* readings stabilized 2ml of NaOH was run to the loop.
19. Once *f* and *d* were stable The sensor surface was washed by running 80$\mu$l of NaOH to the sensor.
20. The *f* and *d* were then allowed to stabilize.
21. Steps 19 and 20 were repeated until NaOH could be washed across the surface with *f* and *d* spiking then returning to the same pre- wash levels.

a) Influence of different polymer chemistry:
   The polymer solution in step 5 was either Zetag™ 7109 or UCARE™ polymer JR-125.
b) Influence of polymer concentration:
   The polymer solutions in step 5 were made up to two different concentrations of 0.3g/l and 0.03g/l to evaluate if the concentration of the polymer can affect the adherence of the nanoparticles.
c) Influence of silica sols:

Three different silica sols were used in step 14: Ludox® SM-30 (7nm particle diameter), Ludox® HS-40 (14nm particle diameter), and Ludox® TM-50 (21nm particle diameter).

d) Influence of QCM-D crystal surface:

Two different surface were used gold and HA (The different coatings tested on each surface are listed in table 3.1).

| **Silica** / **Surface and Polymer** | Ludox® SM (7nm) | Ludox® HS-40 (14nm) | Ludox® (21nm) |
|---|---|---|---|
| **Gold** no polymer | • | • | • |
| **Gold** then Zetag™ 7109 0.3g/l | • | • | • |
| **Gold** then Zetag™ 7109 0.03g/l | • | • | • |
| **Gold** then JR-125 0.3g/l | • | • | • |
| **Gold** then JR-125 0.03g/l | • | • | • |
| **HA** no polymer | | | • |
| **HA** then Zetag™ 7109 0.03g/l | | | • |
| **Dentine** no polymer | | | • |

**Table 3.1** Table of different coatings and surface investigated using the static method of QCM-D. A • indicated that the combination of silica and surface were investigated.

When the dentine surfaces were tested the samples were left overnight after addition of the silica sol and washing of the surface. This was to assess the stability of the surface. The following morning the surface was washed, prior to an excess of silica being added to the surface followed again by washing steps. In all other cases the experiments were stopped once a stable non fluctuating $f$ and $d$ had been achieved.

### 3.3.4 Flow Experiments.

To assess the longevity of the coatings in a flow system as well as the effect of artificial saliva on the nanoparticulate coatings a second setup for the QCM-D was devised (figure 3.2). The addition of a tap allowed easy conversion between a static system (as previously described) for creating the coatings to a flow system using a peristaltic pump to assess their ability to withstand fluid flow over prolonged periods of time (16 hours).

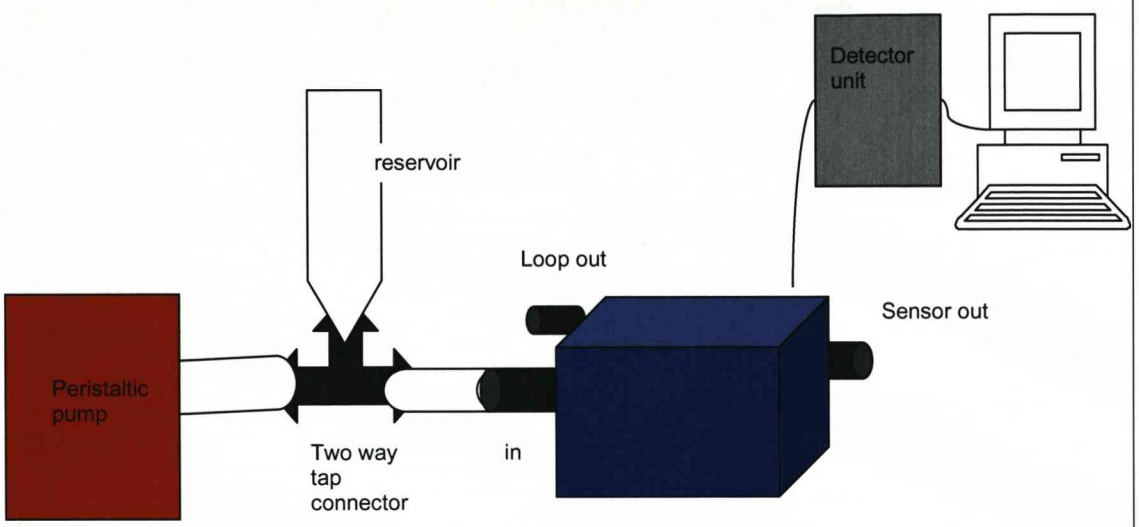


**Figure 3.2** Schematic diagram of the QCM-D setup when a flow system was required. The addition of a two tap connector between the reservoir and the QCM-D allowed the addition of a peristaltic pump that creates the flow system. This set up allowed the system to be easily altered from a static system to a flow system by just closing the valve on the tap to the static system and allowing the flow system to precede and vice versa

The creation of the coatings on the surface using a polymer to create a polymer layer is conducted in the same manner as described in method 2 for the static system. The tap is set to close for the pump and to open for the reservoir. Once the stable coating has been created following steps 1-21of method 2 for the static system, the flow system was started.

1. The tap was moved to the closed position for the reservoir, so the tap was set to open for the pump
2. The pump was set up with tubing running from a conical flask containing 300ml of the flow solution as a reservoir.
3. The pump was set to 50.2$\mu$l per minute and turned on so the solution flows to the loop.
4. After 20 minutes the flow was then diverted to the sensor.
5. The QCM-D was left with the pump running to sensor overnight.
6. After 16 hours the pump was stopped.

a) Influence of silica sols:
   Two different silica sols were used in step 14 (method 2 section 3.3.3): Ludox® (7nm particle diameter), and Ludox® TM-50 (21nm particle diameter).

b) Influence of different polymer chemistry:
   The polymer solution in step 5 (method 2 section 3.3.3) was either Zetag™ 7109 or UCARE™ polymer JR-125.

c) Influence of a continuous flow:
   Either $dH_2O$ or artificial saliva is used as the flow solution in step 2. The artificial saliva comprised of 50mM NaCl, 1.1mM $CaCl_2x2H_2O$, 0.6mM $KH_2PO_4$, 0.1% (W/V) bovine serum albumin and 0.1% (W/V) porcine stomach mucin as the flow solution in step 2.

d) Influence of the QCM-d Crystal surface:
   Two crystal surfaces were investigated: Gold and HA.

When artificial saliva was used as the flow solution after stopping the pump, the static system was used to wash the sensor surface with $dH_2O$ allowing 80$\mu$l of water to wash the surface at a time, until there were no further fluctuations in $f$ and $d$. Table 3.2 lists the different surfaces and flow systems tested in this way.

| Flow Solution. / Surface | $dH_2O$ | Artificial Saliva |
|---|---|---|
| **Gold**<br>No further coating | | • |
| **Gold** with<br>Zetag™ 7109 0.03g/l<br>And Ludox® SM ( 7nm ) | • | |
| **Gold** with<br>Zetag 7109 0.03g/l and<br>Ludox® TM-50 (21nm) | • | • |
| **Gold** with<br>JR 125 0.03g/l and<br>Ludox® TM-50 (21nm) | • | |
| **HA**<br>No further coating | | • |
| **HA** with<br>Zetag™ 7109 0.03g/l and<br>Ludox® TM-50 (21nm) | • | • |

**Table 3.2** Table of the different coatings and surfaces investigated using QCM-D with a pump to create a flow system to asses the effect of flow as well as physiologically relevant solutions on the coatings and test surfaces.

### 3.4 Results

#### 3.4.1 Static Experiments

The absence of a polymer binding layer

a) influence of silica sol

Gold surface

When the nanoparticulate silica was introduced to the gold crystal surface in the absence of a polymer binding layer the nanoparticles were washed off the surface (figure 3.3). As demonstrated with Ludox® SM (7nm) sol (figure 3.3) there was a decrease in $f$ when the particles were added (a) which was coupled with an increase in $d$. The decrease in $f$ is related to the increase in mass on the surface due to the presence of the nanoparticles. After several minutes both $f$ and $d$ stabilized at their new levels and the wash process could begin (b). With each wash there was a spike in the $f$ and $d$ readings followed by an increase in $f$ back towards the original value prior to addition of the silica sol. This is paired with the decrease in $d$ back towards the level prior to the silica sol being added. The increase in $f$ is related to the loss of mass from the surface. After just seven washes there was no further loss of mass and each subsequent wash resulted in a spike but both $f$ and $d$ returned to the same pre wash level.

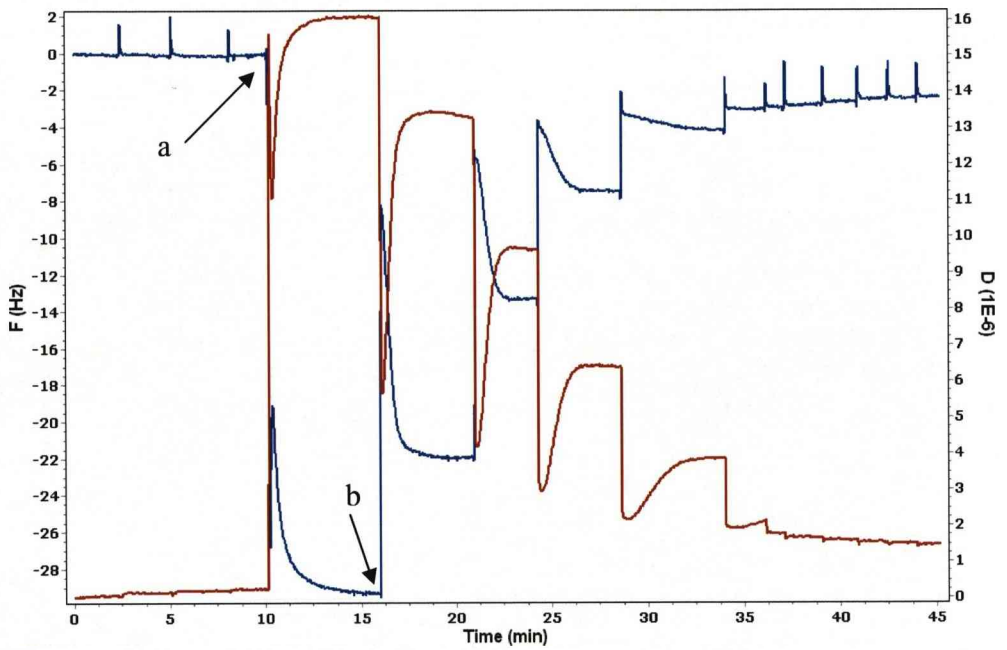


**Figure 3.3** QCM-D plot of *f* (blue line) and *d* (red line) over time
a) Addition of Ludox® SM (7nm) sol to the gold surface.
b) Begin wash steps with NaOH $10^{-5}$M

When the size of the nanoparticulate silica used was increased, the drop in *f* upon addition of the silica sol decreased (table 3.3). After washing the increase in *f* was reversed when both the Ludox® SM and HS-40 were used. There was however an increase in *f* above the starting *f* of 2.4 and 0.97 respectively, this could just be due to drift. However when the Ludox® TM-50 was used only 86% of the *f* decrease was reversed.

| Silica size | Addition of silica | | After first wash | | End point | | % $f$ increase remaining after washes |
|---|---|---|---|---|---|---|---|
| | $\Delta f$ | $\Delta d$ | $\Delta f$ | $\Delta d$ | $\Delta f$ | $\Delta d$ | |
| Ludox® SM | -29.5 | 15.9 | 7.6. | -2.7 | 31.9 | -14.6 | 0% |
| Ludox® HS-40 | -14.2 | 10.6 | 3.44 | -1 | 15.2 | -5.9 | 0% |
| Ludox® TM-50 | -8.5 | 10.5 | 3.3 | -1.2 | 7.3 | -9.7 | 14% |

**Table 3.3** Table of the $f$ and $d$ changes when the different sized silica nanoparticulate sols were added to a gold surface.

HA surface

HA coated quartz crystals are a new product used in this study because they provided a more physiologically relevant surface to study the adhesion of nanoparticulates. Figure 3.4 demonstrates the effect of addition of Ludox® TM-50 silica sol to the surface; only $f$ is shown for clarity although $d$ was also recorded.

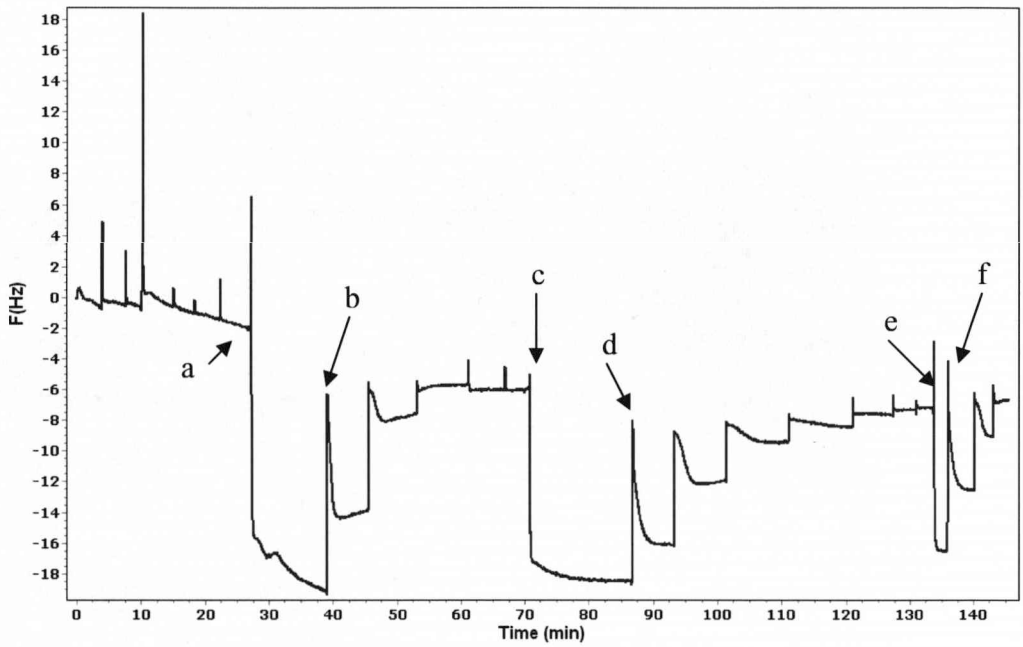


**Figure 3.4** QCM-D plot of *f* for the addition of Ludox® TM-50 (21nm) sol to a HA coated surface.

a) Addition of 4%(w/v) Ludox® TM-50 (21nm) silica sol
b) Begin washes with NaOH $10^{-5}$M
c) Addition of excess Ludox® TM-50
d) Begin washes with NaOH $10^{-5}$M
e) Addition of excess Ludox® TM-50
f) Begin washes with NaOH $10^{-5}$M

It was difficult to gain a stable *f* when the HA crystals were used, there is a *f* drift of 1.5Hz per 30 minutes. Upon addition of the silica sol there was a drop in *f* of 19Hz however after only five washes a stable *f* which was not affected by a further washing was achieved this was only 6Hz lower than the starting *f*. Upon addition of an excess of Ludox® TM-50 there was a second decrease in *f* again of 19Hz. However with washing the *f* returned to just 1 Hz lower than prior to the addition of the excess nanoparticles. The addition of excess nanoparticles was repeated a third time and again upon washing the *f* returned to the same level 7Hz below the original *f* (prior to addition of any nanoparticles to the surface).

Dentine surface

If a dentine disc of a suitable height (less than 0.1mm) was suitably adhered to a gold crystal surface it was possible to gain *f* and *d* readings. If the dentine disc was above 0.1mm in height the upper surface of the dentine disc would be in contact with the upper surface of the QCM-D cell and therefore upon application of the resonant frequency the frequency would be quickly dampened and the QCM-D would be unable to calibrate. However due to the variable nature of dentine not all samples despite being less than 0,1mm in height would enable *f* and *d* readings to be acquired therefore the following figure can only be used as a guide and further work will be needed to investigate the possibility of using dentine adhered to a gold quartz crystal to monitor adhesion of nanoparticulate silica. Addition of 21nm silica nanoparticles (Ludox® TM-50) resulted in a decrease in *f* (figure 3.5). There was also an increase in *d* (data not shown). There was a steady decrease in *f* with washing that may be due to drift as there was a 3Hz per 20 minute drift prior to addition of the silica sol. However there was no increase in *f* with washing relating to a loss of mass. Once the *f* had stabilized around -40Hz an excess of nanoparticulates were added to the surface. This resulted in a second drop in *f* of 10Hz. However this time the washing with $dH_2O$ resulted in a small increase of 3Hz before the *f* formed a reasonably stable line at -47Hz and repeated wash steps resulted in no further fluctuations in *f* or *d*.

The sample was then left overnight with the QCM-D continuing to take readings. There was a steady decline in the *f* overnight however the *d* remained stable. This was until around 700 minutes were there was a steep decline in both *f* and *d*. This decline to -95Hz ended when the surface was washed with $dH_2O$ the following morning after 960 minutes. There was increase in *f* with washing but only of 2Hz.

There was then an addition of excess silica to the surface. Although this did result in a decrease in *f* it returned to the pre silica addition level after washing.

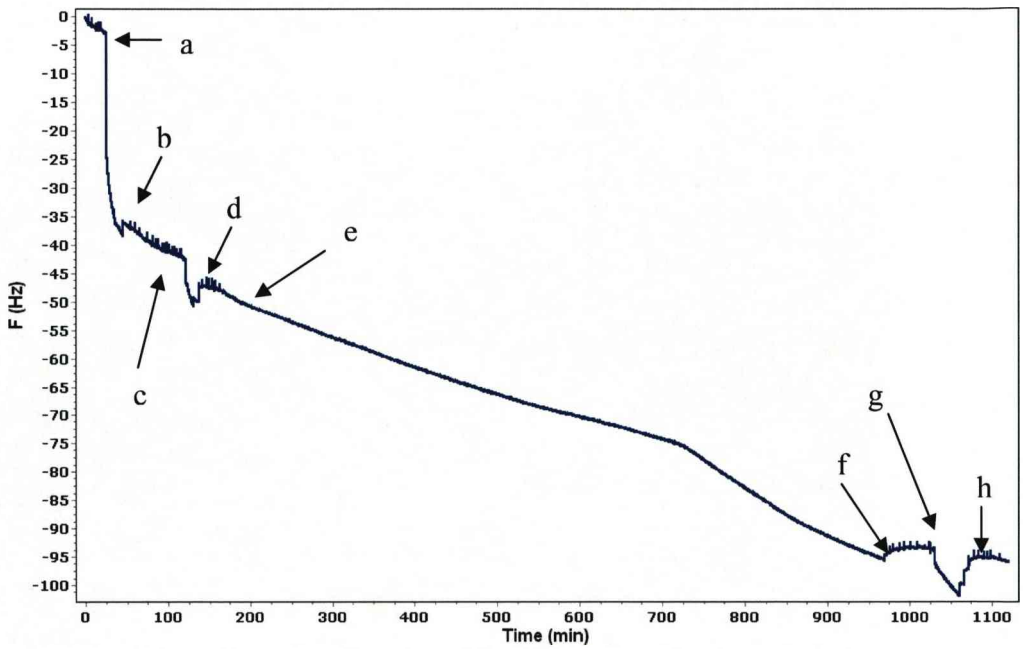


**Figure 3.5** QCM-D plot of *f* of the addition of Ludox® TM-50 (21nm) silica sol to a gold coated quartz crystal with a bovine dentine disc attached.

a) Addition of Ludox® TM-50 4%(w/v)
b) Begin wash steps with $dH_2O$
c) Addition of excess Ludox® TM-50
d) Begin wash steps with $dH_2O$
e) Leave overnight
f) Begin wash steps with $dH_2O$
g) Addition of an excess of Ludox® TM-50
h) Begin wash steps with $dH_2O$

The reliability of the data after 200 mins is uncertain (figure 3.5). This is because after 200 minutes each of the three overtures began recording different fluctuations in *f* and *d*. The three overtures should show the same readings but at multiples of each other. Therefore the stability of the dentine attachment after this point can not be guaranteed.

b) Influence of crystal surface

When Ludox® TM-50 was added to either gold or HA surfaces the *f* increase due to addition of the silica sol to the system was easily removed after washing Table 3.4. When the dentine surfaces were used there was a greater decrease in *f*, this decrease was

maintained after several washes and even increased by a further drop of 4.5Hz. However after just one wash there was an increase in *f* of 1.3Hz which is very small and these fluctuations as discussed above are most probably due to a drift on the output.

| **QCM-D surface** | **Upon addition of silica** | | **After 1 wash** | | **After washes** | | **% *f* remaining after washes** |
|---|---|---|---|---|---|---|---|
| | **$\Delta f$** | **$\Delta d$** | **$\Delta f$** | **$\Delta d$** | **$\Delta f$** | **$\Delta d$** | |
| Gold | -8.5 | 10.5 | 3.3 | -1.2 | 7.3 | -9.7 | 14% |
| HA | -17.2 | 13.4 | 5.2 | -2.5 | 13.0 | -12.6 | 25% |
| Dentine | -35.2 | 7.6 | 1.3 | -1.1 | -4.5 | -2 | 100% |

**Table 3.4.** Table of the *f* and *d* changes when Ludox® TM-50 is added to Gold, HA and Dentine surfaces followed by washing of the surface.

The use of a polycationic polymer prior to addition of the silica nanoparticles.

a) influence of polymer chemistry

gold surface

When 0.3g/l Zetag™ 7109 polymer was adhered to the surface prior to addition of the Ludox® silica sol, the nanoparticles adhered to the surface (figure 3.6). This can also be noted when 0.3g/l UCARE™ polymer JR-125 was used (figure 3.8). As demonstrated in table 3.5 it is clear that following washing for both polymers the *f* continued to decrease. The average *f* decrease was greater when the UCARE™ polymer JR-125 was adsorbed onto the surface to create the polymer binding layer.

| Polymer | Addition of polymer | | After 1 wash | | At end point of washes | |
|---|---|---|---|---|---|---|
| | $\Delta f$ | $\Delta d$ | $\Delta f$ | $\Delta d$ | $\Delta f$ | $\Delta d$ |
| **Zetag™ 7109 average** | -2.4 | 0.7 | -1.2 | -0.7 | -2.3 | -3 |
| **UCARE™ polymer average** | -14.7 | 0.8 | -5.1 | 0.3 | -7.8 | 0.4 |

**Table 3.5** Table showing the effect of addition of 0.3g/l of either Zetag™ 7109 or UCARE™ polymer JR-125 to a gold coated Quartz surface.

Figure 3.6 demonstrates the effect of adding the silica sol to a system after the creation of a polymer layer. The addition of the nanoparticles to the surface resulted in a large drop in *f,* twenty times greater than that of when the polymer was added. The addition of the silica also resulted in a similar fold increase in the *d*. Once both *f* and *d* had stabilized at their new levels, the washing process could begin. Within just four washes there was no further increase in *f* due to loss of mass from the surface and the *f* had stabilized at a new level lower than that prior to addition of the silica sol. This indicated an increase in mass and thus the adhesion of nanoparticles to the polymer coated surface. There were still some fluctuations of *d* with each wash but this could be due to interactions between the nanoparticles the polymer and any trapped liquid.

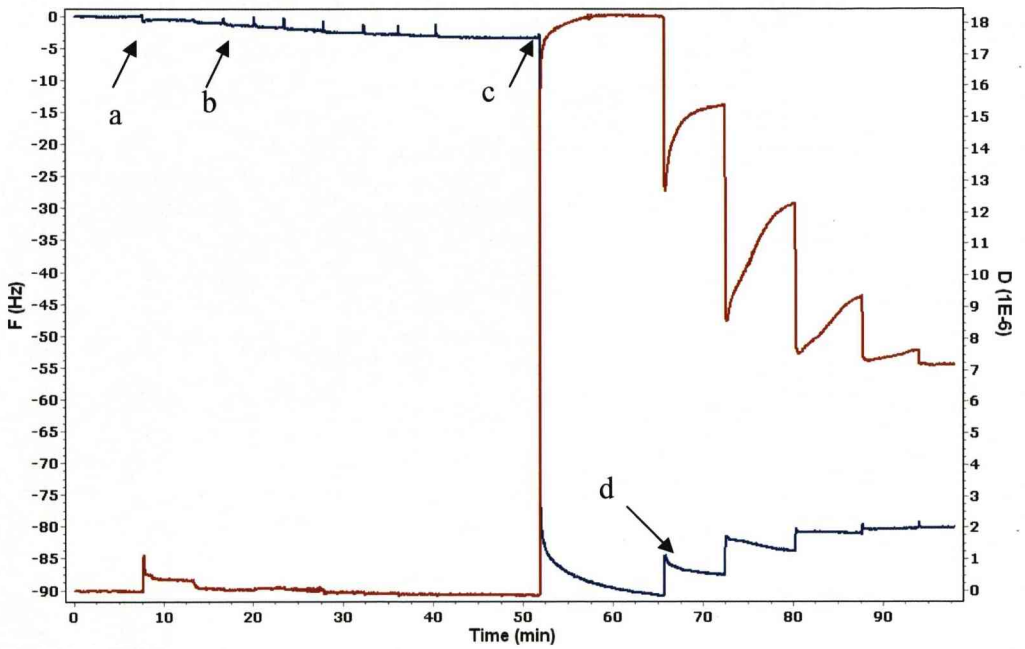


**Figure 3.6** QCM-D plot of *f* (blue line) and *d* (red line) after Zetag 7109 0.3g/l as a polymer binding layer prior to addition of the Ludox® silica sol to a gold coated quartz crystal.

a) Addition of 0.3g/l Zetag™ 7109
b) Begin NaOH $10^{-5}$M washes
c) Addition of Ludox® SM (7nm) silica sol
d) Begin washes with NaOH $10^{-5}$M.

Despite the differences in particle size following washing there was a maximum increase in *f* of 10Hz. Following washing an average of 94% of the *f* decrease observed upon addition of the Ludox® silica sol remained. This would indicate that a nanoparticulate coating had been created when all three of the silica particle sizes were used in conjunction with 0.3g/l Zetag™ 7109 polymer.

| Silica sol | Addition of silica sol | | After 1 washes | | Overall change after washing | | % *f* remaining after washes |
|---|---|---|---|---|---|---|---|
| | $\Delta f$ | $\Delta d$ | $\Delta f$ | $\Delta d$ | $\Delta f$ | $\Delta d$ | |
| Ludox® SM | -87.3 | 18.3 | 2.3 | -2.9 | 3.3 | -11.1 | 96% |
| Ludox® HS-40 | -70.3 | 10.5 | 5.4 | -3.2 | 8.2 | -6.7 | 88% |
| Ludox® TM-50 | -142.5 | 15.92 | 4.7 | -2.2 | 5.8 | -7.8 | 96.% |

**Table 3.6** Table showing the effect of the addition of different particle size Ludox ® silica sols to a Zetag™ 7109 0.3g/l coated gold surface upon *f* (Hz) and *d*.

Comparison of the *d* as a function of the *f* shift (figure 3.7) is commonly used to reveal information regarding the strength of the film/ film interactions and the various phases of undergone during attachment (Fogel, Mashazi et al. 2007). As demonstrated in figure 3.7 there appears to be a 2 stage process of nanoparticulate silica adsorption onto the polymer coating. The first is a fast phase that results in a steady increase in *f* in comparison to *d* this was accompanied by a secondary phase that is very steep relating to a large change in *d* indicating that there is a high degree of viscosity to the second phase of the coating. This plot was representative of all size nanoparticles on all the polymer coatings on all surfaces.

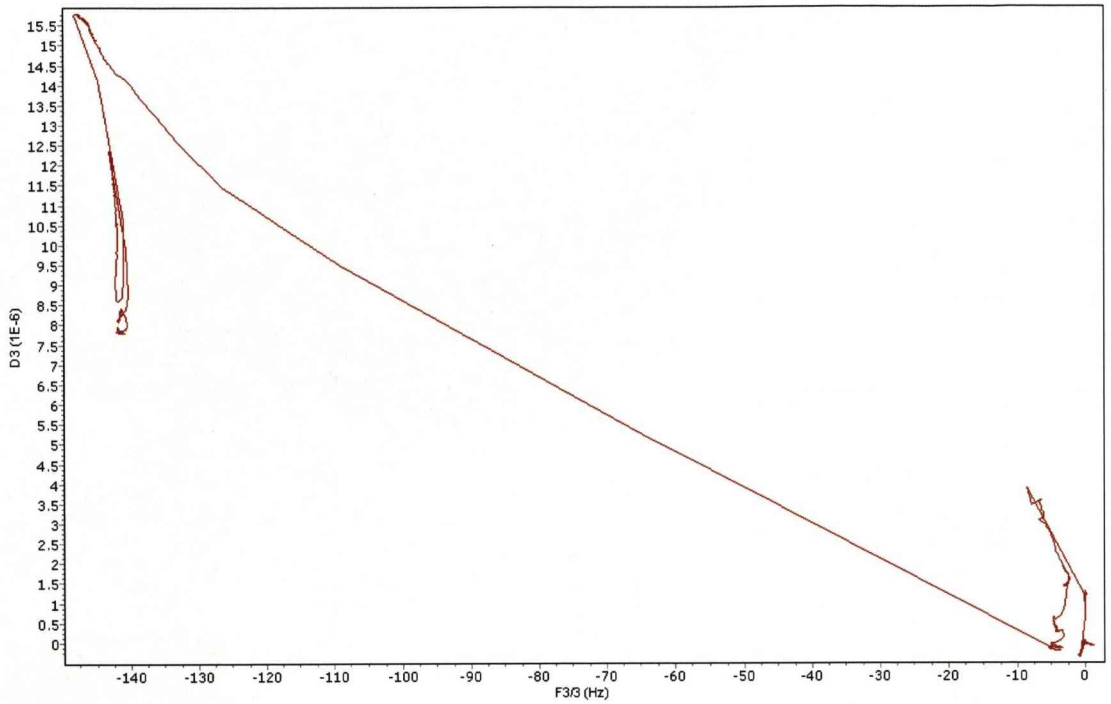


**Figure 3.7** QCM-D plot of *f* vs *d* demonstrating the effect of using Zetag 7109 0.3g/l as a polymer binding layer prior to addition of the Ludox® silica sol to a gold coated quartz crystal.

Figure 3.8 demonstrates the effect of addition of nanoparticles when the lower molecular weight UCARE™ polymer JR-125 was used to create a polymer binding layer. After creation of the polymer layer and the stabilization of *f* and *d* Ludox® TM-50 was added to the surface. There was again a drop in *f* relating to an increase in mass on the surface (the presence of the silica nanoparticles). After just 3 washes there was no further increase in *f* relating to a loss of mass from the surface. The final *f* was 110Hz lower than prior to the addition of the nanoparticles. This indicates a nanoparticulate coating had been formed and remained adhered to the gold surface.

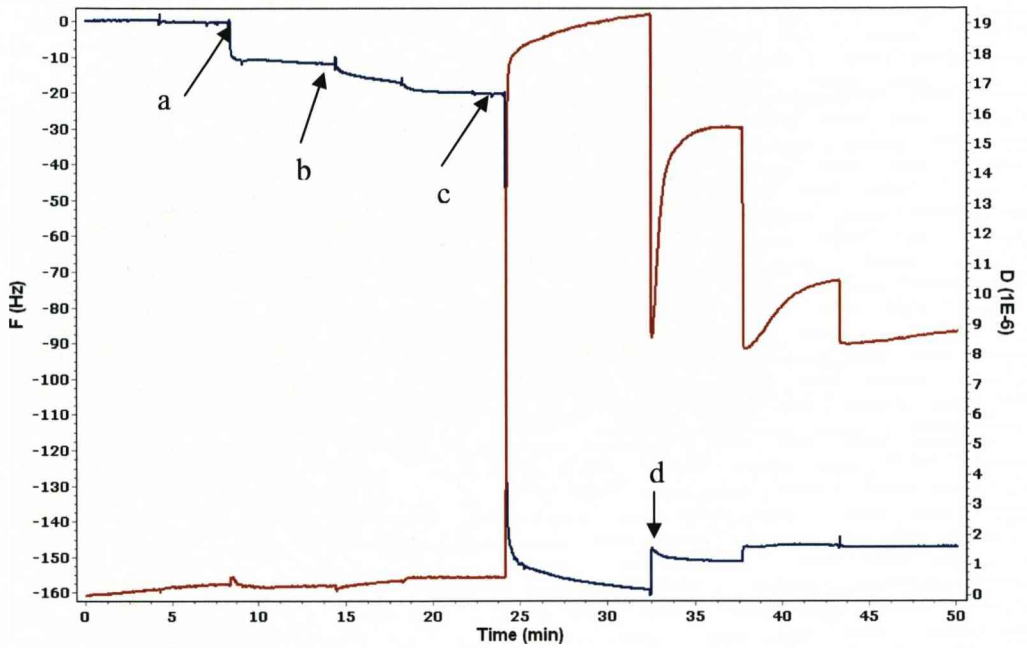


**Figure 3.8** QCM-D plot of *f* (blue line) and *d* (red line) the effect of UCARE polymer JR-125 at 0.3g/l as a polymer binding layer prior to addition of the Ludox® silica sol to a gold coated quartz crystal.

a) Addition of 0.3g/l Ucare polymer JR125
b) Beginning of wash stage using NaOH $10^{-5}$M.
c) Addition of Ludox® TM-50 (21nm) silica sol.
d) Beginning of wash stage using NaOH $10^{-5}$M.

When the effect of using UCARE™ polymer JR-125 with different silica sols was investigated (table 3.7), the greatest drop in *f* was noted when the largest diameter particles (Ludox® TM-50) were used. In all cases although there was some increases in *f* with washing, these increases relating to the loss of mass from the surface were minimal with on average 90% of the *f* decrease remaining after washing.

| Silica sol | Addition of silica | | After 1 wash | | Overall change after washes | | % $f$ remaining after washes |
|---|---|---|---|---|---|---|---|
| | $\Delta f$ | $\Delta d$ | $\Delta f$ | $\Delta d$ | $\Delta f$ | $\Delta d$ | |
| Ludox® SM-30 | -77.9 | 11.6 | 3.2 | -2.5 | 5.8 | -5.5 | 92% |
| Ludox® HS-40 | -56.9 | 6.1 | 5.2 | -3.4 | 6.89 | -5.1 | 89% |
| Ludox® TM-50 | -138.9 | 18.7 | 7.7 | -3.4 | 11.9 | -10.7 | 91% |

**Table 3.7** Table showing the effect of the addition of different particle size Ludox ® silica sols to a UCARE™ polymer JR-125 0.3g/l coated gold surface upon $f$ (Hz) and $d$.

b) Influence of lowering the polymer concentration.

Gold Surface

When a 10 fold lower concentration of Zetag™ 7109 of 0.03g/l was adhered to the surface prior to addition of the Ludox® silica sol, the nanoparticles adhered to the surface (figure 3.9). This can also be noted when a10 fold reduced concentration of UCARE™ polymer JR-125 was used (figure 3.10). As demonstrated in Table 3.8 there was a smaller decrease in the $f$ upon addition of the 0.03g/l Zetag™ 7109 compared to when 0.3g/l was used. However the $\Delta d$ upon addition of the polymer was the same for both concentrations of Zetag™ 7109.

When the UCARE™ polymer JR-125 was used at the lower concentration a similar $\Delta f$ was witnessed as when the higher 0.3g/l concentration was used. However the continuing drop in $f$ with washes was diminished in comparison to the higher concentration polymer solution. As before there was a greater $\Delta f$ when UCARE™ polymer JR-125 was used to compared to Zetag™ 7109 at the lower concentration of 0.03g/l.

| Polymer | Addition of Polymer | | After 1 wash | | After all washes | |
|---|---|---|---|---|---|---|
| | *Δf* | *Δd* | *Δf* | *Δd* | Δ*f* | Δ*d* |
| Zetag™ 7109 0.03g/l average | -1.3 | 0.7 | -1.2 | -0.3 | -0.9 | -0.4 |
| Zetag™ 7109 0.3g/l average | -2.4 | 0.7 | -1.2 | -0.7 | -2.3 | -3 |
| UCARE™ JR-125 0.03g/l average | -14.1 | 0.9 | -1.18 | 0.3 | -3.5 | 0.5 |
| UCARE™ JR-125 0.3g/l average | -14.7 | 0.8 | -5.1 | 0.3 | -7.8 | 0.4 |

**Table 3.8** Table showing the effect of addition of both Zetag™ 7109 and UCARE™ polymer JR-125 at a 0.03g/l and 0.3g/l to a gold coated quartz surface.

Figure 3.9 demonstrates the effect of adding the silica sol to a system after the creation of a polymer layer using Zetag™ 7109 at the lower concentration of 0.03g/l. Following creation of the polymer layer the introduction of the nanoparticles resulted in second larger decrease in *f*. This drop in *f* was coupled with an increase in *d*. After just one wash there was an increase in *f* of 2Hz relating to some mass being removed from the surface however after only seven washes a stable *f* and *d* had been achieved, with an overall increase in *f* of only 8Hz. As before a stable coating of nanoparticles had been achieved, this was highlighted by the fact 88% of the Δ*f* due to the addition of the silica sol remained after washing.

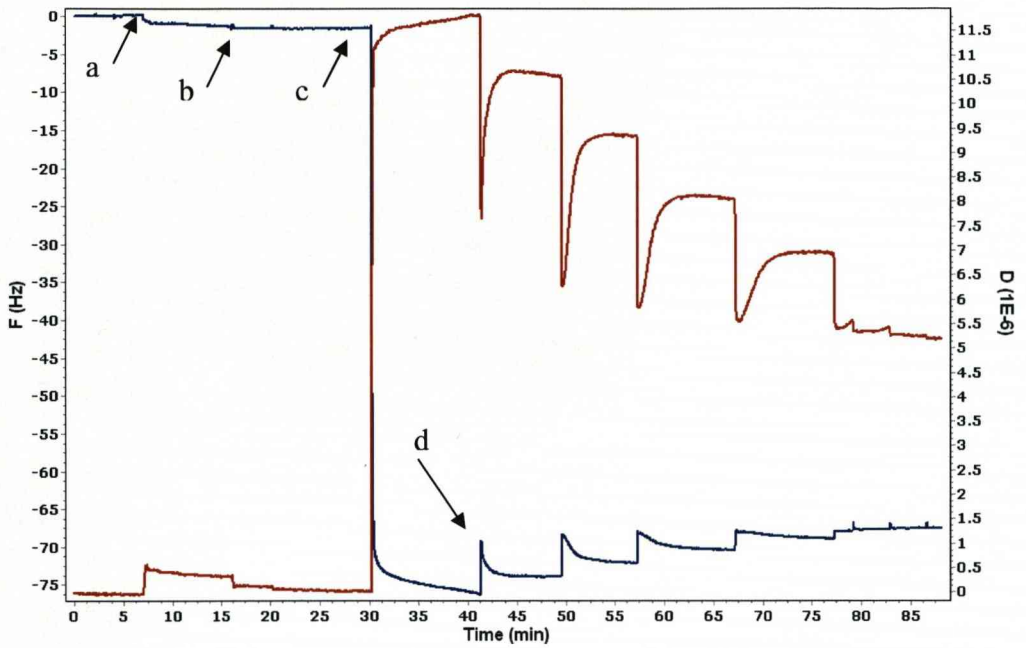


**Figure 3.9** QCM-D plot of *f* (blue line) and *d* (red line) demonstrating the effect of using Zetag 7109 0.03g/l as a polymer binding layer prior to addition of the Ludox® silica sol to a gold coated quartz crystal.

a) Addition of 0.03g/l Zetag™ 7109
b) Begin NaOH $10^{-5}$M washes
c) Addition of Ludox® HS-40 (14nm) silica sol
d) Begin washes with NaOH $10^{-5}$M.

Figure 3.9 is representative of what happened when either of the three different particle size sols was used in conjunction with a Zetag™ 7109 0.03g/l polymer layer. Table 3.9 shows the $\Delta f$ and $\Delta d$ changes upon addition of the other sols to 0.03g/l Zetag™ 7109 polymer coated surface. The decrease in initial $f$ upon addition of the silica sols increased with increasing particle size with the largest $\Delta f$ seen when the 21nm diameter particles where used. In all cases the majority of the $f$ decrease relating to the addition of the silica nanoparticles to the surface remained after repeated washing with on average 89% of the $\Delta f$ due to addition of the nanoparticulate silica sol was maintained following washing.

| Silica Sol | Addition of silica sol | | After 1 wash | | Overall change after washing | | % *f* remaining after washes |
|---|---|---|---|---|---|---|---|
| | $\Delta f$ | $\Delta d$ | $\Delta f$ | $\Delta d$ | $\Delta f$ | $\Delta d$ | |
| Ludox® SM-30 | -67.9 | 16.8 | 3.6 | -2.6 | 12.0 | -11.5 | 82% |
| Ludox® HS-40 | -74.4 | 11.8 | 2.15 | -1.3 | 8.5 | -6.553 | 88% |
| Ludox® TM-50 | -127.2 | 18.2 | 1.8 | -6.05 | 3.0 | -6.3 | 98% |

**Table 3.9.** Table showing the effect of the addition of different particle size Ludox® silica sols to a 0.03g/l Zetag™ 7109 coated gold surface upon *f* (Hz) and *d*,

Figure 3.10 demonstrates the effect of using JR -125 at the lower (0.03g/l) concentration. It is possible to identify the addition of the UCARE™ polymer JR-125 as a drop in *f* of 14Hz (table3.8). After washing there was a further drop of only 2Hz. The addition of the Ludox® silica sol resulted in a second larger drop in *f* of 50Hz (table 3.10). After washing there was a small increase in *f* of 4Hz. After only one wash there was no further increase in *f* relating to the loss of mass from the surface. After 4 washes there was no further decrease in *d*. This indicated that despite lowering the concentration of the polymer solution there was still substantial adherence of nanoparticles to the surface.

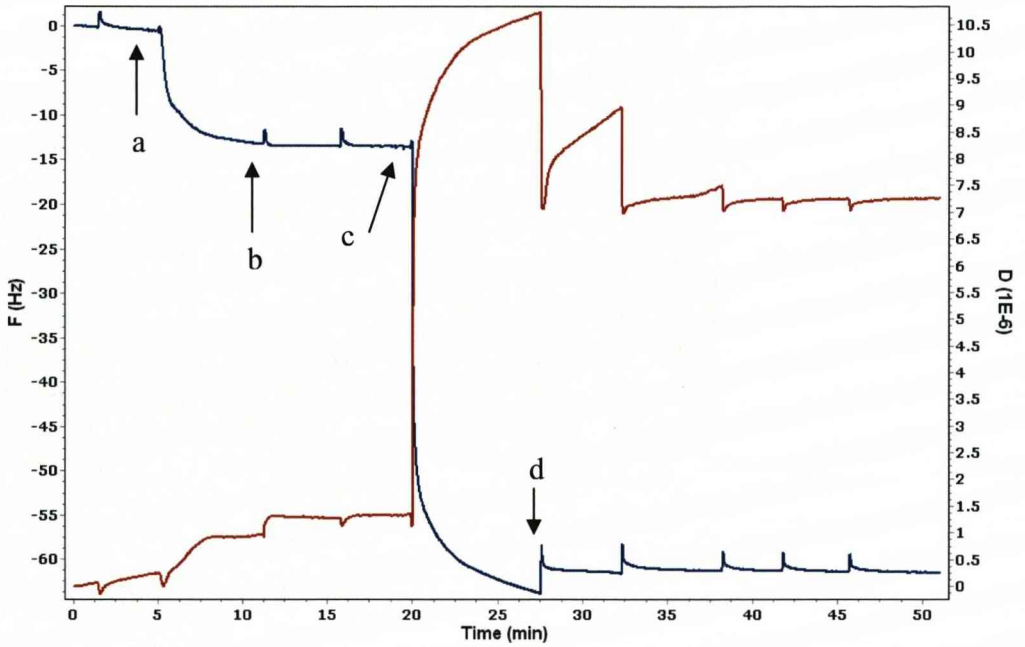


**Figure 3.10** QCM-D plot of $f$ (blue line) and $d$ (red line) the effect of using UCARE polymer JR-125 at 0.03g/l as a binding layer prior to addition of the Ludox® silica sol to a gold coated quartz crystal.

a) Addition of 0.03g/l of UCARE polymer JR-125
b) Begin wash with NaOH $10^{-5}$M
c) Addition of 4%(w/v) Ludox® SM (7nm) silica sol
d) Begin wash with NaOH $10^{-5}$M

This was also noted when the different particle size Ludox® sols were used (table 3.10). There was an increased $\Delta f$ with increasing particle size of the Ludox® silica sols. It was also identified that after washing on average 94% of the $\Delta f$ due to the addition of the nanoparticles remained. This highlights that the nanoparticles had adhered to the lower molecular weight lower concentration polymer coated surface and have formed a substantial coating.

| Silica Sol | Addition of silica | | After 1 wash | | Overall Change after washes | | % *f* remaining after washes |
|---|---|---|---|---|---|---|---|
| | Δ*f* | Δ*d* | Δ*f* | Δ*d* | Δ*f* | Δ*d* | |
| Ludox® SM-30 | -50.2 | 9.4 | 1.7 | -1.7 | 2.4 | -3.5 | 95% |
| Ludox® HS-40 | -78.5 | 9.2 | 4.2 | -3.3 | 6.1 | -6.3 | 92% |
| Ludox® TM-50 | -186.4 | 22.3 | 5.4 | -3.75 | 6.6 | -10.4 | 96% |

**Table 3.10.** Table showing he effect of addition of different particle size Ludox® silica sols to a 0.03g/l UCARE™ polymer JR-125 coated gold surface upon *f* (Hz) and *d*.

HA Surfaces

When 0.03 g/l of Zetag™ 7109 was added to the HA coated Quartz crystals there was a sharp drop in *f* of on average 32Hz (table 3.11). As highlighted in table 3.11 this drop was much larger than that when a gold coated surface was used. There was also an increased *d* fluctuation that did not lower with continued washing as when gold surfaces where investigated. The Δ*f* remained stable despite several wash steps as can be observed in figure 3.11.

| Polymer | Addition of polymer | | After 1 wash | | At end point of washes | |
|---|---|---|---|---|---|---|
| | Δ*f* | Δ*d* | Δ*f* | Δ*d* | Δ*f* | Δ*d* |
| Zetag™ 7109 0.03g/l on **gold** | -1.3 | 0.7 | -1.2 | -0.3 | -0.9 | -0.4 |
| Zetag™ 7109 0.03g/l on **HA** | -31.9 | 11.5 | -1.4 | 0.1 | -2.1 | 0.5 |

**Table 3.11** Table showing the effect of addition of 0.03g/l of Zetag™ 7109 to a Gold and HA coated Quartz crystal surface.

Figure 3.11 highlights the large sharp drop in $f$ upon introduction of the Zetag™ 7109 polymer. Despite washing the $\Delta f$ remains relatively stable with minimal fluctuations. Twenty minutes after the addition of the Zetag™7109 polymer the Ludox® TM-50 (21nm diameter particles) silica sol was introduced to the surface, This resulted in the second drop in $f$ of 191Hz. After one wash there was an increase of 9Hz, however, upon completion of three more washes there was only a further increase in $f$ of 6Hz. Therefore 91% of the $f$ decrease due to the introduction of the silica nanoparticles to the surface remained after washing. Demonstrating that a substantial coating of nanoparticles had been achieved.

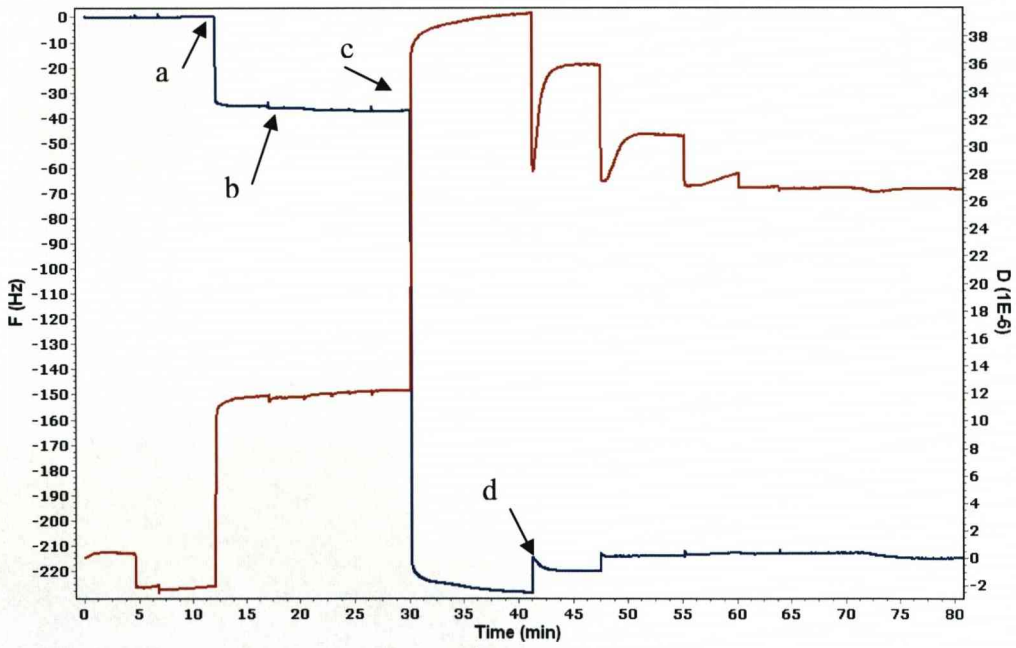


**Figure 3.11** QCM-D plot of $f$ (blue line) and $d$ (red line) the effect of using Zetag™ 7109 at 0.03g/l as a binding layer prior to addition of the Ludox® TM-50 (21nm) silica sol to a HA coated quartz crystal.

a) Addition of Zetag™ 7109 0.03%
b) Begin washes with NaOH $10^{-5}$M
c) Addition of Ludox® TM-50 4%(w/v)
d) Begin washes with NaOH $10^{-5}$M

### 3.4.2 Flow Experiments

To assess the integrity of the coatings, it was important to investigate whether or not the coatings could withstand a flow system overnight. Any increase in *f* would relate to a loss of mass from the surface.

a) influence of particle size in the silica sol

Gold Surfaces

When Zetag™ 7109 0.03g/l was used to adhere 7nm silica particles (Ludox® SM) and then subjected to a continuous flow of $dH_2O$ overnight, there was no fluctuation in the *f* overnight (figure 3.12). There was a blip where the pump was turned on at 65 minutes, although the *f* soon settled back to -122.04Hz and the *d* to 14.3. After 16 hours of flow conditions, the *f* remained at -122Hz and the *d* remained at 14.3.

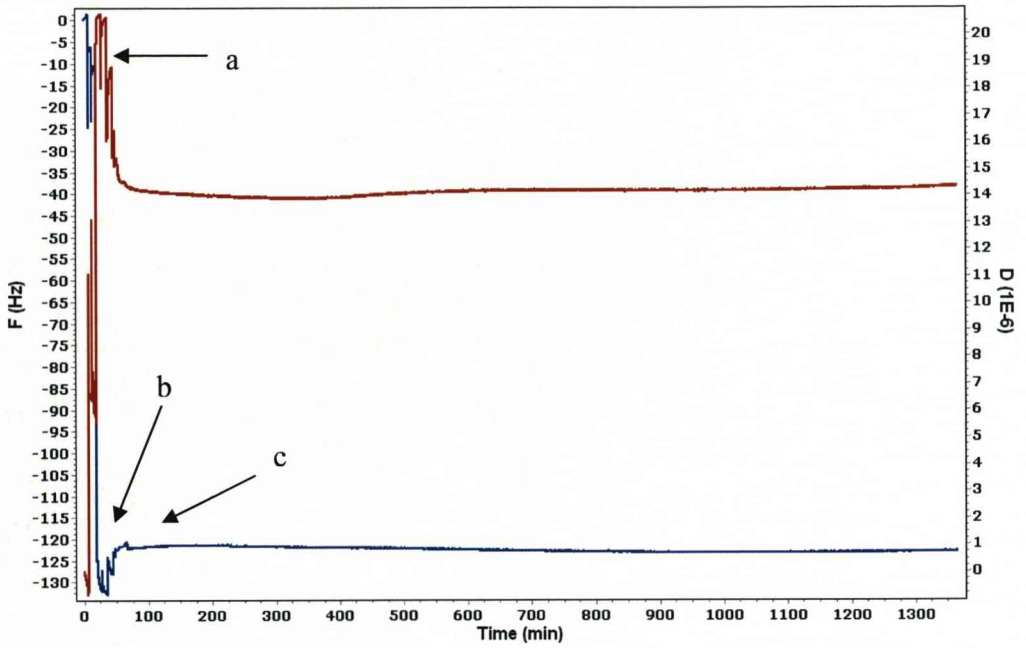


**Figure 3.12** QCM-D plot of *f* (blue line) and *d* (red line) demonstrating the effect of using Zetag™ 7109 at 0.03g/l as a polymer binding layer for adhesion of the Ludox® SM (7nm) silica sol to a gold coated quartz crystal prior to running $dH_2O$ across the surface at a rate of 50.2$\mu$l overnight.

a) Creation of the Zetag™ 7109 polymer layer and addition of the silica nanoparticles (Ludox® SM).
b) Wash steps with NaOH $10^{-5}$ M.
c) Begin continuous flow of $dH_2O$ at 50.2 $\mu$l per minute overnight.

The polymer and silica coating was created in the same manner as in figure 3.5, and the lack of fluctuation of both *f* and *d* suggested there was no loss of mass due to a continuous flow of $dH_2O$. Thus, a stable nanoparticulate coating can be achieved, using the lowest concentration of the Zetag™ 7109 polymer with the smallest diameter silica nanoparticles (Ludox® SM) tested.

To assess whether or not the size of the nanoparticles adhered to the surface alters the coatings ability to withstand flow, a gold coated crystal was coated in Zetag™ 7109 0.03g/l, followed by the largest diameter silica nanoparticles (Ludox® TM-50) before being subjected to a constant flow of 50.2$\mu$l per minute of $dH_2O$ (figure 3.13). This resulted in an initial decrease in *f* of 2Hz and a decrease in *d* of 2.

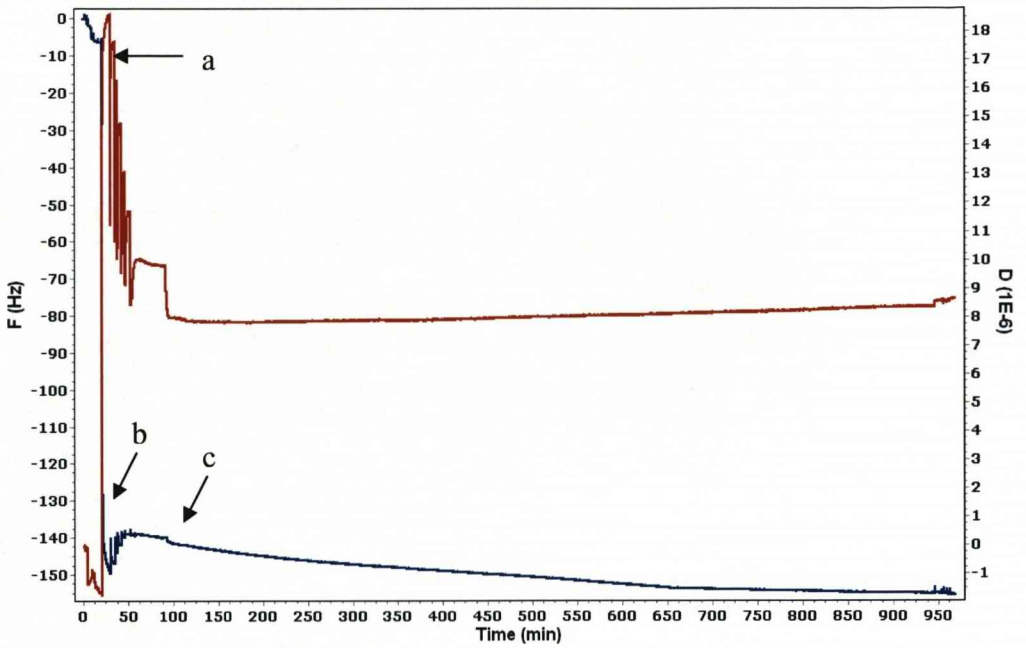


**Figure 3.13** QCM-D plot of *f* (blue line) and *d* (red line) demonstrating the effect of using Zetag™ 7109 at 0.03g/l as a polymer binding layer for adhesion of the Ludox® TM-50 (21nm) silica sol to a gold coated quartz crystal prior to running $dH_2O$ across the surface at a rate of 50.2$\mu$l overnight.

a) Creation of the Zetag™ 7109 polymer layer and addition of the silica nanoparticles (Ludox® TM-50)
b) Wash steps with NaOH $10^{-5}$M
c) Begin flow of $dH_2O$ at 50.2$\mu$l per minute overnight

Over 16 hours of flow conditions, there was no increases in *f* relating to the loss of mass from the surface. However, there was a steady decrease in *f*, which resulted in an overall decrease of 14Hz over the duration of flow conditions. This is less than 1Hz per hour. This was coupled with an overall decrease in *d* of 0.5. These small decreases are, therefore, negligible and do not suggest any alteration to the surface, implying that the 21nm nanoparticulate silica coating was also able to withstand flow conditions.

HA surface

Figure 3.14 demonstrates Zetag™ 7109 0.03g/l Ludox® TM-50 coated HA surface which was then subjected to a continuous flow of $dH_2O$ overnight. The polymer/ nanoparticulate coating portion of the plot (under 100 minutes) closely resembled that in figure 3.10. After the system was switched to a flow system at seventy minutes, there was a drop in *f* of 2 Hz but, after sixty minutes, it had returned to the level prior to the flow system being started. The *d* remained stable throughout this initial sixty minutes of the flow experiment.

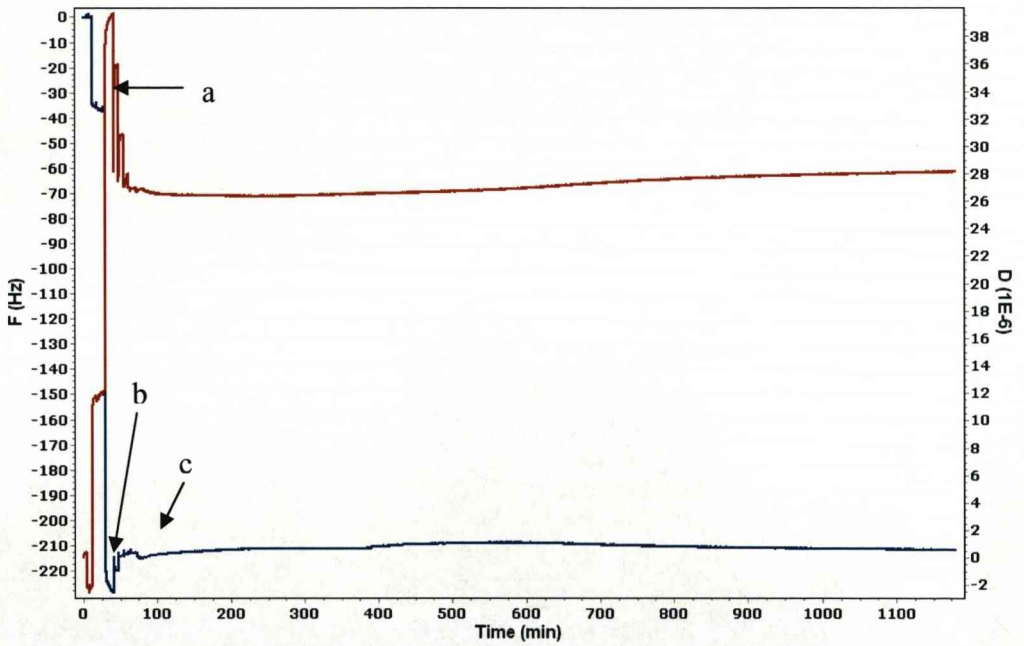


**Figure 3.14** QCM-D plot of *f* (blue line) and *d* (red line) demonstrating the effect of using Zetag™ 7109 at 0.03g/l as a polymer binding layer for adhesion of the Ludox® TM-50 (21nm) silica sol to a HA coated quartz crystal prior to running $dH_2O$ across the surface at a rate of 50.2$\mu$l overnight.

a) Creation of the Zetag™ 7109 polymer layer and addition of the silica nanoparticles (Ludox® TM-50)
b) Begin washes with NaOH $10^{-5}$M
c) Begin flow of $dH_2O$ over the surface at 500.2$\mu$l per minute overnight

After being left overnight, the *f* and *d* had remained stable under flow conditions for 16 hours. The *f* had increased by 2 Hz and the *d* had increased by 2. These are minimal increases and do not indicate any loss of mass from the surface, demonstrating that the Zetag™ 7109 0.03g/l and Ludox® TM-50 coating of the HA crystal is stable under these flow conditions.

b) influence of different polymer chemistry

Gold surfaces

The ability of the lower molecular weight polymer UCARE polymer JR -125 at the lower concentration of 0.03g/l to adhere 21nm silica particles (Ludox®TM-50) under flow conditions was studied (figure 3.15).

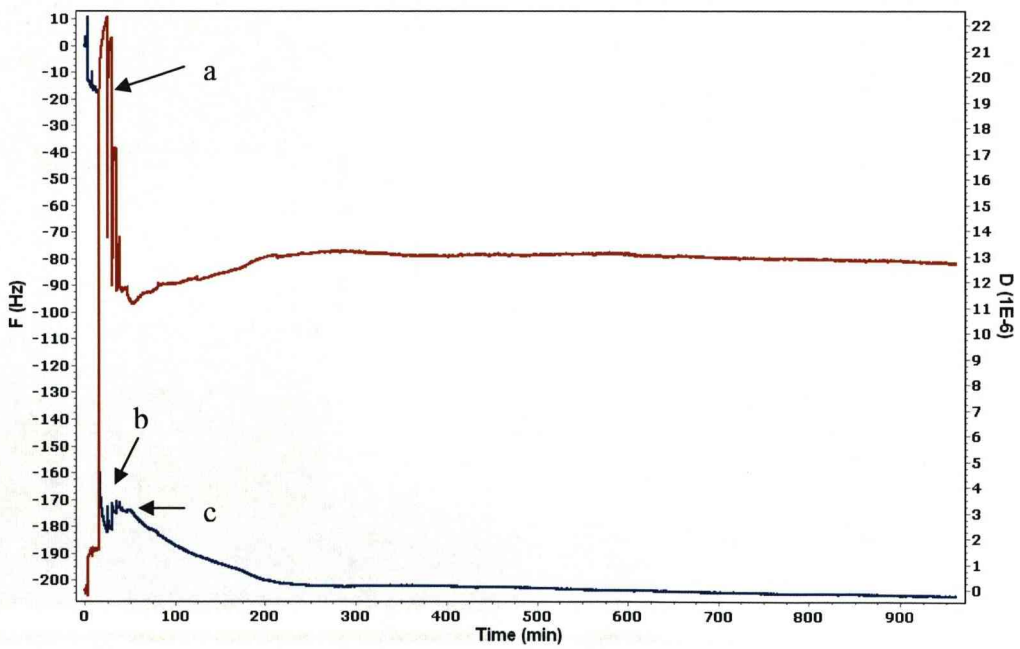


**Figure 3.15** QCM-D plot of *f* (blue line) and *d* (red line) UCARE Polymer JR-125 at 0.03g/l and Ludox® TM-50 (21nm) silica sol on a gold coated quartz crystal prior to running $dH_2O$ across the surface at a rate of 50.2$\mu$l overnight.

a) Creation of the UCARE polymer JR-125 layer and addition of the silica nanoparticles (Ludox® TM-50)
b) Begin washes with NaOH $10^{-5}$M
c) Begin flow of $dH_2O$ at 50.2$\mu$l overnight

There was a decrease in *f* during the initial 200 minutes of flow of 26Hz. However, after this, both *f* and *d* stabilized and remained stable for the rest of the duration of the experiment, with only a 5Hz drop in *f* and no alteration in the *d* after the initial increase of 1 at the start of the flow. This fluctuation could be due to the initial increase in pressure on the crystal surface when the pump was switched on. The lack of increase in *f*, however, would indicate that the nanoparticles were adhered securely to the Ucare polymer layer and thus the surface.

c) The effect of artificial saliva

Gold surfaces

Figure 3.16 highlights the effect of a continuous flow of a physiologically relevant protein containing fluid (artificial saliva) on a gold coated quartz crystal. There was a sharp decrease in *f* during the first 10 minutes of flow of 54.5Hz which was coupled with an increase in *d* of 6.1. After the initial drop, both *f* and *d* began to plateau over the next 100 minutes of artificial saliva flow. During this time, the *f* only decreased by a further 13.6Hz and the *d* only increased by 1.7. This decrease continued at a slower rate of only 11Hz over the following 500 minutes but there was a second, sharper, decline in *f* after 800 minutes resulting in a decrease in *f* of 17.3Hz during the final 500 minutes of the flow portion of the experiment.

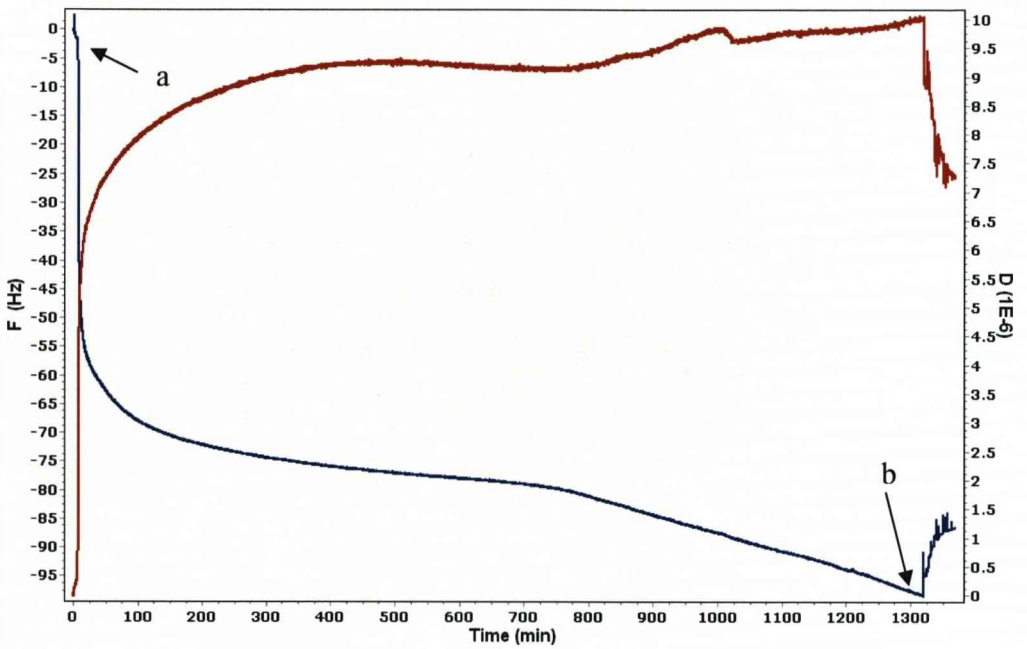


**Figure 3.16** QCM-D plot of *f* (blue line) and *d* (red line) a continuous flow of artificial saliva using a peristaltic pump at a rate of 50.2$\mu$l per minute overnight on a gold coated Quartz crystal

a) Begin flow of artificial saliva at 50.2$\mu$l per minute
b) Begin washing of surface with $dH_2O$.

When the surface was washed with $dH_2O$ the following morning, there was an increase in *f* with each wash After the initial wash, there was an increase of 4.7 Hz and a decrease in *d* of 0.8. After seven washes, there was only a further increase in *f* of 5.7Hz (table 3.12). The new *f* was only 7Hz lower than before the sharp decline at 800 minutes.

When the Zetag™ 7109 0.03g/l 21nm silica (Ludox® TM-50) coating was created and then subjected to a continuous flow of artificial saliva, there was again a sharp decrease in *f* of 133.7Hz (figure 3.17). However, at the end of the flow period of 1100 minutes, there had only been a further decrease in *f* of 10Hz during the final 100 minutes.

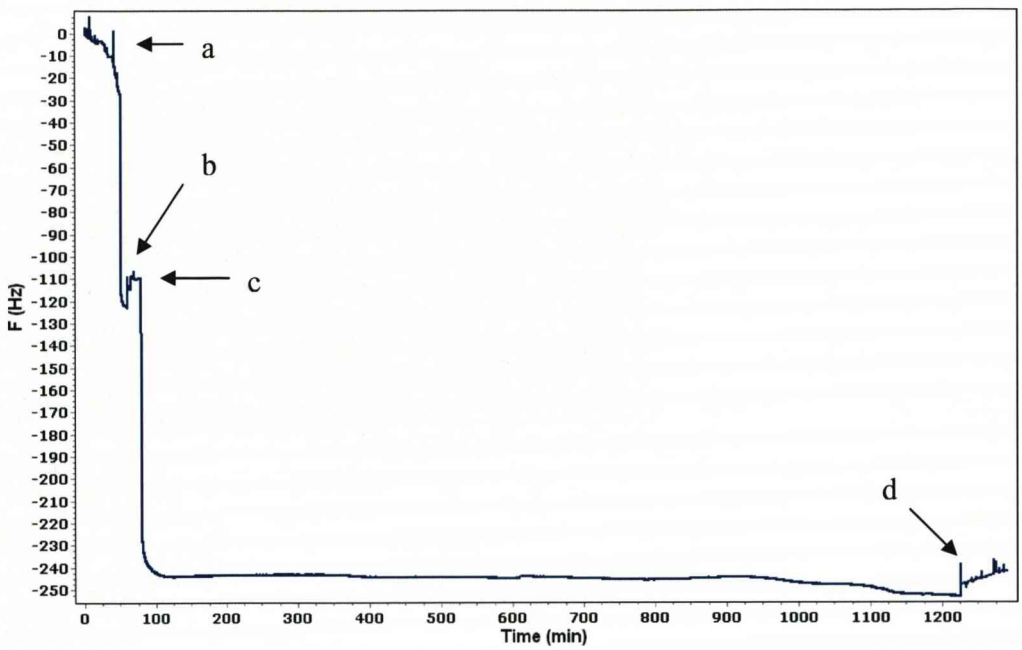


**Figure 3.17** QCM-D plot of *f* (blue line) when a Zetag 7109™ 0.03g/l then 21nm silica (Ludox® TM-50) coating on a gold surface was subjected to a continuous flow of artificial saliva at 50.2$\mu$l per minute overnight

a) Creation of the Zetag™ 7109 polymer layer and addition of the silica nanoparticles (Ludox® TM-50)
b) Begin washes with NaOH $10^{-5}$M
c) Begin flow of 50.2$\mu$l per minute artificial saliva overnight
d) Begin washes with $dH_2O$.

When the surface was washed with $dH_2O$, after one wash there was an increase in *f* of 6Hz. After eleven washes, there was only a further increase in *f* of 5Hz. Once stabilised, the *f* was only 1Hz higher than prior to the 10 Hz dip in the last 100 minutes of artificial saliva flow.

| Coating | Begin flow | | End of flow | | After 1 wash | | After all washes | |
|---|---|---|---|---|---|---|---|---|
| | $\Delta f$ | $\Delta d$ | $\Delta f$ | $\Delta d$ | $\Delta f$ | $\Delta d$ | $\Delta f$ | $\Delta d$ |
| Gold Quartz surface | -54.5 | 6.2 | -41.5 | 3.2 | 4.7 | -0.8 | 10.6 | -2.2 |
| Zetag™ 7109 0.03g/l and Ludox® TM-50 | -133.7 | 6.3 | -9.4 | 2.7 | 5.4 | -1.9 | 10.8 | -2.8 |

**Table 3.12** The effect of artificial saliva flow over gold coated quartz crystals in the absence and presence of a Zetag™ 7109 0.03g/l Ludox® TM-50 coating.

Table 3.12 highlights the effect of altering the surface coating on the gold crystal with artificial saliva flow. There was a larger overall decrease in *f* when the nanoparticulate coating was present. However, the continued decrease in *f* over the duration of artificial saliva flow was smaller when the nanoparticulate coating was present than in its absence. However, the *d* remained relatively similar throughout both experiments, as did the *f* and *d* changes upon washing the surface.

HA surfaces

Artificial saliva flow on a HA coated crystal resulted in a sharp decrease in *f* of 77.4Hz, which, after 50 minutes, began to stabilise (figure 3.18). After 200 minutes, the *f* began to gradually decrease, at a rate of 5Hz. The *f* then remained constant for the following 100 minutes. This was followed by a gradual increase in *f* of 14Hz over the course of the following 500 minutes.

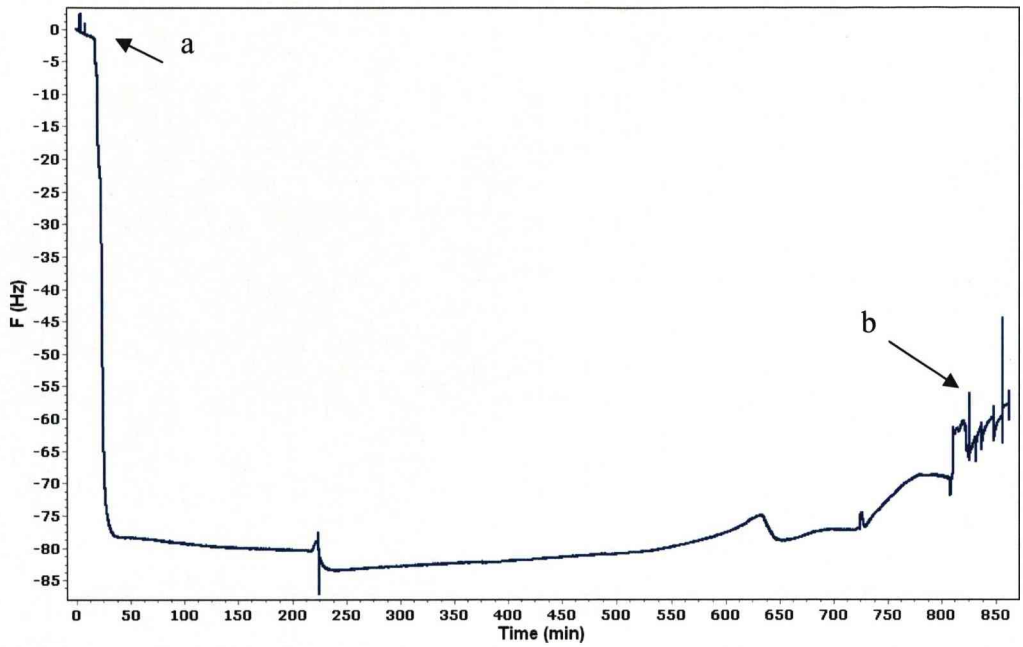


**Figure 3.18** QCM-D plot of *f* (blue line) (*d* is not shown for clarity) demonstrating the effect of a continuous flow of artificial saliva across a HA coated quartz crystal surface

a) Begin flow of 50.2$\mu$l artificial saliva over the surface
b) Begin washes with $dH_2O$

Washing the surface once resulted in a further increase in *f* of 6.7Hz (table 3.13) Following 10 washes there was a further 8.6Hz increase in the *f*. The *d* underwent many fluctuations during the time of the experiment. There was a sustained increase in *d* of 21.4, between 250 minutes and 800 minutes. This increase could be related to the increasing fluidity of the substances adhered to the surface (data not shown).

When the artificial saliva was pumped across a Zetag™ 7109 0.03g/l 21nm silica nanoparticle (Ludox® TM-50) coated HA surface, there was a small initial drop in *f* of 17Hz (figure 3.19) . This was followed, 5 minutes after the start of artificial saliva flow, by a secondary drop of 343.3Hz. The *f* then remained stable for the following 400 minutes. After which, there was a gradual increase of 27.9Hz over the last 500 minutes, until the surface was washed with $dH_2O$.

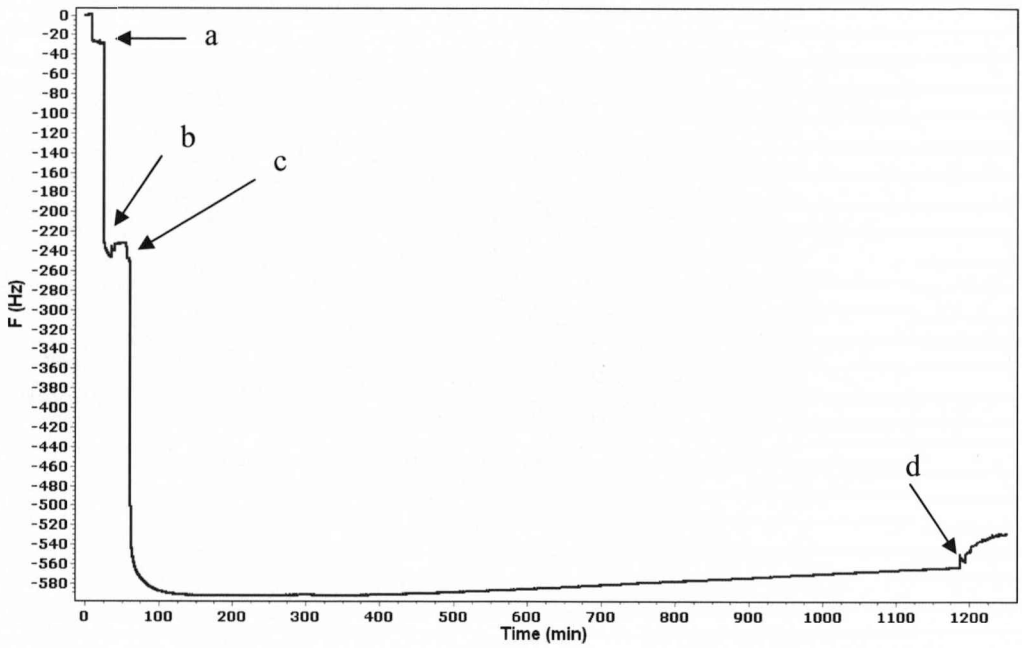


**Figure 3.19** QCM-D plot of *f* (blue line) (*d* is not shown for clarity) Zetag 7109™ 0.03g/l then 21nm silica (Ludox® TM-50) coating on a HA surface was subjected to a continuous flow of artificial saliva at 50.2$\mu$l per minute overnight

a) Creation of the Zetag™ 7109 polymer layer and addition of the silica nanoparticles (Ludox® TM-50)
b) Begin washes with NaOH $10^{-5}$M
c) Begin flow of artificial saliva across the surface at 50.2$\mu$l per minute
d) Begin washes of the surface with $dH_2O$

The first wash of the surface resulted in an increase in *f* of 6.8Hz. Following 16 washes, a stable *f* and *d* had been accomplished and a further increase in *f* of 28.1Hz had occurred. As with *f*, the *d* remained stable for the duration of the experiment, once the flow of artificial saliva was started. Apart from an initial sharp peak, there was a very gradual decrease in *d* after 350 minutes.

Table 3.13 highlights that there was a several times larger initial drop in *f*, when the nanoparticulate coating was present, compared to HA alone. A similar difference can also be seen with the initial values for *d*. In both instances, there was an overall increase in *f* after this initial drop, following the start of artificial saliva flow. However, when the nanoparticulate coating was present, this was coupled with a decrease in the *d*, unlike on

the HA surface where there was a continued increase in *d*. In both instances, following washes, there were increases in *f* and a decrease in *d*.

| **Coating** | **Begin flow** | | **End Flow** | | **After 1wash** | | **After all washes** | |
|---|---|---|---|---|---|---|---|---|
| | **Δ*f*** | **Δ*d*** | **Δ*f*** | **Δ*d*** | **Δ*f*** | **Δ*d*** | **Δ*f*** | **Δ*d*** |
| No coating | -77.4 | 9.2 | 9.3 | 19.5 | 6.7 | -1.2 | 15.3 | -19.2 |
| Zetag™ 7109 0.03g/l and Ludox® TM-50 | -359.5 | 32.9 | 27.9 | -5.1 | 6.8 | 0.6 | 34.9 | -3 |

**Table 3.13** Table showing the effect of artificial saliva flow on HA coated crystals in the presence and absence of a Zetag™ 7109 0.03g/l Ludox® TM-50 coating on *f* and *d*.

e) Effect of different crystal surfaces.

Table 3.14 shows that when the HA coated surfaces were used, the initial drop in *f* was greater compared to that when the gold coated quartz crystals were used. In both instances, there was a larger *f* drop when the nanoparticulate coating was present, compared to the uncoated quartz surfaces. However, there was a continual decrease in *f* during artificial saliva flow on the gold surfaces, compared to an increase in *f* on the HA surface.

| Coating | Begin flow | | End of flow | | After 1 wash | | After all washes | |
|---|---|---|---|---|---|---|---|---|
| | $\Delta f$ | $\Delta d$ | $\Delta f$ | $\Delta d$ | $\Delta f$ | $\Delta d$ | $\Delta f$ | $\Delta d$ |
| **Gold** coated Quartz surface | -54.5 | 6.2 | -41.5 | 3.2 | 4.7 | -0.8 | 10.6 | -2.2 |
| **Gold** Zetag™ 7109 0.03g/l and Ludox® TM-50 | -133.7 | 6.3 | -9.4 | 2.7 | 5.4 | -1.9 | 10.8 | -2.8 |
| **HA** Coated Quartz Surface | -77.4 | 9.2 | 9.3 | 19.5 | 6.7 | -1.2 | 15.3 | -19.2 |
| **HA** Zetag™ 7109 0.03g/l and Ludox® TM-50 | -359.5 | 32.9 | 27.9 | -5.1 | 6.8 | 0.6 | 34.9 | -3 |

**Table 3.14** The effect of artificial saliva flow over gold and HA coated quartz crystals in the absence and presence of a Zetag™ 7109 0.03g/l Ludox® TM-50 coating.

### 3.5 Discussion

The use of the QCM-D in modern scientific research is a rapidly developing area. In this study, the QCM-D was used to monitor nanoparticulate film formation in-situ. The TEM was able to offer a visual analysis of the surface coatings once formed. However, with the aid of the QCM-D, it was possible to monitor the formation of the coatings and the coatings' subsequent ability to withstand different conditions, such as the effect of fluid flow. The QCM-D used for this study was able to record simultaneous measurements of both $f$ and $d$, and was therefore, not only able to indicate the adsorption of nanoparticles to the surface (demonstrated by decreases in $f$) but $d$ readings, which can be used to estimate the nature of the coating with regard to the viscosity and elasticity of the coated layer.

Many QCM-D studies use either the Voight or Sauerbrey equations to calculate the thickness of the coatings of interest (Welle, Chiumiento et al. 2007). The Q-tools programme (Q-Sense, Sweden) was used to analyse the data obtained in this study. This programme offers many useful features, including modelling and automated calculations of thickness and viscosity of adsorbed layers. An attempt was made to use the Q-tools modelling centre to obtain an estimation of the nanoparticulate coatings' thickness. However, when the viscoelastic voight model was used to estimate the thickness of the coating the information gained was unrealistic. The model underestimated the thickness, for example the coating created with a 21nm silica sol was given to be 11nm. The underestimation could be due to the use of nanoparticulate spheres to create the coatings. This adds dimensions to the coatings, that the equation does not account for. It was decided that the use of the modelling centre in the Q-tools programme could result in inaccuracies in data analysis and, as such, would not be used.

As $\Delta f$ is associated with total mass loading, so includes water and ions as well as the viscoelastic contribution from the adsorbing particles, it cannot be used as an absolute measurement of mass (Roach, Shirtcliffe et al. 2006). Therefore, in this study, $\Delta f$ was used as an indication of mass on the surface and not an accurate measurement.

However, the simultaneous measurement of *d* has proven to be useful, as it has allowed some insight into the viscoelastic properties of the coating and the adhesion of macromolecules from artificial saliva in the latter flow experiments.

Using the TEM, it was observed that nanoparticulate adsorption was minimal in the absence of a polymer binding layer. However, the larger diameter nanoparticles (14 and 21nm) demonstrated an increased binding capacity in comparison with the smallest (7nm) particles. It was hypothesised that the larger diameter nanoparticles have an enhanced ability to form van der waals attractions, which would, therefore, increase the potential and possibility of surface adsorption (Napper 1970). This hypothesis was further validated by the observations made with the QCM-D. In the absence of a polymer binding layer following washing of the surfaces, there was a complete reversal of the *f* and *d* shifts, resulting from the introduction of the nanoparticulate sol to the gold coated crystal surface, apart from when the 21nm silica sol was used (table 3.3). When the 21nm nanoparticulate sol (Ludox® TM-50) was used, 14% of the *f* decrease remained following washing and resulted in the stabilisation of *f* at a new level that was lower than the pre addition level suggesting there remained some adsorption to the surface of the nanoparticles. This was accompanied by a decrease in *d* from its increased level which was observed following the addition of the nanoparticles to the surface. This would suggest that the adsorbed particles were irreversibly adsorbed to the surface, with the wash steps removing only the unbound or loosely associated nanoparticles (Fogel, Mashazi et al. 2007).

Surface chemistry is known to influence the adsorption of a variety of molecules (Morrison 1990). It was, therefore, hypothesised that altering the surface chemistry would alter the binding capabilities of the 21nm nanoparticulates. This hypothesis was tested using HA coated quartz crystals. As on the gold surfaces, despite wash steps, a proportion of the *f* shift due to nanoparticulate addition was retained on the HA surface. However, in this instance, 25% of the *f* shift was maintained suggesting a greater portion of the nanoparticulates were able to adsorb to the surface. It could be due to the change in surface chemistry. However, surface topography (roughness) has also been indicated

to either enhance or diminish the adsorption of molecules (Galli, Collaud Coen et al. 2002). The HA coating is created using the electrophoretic deposition method, which produces a continuous layer of high crystallinity HA 10-20nm thick onto a titanium oxide or gold coated crystal. The creation of the HA layer increased the surface roughness of the crystals from 0.97nm for a gold crystal to 6.31nm for HA coated crystals (Monkawa, Ikoma et al. 2006). It can, therefore, be suggested that the enhanced surface roughness of the HA coated crystal could also influence the adsorption potential of the 21nm nanoparticles, in conjunction with the altered surface chemistry.

Although HA coated discs can be used as a more physiologically relevant surface to investigate the creation of nanoparticulate coatings for oral care, its surface chemistry still varies from that of dentine. Dentine is comprised of both organic (collagen-like) and inorganic (HA) phases. The combined effect of these components may also enhance surface adsorption of the nanoparticles. The HA coated crystals are also unable to account for the structure of the dentine, as the presence of the dentine tubules could also affect the adsorption potential of the nanoparticles. The possibility of adhering a dentine disc to a gold coated quartz crystal was investigated. It was hoped that this would allow the QCM-D to be used to investigate a surface that was structurally and chemically relevant to this project. However, as mentioned in the results section, this was not easily achieved. The adhesive used to adhere the dentine to the surface had to be sufficiently thin and rigid to prevent dampening of $f$ and allow continuation of the oscillating $f$ through the dentine. If the disc was not securely and rigidly adhered to the crystal, there would be slipping of the disc upon application of a resonant $f$ that would prevent calibration of the crystal. The dentine disc also had to be sufficiently thin in order to prevent dampening of $f$ that would prevent measurements of $d$. If the height of the disc was above 0.1mm, the upper surface of the dentine would make contact with the upper wall of the sensor cell. Upon application of a resonant $f$ to the crystal, the oscillations would be quickly dampened again, preventing calibration of the QCM-D. To maximise the potential and sensitivity of any $f$ and $d$ readings, the dentine discs were created with a diameter of 2.6mm to fit in the central area of the crystal where sensitivity is a maximum (Andersson, Andersson et al. 2005; Berglin, Olsson et al. 2008). This also minimised

the possibility of contact between the dentine disc and the sensor cell walls, reducing the possibility of *f* dampening.

Attachment of a dentine disc to the crystal surface was attempted several times, from which it was only possible to successfully gain *f* and *d* calibrations and, therefore, readings for two samples, only one of which demonstrated *f* and *d* stability which enabled the effect of nanoparticulate silica addition to be investigated. The unreliability of creating dentine discs adhered to crystal that would result in *f* and *d* measurements being obtained could be due to the internal dentine structure. Dentine can be viewed as a specialised connective tissue. However, dentine is not a continuous tissue but is comprised of tubules. The dentine tubules radiate from the dental pulp throughout the entire thickness of the dentine. The tubules are about 1-3$\mu$m in diameter with about 30,000 tubules per $mm^2$ with an even higher density closer to the pulp (Hildebrand, Fried et al. 1995). Between different dentine discs, the structure and dimensions of the tubules can vary. Therefore, the inconsistency of the production of dentine discs which would allow *f* and *d* readings to be obtained could be due to the variability of the structure of the dentine discs. The structure of some of the dentine discs does not permit the effective continuation of the *f* through the dentine, preventing calibration of the QCM-D and measurements of *f* and *d* being obtained.

The structure of the dentine also resulted in secondary problems. When it was possible to gain *f* and *d* calibrations, a prolonged period of time had to be spent re-hydrating the dentine. Dentine is highly porous and has a high water content. As the sensor surface needs to be dry to be placed in the sensor cell, the dentine has to be dehydrated prior to use. However, when fluid was then reintroduced to the dentine within the sensor cell, a prolonged period of time was required to allow the dentine to rehydrate and stabilise. This process was hampered by the porosity of the dentine, which resulted in the formation of air bubbles. Air bubbles can cause erratic *f* drifts so need to be removed prior to the start of any experimentation on the surface.

The results shown should therefore be viewed with caution due to the lack of reproducibility. However, it is still interesting to note the decrease in $f$ observed upon addition of that nanoparticulate silica to the dentine surface is not reversed following washing. Despite washing, there were no increases in $f$ but the accompanying decrease in $d$ would suggest that the mass adsorbed to the surface is rigidly attached (Fogel, Mashazi et al. 2007). It is hypothesised that the nanoparticles are able to enter the open dentinal tubules, becoming trapped, and, therefore, are not removed with washing. This hypothesis would also explain why upon addition of an excess of silica there was a further decrease in $f$. However, in this instance, following washing there was an increase in $f$ but not back to the original pre-excess addition level to a new lower level. This would indicate that, although some of the additional nanoparticles were not adsorbed to the surface and were removed, some were able to form strong attachments and remained on the surface. This would suggest that, following addition of an excess of silica, the surface had reached saturation point and no further nanoparticulate adsorption could occur. The apparent increase in adsorption of nanoparticulates to the dentine surface may be due to the combined effect of altering the surface chemistry and the porosity of the surface. Never the less, the ability of the nanoparticles to enter the dentinal tubules would be a very desirable attribute for the application of a desensitizing agent. As such this hypothesis requires further experimentation and analysis, as these results are inconclusive but appear to indicate a highly significant ability.

In previous studies, the creation of a polymer binding layer, prior to the addition of the nanoparticulates, was used to alter the surface charge, and increase the adsorption of nanoparticles (Wagberg, Pettersson et al. 2004; Cousins 2005) . Using the QCM-D, it was possible to monitor the creation of both the polymer binding layer and the nanoparticulate silica coating. With the TEM (chapter 2), it was observed that, in the presence of a polymer binding layer an effective coating of nanoparticles across the test surface could be achieved. Data from the QCM-D supported this observation. It was observed that on gold surfaces, for both polymers and at both concentrations, a minimum of 80% of the $f$ shift was maintained following washing, therefore indicating that a nanoparticulate coating had been achieved. It can also be noted that the overall $f$

shift upon addition of the nanoparticles to the surface was greater in the presence of a polymer binding layer. This indicates that the polymer coated surfaces were able to aid the adsorption process by altering the surface charge and, therefore, creating a surface with which the nanoparticles would readily adsorb (Wagberg, Pettersson et al. 2004). This is evidenced by the comparatively small $d$ shifts and would suggest that the adsorption process is fast, with the surface binding positions quickly becoming saturated. Comparison with the $d$ as a function of the $f$ shift can often identify the various phases undergone during adsorption (Fogel, Mashazi et al. 2007). When this was explored, it was apparent there are 2 stages to the $f$ shift, due to the addition of the nanoparticles to a polymer coated surface (figure 3.7). The initial, steady incline would therefore suggest the rigid adsorption of the nanoparticles to the surface.

As discussed, the QCM-D enabled the monitoring of both the polymer and nanoparticulate stages of the coating process. This was of great interest, as it was not possible to use the TEM to visualise the polymer coating in the absence of the nanoparticles. It was apparent that the binding curves produced by the addition of the two different polymers to the gold surface varied considerably. This indicated that there are two different methods of adsorption. When UCARE™ polymer JR -125 was used there was a large sharp decrease in $f$ and then a plateau. This was in stark contrast to the small initial drop in $f$ that was followed by a continuous gradual decrease when Zetag™ 7109 was used. These differences may be related to the manner in which the polymers adhere to the surface. It can be suggested that the lower molecular weight, and therefore smaller chain length of the UCARE™ polymer, minimizes the possibility of the polymer chains interacting and becoming entangled. This increases the possibility of the chain unfolding in solution. If it is assumed that the chain is in an unfolded state, it can be suggested that the polymer is adhering to the surface in an unfolded conformation. This results in uniform adsorption, indicated by the sharp decrease in $f$ upon addition to the surface. The longer chain length of the Zetag™ 7109 polymer will increase the interactions between the chains. This may lead to increased coiling within the solution. (Teraoka 2002), and could result in the adsorption of the polymer chains onto the surface in the coiled form. Adsorption may lead to a conformational change in the polymer due

to the formation of new bonds. This could initiate the uncoiling of the polymer forming a rigidly adsorbed layer and explain the dual phases of the observed binding curve.

It is important to note that despite the apparent differences in the adsorption processes of the two polymers, both of them resulted in similar binding curves with the addition of the nanoparticles. There were similar decreases in $f$ on addition of the nanoparticles to both polymer coatings, and, following washing, a similar level of the $f$ shift was conserved, with 88% on the Zetag™ 7109 coated surface and 90% on the UCARE™ Jr-125 coated surfaces retained. Therefore, it can be surmised that both polymer coatings were able to act as an effective binding layer for nanoparticulate adsorption.

When the HA coated crystals were used the binding curve produced from Zetag™ 7109 addition closely resembled that of the UCARE™ Jr-125 polymer on the gold surfaces. The $f$ decrease on addition of the Zetag™ 7109 polymer was thirty times greater on the HA surfaces in comparison to gold. The increased $f$ shift was accompanied by a sixteen times greater increase in $d$. Unlike on the gold surfaces, the $d$ increase did not diminish as the coating was allowed to settle and, following washing was maintained at the same level. It could be suggested that the Zetag™ 7109 polymer coating has an increased viscosity when adhered to the HA surfaces, which would suggest that the polymer chains are adhering in the coiled state and are unable to uncoil once adsorbed onto the surface. This would account for the increased $d$ because, when a polymer is in the coiled state, it will include water and solvents which have become incorporated within the polymer molecule (Young 1981). The increased $f$ and $d$ shifts observed on the HA coated surface, could be explained by. that as the $f$ change is associated with the total mass loading, including the water and solvent ions that may be associated with the adsorbing polymer (Roach, Shirtckiffe et al. 2006). This was represented by the increased $d$ which would indicate that a more viscoelastic coating had been achieved in comparison with the gold coated surface. It can be hypothesised that there is a greater surface affinity of the polymer chain for the HA coated surface, as altering the surface chemistry has been shown to influence the binding of molecules, such as proteins (Roach, Eglin et al. 2007) . If the surface affinity of the polymer was increased, it could

induce the rapid saturation of the surface and would hinder the uncoiling of the polymer, due to spatial constraints.

However, it should be noted that any conformational alterations resulting from adsorption to the HA coated surfaces had no effect on the binding affinity of the nanoparticles for the surface. A similar decrease in $f$ was observed for both surfaces when 0.03g/l of the Zetag™ 7109 polymer was used, with 91% of the $f$ shift being maintained on the surface following washing. When the ability of the coatings to withstand a shear force in the form of a continuous flow of distilled water was assessed, it was apparent that all the coatings tested were able to withstand the flow conditions for a period of 16 hours. Lowering the molecular weight and concentration of the polymer used to create the binding layer and changing the test surface, had no effect on the coatings' ability to withstand fluid flow.

Protein adsorption onto surfaces is of relevance to a wide audience, including biochip developments, biosensors, drug delivery and biomaterials (Roach, Farrar et al. 2006). The oral environment is no different; the adsorption of salivary proteins onto dentine and enamel surfaces forms a vital step in the protection of both these mineralised tissues and the oral health of the mouth (Whelton 2004). The importance of this coating is its ability to minimise demineralisation during acid attack, forming a protective layer over the dental surface, and it can also facilitate the remineralisation process (Hannig and Balz 2001; ten Cate 2004). Saliva is the glandular secretion that constantly bathes the teeth and the oral cavity. It is comprised predominantly of water but it also contains several inorganic constituents, such as sodium, potassium, calcium, chloride and hydrogen carbonate, and organic compounds (proteins), such as serum albumin, mucins immunoglobulins and histatins (Schenkels, Veerman et al. 1995; Whelton 2004). Saliva has several important functions within the oral cavity, including lubrication, acting as a buffer to neutralize pH and, also, in pellicle formation. A pellicle is a thin (1-10 $\mu$m) protective diffusion barrier formed on enamel from salivary proteins (ten Cate 2004). It was for these reasons the difference in the binding curves for the adsorption of the artificial salivary components was of interest.

The adsorption of proteins onto surfaces is a complex process. Proteins may adsorb in differing quantities, densities, conformations and orientations, depending on the chemical and physical characteristics of the surface (Roach, Farrar et al. 2005). Protein adsorption is a dynamic process and may involve binding, rearranging and detachment. It can involve van der waals forces, hydrophobic and electrostatic interactions and hydrogen bonding. Surface chemistry has been shown to play a fundamental role in the protein adsorption process (Roach, Farrar et al. 2005; Deschaume, Shafran et al. 2006; Roach, Farrar et al. 2006; Welle, Chiumiento et al. 2007). The QCM-D was used in this study to monitor the adsorption of proteins contained within the artificial saliva, including mucins and albumin. It was possible to measure the effect of artificial saliva flow on both gold and HA surfaces as well as HA and gold surface subsequently coated in 0.03g/ Zetag™ 7109 and Ludox® TM-50.

Comparison of the gold and HA surfaces revealed that, although on both surfaces artificial saliva flow resulted in a large initial decrease in $f$, on the HA surface, it was followed by many fluctuations, including increases and decreases in $f$ and $d$ over the time course of the experiment. However, on the gold surface, there was a continuous steady decline in $f$ until washing. This would suggest there are several fundamental differences in the adsorption process on the two samples.

The large initial decrease in $f$ on the gold coated surfaces may be attributed to the high affinity of the serum albumin present within the solution for hydrophobic surfaces. Serum albumin has been shown to have a high affinity for gold surfaces, is thought to be due to the formation of covalent sulphur- thiol linkages (Stadler, Mondon et al. 2003) This would account for the rapid decrease in $f$ observed that was not reversed following washing, indicating that the initial decrease was due to the irreversible adsorption of proteins onto the surface. This protein layer would then be accessible for further interactions with the inorganic and organic components of the saliva, which would also explain the continual slow decrease in $f$ that was accompanied by an increase in $d$ following the initial decrease. In the final 500mins of flow, there was a steeper decrease

in the *f*. However, following washing, the *f* change that occurred during this period was easily removed. Analysis of the *d* readings would suggest that the adsorption of molecules, which resulted in the *f* increase observed in the final 500mins, was water rich and, with the ease of removal, it can be suggested that the *f* shift was due to the formation of loose reversible attachments with the newly created adsorbate layer (Chitpan, Wang et al. 2007).

The fluctuations in both *f* and *d* observed on the HA coated surfaces may be attributed to the dynamic nature of protein adsorption, involving adsorption and desorption from the surface (Feiler, Sahloholm et al. 2007; Roach, Eglin et al. 2007). It may be suggest that following creation of an adsorbate layer, represented by the initial sharp decrease in *f*, there are several adsorption, desorption processes occurring on the newly acquired protein layer as demonstrated by the steady decrease in *f* over time. The differences in the binding curve would suggest that altering the surface chemistry has altered the composition of the adsorbate layer, although this can not be proven conclusively without further analysis of the protein composition of the acquired coating.

In the presence of the nanoparticulate silica coating, there were further difference in the binding curves produced. On both HA and gold surfaces, there was a fast initial decrease in *f*, which was followed by a plateau. However, unlike on the gold surface, in the absence of a nanoparticulate coating, this was followed by a plateau prior to a small secondary decrease during the final 400 mins. On the HA surfaces, the presence of the coating resulted again in a plateau following the initial decrease but during the final 400mins there was a steady but small increase in *f*, unlike on the HA surfaces where there were several fluctuations in both *f* and *d* over the time of the experiment. On the HA surfaces, the presence of the nanoparticulate coating also altered the initial sharp decrease in *f*. There was a small initial decrease, which was followed 5 minutes later by a second larger decrease. These differences in the binding curves would suggest that both the underlying surface chemistry and the increased surface topography have affected the protein adsorption process.

The large *d* increase that accompanied the secondary decrease in *f* on the nanoparticulate coated gold surfaces would suggest that this *f* shift was caused by the adsorption of loosely affiliated molecules and any adsorption layer produced is highly viscous. This hypothesis was supported, as following washing, the *f* shift that occurred during this time period was quickly reversed as was the *d* shift. The stability of the *f* following the initial decrease may be due to the conformation of the protein adsorbing to the surface being altered. The role of surface topography in the protein adsorption process is a relatively new area of interest, albeit a growing one. It has been demonstrated that altering the surface topography or curvature of a surface on the nanometre scale can have an impact on the conformation of the bound protein (Roach, Farrar et al. 2005). The increased curvature of the nanoparticulate coated surfaces may, therefore, alter the conformation of the bound protein and obscure further adsorption sites, preventing the further steady secondary decrease in *f* observed on the gold surfaces. Other studies have demonstrated that the presence of a nanoparticulate silica coating resulted in significant differences in the adsorption of proteins from a growth media compared to a silica surface. When the composition of the protein coating was probed with an assay, there appeared to be a reduction in fibronectin adsorption despite comparable levels of protein adsorption being observed with QCM-D for the two surfaces. It was suggested that the conformation of the fibronectin on the nanoparticulate coated surface was altered, hiding or stericly hindering binding sites for the assay (Lord, Cousins et al. 2006). Therefore, suggesting that the lack of secondary binding observed, following the initial decrease on the nanoparticulate silica coated HA and gold surfaces, is due the surface topography altering the conformation of the proteins that adsorb in the initial *f* decrease, masking the binding sites for possible secondary binding to the newly created coating.

The two stages to the initial decrease in *f*, observed on the nanoparticulate coated HA surfaces would suggest surface rearrangement of the adsorbed protein layer was occurring. The initial rapid decrease maybe linked with the adsorption of smaller proteins within the artificial solution that are able to reach the surface first and saturate the surface binding sites. However, rearrangement of the protein layer could allow further protein adsorption, possibly larger proteins that would be thermodynamically

preferable to adsorb to the surface in the place of the smaller proteins. This would result in the second sharp decrease in $f$ that was greater than that observed in the first instance. which was accompanied by an increase in $d$, an indication that the secondary layer is highly viscous and may involve the incorporation of a large water content. It may explain the increase in $f$ and accompanying decrease in $d$ over the final 400mins that may be related to a loss of fluid from the adsorbed layer, as suggested by the decrease in fluidity represented by the steady decrease in $d$.

The results obtained using the QCM-D have been informative allowing the real-time monitoring of the process by which the coatings adhere and the creation of an adsorbed protein coating. However, the adsorption of proteins to surfaces is a complex process and although the QCM-D has indicated that the adsorption of molecules does occur it is unable to offer any insight into the composition of the adsorbed layer, therefore further work is required.

# Chapter 4

## In- vitro dentine permeability evaluation of the nanoparticulate coatings as a method for occluding dentinal tubules

*This chapter explains the procedure for creating nanoparticulate coatings on dentine for permeability analysis. In this study, the use of different molecular weight polymers and chlorhexidine (a common component of oral rinses or washes) were investigated. Based on Pashley's hydrodynamic model for dentine sensitivity, measurements of hydraulic conductance compared in the form of a percentage reduction in fluid flow. Hydraulic conductance, is a standard test of the ability of a possible agent to coating to reduce fluid flow via occlusion of the dentinal tubules and, thus, an indication of their effectiveness as a desensitising agent.*

### 4.1. Introduction

#### 4.1.1 The Hydrodynamic Theory

As discussed previously, (chapter 1) teeth exhibiting dentine sensitivity, have many more, and wider, dentinal tubules open at the dentine surface and patent to the pulp (Banfield and Addy 2004). This is consistent with the hydrodynamic theory of dentine sensitivity. The hydrodynamic theory states that the rapid displacement of the dentine tubule contents at the pulp-dentine border excites mechanosensitive nerve endings, inciting a pain response (Seltzer 1971; Brannstrom and Astrom 1972; Dowell and Addy 1983). To prevent dentine sensitivity a logical conclusion is tubule occlusion. Occluding the tubules blocks fluid movement and, therefore, desensitized the dentine (Gillam, Mordan et al. 1997).

#### 4.1.2 Dentine permeability and hydraulic conductance

Based on the hydrodynamic theory, dentine permeability is often used as an in-vitro method of measuring tooth sensitivity and measuring the effectiveness of potential desensitizing agents, to occlude the dentinal tubules and prevent sensitivity. A model for investigating dentine permeability was first proposed by Pashley in 1974 and was

based on a split cell chamber. A dye was used to measure fluid flow through the tubules and therefore permeability of the dentine (Gillam, Mordan et al. 1997). The method quantifies dentine permeability, using its hydraulic conductance. The hydraulic conductance measure the ease with which fluid can shift across a unit surface area of dentine, in a unit of time, under a unit of pressure gradient (Pashley 1996). A split level chamber was used wherein thin slices (approximately 1mm thick) of coronal dentine from human third molars were placed between fixed surface area plexi glass reservoirs, one end of which could be attached to a source of hydrostatic pressure and the other to a means of measuring flow rate or to collect diffusal fluid (Gillam, Mordan et al. 1997). Many investigations have used either Pashley's flow cell method or a slightly modified version of his original flow cell to investigate dentine permeability. Investigations have shown that hydraulic conductance can be affected by the thickness of the dentine slice, the presence of a smear layer and the number of open dentinal tubules (Gillam, Mordan et al. 1997).

The general practice for measuring hydrodynamic conductance still relies on a split level chamber, in which a dentine disc is clamped between two O-rings, creating a fixed surface area for testing. The split cell chamber is linked on one side to a micropipette and a reservoir of fluid at a constant pressure. The linear displacement of a bubble in the micropipette is converted into a volume and used to measure fluid flow via the dentine disc (Gregoire, Guignes et al. 2005). By combining the hydrostatic pressure, the area of the dentine surface and the time taken for the fluid shift, the hydraulic conductance (Lp) of the dentine can be calculated using the following equation:

$$Lp = \frac{Jv}{A\ (\Delta P)}$$ (Cherng, Chow et al. 2004)

Jv = fluid flow rate ($\mu l min^{-1}$)

A = dentine surface area ($cm^2$)

$\Delta P$ = hydrostatic pressure gradient across the dentine disc (cm of $H_2O$)

Lp = hydraulic conductance ($\mu l cm^{-2} min^{-1} H_2O cm^{-1}$)

Due to the biological variability of dentine in hydraulic conductance experiments, each dentine specimen acts as its own control, with a base reading prior to treatment and a

second reading following treatment. These are then expressed as a relative rather than absolute value (Gregoire, Guignes et al. 2005). This is mainly due to the variation in the incidence and size of the dentine tubules between samples which can lead to large variations in standard deviation (Pereira, A.D. Segala et al. 2005).

Hydraulic conductance is a good indication of the ability of a potential desensitising agent to occlude the dentinal tubules. As such, hydraulic conductance was used in this study to monitor the ability of the silica nanoparticulate coatings to occlude the tubules and thus diminish dentine permeability. The effect of different polymers and chlorhexidine, a commonly used chemotherapeutic for oral care, (Pietruska, Paniczko et al. 2006) and the "one-step" sonicated UCARE™ polymer JR-125 and Ludox® HS-40 on hydraulic conductance was explored. The results were expressed as a percentage reduction in hydraulic conductance and the mean values for each treatment group of six samples are shown.

## 4.2 Materials

Bovine dentine discs were obtained from teeth donated by GlaxoSmithKline, Weybridge. Two polymers, Zetag™ 7109 (Ciba Scientific) and UCARE™ polymer JR-125 were used to create coatings with a variety of Ludox® silica sols, having average particle sizes of 7,14 and 21nm (as previously described section 2.2). A solution was prepared as described in section 2.3.3 method one of UCARE™ polymer JR-125 and Ludox® HS-40 (14nm) through ultrasonic mixing and was also tested. As a control, chlorhexidine digluconate (figure 4.1), a commonly used antimicrobial agent was also tested. Chlorhexidine is used in many oral treatments, including the over-the counter mouth rinse Corsodyl™ (GlaxoSmithKline). It has exhibited an action against fungi and both gram negative and positive bacteria in the treatment of periodontitis (Pietruska, Paniczko et al. 2006). It is hypothesised that the chlorhexidine will render the surface positive in the same manner as the cationic polymer, facilitating nanoparticulate adhesion to the surface.

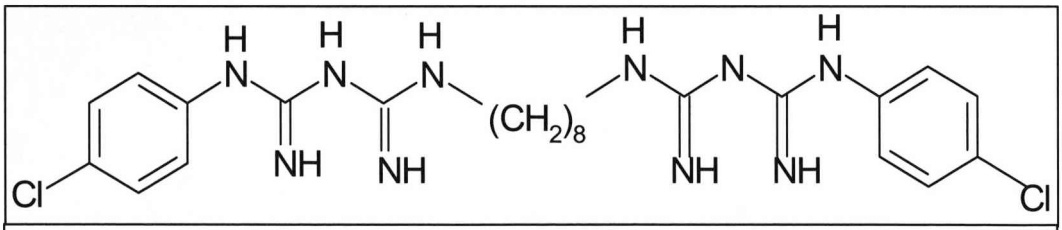


**Figure 4.1** The chemical structure of the anti microbial agent Chlorhexidine.

## 4.3 Methods

### 4.3.1 Preparation of the dentine discs

As in chapter 3, dentine discs were prepared from Bovine teeth donated by GlaxoSmithKline, Weybridge, UK using a slow speed saw.

1. Cut dentine discs were polished using 4,000 grit silicon carbide paper, to a thickness of 0.4mm.
2. The samples were submerged in 6% (w/v) citric acid and placed in a sonic bath for 10 minutes.

3. The samples were rinsed in $dH_2O$ for 5 minutes.

### 4.3.2 Measurement of hydraulic conductance

A modified Pashley flow cell, consisting of two parts, was used to measure the hydraulic conductance (figure 4.2)

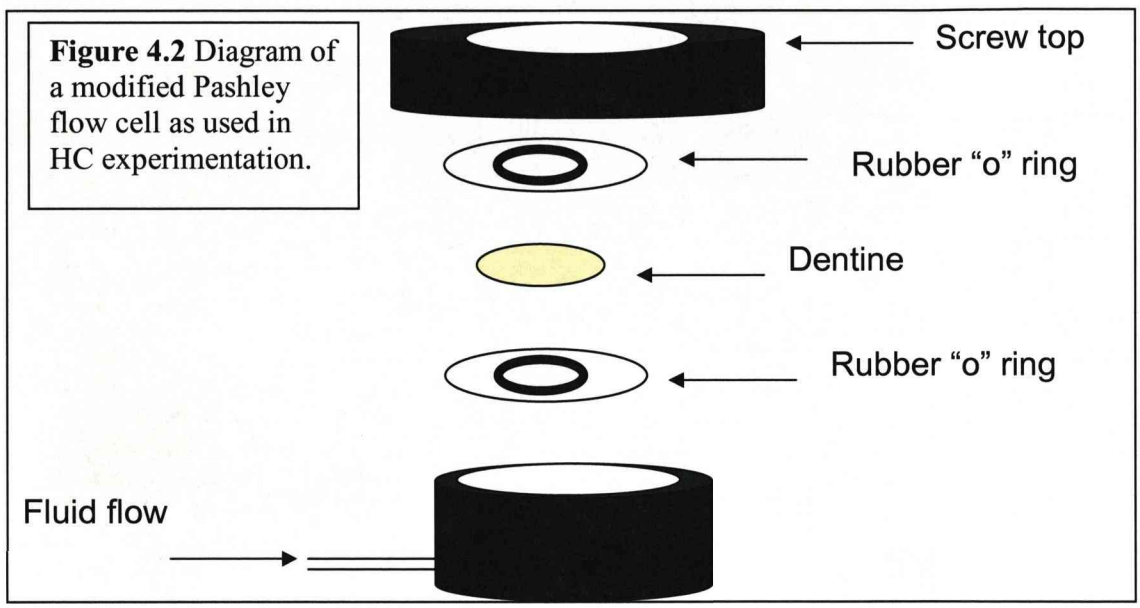


**Figure 4.2** Diagram of a modified Pashley flow cell as used in HC experimentation.

The lower part was connected via a three way tap to a glass capillary with a diameter of 3.8mm and a metal ruler running alongside its 20cm length (figure 4.3). This was positioned 1.4m below a reservoir of Earle's solution ($NaH_2PO_4$ 0.122g/l, NaCl 6.9g/l, $NaHCO_3$ 2.2g/l, KCl 0.4g/l. $MgSO_4$ 0.09g/l and $CaCl_2 \cdot H_2O$ 0.265g/l in $dH_2O$). Also attached to the three way tap was a syringe containing Earle's solution for introduction of an air bubble.

1. Dentine discs were clamped in the flow cell between two O-rings.
2. A bubble is introduced to the glass capillary using the syringe.
3. The position of the bubble was recorded and the tap moved to allow flow from the capillary into the flow cell.
4. After 30 minutes, the position of the bubble in the capillary was recorded ad flow stopped.

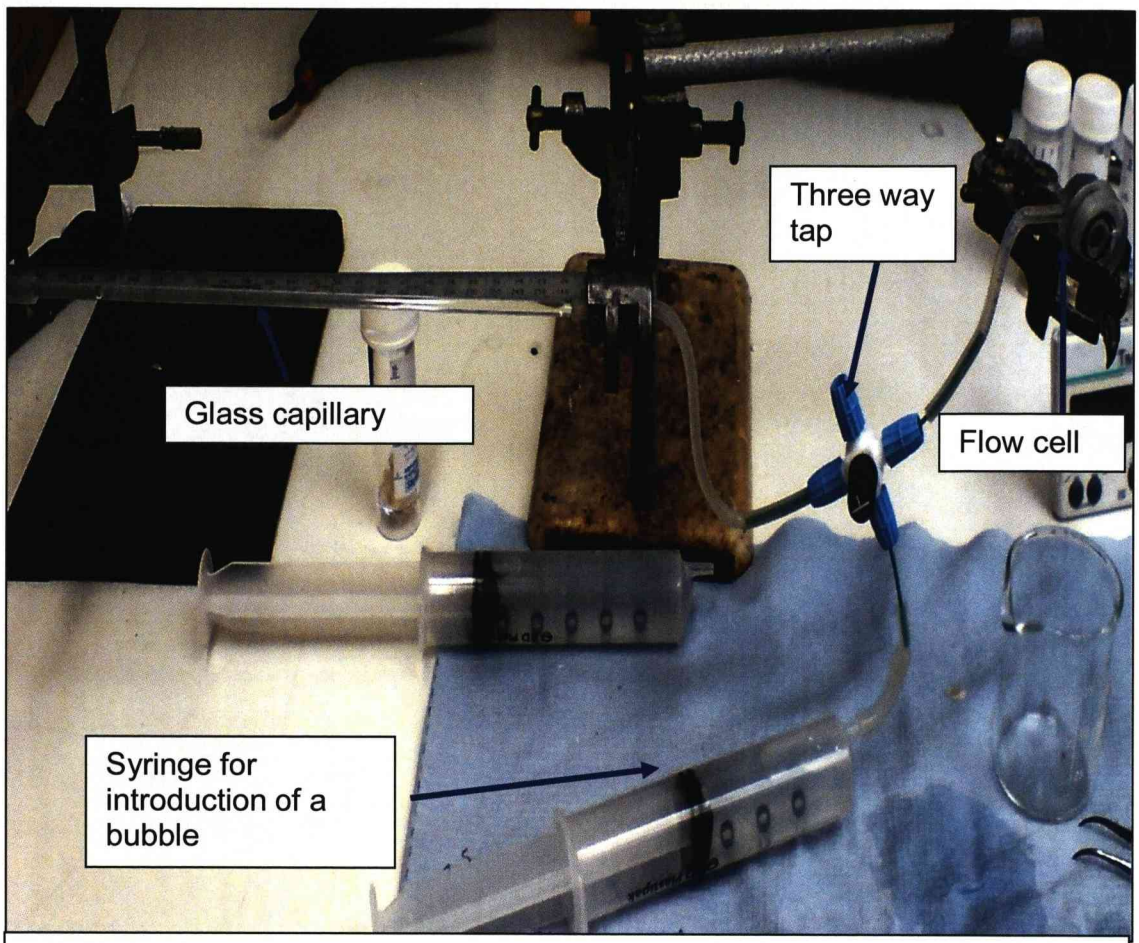


**Figure 4.3** The hydraulic conductance experimental set up.

### 4.3.3 Treatment of dentine

As discussed in section 4.1.2., due to the structural variability between dentine samples, each dentine disc acts as its own control. After taking an initial baseline reading of hydraulic conductance, the samples were treated by one of the following two methods and a second post treatment hydraulic conductance was measured.

Method 1

One step coating procedure.

1. Dentine discs had 250$\mu$l of test solution added to the coronal surface.
2. A dental applicator brush (Dentsply) was used to manipulate the solution over the surface for 2 mins.
3. The sample was rinsed in copious amounts of $dH_2O$

4. The dentine disc was placed in 8ml of artificial saliva (as described in section 3.3.4) in an incubator set at 37°C for 1 hour.
5. The sample was rinsed in $dH_2O$ and placed back in the hydraulic conductance chamber
6. As described in section 4.3.2., a second hydraulic conductance reading following treatment was then made.

a) Influence of silica sol:
   Three different silica sols were used in step 1: Ludox® SM-30 (7nm particle diameter), Ludox® HS-40 (14nm particle diameter), and Ludox® TM-50 (21nm particle diameter).
b) Influence of a polymer chemistry:
   Two different polymer solutions were tested in step 1: 0.3g/l of Zetag™ 7109 and 0.3g/l UCARE™ polymer JR-125.
c) Influence of a Chlorhexidine:
   In step 1 20% (w/v) of chlorhexidine was used.
d) Influence of a "one-step" coating:
   The "one-step" preparation of UCARE™ polymer JR-125 sonic mixed with Ludox® HS-40 (as described in chapter 2) was used in step 1.

Method 2

A two step method for creating a nanoparticulate coating, consisting of a binding layer and followed by the addition of a silica sol to create the nanoparticulate layer.

1. Dentine discs had 250$\mu$l of a binding solution added to the coronal surface.
2. A dental applicator brush (Dentsply) was used to manipulate the solution over the surface for 2 minutes.
3. The dentine disc was rinsed in copious amounts of $dH_2O$
4. The dentine disc had 250$\mu$l of Ludox® silica sol added to the coronal surface.
5. A dental applicator was used to manipulate the solution over the surface for 2 min

6. The sample was rinsed in copious amounts of $dH_2O$
7. The dentine disc was placed in 8ml of artificial saliva in an incubator set at 37°C for 1 hour.
8. The dentine disc was rinsed in copious amounts of $dH_2O$.
9. As previously described, a second reading of hydraulic conductance post treatment was taken.

a) Influence of the silica sol:

   Three different silica sols were used in step 4: Ludox® SM-30 (7nm particle diameter), Ludox® HS-40 (14nm particle diameter), and Ludox® TM-50 (21nm particle diameter).

b) Influence of a polymer chemistry:

   The polymer solution in step 1 was either 0.3g/l Zetag™ 7109 or 0.3g/l UCARE™ polymer JR-125.

c) Influence of a Chlorhexidine:

   In step 1 20% (w/v) of Chlorhexidine was used.

Table 4.1 lists all the coatings investigated, using the hydraulic conductance method. For each treatment tested there were six repeats.

| Polymer / Silica | None | Zetag™ 7109 | UCARE™ polymer JR-125 | Chlorhexidine |
|---|---|---|---|---|
| **None** | | • | • | • |
| **Ludox® SM-30 (7nm)** | • | • | • | |
| **Ludox® HS-40 (14nm)** | • | • | • | |
| **Ludox® TM-50 (21nm)** | • | • | • | • |
| **Sonic mixed Ludox® HS-40 and UCARE™ polymer JR-125** | • | | | |

**Table 4.1** Table of different coatings investigated using hydraulic conductance.

**4.4. Results**

To calculate the hydraulic conductance of the dentine discs, the fluid flow (Q) was first established. Q was calculated from the distance travelled by the bubble in the glass capillary and the known radius of the capillary (1.9mm). Q was then used in the following equation to calculate hydraulic conductance of the sample.

$$Lp = \frac{Q}{A.\ P.\ t}.$$

Lp = hydraulic conductance ($\mu lcm^{-2}s^{-1}kPa^{-1}$)

Q = fluid flow ($\mu l$)

A = dentine surface area ($1.96cm^3$)

P = hydraulic pressure (80kPa)

t = time (1800s)

Both A, P and t are constants. P was calculated using the height of the reservoir from the capillary and the weight of 100ml of Earle's solution, in conjunction with the experimentally arrived volume of fluid flow through the system in one minute in the absence of a dentine disc.

A percentage reduction in hydraulic conductance was calculated for wash sample using the following equation:

$$\% \text{ reduction in } Lp = \frac{Lp_B - Lp_A}{Lp_B} \times 100$$

$Lp_B$ = hydraulic conductance of the dentine disc before treatment.

$Lp_A$ = hydraulic conductance of the dentine disc after treatment

The percentage reductions in hydraulic conductance for each treatment group of 6 dentine discs were then averaged, giving a mean percentage reduction in hydraulic conductance for each treatment, which was plotted on the charts along with the standard deviation as error bars. Statistical analysis was performed using SPSS. The paired t-test with a p-value of 0.05 was used to establish statistical differences between the hydraulic conductance before and after treatment for each of the sample groups. The one way

ANOVA test was used to establish any statistical differences between the different treatment groups.

### 4.4.1. Method 1 (one step treatments).

a) Influence of a silica sol.

Figure 4.4 demonstrates that all three Ludox® silica sols resulted in a percentage decrease in hydraulic conductance following treatment. The paired t-test established that the observed reduction in hydraulic conductance, following nanoparticulate silica sol treatment, was statistically significant at the 95% confidence interval. Although the 21nm diameter silica sol (Ludox® TM-50) appears to have resulted in the greater percentage reduction of hydraulic conductance, statistical analysis with te one way ANOVA post hoc test identified no significant differences between the silica treatments at a 0.05 significance level.

b) Influence of a cationic polymer:

The use of both Zetag™ 7109 and UCARE™ JR-125 resulted in a percentage decrease in hydraulic conductance following treatment (figure 4.4.). The paired t-test established that there was a significant difference in the hydraulic conductance readings before and after treatment for both polymers at the 0.05 significance interval. Using the one way ANOVA test, it was shown that there was no statistical difference between the two polymer treatments.

c) Influence of chlorhexidine:

The observed mean percentage reduction in the hydraulic conductance of 55% following chlorhexidine treatment was shown to be statistically insignificant, using the paired t-test.

d) Influence of a "one-step" coating (ultrasonic mixed Ludox® HS-40 and UCARE™ polymer JR-125).

The reduction in hydraulic conductance following treatment with the one-step solution of ultrasonic mixed Ludox® HS-40 and UCARE™ polymer JR-125 was shown to be statistically significant, using the paired t-test.

Although all of the method 1 treatments, apart from chlorhexidine, resulted in a significant reduction in hydraulic conductance using the paired t-test, the one way ANOVA post hoc test failed to establish any significant differences between the different treatments. It was however apparent that there was a trend for increasing reduction in %Lp with increasing particle size.

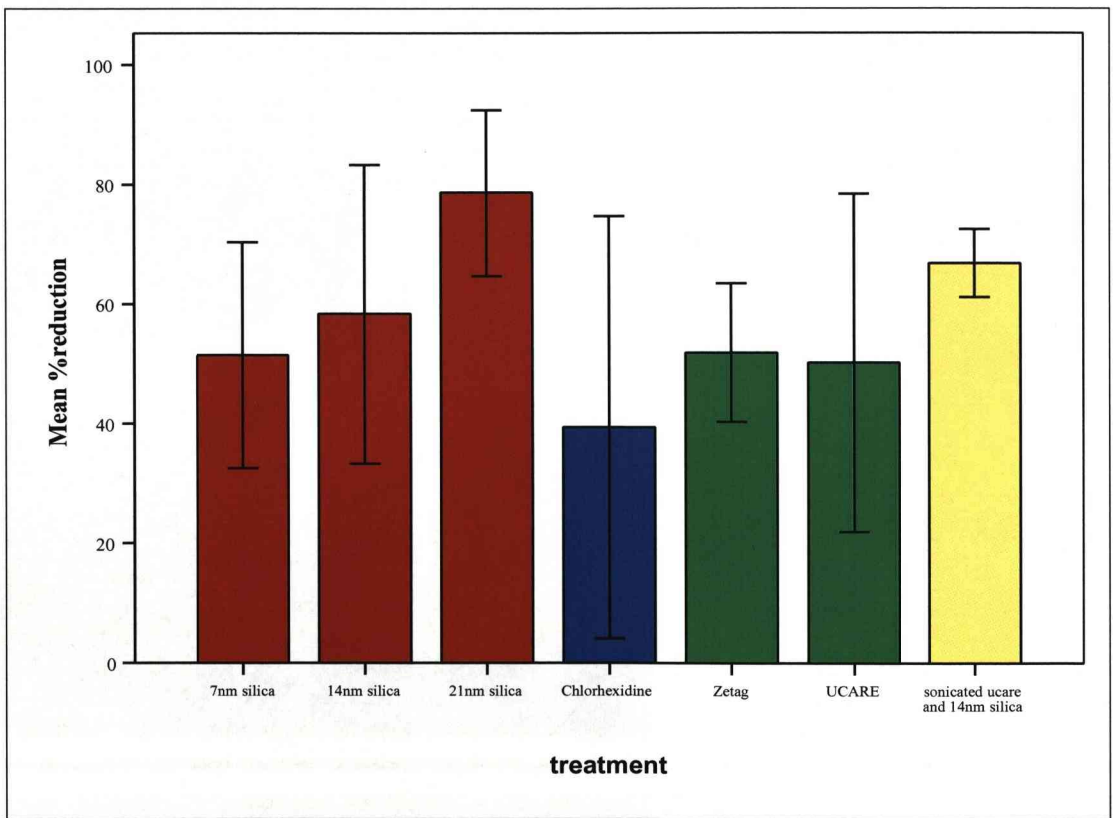


**Figure 4.4** Graph showing the effect of method 1 treatments on the mean %Lp reduction.

### 4.4.2 Method 2 (two step coating procedure)

a) Influence of the silica sol:

Figure 4.5 depicts the effect of a two step coating procedure using the Zetag™ 7109 polymer and the three different diameter Ludox® silica sols. Using the paired t-test all the observed reductions in hydraulic conductance, following treatment of the samples with Zetag™ 7109 and a Ludox® silica sol, were shown to be significant at a 95% significance interval, with p values of 0.009, 0.003 and 0.007 for the 7, 14 and 21nm silica sols respectively.

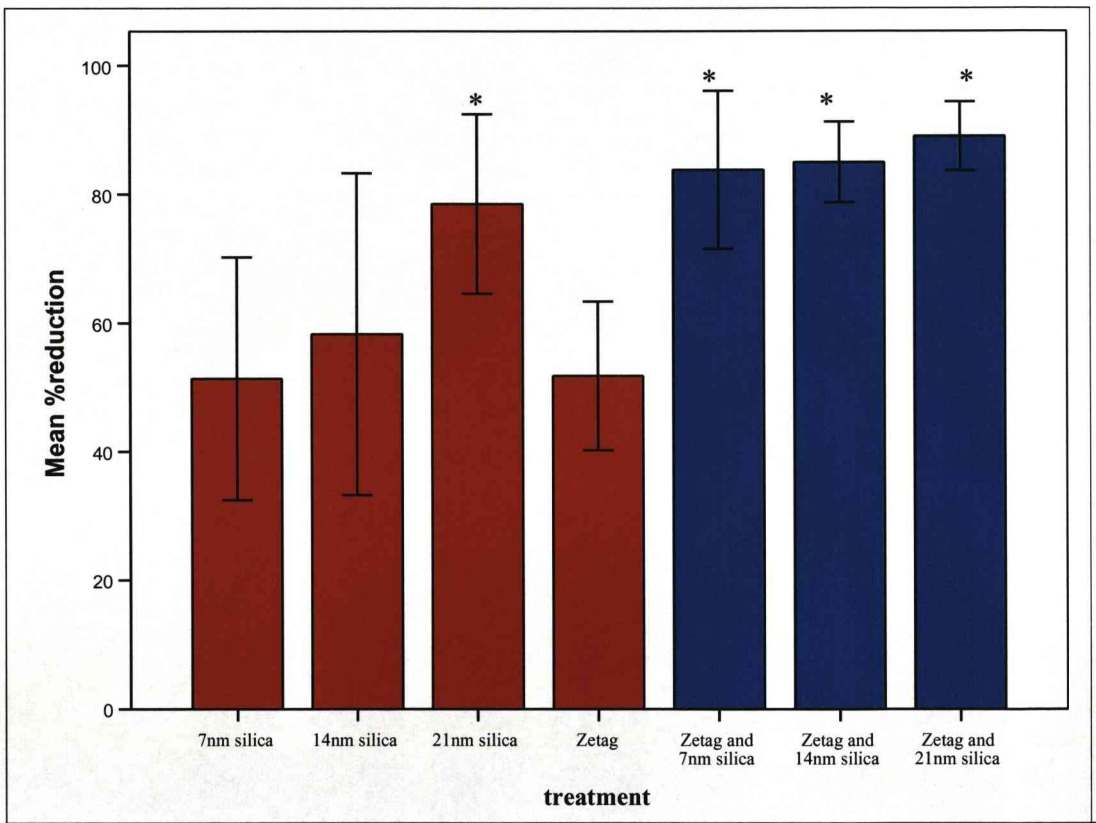


**Figure 4.5:** Graph showing the effect of a two step (blue bars) treatment method using the polymer Zetag™ 7109 and Ludox® silica sols on mean % reduction in hydraulic conductance compared to the single step controls red bars. * denotes a statistically significant difference

From figure 4.5, it would appear that the treatment of the dentine disc with Zetag™ 7109 and 21nm silica sol (Ludox® HS-40) resulted in the largest mean percentage reduction in hydraulic conductance. However, the one way ANOVA test demonstrated

that there were no significant differences between the different method 2 treatments in figure 4.5. There was, however, a statistically significant difference between the combined silica sol and Zetag™ 7109 treated samples and all the method 1 treatments, apart from when 21nm silica sol was used.

When the UCARE™ polymer JR-125 was used in conjunction with a Ludox® silica sol (figure 4.6), there was a statistically significant difference in the hydraulic conductance values before and after treatment, apart from when the 14nm diameter silica sol (Ludox® HS-40) was used. The paired t-test revealed a p-value of 0.054 for the UCARE™ polymer JR-125 and 14nm silica sol treated sample, which is close to the 0.05 significance level.

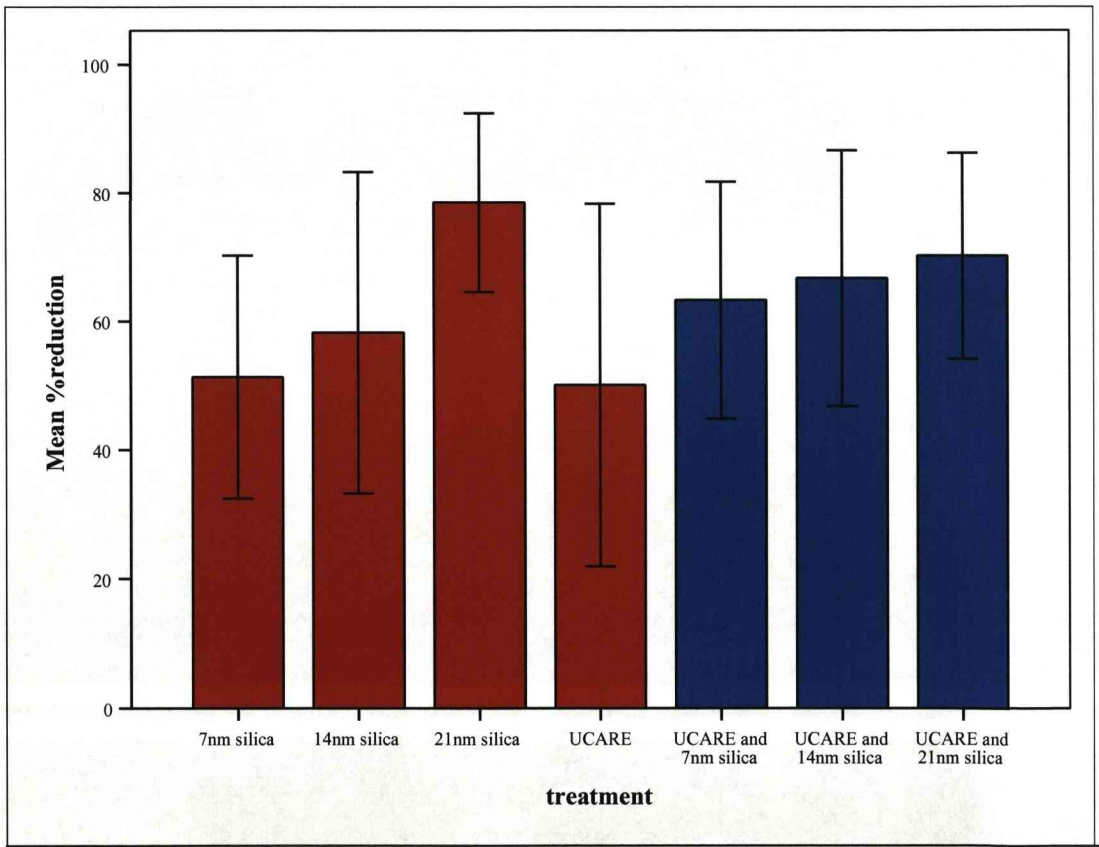


**Figure 4.6:** Graph showing the effect of a two step (blue bars) treatment method using the polymer UCARE™ polymer JR-125 and Ludox® silica sols on mean % reduction in hydraulic conductance compared to the single step controls red bars.

When the one way ANOVA test was conducted, there were no statistically significant differences between the percentage mean reductions, when the two ste coating procedure using UCARE™ polymer JR-125 was employed.

b) Influence of the polymer chemistry

Figure 4.7 depicts the effect of altering the polymer chemistry in the two step coating process. Statistical analysis showed there was a statistically significant difference between the UCARE™ polymer JR-125 and 7nm silica sol treatment and the Zetag™ 7109 and 21nm silica treated dentine. But there was no overall significant difference between the two polymers.

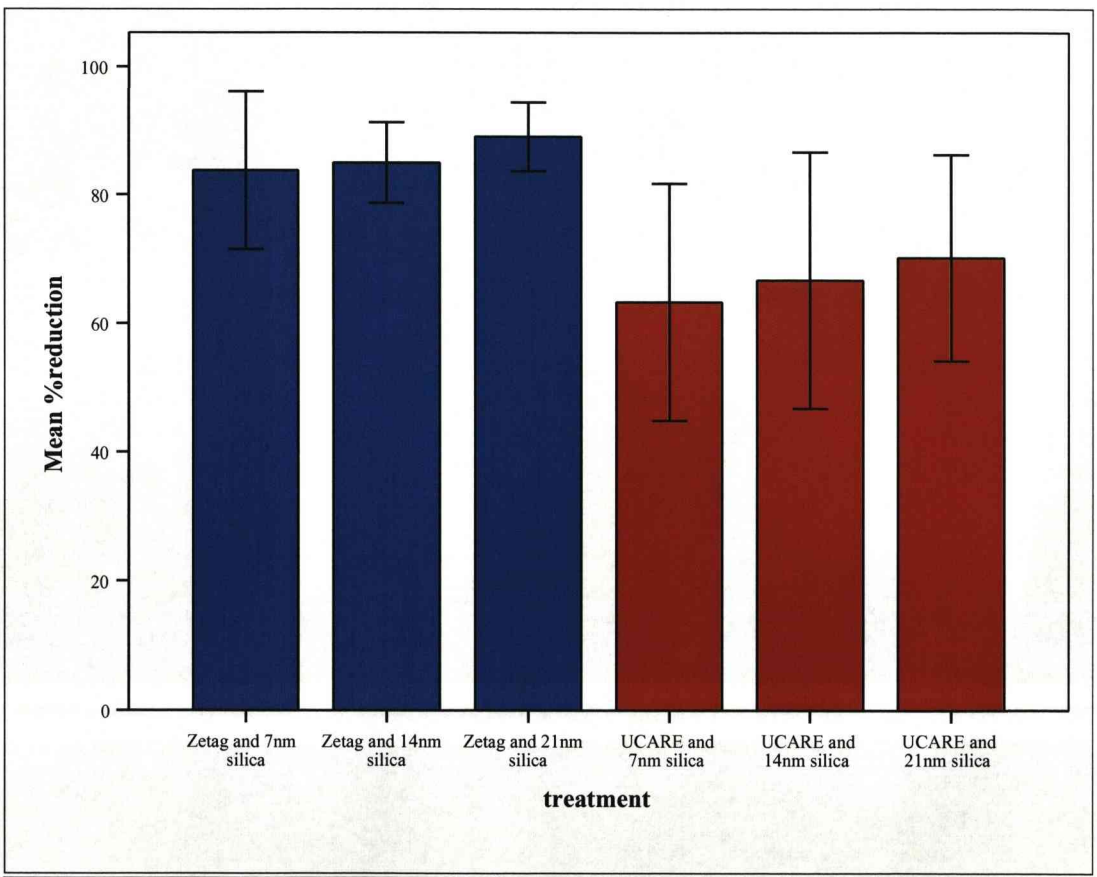


**Figure 4.7:** Graph showing the effect of a two step treatment method using the polymer Zetag™ 7109 (blue bars) and UCARE™ polymer JR-125 (red bars) with Ludox® silica sols on mean % reduction in hydraulic conductance.

c) Influence of chlorhexidine

As discussed in section 4.4.1., although there appeared to be a mean percentage reduction in hydraulic conductance following chlorhexidine treatment of 55%, this was shown not to be statistically significant using the paired t-test. However, when chlorhexidine was used as part of the two step procedure in conjunction with Ludox TM-50 (21nm) silica sol, there was a mean percentage reduction in hydraulic conductance following treatment. Using the paired t-test, this reduction in hydraulic conductance was shown to be significant with a p-value of 0.028.

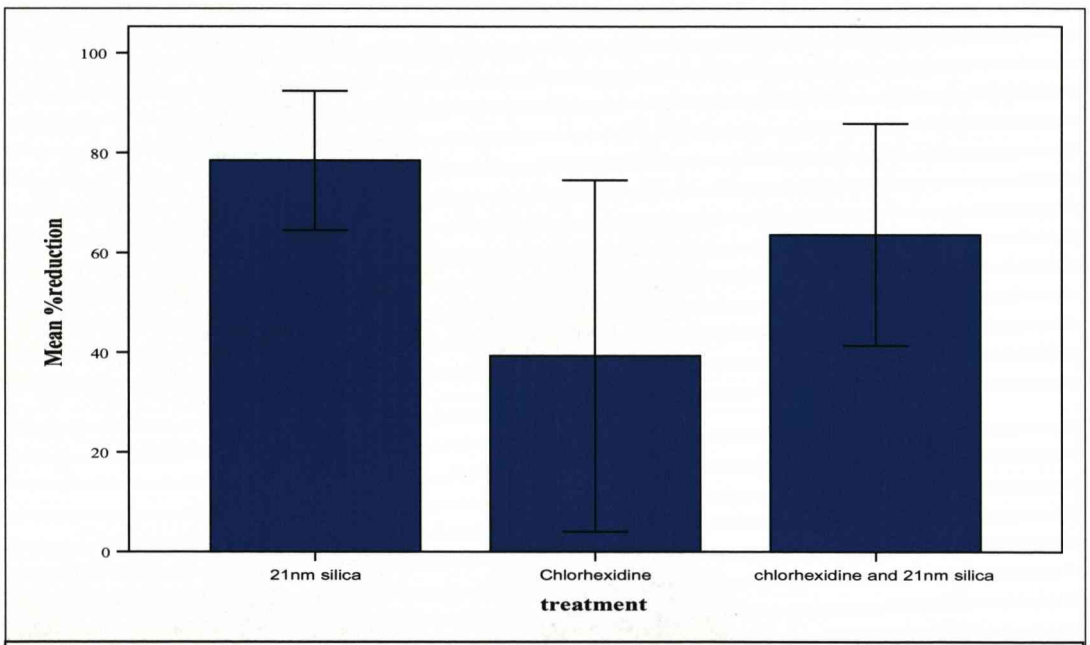


**Figure 4.8** Graph showing the effect of chlorhexidine and Ludox® TM-50 (21nm) silica sol on mean % reduction in hydraulic conductance.

As demonstrated in figure 4.8., there was an apparent increased reduction in hydraulic conductance, when chlorhexidine was used in conjunction with the 21nm silica sol. However, statistical analysis using the one way ANOVA test identified no statistical differences between the three treatments shown in figure 4.8 (Ludox® TM-50, chlorhexidine and combined chlorhexidine and Ludox® TM-50 treatment).

Comparison of the one and two step methods of treatment with Zetag™ 7109 and UCARE™ JR-125 polymers, chlorhexidine and Ludox® TM-50 (21nm) silica sol

(figure 4.9), demonstrated that the two step treatment using Zetag™ 7109 and Ludox® TM-50 resulted in the greatest mean percentage reduction in hydraulic conductance (90% reduction). Using the one way ANOVA test, it was shown there were no statistical differences between the two step coating methods using Ludox® TM-50 silica sol. But there was a significant difference between the two step Zetag™ 7109 and Ludox® TM-50 (21nm) silica treatment and the one step, Zetag™ 7109, UCARE™ polymer JR-125 and chlorhexidine treatments.

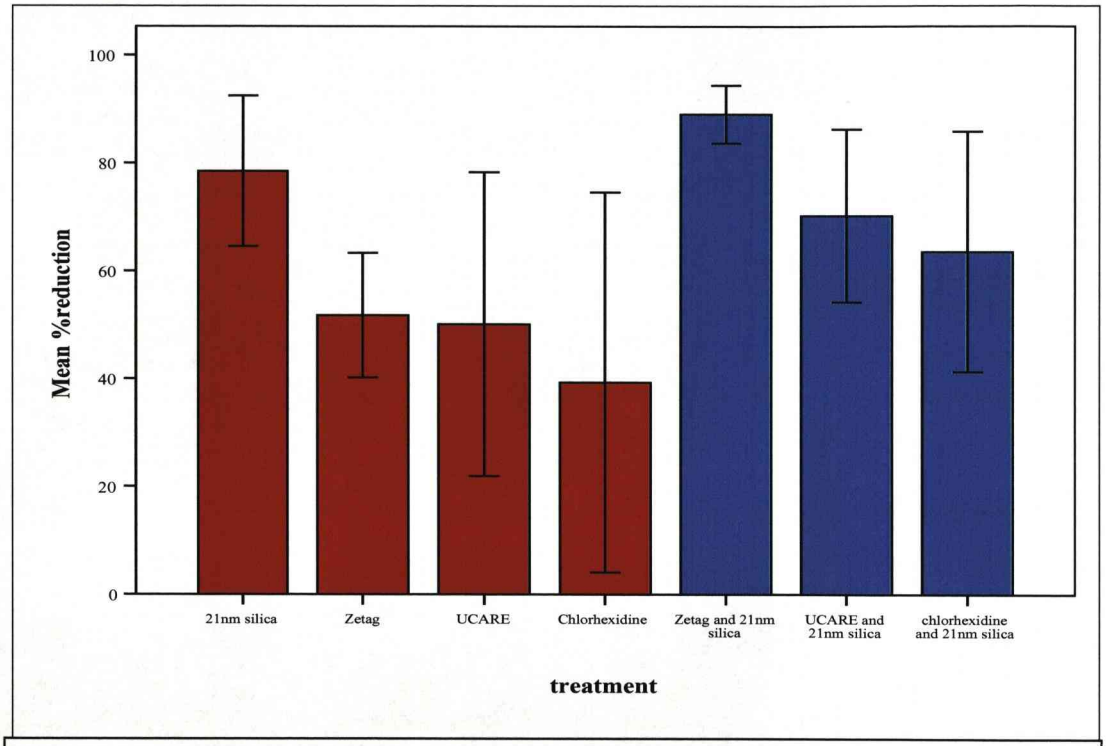


**Figure 4.9:** Graph showing the effect of a two step (blue bars) treatment method using Ludox® TM-50 (21nm) silica sol on mean % reduction in hydraulic conductance compared to the single step controls (red bars).

Comparison of all the treatments suggested treatment of dentine discs with the two step process using Zetag™ 7109 and Ludox® TM-50 resulted in the greatest mean percentage reduction in hydraulic conductance (figure 5.10).

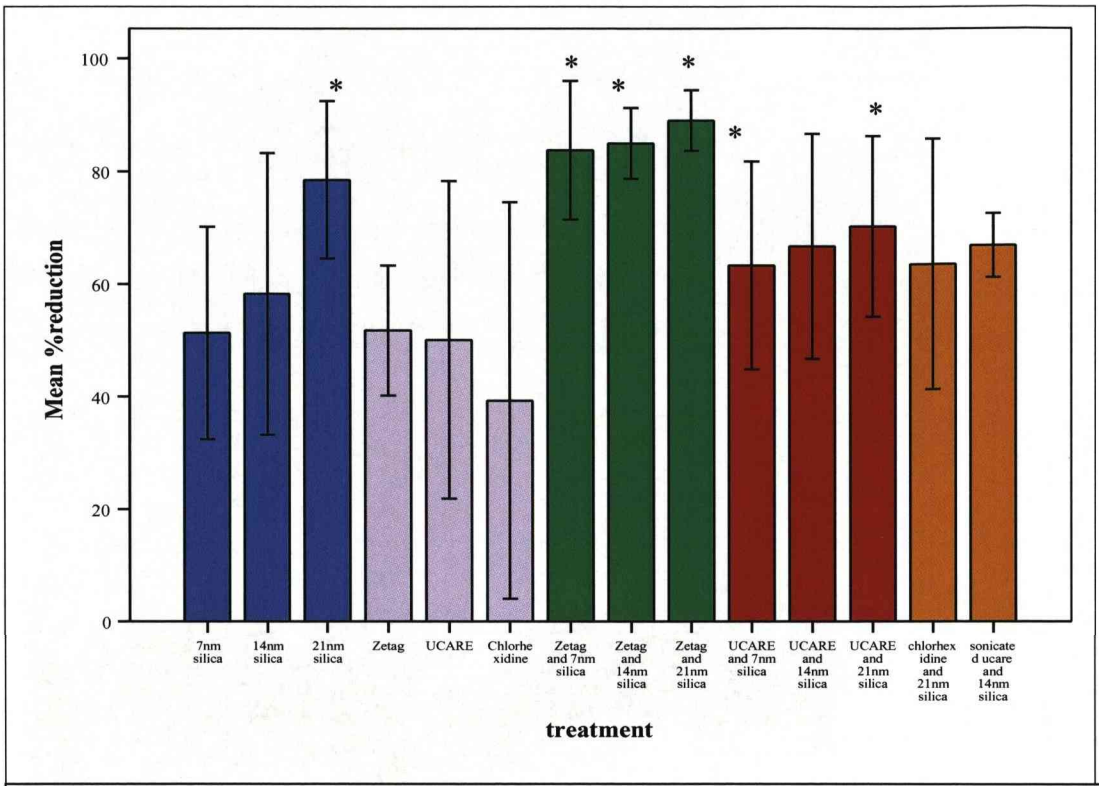


**Figure 4.10:** Graph showing the effect of the different treatments tested Ludox® silica sols (blue bars), Polymers and Chlorhexidine (purple bars), Zetag™ 7109 and Ludox® silica sols (green bars) UCARE™ polymer JR-125 and Ludox® silica sol (red bars) and Chlorhexidine and Ludox® TM-50 and Sonicated UCARE™ polymer JR-125 and Ludox® HS-40 solution (orange bars) a * denotes a statistically significant difference.

## 4.5. Discussion

The dentine disc model is a common method for *in-vitro* evaluation of potential desensitizing agents (Ling, Gillam et al. 1997). The basis of the dentine disc model is the hydrodynamic theory of dentine sensitivity. The theory states that the application of a pain provoking stimulus (typically thermal, evaporative or osmotic) to the dentine increases the flow of dentinal tubular fluid mechanically activating nerves situated in the outer layer of the pulp, eliciting pain (Orchardson and Gillam 2006). The hydrodynamic theory proposed the dentine can be thought of as being composed of hollow tubules containing fluid or semi-fluid material. The dentinal fluid within the tubules would therefore obey the physical laws as a fluid in fine capillary tubes (Poiseuille's Law) (Gillam, Mordan et al. 1997). According to Poiseulle's law, the flow through the capillary tubes is directly proportional to the fourth power of the radius. Therefore, a small reduction in tubular radius will greatly decrease dentinal fluid flow (Mongiorgi and Prati 1994). Due to this many clinical treatments for dentine sensitivity aim by occluding the tubule orifice to decrease the hydraulic conductance (permeability) of the dentine (Hsiao, Ogawa et al. 1994). The dentine disc model has been reported as a useful screening method of the potential occluding abilities of a desensitizing agent (Absi, Addy et al. 1995). Therefore, the ability of the different coatings to occlude the dentinal tubules and their potential as a desensitizing agent was investigated, using the hydraulic conductance model. Agents that elicit a positive response (a significant occlusion of dentine tubules) are easily identified as agents that may in turn be effective clinically. However, a positive response does not guarantee clinical success (Ling, Gillam et al. 1997).

Several over-the-counter treatments for dentine sensitivity employ occluding agents as their active ingredients, including calcium phosphates, oxalates and fluorides (Orchardson and Gillam 2006). Treatments containing oxalates, such as ferric oxalate as the active ingredient, have been shown to form crystal like structures on the surface of the dentine, which results in reductions in hydraulic conductance (Ling, Gillam et al. 1997). However, it has been suggested that, although there was occlusion of the tubules following oxalate treatment, the crystals formed did not penetrate a great distance into

the tubules (Hsiao, Ogawa et al. 1994). This may hinder the long term effectiveness of the treatments, as removal of the surface coating due to attrition or acid challenge would lead to the reoccurrence of patent tubules. A coating that was able to penetrate further into the tubules occluding them would offer greater protection. It was hypothesised that the smaller dimensions of the silica nanoparticles in comparison to the dentinal tubules would ensure their entry into the tubules with minimal resistance, resulting in the occlusion of the tubules. The results of the hydraulic conductance experiments would appear to support this theory, with a reduction in hydraulic conductance ranging between 52 and 78% following treatment of the dentine with the Ludox® silica sols. Previous studies identified the occlusion of the dentinal tubules with gold nanoparticles with a diameter of 30 ±8nm using SEM analysis. This study identified a fill in depth of the gold nanoparticles of 2$\mu$m (Liu, Chan et al. 2007). The similarities in the dimensions of the gold and silica nanoparticles would suggest that the reductions in permeability observed, following nanoparticulate silica treatment are due to the ability of the nanoparticulate silica to enter the dentinal tubules. The preliminary results from the QCM-D study, using a dentine disc adhered to a quartz crystal (chapter 3), also indicated the possibility that the 21nm diameter nanoparticles were able to enter the tubules. This would indicate that the reductions in hydraulic conductance following nanoparticulate silica treatment, are due to the ability of the nanoparticles to penetrate the tubules.

The largest reductions in hydraulic conductance were observed when the largest diameter (21nm) Ludox® silica sol was used. However, statistical analysis failed to established a statistically significant difference between the different sizes of nanoparticulate silica sols could be due to the comparative differences in dimensions between the sols and the dentinal tubules. There is a variation of only 7nm between each grade of nanoparticulate sol tested weheras the dentinal tubules can have a diameter of between 1 and 3$\mu$m (Mjor and Nordahl 1996).

The use of fluoropolymers in oral care has been previously investigated. It was demonstrated that fluoropolymers were able to reduce hydraulic conductance in the range of 30 – 55% (Churchley, Rees et al. 2007). The observed decreases in hydraulic

conductance, following both Zetag™ 7109 and UCARE™ polymer JR-125 of 51 and 41% respectively, are, therefore, comparable to those observed for fluoropolymers. It was anticipated that the polymers would enter the tubules in a similar manner, as the nanoparticles adhere to the walls of the dentinal tubules as well as the dentinal surface.

The reduction of hydraulic conductance following UCARE™ polymer JR-125 treatment was lower that that achieved following Zetag™ 7109 treatment. This may be linked to the differences in the adsorption of the polymer to the surface. As demonstrated using the QCM-D (chapter 3), there were differences in the binding curves produced by the different polymers upon addition to the test surfaces. The UCARE™ polymer is known to adhere to surfaces in a smooth manner. It was surmised that the differences in the binding curves may be due to the Zetag™ polymer adhering in a coiled manner and uncoiling once adsorbed. It was suggested, however, when the HA crystals were used that Zetag™ 7109 has a high affinity for the surface and rapid saturation hindered the uncoiling of the polymer due to spatial constrictions. This may explain why the reduction in hydraulic conductance was greater following Zetag™ 7109 treatment, as the polymer was forming a denser coating of the tubule walls than the smooth uniform coatings UCARE™ polymer JR-125 had been shown to produce on several surfaces. UCARE™ polymer JR-125 would still be able to elicit a reduction in hydraulic conductance, despite the surmised smooth manner in which it adsorbs to the surface.

It was hypothesised that chlorhexidine treatment alone would produce a minimal reduction in hydraulic conductance and, as such, could be used as a control. As expected, chlorhexidine treatment failed to produce a statistically significant reduction in hydraulic conductance. Previous studies support this finding with chlorhexidine treatment of etched dentine resulting in a large variation in the results. SEM analysis demonstrated that, in several cases, chlorhexidine treatment failed to occlude the tubules with identifiable changes in the tubule outline in comparison to controls, while other samples were able to demonstrate differential levels of tubular occlusion varying from total to partial occlusion of some of the tubules (Banfield and Addy 2004).

Creation of a Zetag™ 7109 polymer binding layer prior to addition of the nanoparticulate sol did produce a decrease in permeability that was statistically greater than treatment with either the polymer or the 7 and 14nm silica nanoparticles alone. The lack of a statistically significant difference between the 21nm particles alone and the combined polymer, silica coating could be due to the size of the particles and their increased ability to form van der waals attractions (Napper 1970). It can be suggested that this would allow a closer relationship between the particles within the tubules and this may lead to the increased occlusion abilities that were on par with those achieved with the smaller size nanoparticles in the presence of a Zetag™ 7109 polymer binding layer.

It was hypothesised that the use of UCARE™ polymer JR-125 as a binding layer for the nanoparticles would also result in an increased reduction of hydraulic conductance. However, this was not the caries. There were no statistically significant differences between the two step treatments with UCARE™ polymer and the Ludox® silica sols and the individual silica and polymer coatings in reducing hydraulic conductance. This could again be related to the manner in which the UCARE™ polymer JR-125 adheres to the surface in a smooth flat manner. As demonstrated in chapter 2 using UCARE™ polymer JR-125 to create the binding layer resulted in the creation of an even and uniform coating. It could be suggested that, due to the smooth manner in which the UCARE™ polymer adsorbs to the surface, there is minimal influences of the polymer layer in increasing the density of the coating. However, if as proposed the Zetag™ polymer bound in a coiled manner, this would increase the density of the coating within the tubules, therefore enhancing the reduction in permeability.

When chlorhexidine was used to alter the surface charge of the dentine (in the same manner as the creation of a polymer binding layer), prior to addition of the 21nm nanoparticulate silica sol, there was a statistically significant decrease in permeability/ However, this decrease was lower than that of the 21nm particulate silica sol treatment alone. It was also diminished in comparison to the polymer and silica coatings.

Comparison of the different coatings failed to establish a single statistically superior coating. Instead a group of treatments were identified as offering superior reductions in dentine permeability. The only single step treatment within the group used the largest size (21nm) nanoparticulate silica sol (Ludox® TM-50). These results would suggest that the added complexity of creating a polymer binding layer for the purpose of reducing dentine permeability was not strictly necessary. This would also be a more commercially favourable treatment, as ease of use is an important consideration in the creation of any new oral care products and would aid the commercial viability of the product (Zappa 1994)

Although hydraulic conductance can indicate the suitability of a treatment as an occluding agent, it cannot accurately predict its success in a clinical setting (Ling, Gillam et al. 1997). So although these results are promising, further experimentation would be required to obtain a more accurate prediction of success in clinical trials.

# Chapter 5

# Characterisation of nanoparticulate silica treated dentine discs with X-ray Photoelectron Spectroscopy

*In this study, X-ray photoelectron spectroscopy (XPS) has been used to monitor the chemical composition of non etched and citric acid etched dentine. XPS was used to monitor shifts in peak positions and heights of several key components of dentine, including carbon, oxygen, nitrogen, calcium, phosphorous, silicon, fluorine and sodium and the percentage concentrations calculated. The treatment of both citric acid etched and non etched surfaces with nanoparticulate silica and fluoride was investigated, as well as the possibility for dentine remineralisation with artificial saliva treatment. The ability of the coatings to withstand acid attack and protect the underlying dentine was also assessed.*

## 5.1 Introduction

X-ray photoelectron spectroscopy (XPS also known as electron spectroscopy for chemical analysis ESCA) involves the absorption of x-rays by the atoms in the sample leading to the ejection of core and valance electrons (photoelectrons) (McArthur 2006). The production of a photoelectron is dependent on the incident photon (x-ray) having sufficient energy (hν) to ionize an electronic shell, such that an electron which was bound to the solid with energy ($E_B$) is ejected into the vacuum with kinetic energy ($E_K$) so:

$$E_K = h\nu - E_B \qquad \text{Equation 1 (Prutton 1998).}$$

The energy emitted as a photon is equivalent to the absolute energy difference between $E_B$ of the initial and final states of the transferred electron in the excited atom. Therefore, the wavelength of the photon is dependent upon the distribution of electrons in the excited atom, hence the atomic number (Jenkins 1986; Prutton 1998). So, for each and every element, there will be a characteristic binding energy associated with each core atomic orbital, giving rise to a characteristic set of peaks in the photoelectron spectrum determined by the photon energy and respective binding energies (Carlson 1975).

An important and useful phenomenon of the XPS spectrum in analysis is the chemical shift. It was observed that a chemical shift in electron binding energies correlated with the chemical state of the atom (Hercules 2004), in that non-equivalent atoms of the same element gave rise to core level peaks with measurably different $E_B$'s. The non equivalence of atoms can arise in several ways, including differences in the formal oxidation state differences in molecular environment (Briggs and Riviere 1983). This allows not only the production of a spectrum identifying the atoms present in the sample but it is also possible to characterize the molecular environment of the atoms, using reference texts listing known chemical shifts in binding energies (Moulder, Stickle et al. 1992; McArthur 2006).

Due to its ability to provide spectra for all elements except hydrogen and helium, XPS has proven a useful tool for surface analysis (Hercules 2004). Although x-rays penetrate to a depth of several micrometers, ejected photoelectrons generally come from the outer most nanometers (about 10nm) of the material, resulting in a highly surface sensitive technique (Lambert, McLauglin et al. 1999). The depth resolution in electron spectroscopy is due to the mean escape depth (or effective escape depth) of the photoelectron, not the penetrating depth of the x-ray (Hofman 1986). This can be explained by considering equation 1, which assumes that the photoemission process is elastic, with every x-ray giving rise to a series of photoelectron peaks which reflect discrete binding energies of the solid. However, the photoelectron process is inelastic if the photoelectron suffers an energy change between photo emission from an atom in the solid and detection in the spectrometer (Briggs and Riviere 1983). Electrons can lose energy in a number of ways, including the excitation of lattice vibrations and various single and double particle excitations. Thus, an electron may lose energy by raising a second electron from its ground state to an empty state in the solid or it may ionize an electron level with the ejection of another photoelectron (an auger electron) (Prutton 1998). The inelastic free mean path ($\lambda$) of a photoelectron, therefore, depends, not only on its energy, but on the matrix of the sample from which the atom is contained (Hofman 1986).

It is possible to increase surface sensitivity by decreasing the angle of electron exit to the surface (also known as the "take off angle" (figure 5.1). If $\lambda$ is the inelastic free

mean path of the emerging electron then 95% of the signal intensity is derived from a distance of 3 λ within the solid. The vertical depth (d) sampled is given by:

$$d = 3\lambda \sin \alpha$$

The vertical depth sampled is a maximum when the "take off angle" ($\alpha$) is 90°. By reducing the "take off angle", it is possible to increase the surface sensitivity (reducing the vertical depth sampled) (Briggs and Riviere 1983).

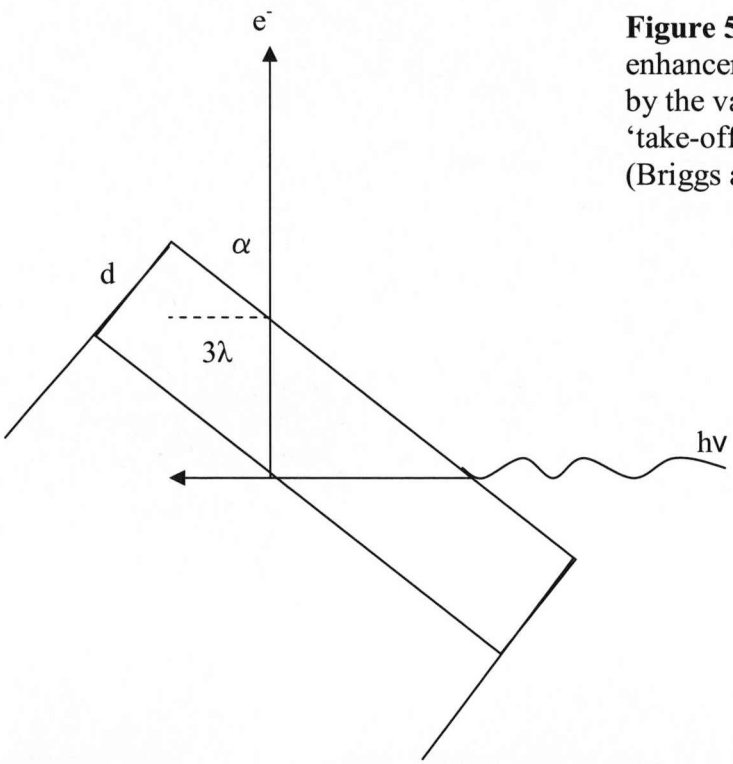


**Figure 5.1.** Diagram of the enhancement of surface sensitivity by the variation of the electron 'take-off' angle adapted from (Briggs and Riviere 1983)

It was due to its high surface sensitivity that XPS was selected as a surface analysis technique to probe the coated dentine surfaces. For all experiments the Scienta ESCA 300 at NCESS (The National Centre for Electron Spectroscopy and Surface analysis) Daresbury Laboratory was used. The ESCA 300 uses a high power rotating anode x-ray source with a focusing quartz monochromator. The monochromator enables the focusing of the x-rays at the sample onto a line of about 0.5mm wide and 6mm long. It also removes x-ray satellites, reducing spectral background radiation and therefore damage to sensitive samples. However this, also, has the disadvantage of eliminating the flood of low energy electrons that the x-ray source also generates, which leads to severe charging problems. To minimize this, in the analysis chamber of the ESCA

300 there is an unchromated dual anode (Mg/Al) x-ray source (a flood gun). This is used to flood the sample with low energy electrons for charge compensation, minimising the differential charging and therefore the large peak shifts and peak broadening that would result (Beamson, Briggs et al. 1990).

Photoelectrons from the sample are collected by a multi element lens and focused to a slit aperture pair at the entrance plane of the hemispherical electron analyser. This allows for two modes of operation: high transmission which accepts electrons from the whole of the x-ray line but has poor binding energy resolution, or high binding energy resolution, which accepts electrons from only a small part of the x-ray line and results in high resolution spectra for a selected element and can be used for quantification calculations.

The Scienta ESCA 300 used in the following experiments had an argon ion gun, fitted to the sample preparation chamber, which can be used for depth profiling. As discussed, it is possible to alter the analysis depth in XPS experiments by altering the "take off angle" of the measured electrons. Increasing the angle increases the vertical depth at which the sample is being probed. By taking measurements at multiple take off angles, it is possible to create a depth profile of the upper surface. However this method is limited to probing between 5 and 200nm of the surface, depending on the material being probed. So a universally applicable sectioning method for depth profiling is surface erosion by ion sputtering. Sputtering is a destructive method of depth profiling, whereby the sample is bombarded with ions accelerated in an ion gun to an energy above 100eV (usually between 0.5 and 5keV). Argon ion bombardment results in the transference of a small fraction of the energy of the ion to the surface atoms, causing them to leave the surface. Analysis depth profiling using an argon ion gun minimises the influence of the matrix on elemental detection that is a limiting factor in the efficiency of the non destructive angle dependent depth profiling method discussed above (Hoffman 1983).

XPS enabled the examination of the surface chemistry following several different surface treatments and coatings. Due to its high surface sensitivity and by using a take off angle of 45°, it was possible to probe the surface with minimal interference from the bulk. The use of an argon ion gun to sputter the surface enabled the

analysis depth to be altered and information regarding the depth of penetration into the bulk of dentine following different treatments to be analysed. A limitation of the argon ion sputtering method is that it was not possible to ascertain the depth probed following sputtering. To maintain consistency, all samples were sputtered for the same length of time (10 minutes) and with ions of the same energy (5KeV).These parameters on a uniform metal surface would suggest a profile depth of 50nm, but this depth would vary on the non uniform dual phase surface of the dentine. The ability to produce high spatial resolution spectra for specific elements of interest allowed for quantification of the main components of the surface and therefore, information regarding the percentage elemental composition and the ratio of organic to inorganic components of the sampled dentine.

## 5.2 Materials

Dentine discs were created from extracted wisdom teeth from patients at the University of Liverpool Dental Hospital. These teeth were from an archival store of teeth for research and teaching purposes and, as such, did not require ethical approval. To create the nanoparticulate coating, Ludox® TM-50 silica sol (21nm diameter) was used (section2.2). A sodium fluoride solution (Sigma-Aldrich) was used as a control. Fluoride is a common component of many over the counter and in house dental treatments and is used to minimise mineral loss (Schlueter ref 2007). Artificial saliva created as described in section 3.3, was used as a remineralising solution.

## 5.3 Methods

### 5.3.1 Fabrication of dentine discs

Dentine discs were prepared from human wisdom teeth collected from the University of Liverpool Dental Hospital (section 5.2).

1. The teeth were stored in ethanol until required, and rinsed in $dH_2O$ before use.
2. Dentine discs were prepared by sectioning the human teeth in a plane perpendicular to the long axis of the tooth, between the enamel dentine junction and the pulp. Using a slow speed saw (Isomet, Buehler, UK.) with a diamond edged wafering blade (Buehler LT 11-44254, Buehler, UK.), a first cut was made approximately 0.5mm from the crown of the tooth.
3. A second cut was made to create a dentine disc of an approximate thickness of 0.75mm.
4. The dentine discs were then placed in $dH_2O$ in a sonic bath for 10 minutes to remove wear debris.

a) Influence of citric acid etching.

   To investigate the effect of acid etching on the dentine, following step 4, dentine discs were subjected to 6% (w/v) citric acid (sigma, UK) for 2 minutes and then rinsed in $dH_2O$.

### 5.3.2 Coating the dentine discs

Both acid etched and non etched dentine were subjected to the following coating procedure.

1. Using a pipette 10µl of treatment solution, was added to the coronal surface of the dentine
2. A small dental applicator brush was used to manipulate the solution over the surface for 2 minutes.
3. The samples were rinsed in $dH_2O$.
4. All samples were dried in a desiccator for a minimum period of 72 hours prior to use.

a) Influence of nanoparticulate silica sol:
   Ludox® TM-50 (21nm) silica sol was used as the treatment solution in step 1.

b) Influence of fluoride
   1000ppm sodium fluoride solution (NaF) was used as the treatment solution in step1.

c) Influence of acid challenge:
   To investigate the ability of the different treatments to withstand acid challenge, the samples were subjected to a 1% (w/v) citric acid challenge. The coated samples were place in a 1% (w/v) citric acid solution for 30 minutes, 7 days after treatment. After acid challenge, the samples were rinsed in $dH_2O$ and stored in the desiccator for a minimum of 72 hours prior to analysis.

### 5.3.3 Dentine remineralisation

To assess the possibility of remineralising dentine, artificial saliva (section3.3) was used as a remineralising solution that would closely mimic physiological conditions in the mouth. Both citric acid etched and non etched dentine were subjected to the following treatment:

1. Samples were prepared as described above (sections 5.3.1 and 5.3.2).
2. Samples were placed in 10ml of artificial saliva and placed on a rotating stand at 37°C.

3. After 7 days the samples were rinsed in $dH_2O$ and dried in a desiccator for a minimum of 7 days.

a) Influence of nanoparticulate silica:

The influence of nanoparticulate silica on remineralisation was tested using samples coated in 40% (w/v) Ludox® TM-50 (21nm silica sol) as previously described in section 5.3.2

b) The influence of fluoride

The effect of fluoride treatment was investigated using 1000ppm NaF solution as previously described in section 5.3.2

c) Influence of acid challenge:

To assess the ability of the coatings to withstand acid, samples were subjected to acid challenge, using 1% (w/v) citric acid as described in section 5.3.2

| **Surface challenge. / Coating** | **None** | **Acid challenge** | **Artificial saliva** | **Artificial saliva and acid challenge** |
|---|---|---|---|---|
| **None** | • | | • | • |
| **Ludox ® TM-50 (21nm silica)** | • | • | • | • |
| **NaF** | • | • | • | • |

**Table 5.1** List of coatings and subsequent challenges subjected to both citric acid etched and non etched dentine surfaces.

### 5.3.4 XPS of dentine discs

XPS was conducted using the Scienta ESCA300 (NCESS, CCLRC, Daresbury Laboratories, Daresbury, UK). It uses a high powered rotating anode and monochromated Al k$\alpha$ ($h\nu$= 1486eV) x-ray source.

1. Samples were mounted on a metal stub.

2. Carbon conducting putty (Neubauer Chemikalien 004400 Minster Leit C-Plast Plastic conductive carbon cement, Agar Scientific, UK) was placed around the sample on the stub and used to hold a silver screen in place over the dentine sample.
3. The silver screen had a window of 0.4 cm wide and 1.2 cm long and was used in conjunction with a flood gun set to 6eV to minimise the surface charging of the samples.
4. The take off angle was set to 45°.
5. A survey scan (1325-0 eV binding energy) of the sample surface was taken using a slit width of 1.9 mm.
6. High resolution scans of the oxygen, carbon, nitrogen, sodium, calcium, fluorine, phosphorous and silicon regions were taken with a slit width of 0.8mm.

a) Argon ion sputtering

Samples were removed from the vacuum following the initial data collection. The carbon putty and silver mask were removed from the specimens and then the specimens were placed back into the preparation vacuum chamber. The samples were subjected to argon ion etching (for the purpose of clarity in this study this will be referred to as sputtering). An argon ion gun set to 5KeV was focused on the samples at a 45° angle for 10 minutes to remove the surface layer. The sample was removed from the preparation chamber and the carbon putty and silver mask replaced prior to re entry into the vacuum system and re analyses following the steps described in section 5.3.4.

All spectra were corrected to the C1s peak at 285eV to take into account the shift in binding energy due to surface charging. Quantification was undertaken, using the ESCA 300 series analysis programme, which lead to the calculation of the relative atomic concentrations for the selected elements. The area under the peaks was measured and combined with the known atomic sensitivity factors for this instrument for each element. This allowed the calculation of the relative percentage concentrations of the different elements in the sample.

## 5.4 Results

For clarity the samples will be referred to by the number given in table 5.2 throughout the results section.

| Treatment Number | Treatment |
|---|---|
| 1 | Silica coated |
| 2 | NaF coated |
| 3 | Silica coated and acid challenged |
| 4 | NaF coated and acid challenged |
| 5 | Artificial saliva treated |
| 6 | Silica coated and artificial saliva treated |
| 7 | NaF coated and artificial saliva treated |
| 8 | Artificial saliva treated and acid challenged |
| 9 | Silica coated and artificial saliva treated and acid challenged |
| 10 | NaF coated and artificial saliva treated and acid challenged |

**Table 5.2** Table listing the treatment to which each treatment refers. All treatments were conducted on both etched and non etched dentine.

### 5.4.1 Acid challenged

Comparison of the calcium (Ca2p) spectra revealed that citric acid etching resulted in a decrease in the intensity of the Ca2p peak (figure 5.2). There was also a decrease in the phosphorous (P2p) peak intensity (data not shown). Both these elements are associated with the mineralised phase of the dentine and would indicate that acid etching had resulted in some surface demineralisation.

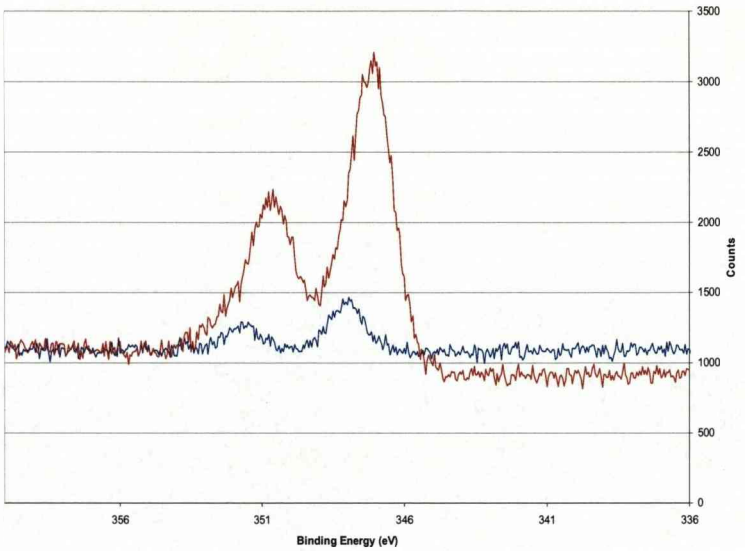


**Figure 5.2** Ca2p spectra for etched (blue line) and non etched (red line) dentine.

Comparison of the carbon (C1s) spectra following acid challenge identified an increase in the peak intensity around 285eV (figure 5.3). On the etched dentine sample, there was the presence of a shoulder at 287eV. On the non etched dentine sample, this appears to be merged with the 285eV peak and appears as a single wide peak.

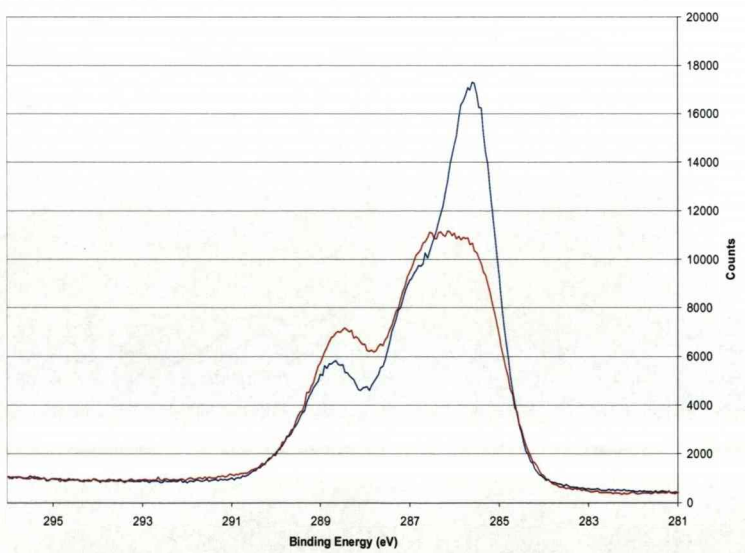


**Figure 5.3** C1s spectra for etched (blue line) and non etched (red line) dentine.

The carbon and nitrogen spectra are associated with the organic component of the dentine, while the calcium and phosphorous are associated with the inorganic mineral phase. When the concentrations of the mineral (Ca2p) and organic (C1s) phases were compared, it was clear that acid etching resulted in demineralisation of

the surface (table 5.3). Acid etching resulted in a five fold relative reduction in the calcium (mineralised) content of the dentine.

| Dentine treatment | Concentration Atomic % | | C: Ca |
|---|---|---|---|
| | C1s | Ca2p | |
| **Etched** | 66.9 | 0.8 | 1:0.01 |
| **Non etched** | 54.5 | 3.3 | 1:0.06 |

**Table 5.3** Table showing the effect of citric acid etching on dentine on the Ca2p and C1s concentrations and C: Ca ratios.

Argon ion sputtering to remove the surface layer resulted in an increase in the Ca2p intensity on the etched dentine sample (figure 5.4), and was coupled with a small increase in the P2p peak intensity (data not shown). These increases would appear to indicate the reappearance of the mineralised component of dentine underlying the demineralised zone on the surface, an assumption which was further strengthened when the ratio of Ca:C was considered. Following argon ion sputtering, there was an increase in the ratio to 0.04 which was just below the ratio achieved on the surface of the non etched sample. This suggests that argon ion sputtering revealed the mineralised bulk dentine underneath the surface demineralised zone.

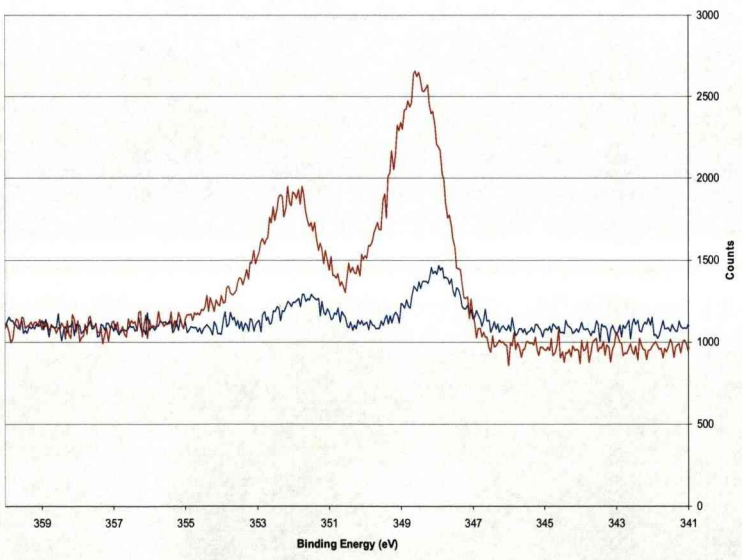


**Figure 5.4.** Ca2p spectra for etched dentine before (blue line) and after 10 mins 5KeV argon ion sputtering (red line).

### 5.4.2 Effect of coating the dentine surfaces

**a) The influence of nanoparticulate silica**

Etched dentine.

Acid etched → Silica treated

Coating of the dentine with nanoparticulate silica resulted in the appearance of a silicon peak (100eV) on the survey spectra and an increase in the intensity of the O1s peak (figure 5.5)

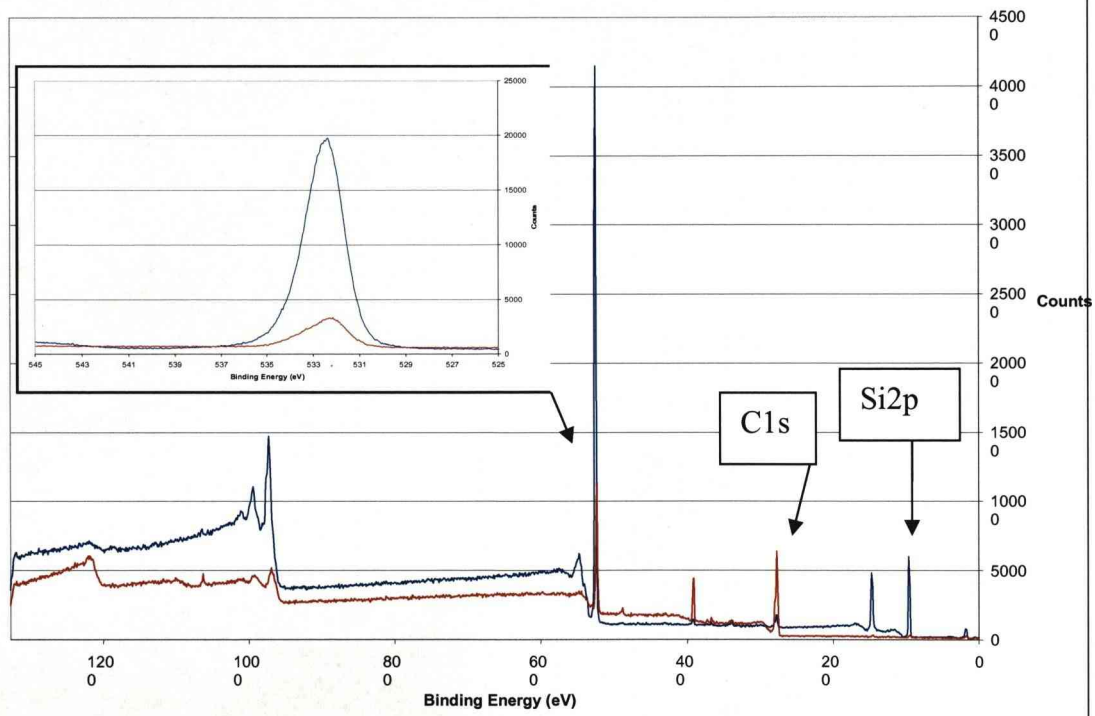


**Figure 5.5.** Survey spectra for etched dentine (red line) and etched dentine and nanoparticulate silica (blue line). Inserted spectra for O1s again etched dentine (red line) and etched dentine and nanoparticulate silica (blue line).

When the O1s peak of the silica treated dentine was compared with etched dentine there was a clear increase in intensity (Figure 5.5 insert). There is a slight shift in the peak position of 1eV. The peak position in the presence of a silica coating of 532eV would indicate that the oxygen is associated with silica (Moulder, Stickle et al. 1992). Therefore, it would also account for the increase in O1s peak intensity upon addition of a nanoparticulate coating to the surface.

Upon addition of the nanoparticulate silica coating, there was a decrease in the intensity of the peaks associated with dentine such as carbon 285 eV (figure 5.5). The Ca2p peak, which was low on the etched dentine sample, underwent a further reduction and the phosphorous peak was undetectable, thus indicating that a substantial surface coating of nanoparticulates had been achieved and that this coating was masking the underlying dentine.

Argon ion sputtering of the surface appeared to have little overall effect on the intensity of either the P2p or Ca2p signals, with the P2p peak remaining undetectable (data not shown). Figure 5.6 highlights the effect of argon ion sputtering of the nanoparticulate coated dentine surface. There was no alteration to the Si2p concentration but there was a small increase in the O1s concentration. This could be due to the re-emergence of some of the dentine components with an increase in both the N1s and Ca2p concentrations following argon ion sputtering. The continued intensity of the Si2p peak following argon ion sputtering would indicate a substantial coating of silica remained, following removal of the surface layers. Therefore, it could indicate that the nanoparticulates were able to penetrate the tubules and removal of the surface layers will not remove the entire coating.

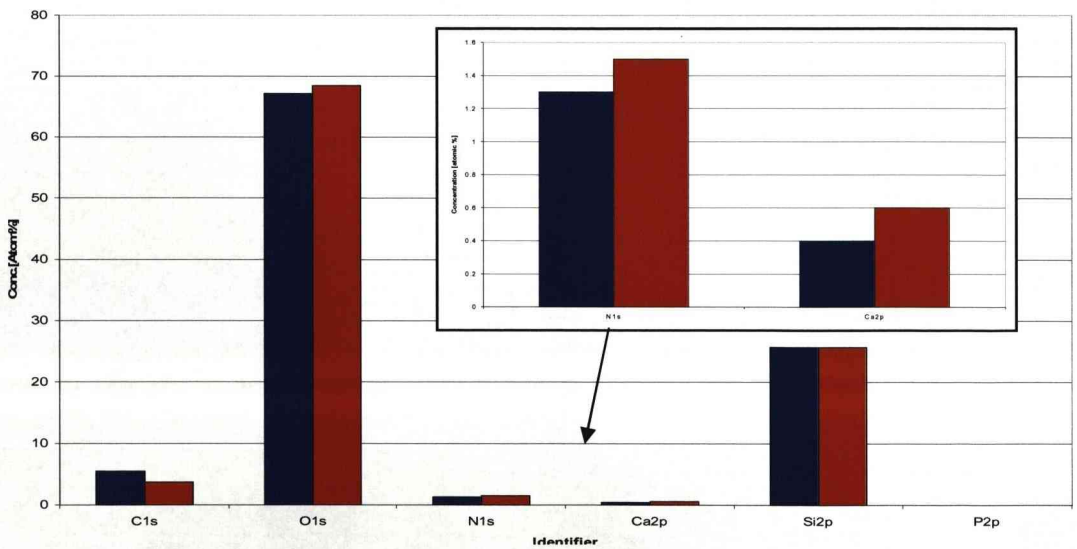


**Figure 5.6.** Graph showing the effect of argon ion sputtering on the concentration [atomic %] of etched dentine treated with nanoparticulate silica before sputtering (blue) after sputtering. (red).

Non Etched dentine

Non etched → Silica treated

Treatment of a non etched dentine surface with nanoparticulate silica resulted in the appearance of a silicon peak (figure 5.7). The appearance of a strong silica peak was accompanied by an increase in the O1s peak intensity.

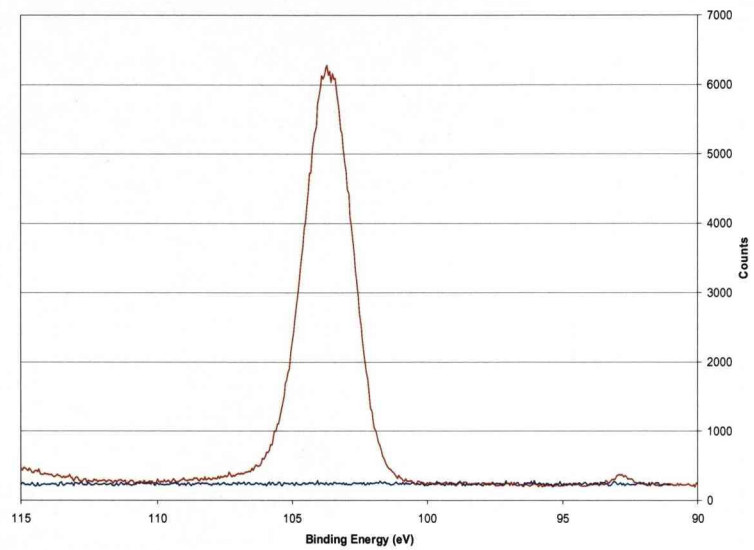


**Figure 5.7** Si2p spectra for non etched dentine (blue line) and following nanoparticulate silica treatment (red line).

Figure 5.8 highlights the increase in O1s peak intensity upon the treatment of non etched dentine with nanoparticulate silica. There is a shift in peak position of 2eV. The shift and increase is due to the O1s now being associated with silica as well as the underlying dentine. When this was compared with the etched dentine peak, it was apparent that the peak shift due to the presence of silica is more obvious on the non etched dentine surface.

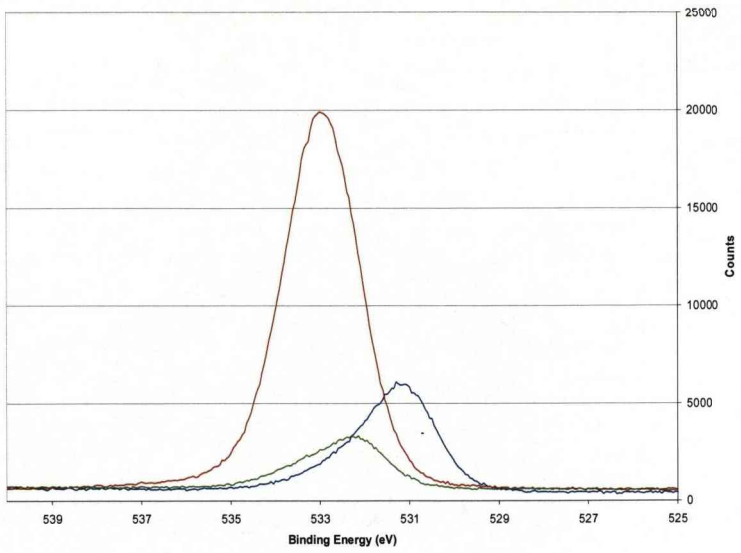


**Figure 5.8** O1s spectra for non etched dentine (blue line) and non etched dentine following nanoparticulate silica treatment (red line) and etched dentine (green line).

Figure 5.9 highlights the effect of nanoparticulate silica treatment on non etched dentine, as, on the etched dentine sample, treatment with nanoparticulate silica resulted in a decrease in the relative concentrations of the major dentine components (carbon, calcium, nitrogen and phosphorous). Again it could suggest that the dentine surface was masked by the presence of a nanoparticulate coating.

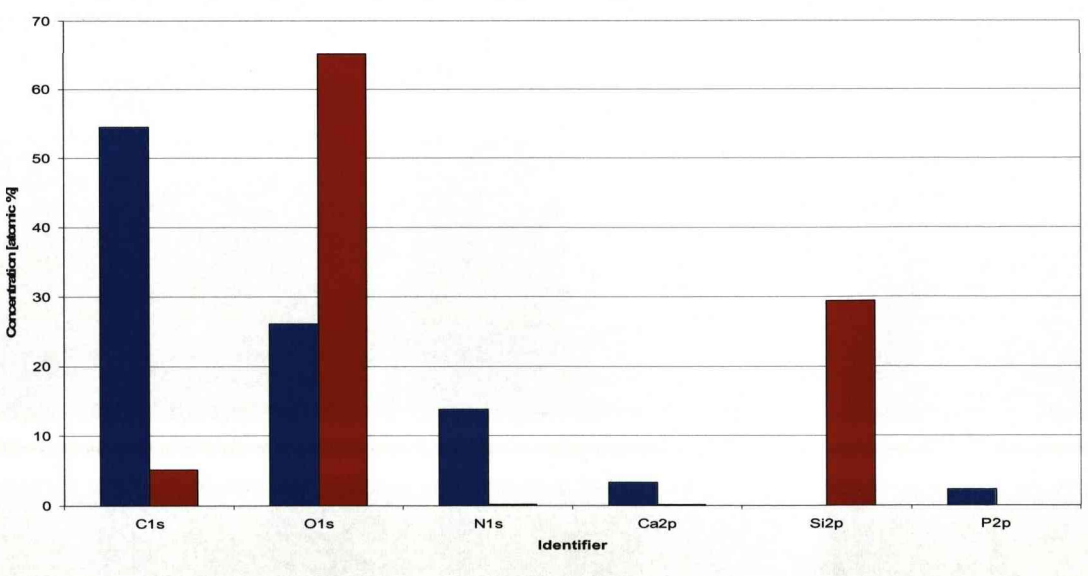


**Figure 5.9** Graph showing the effect of silica treatment of non etched dentine on concentration [atomic %]. Non etched dentine (blue) non etched and nanoparticulate silica (red)

Argon ion sputtering resulted in a decrease in the concentration of Si2p (figure 5.10). Despite the decrease in the Si2p concentration, there was no corresponding decrease in O1s. This may be due to an increase in the C1s and Ca2p concentrations (Figure 5.10). The increased intensity of elements associated with the dentine indicates that, although a substantial amount of the silica remains on the surface, there was the emergence of the underlying dentine surface.

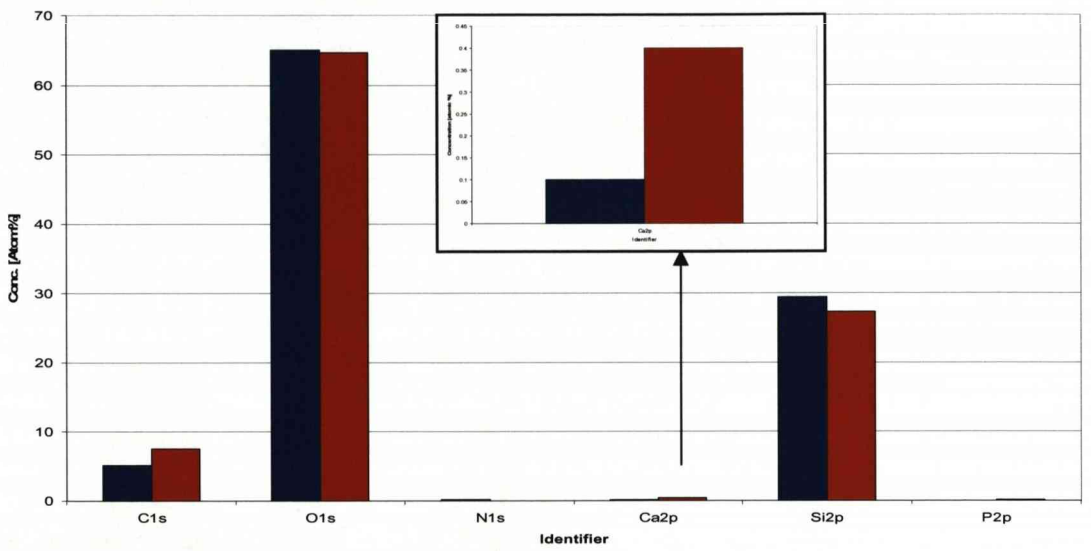


**Figure 5.10.** Graph showing the effect of silica treatment non etched dentine on concentration [atomic %]. Non etched dentine (blue) non etched and nanoparticulate silica (red) Insert Ca2p concentration changes

**b) Influence of NaF**

Etched dentine


Following NaF treatment there was the appearance of sodium (Na1s) and fluorine (F1s) peaks (data not shown), and this is highlighted in figure 5.11 as the appearance of Na and F concentrations.

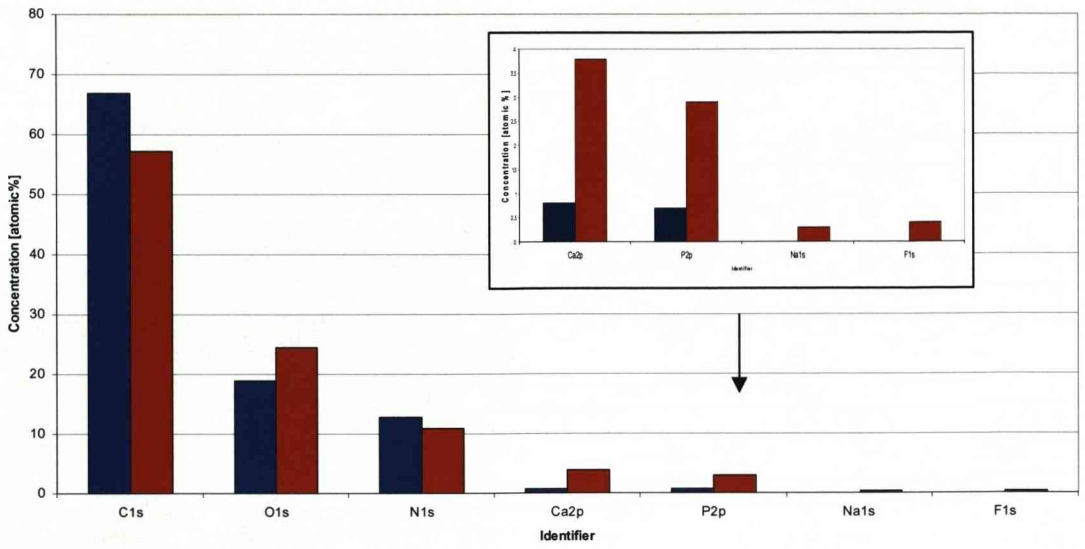


**Figure 5.11.** Graph showing the effect of NaF treatment of etched dentine on concentration [atomic %]. etched dentine (blue), etched and NaF (red) Insert Ca2p, P2p Na1s and F1s concentration changes

Figure 5.11 also highlights an increase in the Ca2p concentration. The increase in inorganic components was accompanied by a decrease in the organic components.

There was no change to the Na1s and F1s peak heights or positions following argon ion sputtering. This would indicate that the NaF solution had entered the dentinal tubules. Therefore, NaF was able to penetrate further than the surface layers alone and appears to be reaching the subsurface layers of dentine.

Following argon ion sputtering, there was an increase in the Ca2p signal (figure 5.12). This increase was greater than that observed for the etched dentine sample alone following argon ion sputtering (green line figure 5.12). It was also apparent there was a 1eV peak shift on the NaF treated samples compared to non NaF treated sample. The peak shift would position the Ca2p peak within the range of a Ca atom associated with fluorine. Therefore, the shift in the Ca2p peak position can be used to highlight the incorporation of the NaF into the inorganic phase of the dentine.

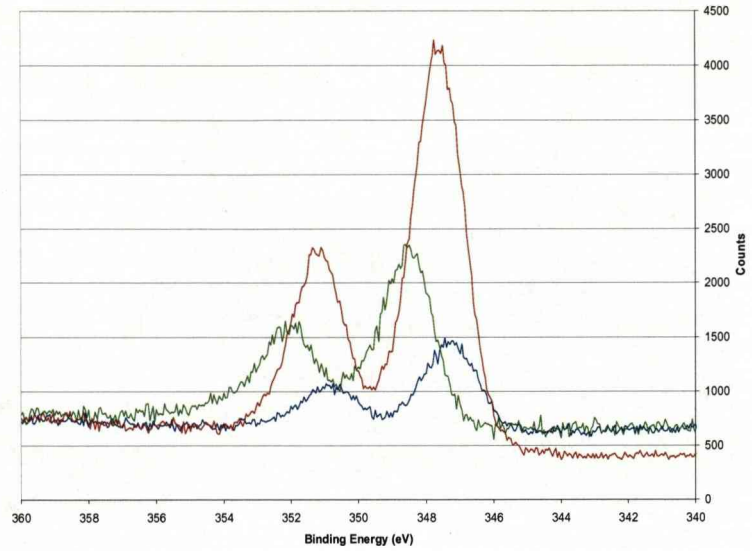


**Figure 5.12** Ca2p spectra for etched dentine and NaF treated before (blue line) and after 10 mins argon ion sputtering (red line) and etched dentine after 10 mins argon ion sputtering (green line).

There was a decrease in the relative concentration of C1s following argon ion sputtering. When the Ca2p and C1s concentrations were compared (table 5.4), there was an increase in the inorganic phase of the dentine following NaF treatment. There was a further increase in the inorganic phase, following argon ion sputtering of the NaF treated surface. The ratios of C:Ca were higher on the NaF treated samples than on the non etched dentine samples which had undergone no further treatment (table 5.4).

| **Dentine Treatment** | **Concentration [Atomic %]** | | **Ratio** |
|---|---|---|---|
| | **C1s** | **Ca2p** | **C : Ca** |
| Etched before $Ar^+$ | 66.9 | 0.8 | 1: 0.01 |
| Etched after $Ar^+$ | 77.3 | 3.1 | 1: 0.04 |
| Etched and NaF before $Ar^+$ | 57.2 | 3.8 | 1: 0.07 |
| Etched and NaF after $Ar^+$ | 38.7 | 12.8 | 1: 0.33 |

**Table 5.4** The effect of argon ion sputtering ($Ar^+$) of etched and NaF treated dentine on the C1s and Ca2p concentrations and ratio.

Non etched dentine

Non etched → NaF treated

Following NaF treatment of the non etched dentine, there was the appearance of Na1s and F1s peaks (figure 5.13). It was also apparent that the NaF treatment of the non etched dentine surface led to a decrease in the concentrations of the organic components of dentine (C1s and N1s) (figure 5.13).

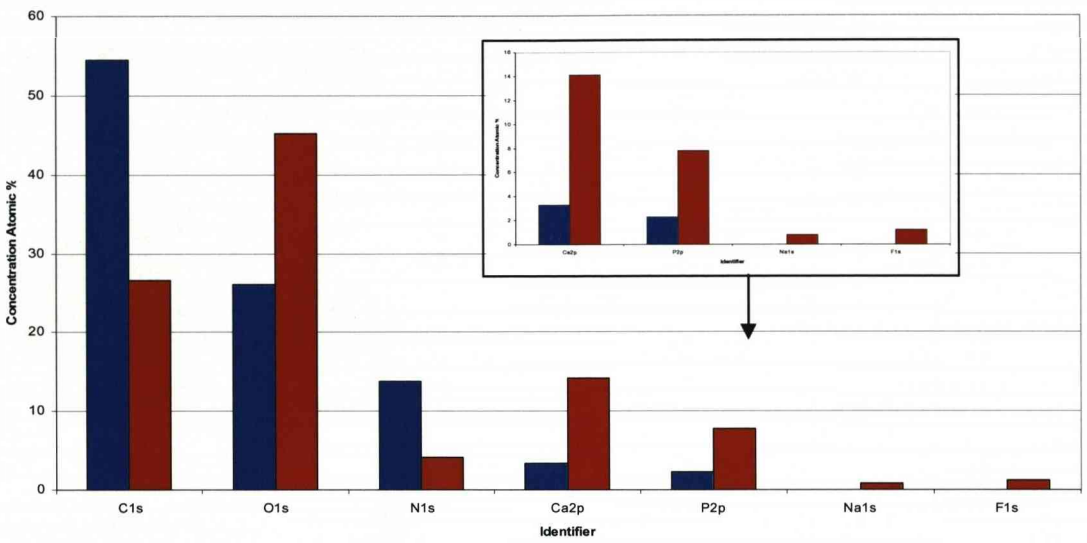


**Figure 5.13.** Graph showing the effect of NaF treatment of non etched dentine on concentration [atomic %]. Non etched dentine (blue), non etched and NaF (red) Insert Ca2p, P2p Na1s and F1s and Si2p concentration changes

As with the etched dentine sample, NaF treatment resulted in an increase in the Ca2p and P2p concentration (figure 5.13). Accompanying the increased inorganic phase concentrations, was an increase in the O1s concentration (figure 5.13).

Following 10 minutes argon ion sputtering there was no alteration to the Na1s and F1s peak intensities. This would indicate that the NaF treatment was able to penetrate the surface of the dentine. Argon ion sputtering resulted in an increase in the Ca2p and P2p concentrations and a decrease in the C1s and N1s concentrations (data not shown). The effect of both NaF treatment and argon ion sputtering on the

inorganic and organic phases of dentine are highlighted in table 5.5. There is an increase in the inorganic phase on the NaF treated samples, following argon ion sputtering. As with the etched dentine sample, it is apparent that the Ca2p concentrations are considerably higher on the NaF treated samples compared to the non treated dentine samples.

| **Dentine Treatment** | **Concentration [Atomic %]** | | **Ratio** |
|---|---|---|---|
| | **C1s** | **Ca2p** | **C : Ca** |
| Non etched before $Ar^+$ | 54.5 | 3.3 | 1 : 0.06 |
| Non etched after $Ar^+$ | 74.3 | 5.3 | 1 : 0.07 |
| Non etched and NaF before $Ar^+$ | 26.6 | 14.1 | 1 : 0.53 |
| Non etched and NaF after $Ar^+$ | 18.6 | 18.8 | 1 : 1.01 |

**Table 5.5** The effect of NaF treatment of non etched dentine on the ratio C : Ca and the effect of subsequent argon ion sputtering ($Ar^+$) of the treated surfaces.

**c) Effect of acid challenge**

i) silica treated

Etched dentine.

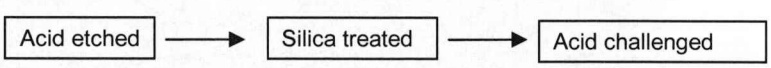


Citric acid was selected for these experiments following discussions with GlaxoSmithKline. Citric acid is commonly found in fruit juices at this concentration and as such is often used as a standard industry test of a coatings ability to withstand acid. Acid challenge of the nanoparticulate silica coated etched dentine surface (sample 3) resulted in a decrease in the O1s concentration (figure 5.14), which can be linked to the decrease in Si2p concentration.

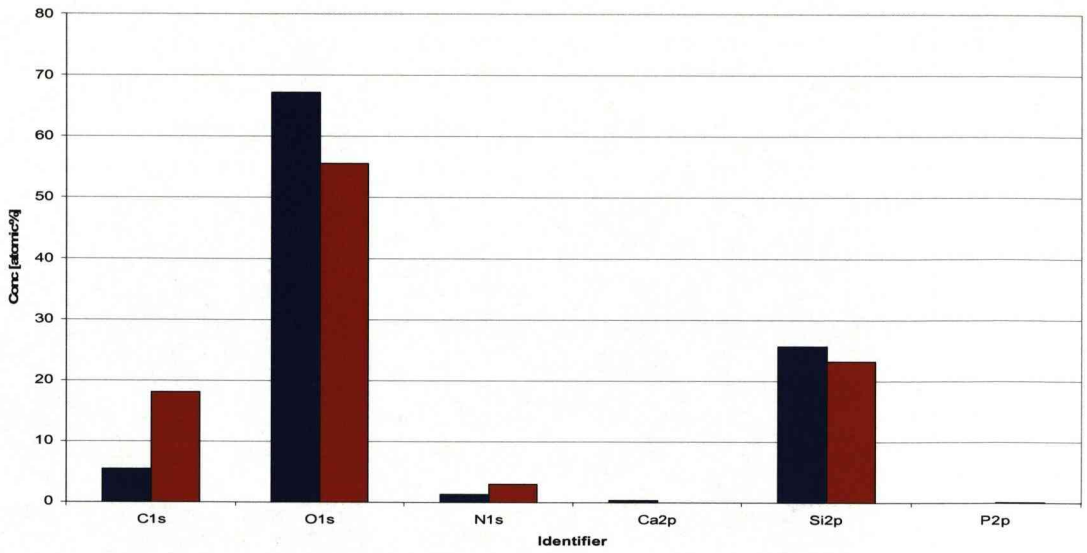


**Figure 5.14.** Graph showing the effect of acid challenge of nanoparticulate silica treated etched dentine on concentration [atomic %]. etched dentine and nanoparticulate silica (blue), and following acid challenge (red).

The small decrease in the relative concentration of Si2p following acid challenge would indicate that a substantial amount of the nanoparticulate silica coating had remained intact despite acid challenge. This theory is supported by the lack of dentine associated components such as Ca2p and P2p. Although there are small increases in the organic components such as C1s (figure 5.15), these increases are minimal compared to the C1s peak observed on the etched dentine sample (blue line figure 5.15), therefore, suggesting that the nanoparticulate silica coating had been able to withstand acid challenge.

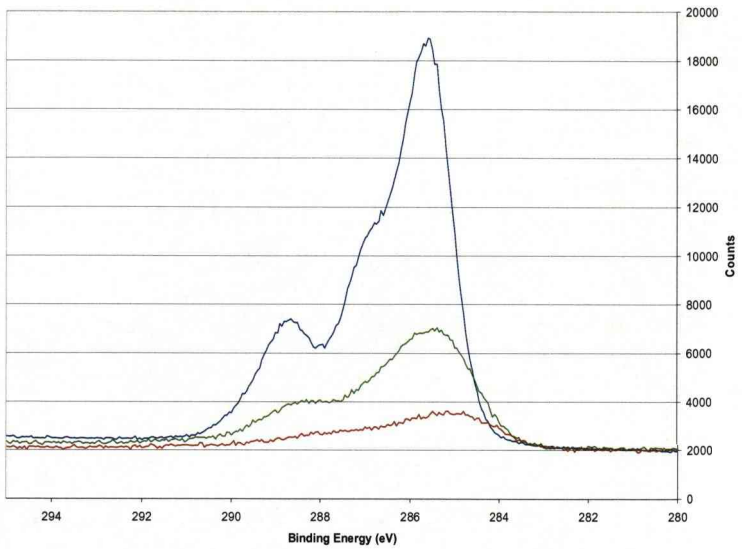


**Figure 5.15** C1s spectra for etched dentine (blue line) and etched dentine and silica (red line) and following acid challenge (green line).

Following argon ion sputtering, there was a further decrease in the Si2p peak intensity and a corresponding decrease in the O1s peak intensity (data not shown), which would indicate that some of the residual silica had been removed from the surface. But, as highlighted in figure 5.16, the majority of the underlying dentine was still covered in a substantial coating of nanoparticulates, as the inorganic dentine related spectra remained undetected. Although there was an increase in the organic component of dentine, the intensity of the C1s peak was still below that of the non silica treated sample, therefore, indicating that the silica coating was able to withstand the acid challenge and offered some protection to the underlying dentine.

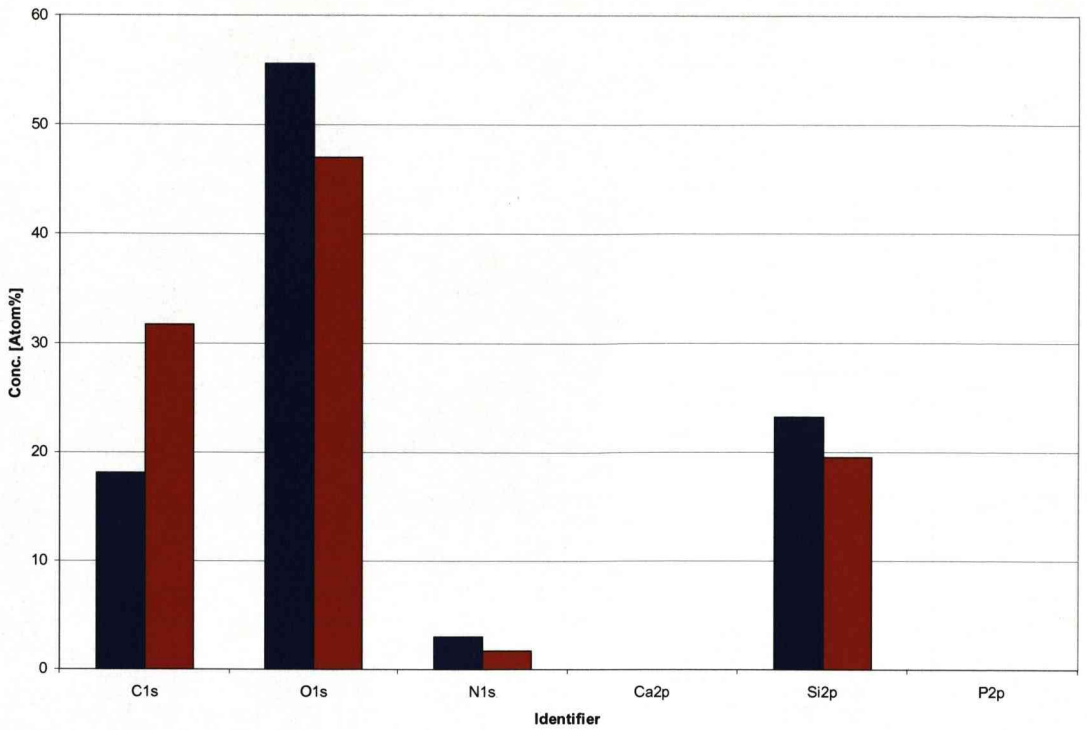


**Figure 5.16.** Graph showing the effect argon ion sputtering of nanoparticulate silica treated etched dentine following acid challenge on concentration [atomic %]. Before (blue), and after 10 mins argon ion sputtering (red).

Non etched dentine

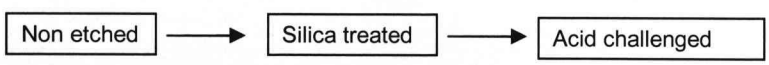


Acid challenge of the silica treated non etched dentine resulted in a decrease in the Si2p concentration (figure 5.17). Following acid challenge and the drop in Si2p intensity, a corresponding decrease in O1s would be expected. However, this does not occur and there is an increase in the O1s concentration (figure 5.17).

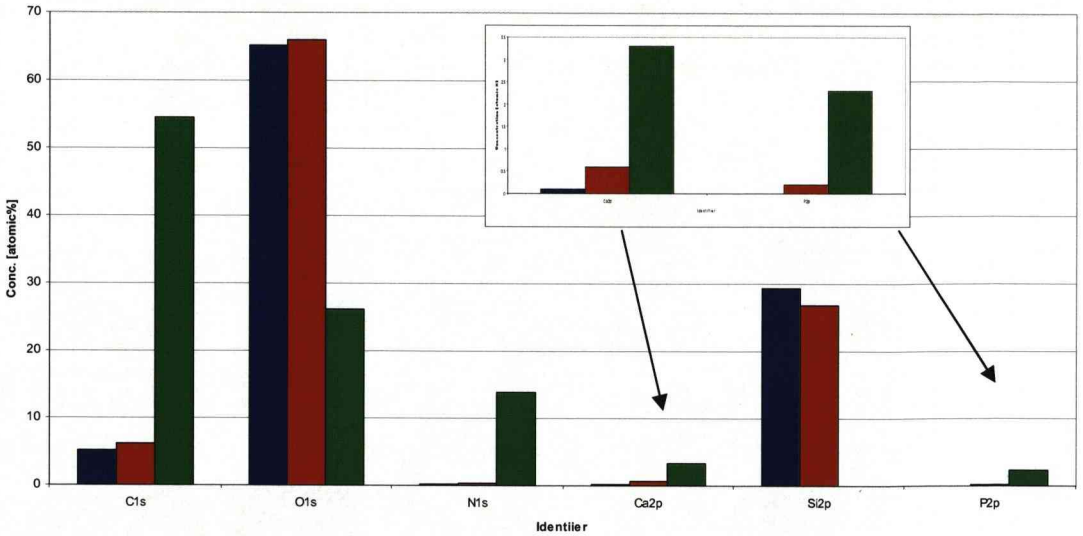


**Figure 5.17.** Graph showing the effect acid challenge of nanoparticulate silica treated non etched dentine on concentration [atomic %]. Non etched dentine and silica (blue), and following acid challenge (red) and non etched dentine (green). Insert Ca2p and P2p.

Acid challenge resulted in an increase in the concentrations of the dentine associated peaks, both organic (C1s and N1s) and inorganic (Ca2p and P2p), as highlighted by the appearance of the Ca2p peak following acid challenge (figure 5.18). Therefore, the increase in O1s concentration was due to the re emergence of dentine related spectra. This would support the suggestion that nanoparticulate silica had been removed from the surface during acid challenge.

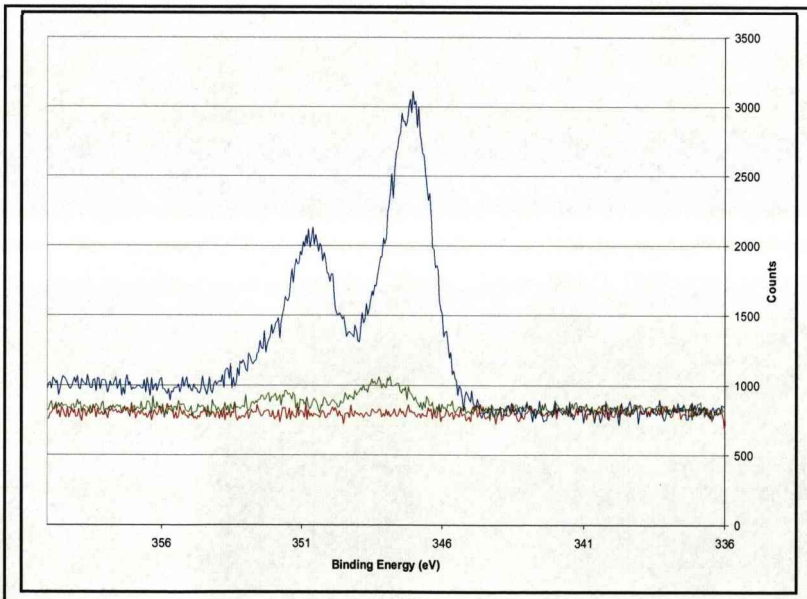


**Figure 5.18** Comparison of the Ca2p spectra of non etched dentine (blue line) following silica treatment (red line) and following acid challenge of the silica coating (green line)

Argon ion sputtering resulted in a decrease in the O1s peak intensity. This decrease is associated with the further removal of nanoparticulate silica from the surface, as there was a corresponding decrease in the Si2p peak intensity (data not shown). In conjunction with the loss of silica from the surface, there was an increase both the Ca2p and the C1s concentrations, therefore, supporting the suggested removal of the nanoparticulate silica from the upper surface and the exposure of the dentine following argon ion sputtering. Although, due the continued presence of a Si2p peak, some silica remains which could be due to the silica penetrating the tubules as well as incomplete removal from the surface.

ii) NaF treated

Etched dentine

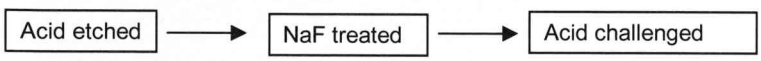


Acid challenge of the NaF treated surface resulted in a decrease in the concentration of Ca2p (figure 5.19), and was accompanied by a decrease in the O1s concentration. However, there was an increase in the concentrations of the organic components such as C1s and N1s following acid challenge. Therefore, it can be surmised that the decrease in O1s intensity can be linked to the decrease in the inorganic dentine components, suggesting that the dentine underwent some level of demineralisation following acid challenge.

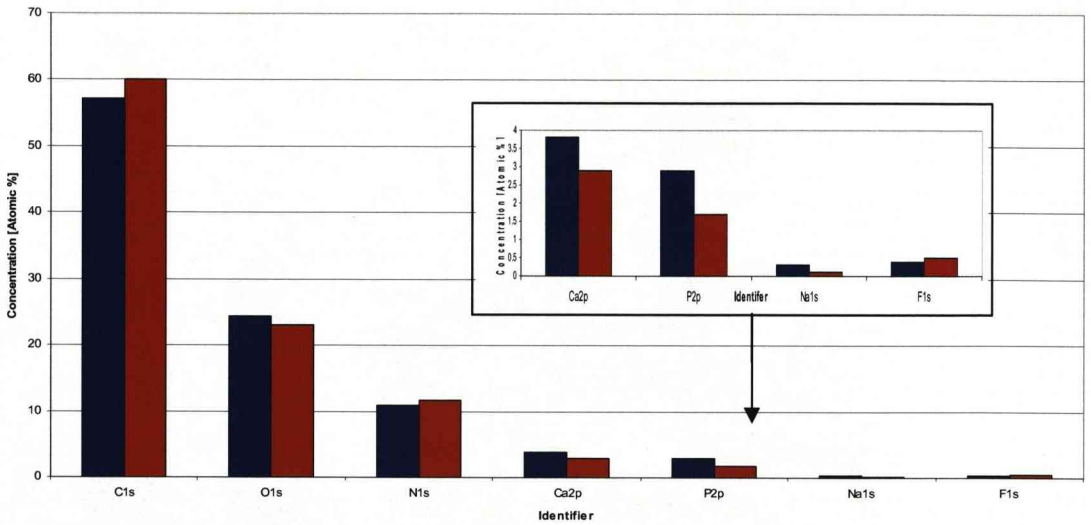


**Figure 5.19.** Graph showing the effect acid challenge of NaF treated etched dentine on concentration [atomic %]. etched dentine and NaF (blue), and following acid challenge (red) Insert Ca2p and P2p Na1s and F1s.

The Na1s and F1s concentrations decreased following acid challenge. The decreases in Na1s and F1s could be linked with the decrease in the inorganic phase of dentine. The decrease in the relative concentration of the mineralised phase of dentine would suggest that the NaF treatment offered little protection to the dentine from acid challenge.

Argon ion sputtering resulted in increases in Ca2p concentration (figure 5.20). This increase was accompanied by a decrease in the relative concentrations of C1s and N1s.

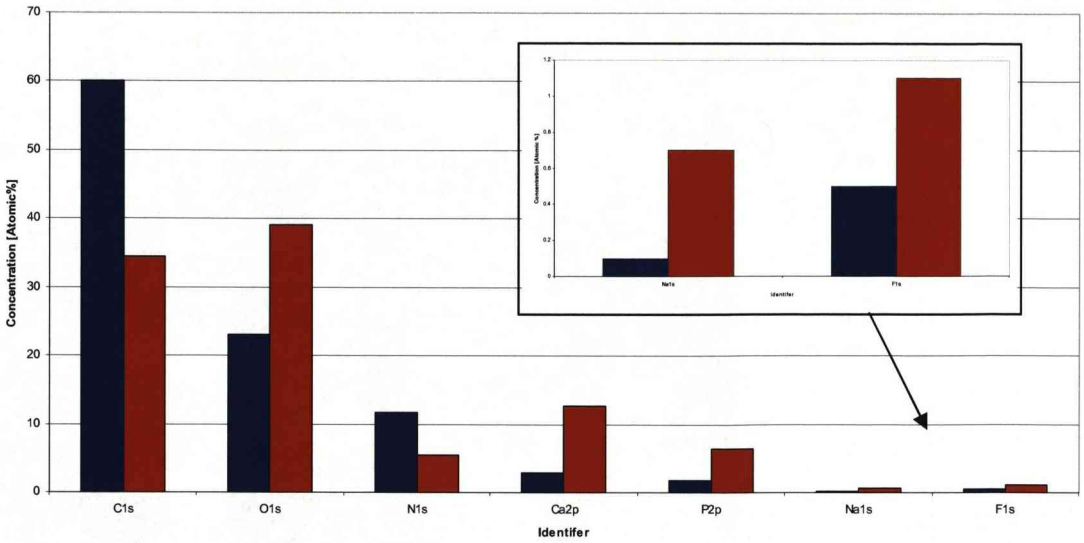


**Figure 5.20.** Graph showing the effect of argon ion sputtering of acid challenged NaF treated etched dentine on concentration [atomic %]. Before argon ion sputtering (blue), and following 10 mins argon ion sputtering (red) Insert Na1s and F1s.

Comparison of the organic to inorganic ratio following different treatments revealed that, following acid challenge and argon ion sputtering, there was an increase in the inorganic phase (table 5.6), indicating that there was some demineralisation at the surface upon acid challenge as observed by the decrease in the C:Ca ratio. However, upon argon ion sputtering, there was an increase in the C:Ca ratio suggesting the demineralised zone at the surface had been removed, indicating that the demineralisation due to acid challenge was confined to the surface. Removal of the demineralised zone through argon ion sputtering reveals the un-affected mineralised dentine of the bulk.

| Treatment | Concentration [Atomic %] | | Ratio |
|---|---|---|---|
| | C1s | Ca2p | C : Ca |
| Treatment 4 before $Ar^+$ | 60 | 2.9 | 1 : 0.05 |
| Treatment 4 after $Ar^+$ | 34.5 | 12.7 | 1 : 0.37 |
| Treatment 2 before $Ar^+$ | 57.2 | 3.8 | 1: 0.07 |
| Treatment 2 after $Ar^+$ | 38.7 | 12.8 | 1 : 0.33 |

**Table 5.6.** Effect of acid challenge (treatment 4) and argon ion sputtering ($Ar^+$) on the inorganic and organic phases of etched dentine treated with NaF (treatment 2).

Non etched dentine

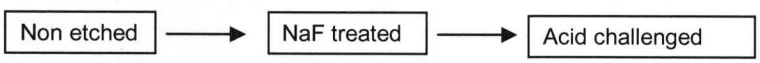


As with the etched dentine samples, there was a decrease in the inorganic peak intensities following acid challenge (figure 5.21 insert). There was also a small decrease in the F1s peak intensity (data not shown). However, the Na1s peak remained unchanged. There was an increase in the relative C1s and N1s concentrations (figure 5.21).

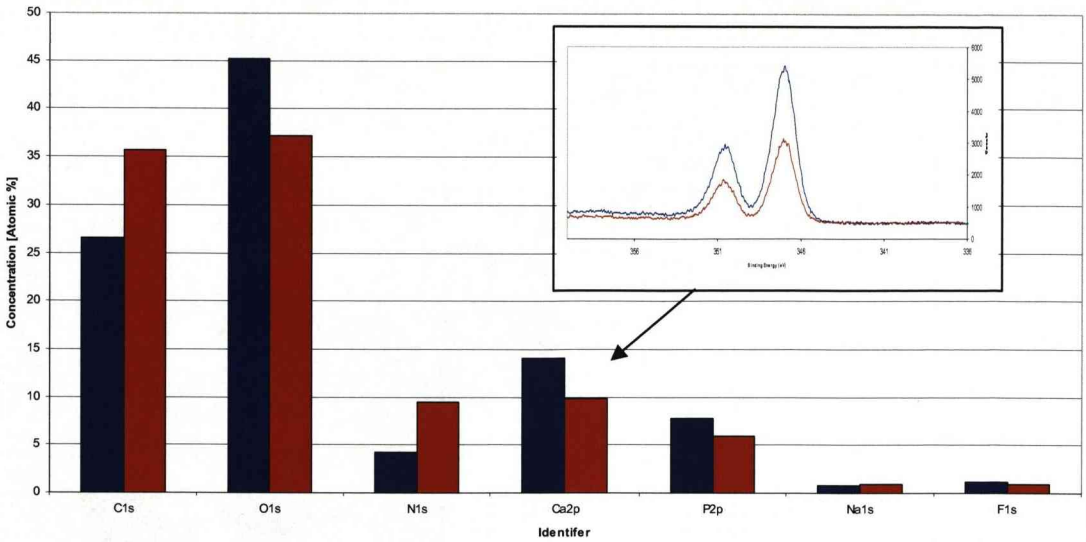


**Figure 5.21.** Graph showing the effect of acid challenged NaF treated non etched dentine on concentration [atomic %]. Non etched and NaF (blue), and following acid challenge (red) Insert Ca2p spectra, NaF treated (blue line) and acid challenged (red line).

Following argon ion sputtering, there was an increase in the inorganic relative concentrations (Ca2p and P2p) (figure 5.22), which was accompanied by an increase in the O1s peak intensity. As on the etched dentine sample, the Na1s and F1s peaks remained unchanged, with only small increases following argon ion sputtering.

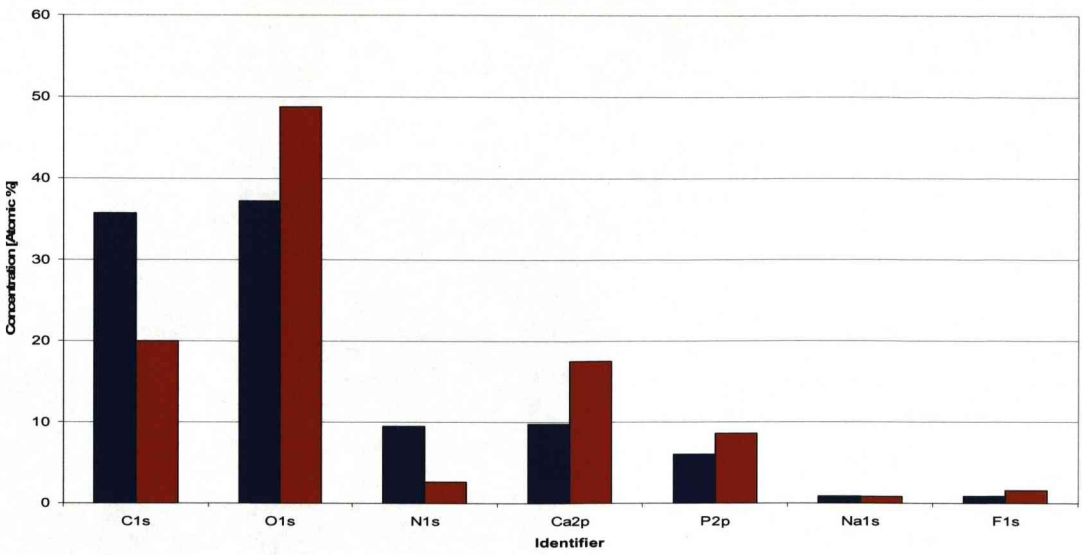


**Figure 5.22.** Graph showing the effect of argon ion sputtering of acid challenged NaF treated non etched dentine on concentration [atomic %]. before (blue), and following 10 mins argon ion sputtering (red).

When the organic component of dentine was considered, there were decreases in both the C1s and N1s relative concentrations following argon ion sputtering (figure 5.22). Comparison of the inorganic to organic ratios (table 5.7) would suggest acid challenge results in surface demineralisation. Argon ion sputtering resulted in an increase in the inorganic phase. However this was still reduced compared to the non acid challenged surface, which could indicate that argon ion sputtering had not removed the entire demineralised zone. This would suggest that NaF treatment offered little protection from acid challenge to mineralised dentine.

| Treatment | Concentration [Atomic %] | | Ratio |
|---|---|---|---|
| | C1s | Ca2p | C : Ca |
| Treatment 4 before $Ar^+$ | 35.7 | 9.8 | 1 : 0.27 |
| Treatment 4 after $Ar^+$ | 20 | 17.5 | 1 : 0.88 |
| Treatment 2 before $Ar^+$ | 26.6 | 14.1 | 1 : 0.53 |
| Treatment 2 after $Ar^+$ | 18.6 | 18.8 | 1 : 1.01 |

**Table 5.7.** Effect of acid challenge (treatment 4) and argon ion sputtering ($Ar^+$) on the inorganic and organic phases of non etched dentine treated with NaF (treatment 2).

### 5.4.3 Remineralisation of the dentine samples

a) non coated dentine

Etched dentine


Artificial saliva treatment of the etched dentine resulted in an increase in the Ca2p peak intensity (figure 5.23) The intensity of the Ca2p peak of etched dentine artificial saliva treated was greater than that of non etched dentine. Accompanying the increase in Ca2p, was an increase in the P2p intensity and the O1s (data not shown). In comparison with the inorganic phase components, there was a decrease in the intensity of both organic associated components (C1s and N1s) (data not shown).

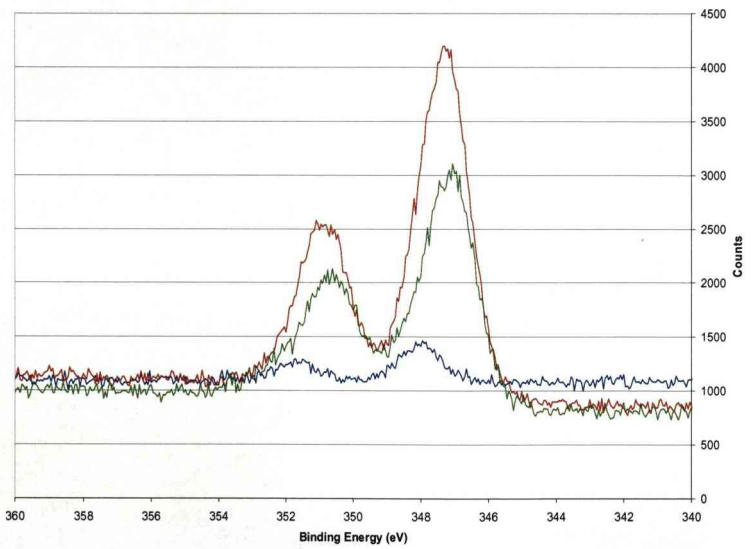


**Figure 5.23** Comparison of the Ca2p spectra of etched dentine (blue line) following artificial saliva treatment (red line) and non etched dentine (green line)

Comparison of the concentrations of an inorganic (Ca2p) and organic (C1s) component (table 5.8) revealed that there was a 10-fold increase in the mineralised phase of the etched dentine surface, following artificial saliva treatment. This was higher than that of the non etched dentine. It can be suggested that artificial saliva treatment resulted in some surface remineralising of the demineralised dentine.

| Treatment | Concentration [Atomic %] | | Ratio |
|---|---|---|---|
| | C1s | Ca2p | C: Ca |
| Etched dentine | 66.9 | 0.8 | 1 : 0.01 |
| Etched and artificial saliva | 50.6 | 5.1 | 1 : 0.1 |
| Non etched dentine | 54.5 | 3.3 | 1 : 0.06 |

**Table 5.8.** The effect of artificial saliva treatment of etched dentine on the ratio of inorganic to organic phases.

Argon ion sputtering of the artificial saliva treated surface resulted in a further increase in the relative concentration of Ca2p (figure 5.24), and was accompanied by increases in the relative concentrations of both P2p and O1s (figure 5.24).

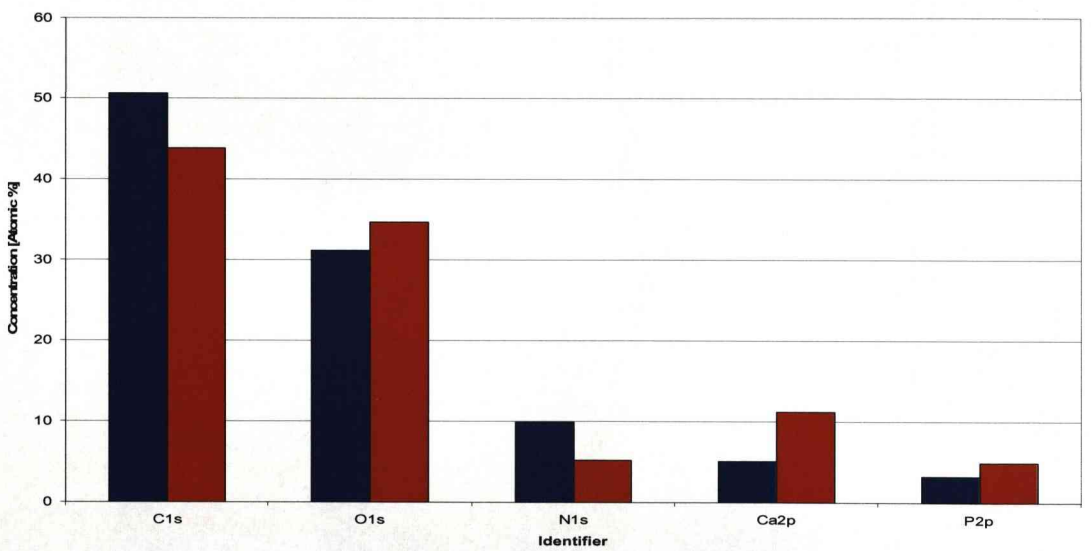


**Figure 5.24.** Graph showing the effect of artificial saliva treatment of etched dentine on concentration [atomic %]. before (blue), and following 10 mins argon ion sputtering (red).

These increases were coupled with further decreases in the relative concentrations of the organic phase, including C1s. However, this was despite the increase in the 285eV peak intensity (figure 5.25), as there was the loss of the shoulders at 286 and 288 eV.

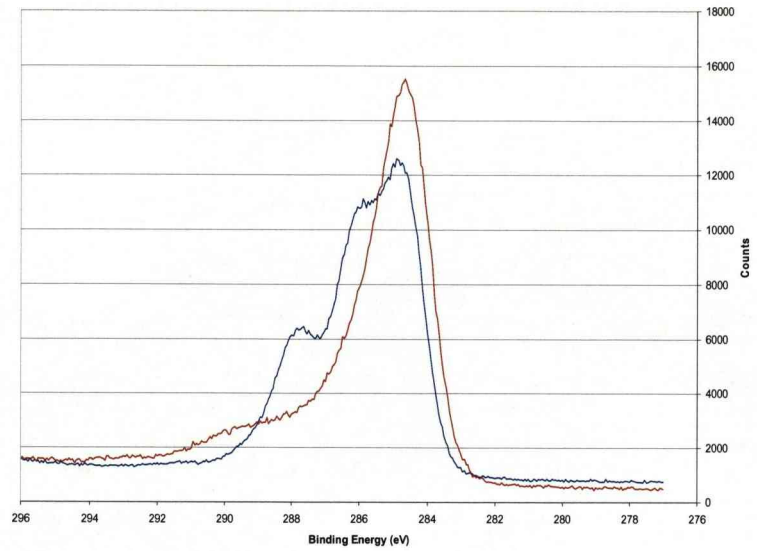


**Figure 5.25** C1s spectra of etched dentine and artificial saliva treatment before (blue line) and after 10 mins Argon ion sputtering (red line).

Argon ion sputtering resulted in a further increase in the C : Ca ratio from 0.1 to 0.26, and would suggest that the artificial saliva treatment was able to penetrate the surface. Again this level was higher than that of the non etched dentine, which had not undergone any further treatments.

Non etched dentine


As on the etched dentine sample, artificial saliva treatment resulted in an increase in the relative concentration of Ca2p (figure 5.26). Which was in conjunction with an increase in the second inorganic associated atom P2p. However, there was a decrease in the organic components C1s and N1s concentrations.

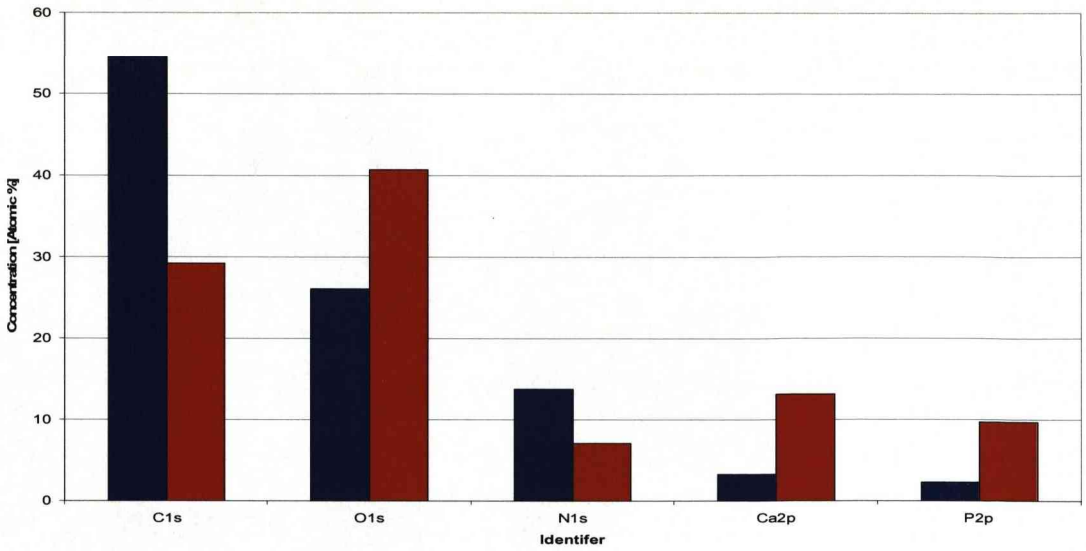


**Figure 5.26.** Graph showing the effect of artificial saliva treatment of non etched dentine on concentration [atomic %] non etched dentine (blue), and following artificial saliva treatment (red).

Argon ion sputtering resulted in a decrease in the N1s peak intensity (data not shown). However, argon ion sputtering led to an increase in the C1s peak intensity (figure 5.27) The increase in the 285eV C1s peak was accompanied by the increase in the secondary peak at 289eV.

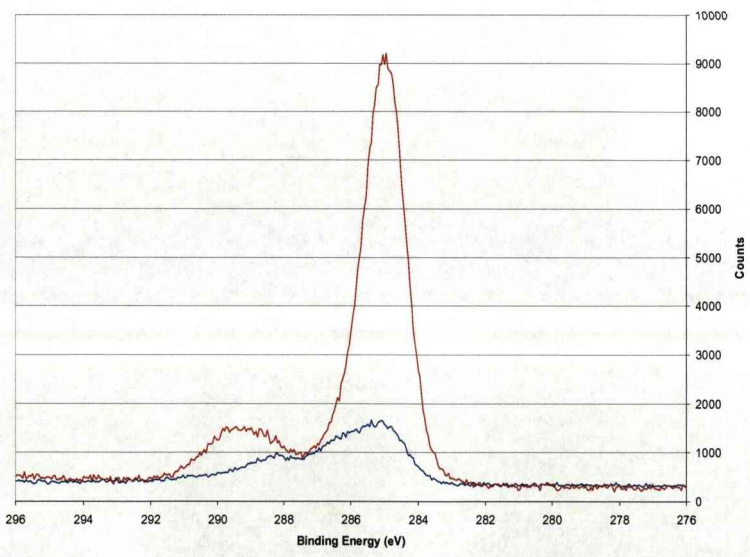


**Figure 5.27** C1s spectra for non etched dentine following artificial saliva treatment before (blue line) and after 10 mins Argon ion sputtering (red line).

A similar pattern was also observed for the two inorganic phase associated atoms, following argon ion sputtering. Although there was a decrease in the P2p peak intensity it was accompanied by an increase in the Ca2p peak height (figure 5.29).

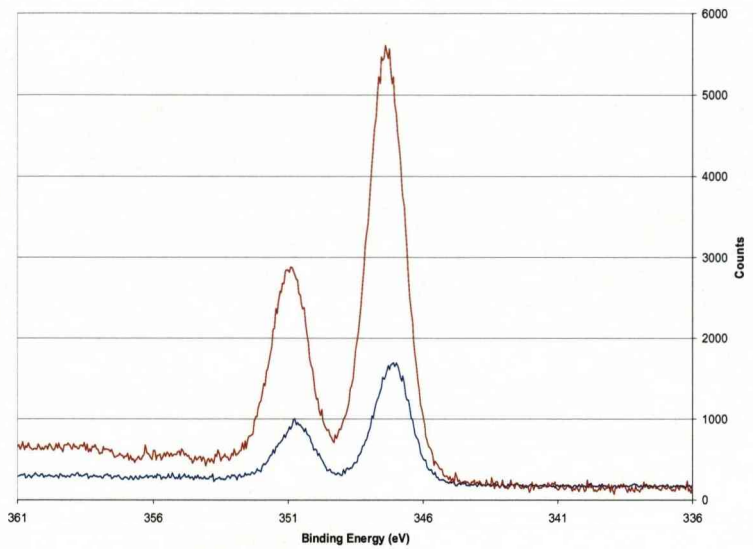


**Figure 5.28** Ca2p spectra for non etched dentine following artificial saliva treatment before (blue line) and after 10 mins Argon ion sputtering (red line).

When the effect of argon ion sputtering on the inorganic and organic phases was compared (table 5.9), it appeared that argon ion sputtering had little affect on the inorganic phase, with the ratio of C:Ca increasing by only a small amount. However, the ratio was greater for the artificial saliva treated dentine in comparison to the non etched dentine, which had undergone no further treatment. This would again suggest that artificial saliva treatment increased mineralization of the dentine, probably through the creation of a pellicle coating by deposition of salivary compounds onto the dentine surface.

| Treatment | Concentration [Atomic %] | | Ratio |
|---|---|---|---|
| | C1s | Ca2p | C : Ca |
| Artificial saliva before | 29.2 | 13.1 | 1 : 0.45 |
| Artificial saliva after $Ar^+$ | 31.8 | 15.6 | 1 : 0.49 |
| Non etched before | 54.5 | 3.3 | 1 : 0.06 |
| Non etched after $Ar^+$ | 74.3 | 5.3 | 1 : 0.07 |

**Table 5.9** Effect of artificial saliva and argon ion sputtering ($Ar^+$) on the organic and inorganic phases of non etched dentine.

b) silica treated

Etched dentine


Treating the silica coated dentine with artificial saliva (treatment 6) resulted in a decrease in the concentrations of Si2p and O1s (figure 5.29). Although there was a decrease in the O1s concentration upon artificial saliva treatment, the concentration was still greater than on the non silica treated surfaces. The continued presence of a heightened O1s concentration and a Si2p peak indicates that a nanoparticulate coating was still present, despite artificial saliva treatment.

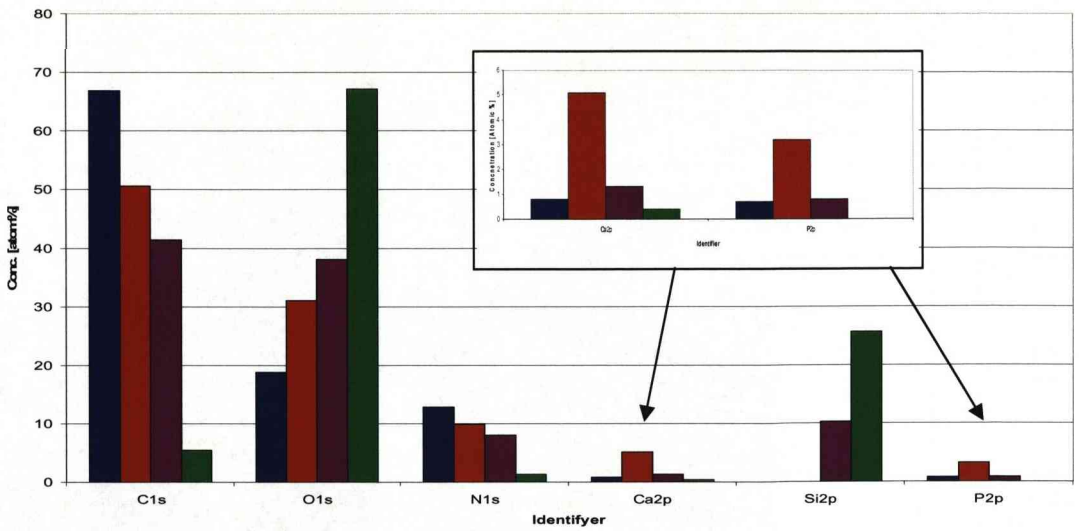


**Figure 5.29.** Graph showing the effect of Treatment 4 on etched dentine on concentration [atomic %]. Etched dentine (blue), and following artificial saliva treatment (red) etched dentine treatment 6 (purple) and etched dentine and nanoparticulate silica (green).

The Ca2p concentration was higher than both etched dentine and treatment 1 (silica treatment) etched dentine. This would indicate that surface mineralization had occurred. However, due to the presence of the nanoparticulate silica coating the Ca2p concentration remains lower than the treatment 5 (artificial saliva treated) etched dentine, as the coating masks any residual Ca2p that is associated with the dentine so only the Ca adsorbed onto the surface is measured.

Artificial saliva treatment resulted in an increase in the C1s peak intensity (figure 5.30). Although the peak height is still below that of etched dentine, it follows a very similar shape as the peak of etched dentine following artificial saliva treatment (red line figure 5.30). Both artificial saliva treated samples had a diminished 285eV peak and a more prominent secondary peak at 286eV, although peak height of the 286eV peak does not appear to increase. The third peak at 288eV remains relatively unchanged for all three spectra.

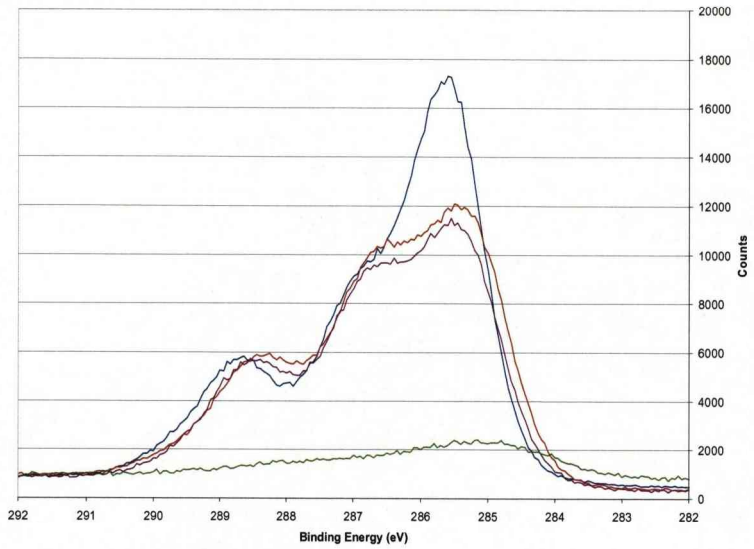


**Figure 5.30** C1s spectra of etched dentine (blue line) and artificial saliva treatment (red line) and etched dentine and silica (green line) and following artificial saliva treatment (purple line).

Argon ion sputtering resulted in further increases in the relative concentrations of Ca2p and P2p (figure 5.31). However, the peak heights were still reduced compared to the non silica treated samples, following artificial saliva treatment. These increases were not coupled with any further increases in the components associated with the organic phase of dentine, but a reduction in the relative concentrations of both C1s and N1s following argon ion sputtering. However all these peaks were elevated in comparison with the silica treated surface which had not undergone artificial saliva treatment (figure 5.6).

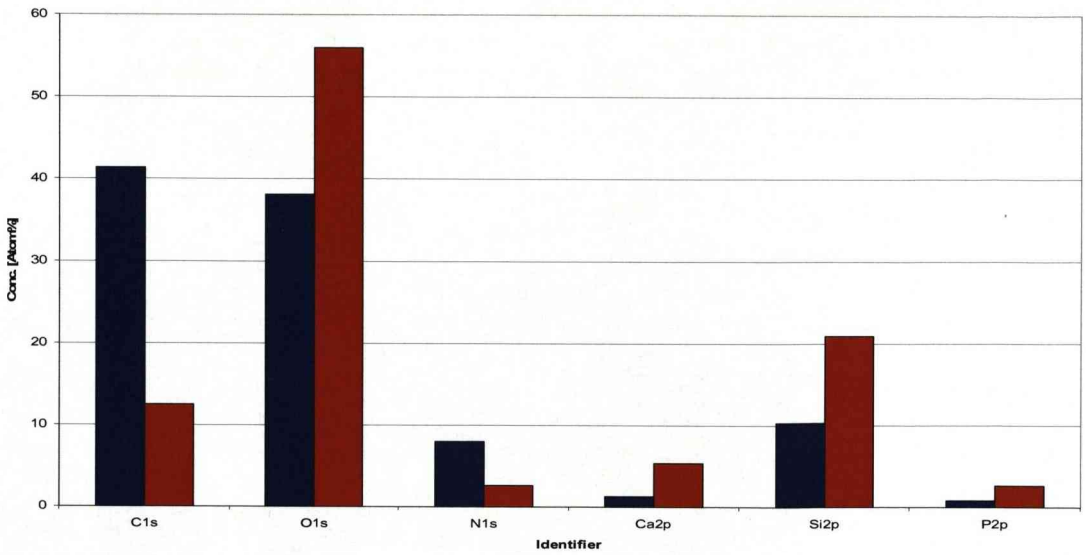


**Figure 5.31.** Graph showing the effect of argon ion sputtering of silica coated and artificial saliva treated etched dentine on concentration [atomic %] before (blue) and after 10 mins argon ion sputtering (red).

There was an increase in the relative concentrations of Si2p and O1s following argon ion sputtering of the surface. Although the concentration was diminished in comparison to the nanoparticulate silica only treated samples, the increased intensity of the silica associated concentrations combined with the decrease in the organic dentine associated concentrations would suggest that argon ion sputtering had preferentially removed the organic components of the adsorbed pellicle layer, revealing more of the nanoparticulate silica layer and unmasking more of the Ca2p containing adsorbents.

Non Etched dentine

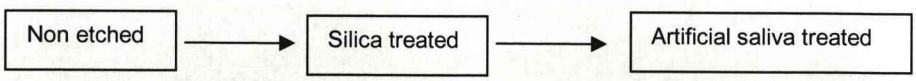


Following artificial saliva treatment of the silica coated non etched dentine surface as on the etched dentine surface, there was a decrease in the relative concentrations of both Si2p and O1s (figure 5.32). These decreases were accompanied by increases in the relative concentrations of both inorganic and organic dentine associated atoms.

As before, this would suggest that there was still silica on the surface but it had been masked by the adsorption of artificial saliva components onto the coating.

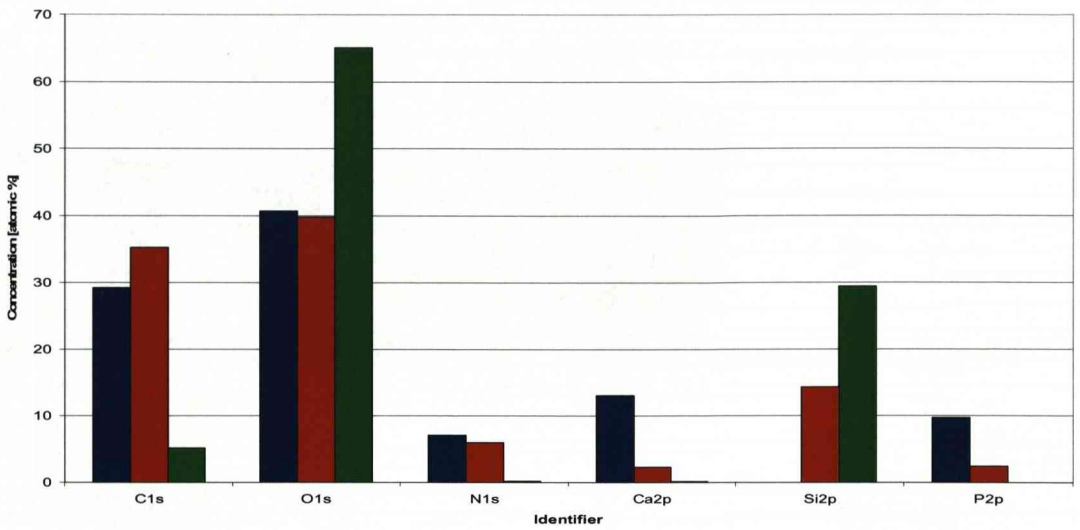


**Figure 5.32.** Graph showing the effect of artificial saliva treating silica coated non etched dentine on concentration [atomic %] non etched dentine and artificial saliva (blue) artificial saliva treated silica coated non etched dentine (red) and silica coated non etched dentine (green).

Argon ion sputtering resulted in an increase in the relative concentrations of both Si2p and O1s. These were accompanied by a decrease in the C1s and N1s concentrations. This would suggest that argon ion sputtering removed the adsorbed layer of artificial saliva proteins, revealing the underlying nanoparticulate silica coating (figure 5.33). When the C1s peak was examined, argon ion sputtering resulted in the loss of the secondary peak at 287eV (data not shown).

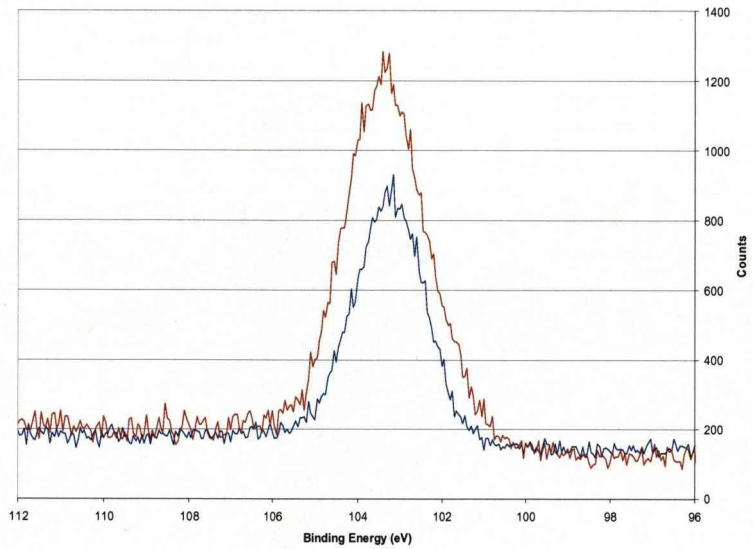


**Figure 5.33** Si2p spectra of non etched dentine silica coated and artificial saliva treated before (blue line) and after 10 mins argon ion sputtering (red line)

However, as on the etched dentine sample, there was an increase in the relative concentrations of the inorganic associated spectra (Ca2p and P2p), following argon ion sputtering. This would suggest that argon ion sputtering has preferentially removed the organic (C1s and N1s) compounds that had adsorbed onto the surface from the artificial saliva. Argon ion sputtering, therefore, exposes the silica coating and the adsorbed Ca2p and P2p containing compounds, from the artificial saliva.

c) NaF treated

Etched Dentine

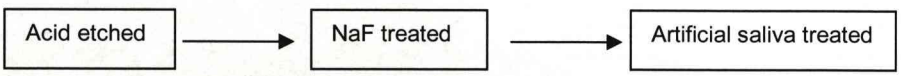


The relative concentrations of Na1s and F1s remained the same, following artificial saliva treatment of NaF treated etched dentine (treatment 7). However, following artificial saliva treatment, there was an increase in the relative concentrations of both Ca2p and P2p (figure 5.34).

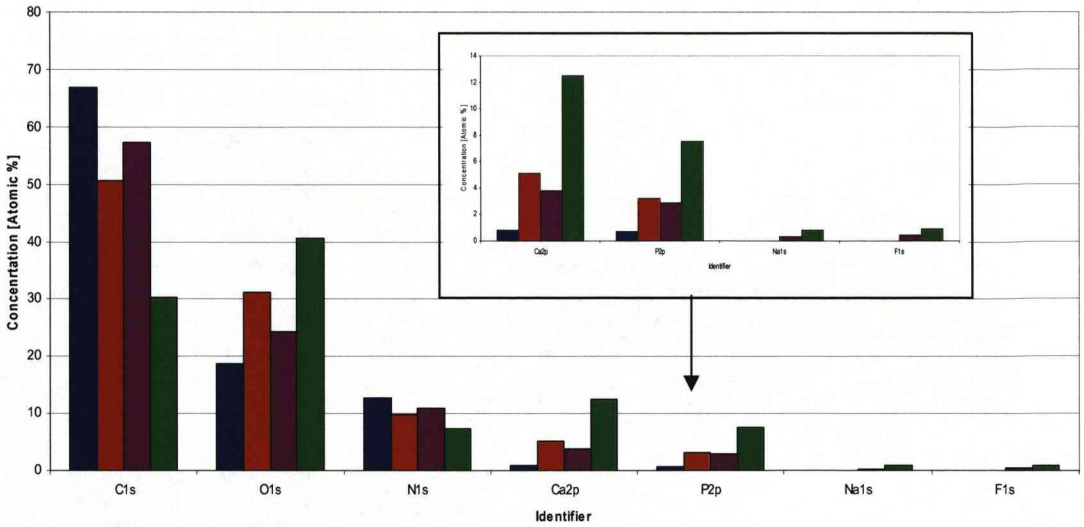


**Figure 5.34.** Graph showing the effect of artificial saliva treating NaF coated etched dentine on concentration [atomic %] etched dentine (blue) etched dentine and artificial saliva (red line) etched dentine and NaF (purple) etched and NaF and artificial saliva (green). Insert Ca2p, P2p, F1s and N1s.

The relative concentration of Ca2p on the NaF treated surface, following artificial saliva treatment (green line Figure 5.34), was greater than that of the etched dentine sample that underwent treatment 5. However, there was a decrease in the relative concentrations of the organic dentine components, following artificial saliva treatment of the NaF treated dentine (figure 5.34).

Argon ion sputtering resulted in further decreases in the relative concentrations of the organic dentine components (C1s and N1s) (figure 5.35). These decreases were accompanied by an increase in the relative concentrations of the inorganic phase (Ca2p and P2p). However, there was no alteration to the Na1s and F1s peak intensities or corresponding concentrations.

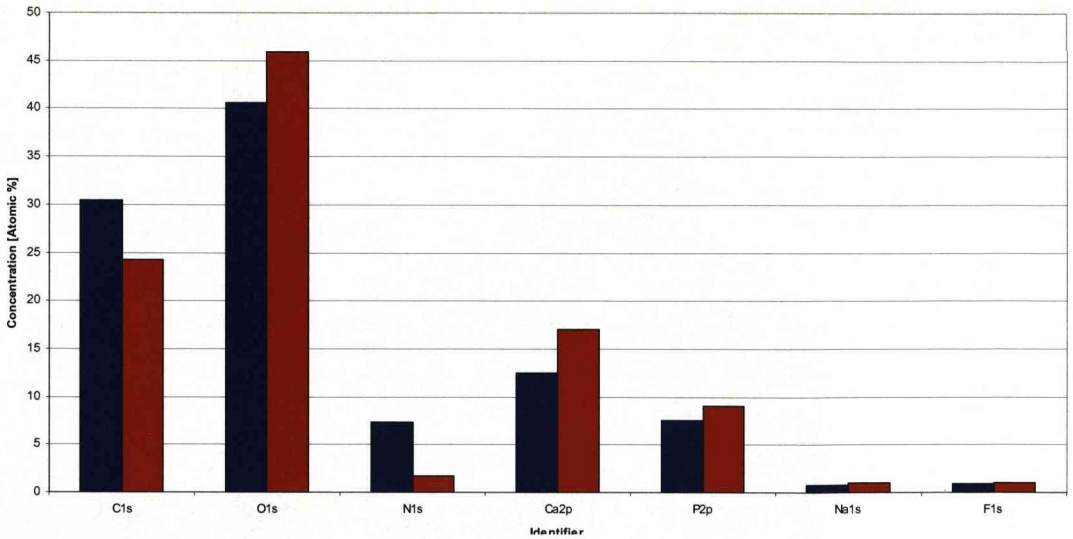


**Figure 5.35.** Graph showing the effect argon ion sputtering of artificial saliva treated NaF coated etched dentine on concentration [atomic %] before (blue) and after 10 mins argon ion sputtering (red line).

When the ratios of organic and inorganic components were considered, there was an increase in the inorganic component of the dentine, following argon ion sputtering of the artificial saliva and NaF treated dentine. When compared to both artificial saliva only and NaF only treated etched dentine, the ratio of inorganic components was increased when both a NaF and artificial saliva treatment was administered. It can be suggested that there was some level of remineralisation due to artificial saliva treatment of the etched dentine and that the level of mineralization was increased in the presence of a NaF coating.

| Treatment | Concentration [Atomic %] | | Ratio |
|---|---|---|---|
| | C1s | Ca2p | C : Ca |
| Treatment 7 before | 30.4 | 12.5 | 1 : 0.41 |
| Treatment 7 after $Ar^+$ | 24.3 | 17 | 1 : 0.7 |
| Treatment 5 before | 50.6 | 5.1 | 1 : 0.1 |
| Treatment 5 after $Ar^+$ | 43.8 | 11.2 | 1 : 0.26 |
| Treatment 2 before | 57.2 | 3.8 | 1 : 0.07 |
| Treatment 2 after $Ar^+$ | 37.9 | 12.8 | 1 : 0.33 |

**Table 5.10** The effect of argon ion sputtering on the ratio of C1s : Ca2p representing organic : inorganic ratio. Following treatment 7 ( artificial saliva treatment and NaF coated), treatment 5 (artificial saliva treatment) and treatment 2 (NaF treatment) of etched dentine and argon ion sputtering ($Ar^+$).

Non etched dentine

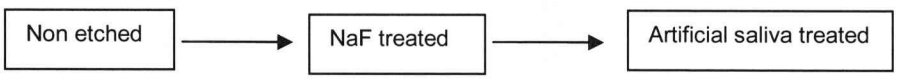


There was no difference in the relative concentration of Na1s following artificial saliva treatment of the NaF coated surface, but there was a decrease in the relative concentration of F1s. Artificial saliva treatment of the NaF coated surface resulted in a decrease in the relative concentrations of the inorganic components of dentine Ca2p and P2p (figure 5.36).

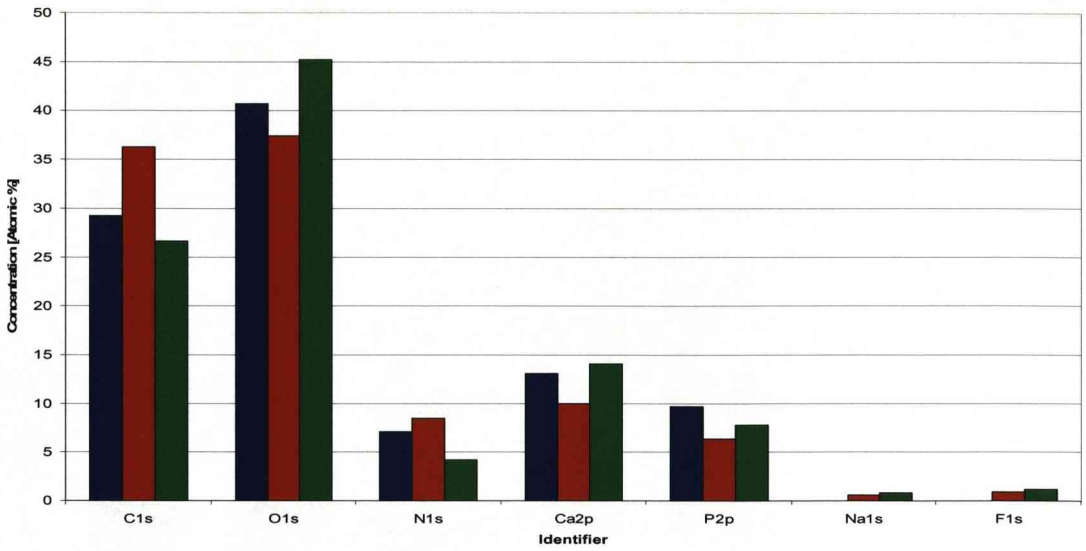


**Figure 5.36.** Graph showing the effect of artificial saliva treating NaF coated non etched dentine on concentration [atomic %] non etched dentine and artificial saliva (blue), non etched dentine and NaF coated and artificial saliva treated(red) and non etched dentine and NaF treated (green).

This would suggest the preferential adsorption of organic compounds from the artificial saliva due to the increases in the C1s peaks, therefore, explaining the decrease in the relative concentration of Ca2p below that observed for NaF treated dentine, which had not undergone artificial saliva treatment. The adsorption of organic components from the artificial saliva masks the mineralised dentine below.

Upon argon ion sputtering, there was a decrease in the relative concentration of C1s (figure 5.37), which was accompanied by an increase in the relative concentrations of Ca2p and P2p (figure 5.37). Argon ion sputtering had no effect on the relative concentration of Na1s, which was unchanged. However, there was an increase in the relative concentration of F1s (figure 5.37).

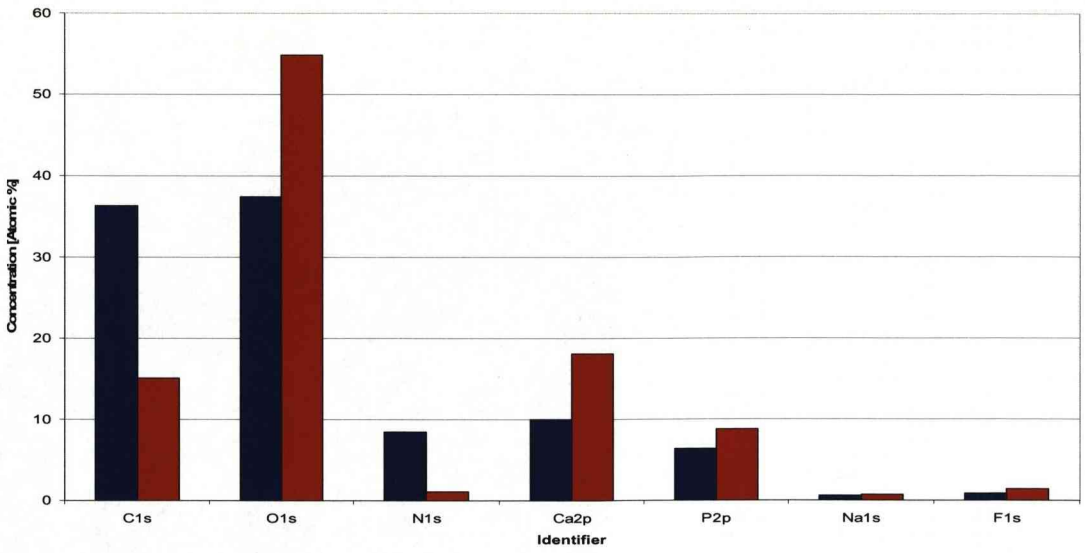


**Figure 5.37.** Graph showing the effect of argon ion sputtering of artificial saliva treated NaF coated non etched dentine on concentration [atomic %] before (blue) and after 10 mins argon ion sputtering (red).

Comparison of the inorganic and organic phases revealed a large increase in the inorganic (mineralised) phase upon argon ion sputtering (table 5.11). However, prior to argon ion sputtering, the ratio of mineralised phase was lower than on both the artificial saliva and NaF treated non etched dentine surfaces. Following argon ion sputtering, the ratio of mineralised phase was greater for the NaF and artificial saliva treated dentine than on any of the other treated surfaces compared in table 5.11. The suggestion would be that argon ion sputtering removed the adsorbed organic components of the artificial saliva, thus revealing the inorganic phase of the dentine that was previously masked by the adsorbed pellicle layer.

| Treatment | Concentration [Atomic %] | | Ratio |
|---|---|---|---|
| | C1s | Ca2p | C : Ca |
| Treatment 7 before | 36.3 | 10 | 1 : 0.28 |
| Treatment 7 after $Ar^+$ | 15.1 | 18.1 | 1 : 1.2 |
| Treatment 2 before | 26.6 | 14.1 | 1 : 0.53 |
| Treatment 2 after $Ar^+$ | 18.6 | 18.8 | 1 : 1.01 |
| Treatment 5 before | 29.2 | 13.1 | 1 : 0.45 |
| Treatment 5 after $Ar^+$ | 31.8 | 15.6 | 1 : 0.49 |

**Table 5.11** Effect of artificial saliva and argon ion sputtering ($Ar^+$) on the organic and inorganic phases of NaF treated non etched dentine. Treatment 7 (artificial saliva and NaF), treatment 2 (NaF) and treatment 5 (artificial saliva) of non etched dentine.

d) acid challenge

i) non coated

Etched dentine

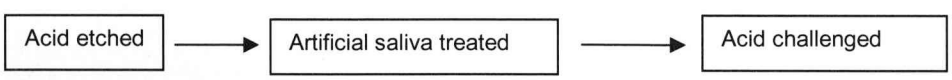


Acid challenge resulted in a decrease in the relative concentration of C1s (figure 5.38). This was accompanied by a decrease in the N1s peak intensity. When the C1s peak was considered, there was a loss of the characteristic peak shape observed for the other artificial saliva treated samples, which would suggest that the decrease in the C1s concentration was related to the removal of adsorbed carbon containing compounds from artificial saliva.

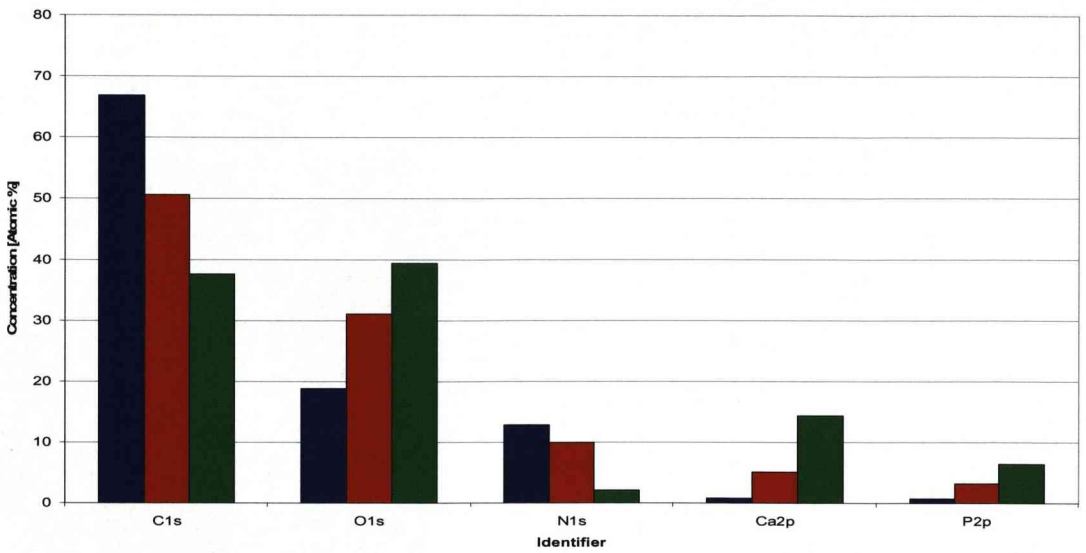


**Figure 5.38.** Graph showing the effect of acid challenge of artificial saliva treated etched dentine on concentration [atomic %] etched dentine (blue) artificial saliva treated (red) and following acid challenge (green).

Following acid challenge, there was an increase in the relative concentrations of Ca2p and P2p (figure 5.38). This would suggest that there was an increase in the inorganic phase and that acid challenge had no effect on the inorganic phase of the dentine. It is probable that acid challenge removed surface carbon rich adsorbents, exposing the underlying mineral rich surfaces created during artificial saliva treatment. Therefore, the organic carbon rich components act as a protective layer to the re mineralised dentine below.

Argon ion sputtering resulted in a small increase in the relative concentration of C1s (figure 5.39). The relative concentrations of N1s and P2p were unchanged following argon ion sputtering. However, there was a decrease in the relative concentration of Ca2p (figure 5.39).

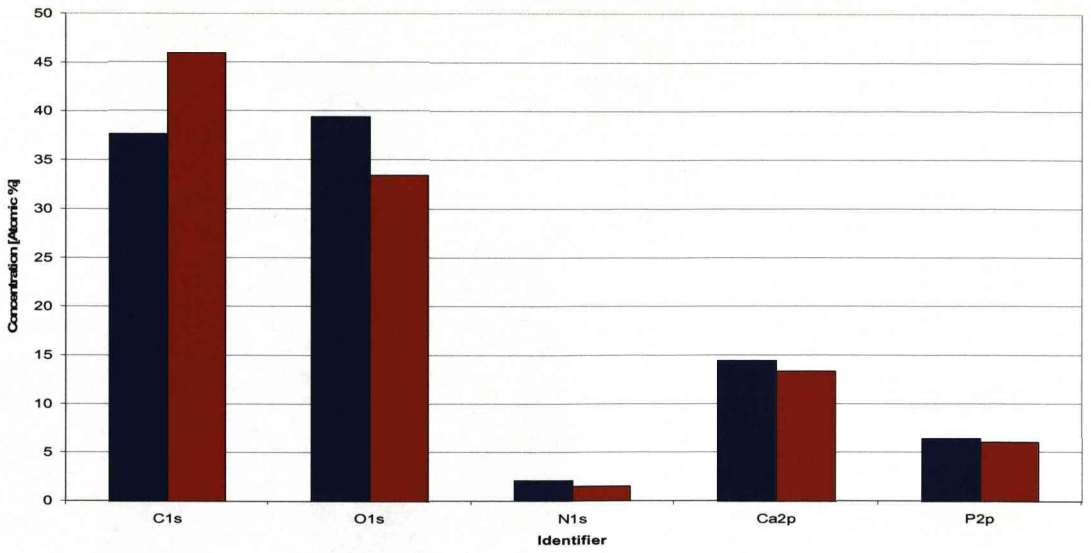


**Figure 5.39.** Graph showing the effect of argon ion sputtering an acid challenged artificial saliva treated etched dentine on concentration [atomic %] before (blue) and after 10 mins argon ion sputtering (red).

When the Ca2p and C1s concentrations were compared, there was a decrease in the inorganic (mineralised) phase, following argon ion sputtering (table 5. 12). However, the mineralised phase was of a similar level as the treatment 5 sample, following argon ion sputtering. Despite the acid challenge, the ratio of inorganic phase was still greater than on the etched dentine sample. This suggests that the mineralised phase created during artificial saliva treatment was able to withstand acid challenge. However, the organic adsorbed phase from the artificial saliva was less able to withstand acid challenge and was reduced upon acid challenge.

| Treatment | Concentration [Atomic %] | | Ratio |
|---|---|---|---|
| | C1s | Ca2p | C : Ca |
| Treatment 8 before | 37.6 | 14.4 | 1 : 0.38 |
| Treatment 8 after $Ar^+$ | 45.9 | 13.3 | 1 : 0.29 |
| Etched dentine before | 66.9 | 0.8 | 1 : 0.01 |
| Etched dentine after $Ar^+$ | 73.3 | 3.1 | 1 : 0.04 |
| Treatment 5 before | 50.6 | 5.1 | 1 : 0.1 |
| Treatment 5 after $Ar^+$ | 43.8 | 11.2 | 1 : 0.26 |

**Table 5.12.** The effect of argon ion sputtering ($Ar^+$) on etched dentine surfaces treated with treatment 8 (artificial saliva then acid challenged) and treatment 5 (artificial saliva).

Non etched dentine

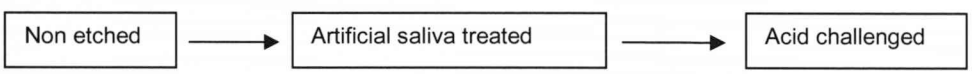


Following acid challenge there was a decrease in the relative concentration of Ca2p. However, the relative concentration was still above that of the etched dentine sample (figure 5.40), which was accompanied by a decrease in the relative concentration of P2p. There were also increases in the relative concentrations of the organic phase components (C1s and N1s) although these levels were still diminished in comparison to the non etched dentine sample (figure 5.40 blue line) These changes indicate that acid challenge of the surface reduced the mineralised phase of the dentine. Removing some of the adsorbed mineral phase appears to have increased the exposure of the organic components that may have been masked by the preferential binding of Ca2p containing compounds to the upper surface.

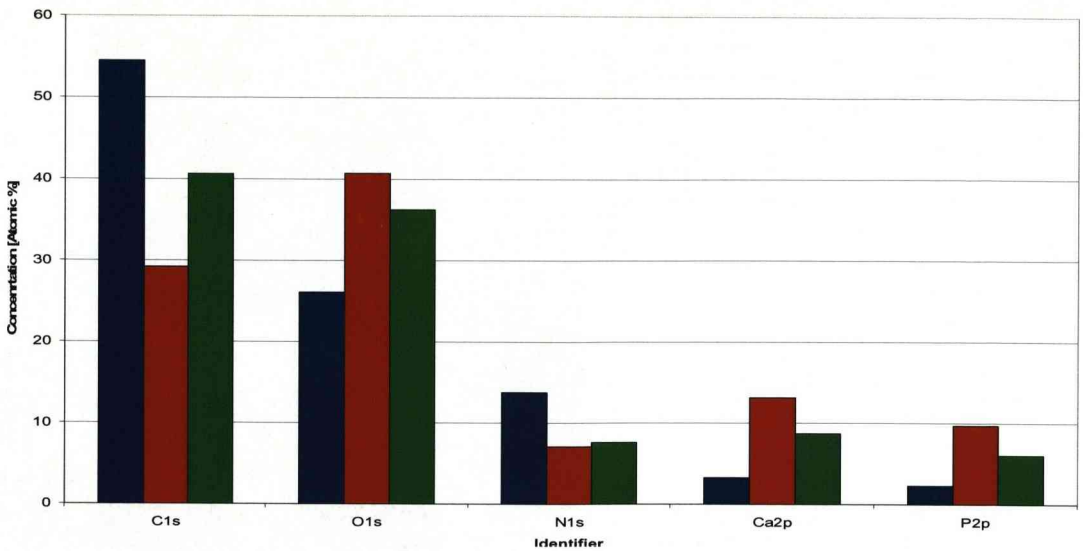


**Figure 5.40.** Graph showing the effect of acid challenge of artificial saliva treated non etched dentine on concentration [atomic %] non etched dentine (blue) and artificial saliva (red) and following acid challenge (green).

Comparison of the ratio of inorganic to organic phases revealed that there was an increase in the inorganic phase, following argon ion sputtering of the acid challenged surface (table 5.13). The ratio of inorganic phase was much higher following argon ion sputtering than on either the non etched sample or the artificial saliva treated sample (treatment 5). It can be suggested that argon ion sputtering removed some of the residual bound carbon containing products, revealing the mineralised dentine phase below the surface, that was previously masked. The continued elevation of the inorganic phase in comparison to the non treated sample would suggest that artificial saliva treatment offered some level of protection from acid challenge, despite the initial decrease in the surface Ca2p levels.

| Treatment | Concentration [Atomic %] | | Ratio |
|---|---|---|---|
| | C1s | Ca2p | C : Ca |
| Treatment 8 before | 40.6 | 8.7 | 1 : 0.21 |
| Treatment 8 after $Ar^+$ | 25.9 | 17.4 | 1 : 0.67 |
| Non etched dentine before | 54.5 | 3.3 | 1 : 0.06 |
| Non etched dentine after $Ar^+$ | 74.3 | 5.3 | 1 : 0.07 |
| Treatment 5 before | 29.2 | 13.1 | 1 : 0.45 |
| Treatment 5 After $Ar^+$ | 31.8 | 15.6 | 1 : 0.49 |

**Table 5.13** The effect of argon sputtering ($Ar^+$) non etched dentine and non etched dentine which had been subjected to treatments 8 (artificial saliva treatment then acid challenge) and 5 (artificial saliva).

ii) Nanoparticulate silica coated

Etched dentine


There was a decrease in the relative concentration of Ca2p, following acid challenge (figure 5.41). This was accompanied by a decrease in the P2p intensity, suggesting there was a loss of adsorbed mineralised compounds from the surface following acid challenge. However, a small P2p peak was still detectable following acid challenge, unlike on the silica only treated sample, where the P2p peak was undetectable.

There was an increase in the relative concentration of C1s, following acid challenge (figure 5.41). Consideration of the second organic phase associated peak revealed that there was also an increase in the relative concentration of N1s, following acid challenge of the treated surface. This suggests that there was removal of the adsorbed

calcium containing compounds from the surface, following acid challenge, revealing underlying adsorbed organic compounds.

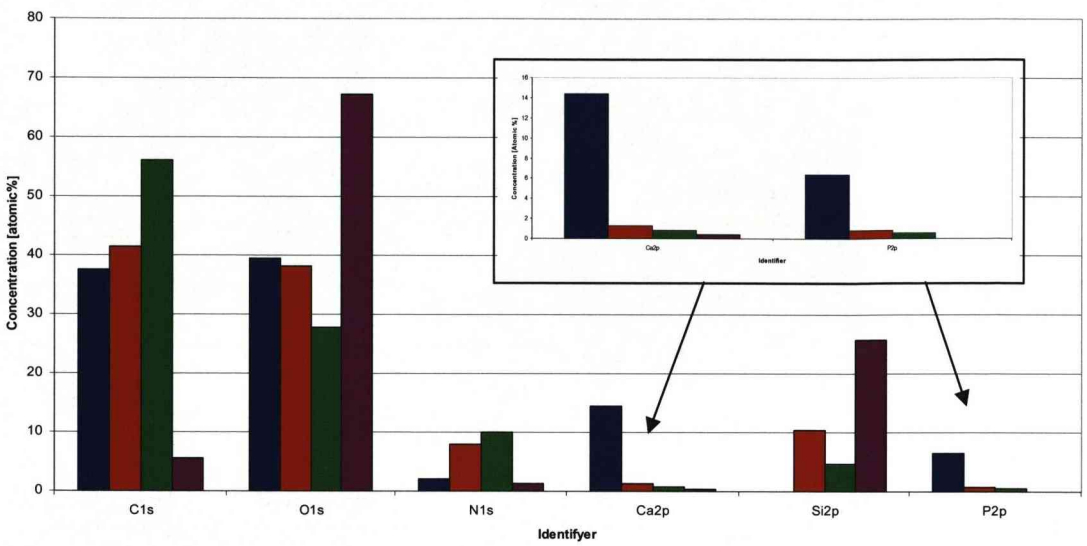


**Figure 5.41.** Graph showing the effect of acid challenge of artificial saliva treated silica coated etched dentine on concentration [atomic %] etched dentine and artificial saliva and acid challenge (blue), etched dentine and silica and artificial saliva (red) and following acid challenge (green) and etched dentine and silica (purple). Insert Ca2p and P2p concentrations magnified.

There was a decrease in the relative concentration of O1s following acid challenge (figure 5.41). Examination of the O1s spectrum revealed that a decrease in the peak intensity at 532eV following acid challenge was accompanied by an increase in the intensity of the shoulder at 531eV (figure 5.42), indicating the removal of some of the silica associated O1s from the surface, as the position of the silica associated O1s peak is 532eV. The increase in the intensity of the shoulder indicates a shift in association of the O1s from the silica to carbonate form as on the non silica treated sample (figure 5.42 blue line) (Moulder, Stickle et al. 1992) This theory is supported by the decrease in the Si2p peak intensity following acid challenge, which indicates the removal of some of the silica nanoparticulates from the surface.

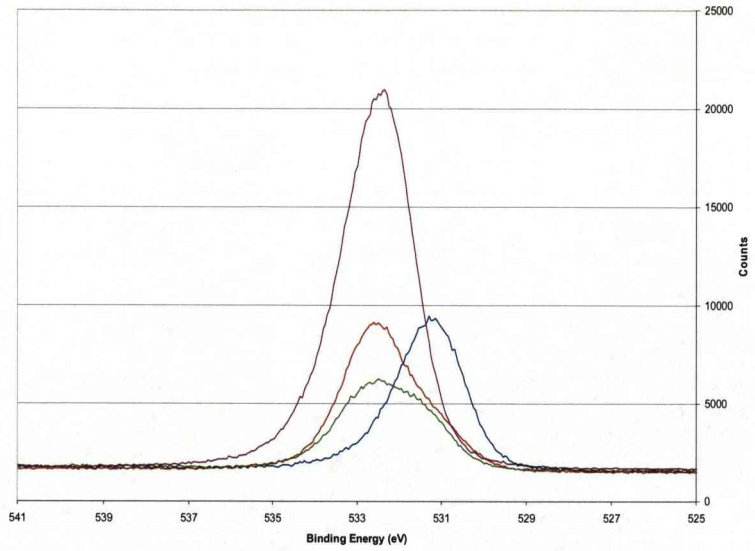


**Figure 5.42** O1s spectra of etched dentine artificial saliva treated and acid challenged (blue line)etched dentine and silica coated and artificial saliva treated (red line) etched dentine and silica treated and artificial saliva and acid challenged (green line) and etched dentine silica coated (purple line).

Argon ion sputtering resulted in a further decrease in the relative concentration of O1s (figure 5.43), which was accompanied by a decrease in the intensity of the shoulder at 321eV. This could be due to the increase in the Si2p signal, indicating the exposure of the nanoparticulate silica coating that remained following acid challenge.

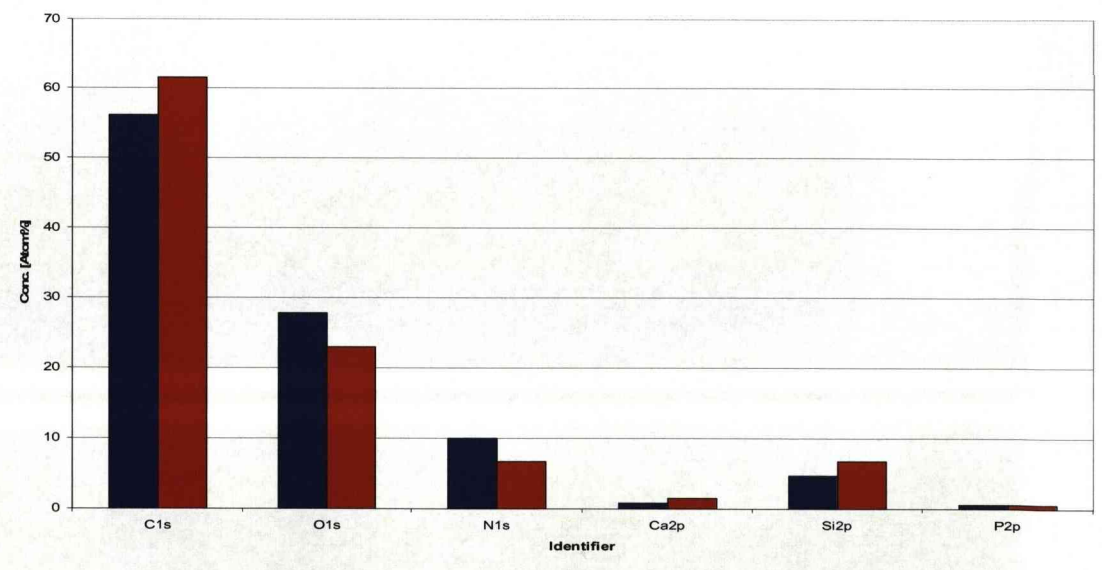


**Figure 5.43.** Graph showing the effect argon ion sputtering acid challenged artificial saliva treated silica coated etched dentine on concentration [atomic %] before (blue) and after 10 mins argon ion sputtering (red).

The increase in C1s concentration was due to the increase in the 285eV peak intensity. However, when the peak shape is examined, there is a decrease in the two shoulders at 288 and 287eV (data not shown), which could be linked to the decrease in the relative concentration of N1s following argon ion sputtering and may indicate the removal of adsorbed carbon containing compounds from the surface. Therefore it would also account for the observed increases in the relative concentrations of Si2p and Ca2p, following argon ion sputtering.

Non Etched Dentine

Non etched → Silica treated → Artificial saliva treated → Acid challenged

Acid challenge resulted in an increase in the relative concentration of Ca2p (figure 5.44), which was accompanied by an increase in P2p concentration, the second peak associated with inorganic dentine phase. However, both peak heights (Ca2p and P2p) were lower than those observed for the non etched dentine following treatment 8 (figure 5.44 blue).

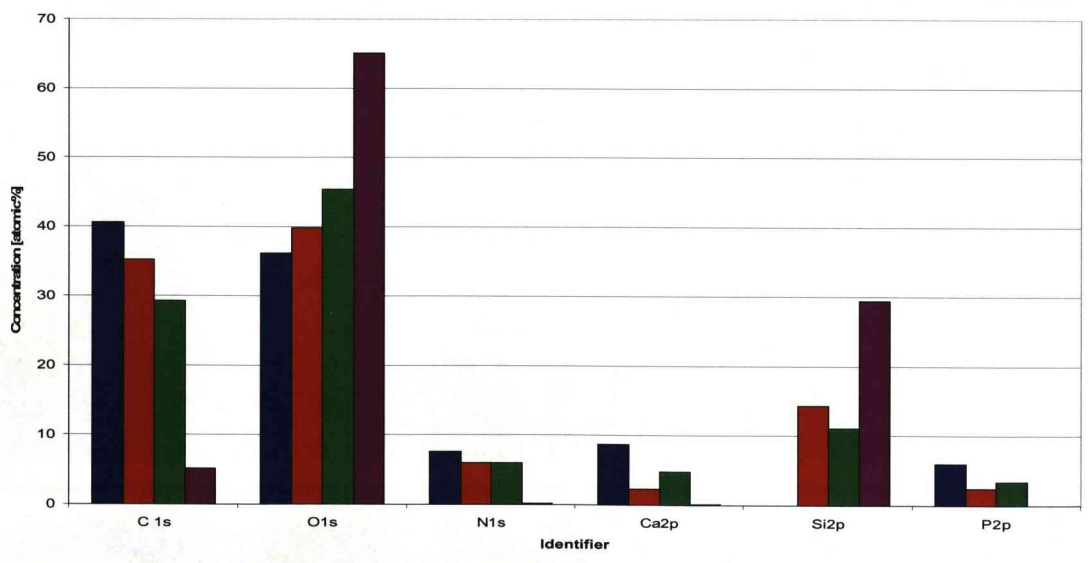


**Figure 5.44.** Graph showing the effect of acid challenging artificial saliva treated silica coated non etched dentine on concentration [atomic %] non etched dentine and artificial saliva and acid challenged (blue) non etched dentine and silica and artificial saliva (red), and following acid challenge (green) and non etched dentine and silica (purple).

There was no alteration to the relative concentration of N1s following acid challenge (figure 5.44). Consideration of the C1s peak revealed that, although the peak at 285eV remained at the same intensity following acid challenge, there was a decrease in the peak intensity of the secondary peak at 287eV (data not shown). This would account for the decrease in the C1s concentration following acid challenge (figure 5.44), suggesting that acid challenge resulted in the loss of some carbon containing compounds, predominantly those associated with the 287 eV secondary peak.

Acid challenge resulted in an increase in O1s peak intensity (figure 5.45). As well as the increase in peak intensity, there was the beginning of a shoulder at 531eV. This was around the position of the O1s peak of the non silica treated dentine. Although the main O1s peak position remains at 532eV, it is still greatly reduced when compared to the peak intensity of the O1s peak of the silica only treated sample. The data would suggest that, although the silica associated O1s is predominant on the surface, there was an increasing non silica associated O1s component.

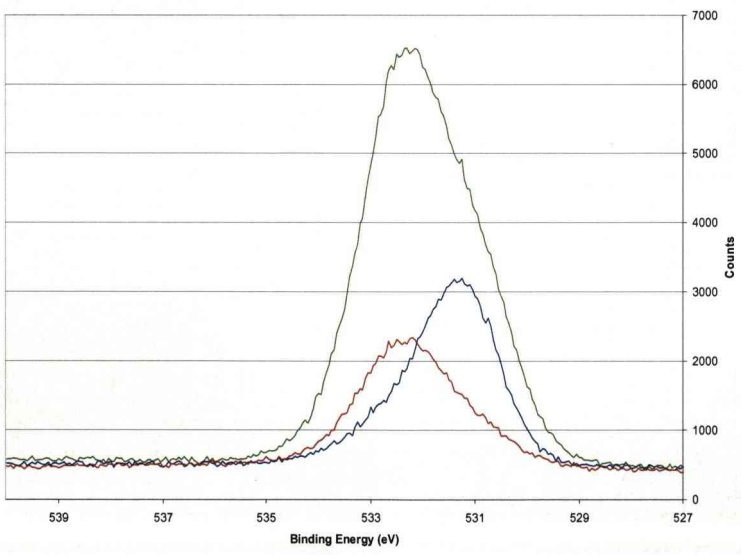


**Figure 5.45** O1s spectra of non etched dentine artificial saliva treated and acid challenged (blue line) non etched dentine and silica coated and artificial saliva treated (red line) non etched dentine and silica treated and artificial saliva and acid challenged (green line).

Argon ion sputtering resulted in an increase in relative concentration of Ca2p (figure 5.46) and was accompanied by an increase in the relative concentration of P2p, both of which are associated with the inorganic phase of dentine and would indicate the presence of a mineralised phase on the surface.

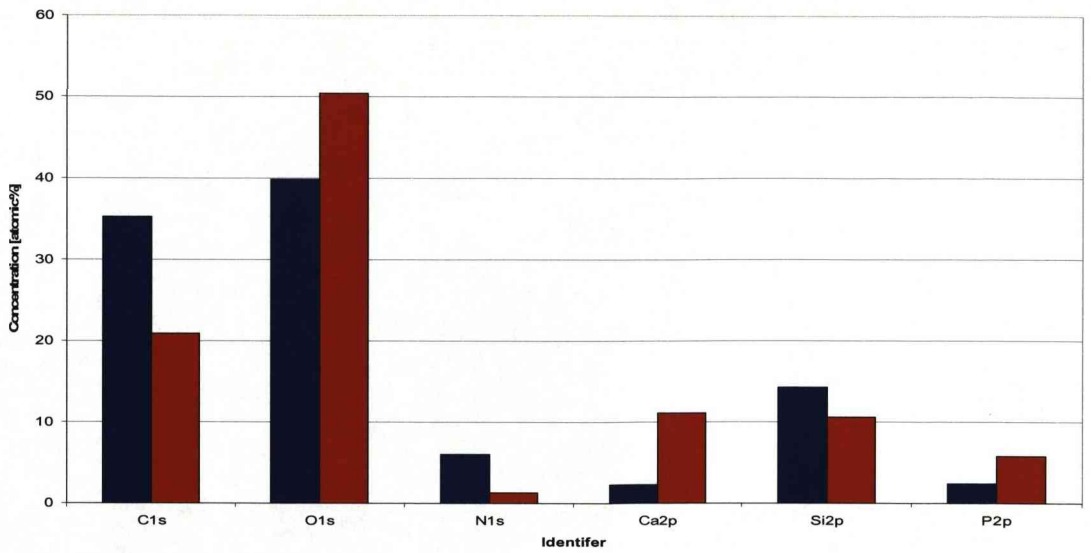


**Figure 5.46.** Graph showing the effect of argon ion sputtering acid challenged artificial saliva treated silica coated non etched dentine on concentration [atomic %] before (blue) and after 10 mins argon ion sputtering (red).

The decreases in the relative concentrations of C1s and N1s would indicate the removal of the organic components. Examination of the C1s spectrum revealed that, although there was an increase in the 285eV peak, the secondary peak at 287eV was undetectable (data not shown), therefore suggesting that argon ion etching removed carbon containing compounds associated with the 287eV peak.

iii) NaF treated

Etched dentine

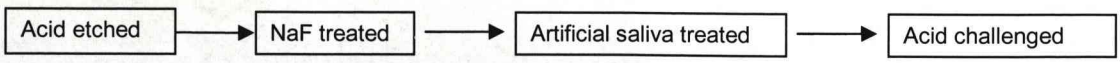


There was a decrease in the relative concentrations of Ca2p and P2p, following acid challenge (figure 5.47). These decreases were accompanied by an increase in the relative concentrations of C1s and N1s organic phase of dentine, which would suggest that the acid challenge had resulted in surface demineralisation. It is interesting to note that there was no variation in the relative concentration of F1s and only a small increase in the Na1s concentration following acid challenge.

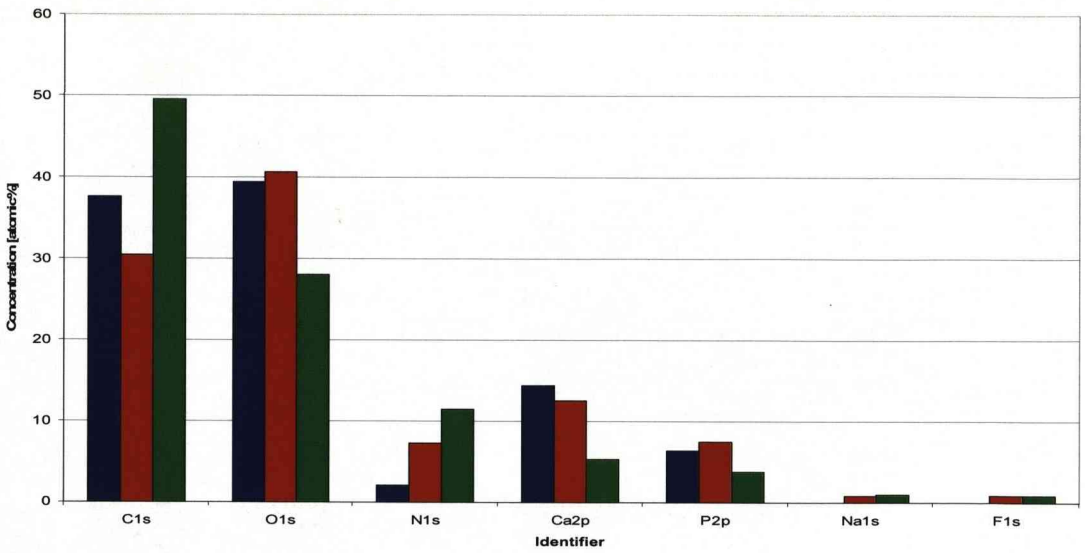


**Figure 5.47.** Graph showing the effect of acid challenging artificial saliva treated NaF coated etched dentine on concentration [atomic %] artificial saliva treated and acid challenged (blue) NaF coated and artificial saliva treated (red) and following acid challenge (green).

Following argon ion sputtering, there was a minimal increase in the relative concentrations of Na1s and F1s (figure 5.48). However, there was a decrease in the relative concentration of C1s (figure 5.48). Examination of the C1s peaks revealed that, accompanying the decrease in the peak height, there was also the loss of a secondary peak at 288eV (data not shown), suggesting the removal of adsorbed organic compounds from the surface.

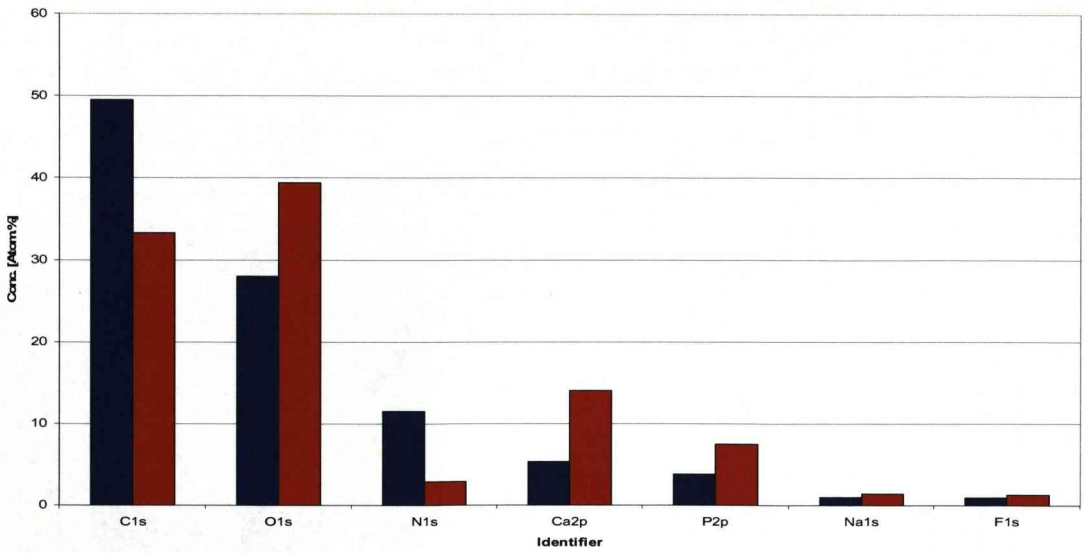


**Figure 5.48.** Graph showing the effect of argon ion sputtering upon acid challenged artificial saliva treated NaF coated etched dentine on concentration [atomic %] before (blue) and after 10 mins argon ion sputtering (red).

The decrease in the organic phase was accompanied by increases in the relative concentrations of the inorganic phase (Ca2p and P2p). Which would suggest the removal of some of the residual carbon containing compounds, revealed the underlying inorganic (mineralised) compounds (figure 5.48).

When the inorganic and organic phases of dentine are compared, it is apparent that there was a decrease in the inorganic phase on the surface (table 5.14). The ratio of inorganic phase was below the level of the non NaF treated sample, which had undergone artificial saliva treatment and acid challenge (treatment 8). However, it was apparent that there was still an increase in the inorganic phase, despite acid challenge when compared to the non artificial saliva treated sample (treatment 2). However, following argon ion sputtering, there was an increase in the inorganic phase above the level for the NaF only treated sample.

| Treatment | Concentration [Atomic %] | | Ratio |
|---|---|---|---|
| | C1s | Ca2p | C : Ca |
| Treatment 10 before $Ar^+$ | 49.5 | 5.3 | 1 : 0.11 |
| Treatment 10 after $Ar^+$ | 33.3 | 14 | 1 : 0.42 |
| Treatment 7 before $Ar^+$ | 30.4 | 12.5 | 1 : 0.41 |
| Treatment 7 after $Ar^+$ | 24.3 | 17 | 1 : 0.7 |
| Treatment 2 before $Ar^+$ | 57.2 | 3.8 | 1 : 0.07 |
| Treatment 2 after $Ar^+$ | 38.7 | 12.8 | 1 : 0.33 |
| Treatment 5 before $Ar^+$ | 50.6 | 5.1 | 1 : 0.1 |
| Treatment 5 after $Ar^+$ | 43.8 | 11.2 | 1 : 0.26 |
| Treatment 8 before $Ar^+$ | 37.6 | 14.4 | 1 : 0.38 |
| Treatment 8 after $Ar^+$ | 45.9 | 13.3 | 1 : 0.29 |

**Table 5.14** The ratio of inorganic and organic phases of dentine following argon ion sputtering ($Ar^+$) of etched dentine following: treatment 10 (NaF and artificial saliva then acid challenge ) treatment 7 (NaF and artificial saliva) , treatment 2 (NaF), treatment 5 (artificial saliva), treatment 8 (artificial saliva and acid challenge)

Non Etched dentine

Non etched → NaF treated → Artificial saliva treated → Acid challenged

Acid challenge did not alter the relative concentrations of both Na1s and F1s (figure 5.49). However, acid challenge did result in a decrease in the relative concentrations of the two inorganic phase atoms Ca2p and P2p. When the Ca2p spectra are compared to that of non etched dentine following artificial saliva treatment and acid challenge in the absence of NaF, the peak shapes and heights are the same (data not shown).

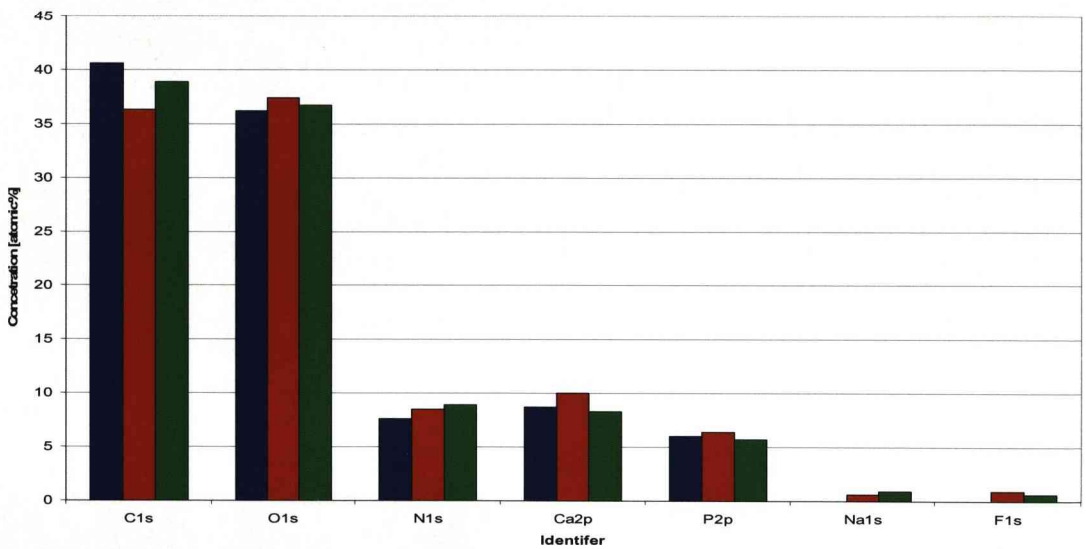


**Figure 5.49.** Graph showing the effect of acid challenging artificial saliva treated NaF coated non etched dentine on concentration [atomic %] artificial salvia treated and acid challenged (blue) NaF and artificial saliva treated (red) NaF and artificial saliva and acid challenged (green).

When the organic phase was investigated, there was an increase in the relative concentrations of both C1s and N1s following acid challenge (figure 5.48). However, comparison of the C1s spectra revealed an increase in the secondary peak intensity at 288eV in comparison with that of the treatment 8 (artificial saliva and acid challenged) non etched dentine. Therefore, it would suggest that, the presence of the NaF coating alters the preferences for adsorption of compounds of the artificial saliva, altering the overall composition of the artificial salvia created pellicle layer.

Argon ion sputtering had minimal effect on the relative concentrations of both Na1s and F1s (figure 5.50). However, there was a decrease in the relative concentrations of the organic phase (C1s and N1s). It would appear that the removal of the carbon rich surface unmasked the underlying inorganic phase, demonstrated by the increases in relative concentrations of both Ca2p and P2p (figure 5.50).

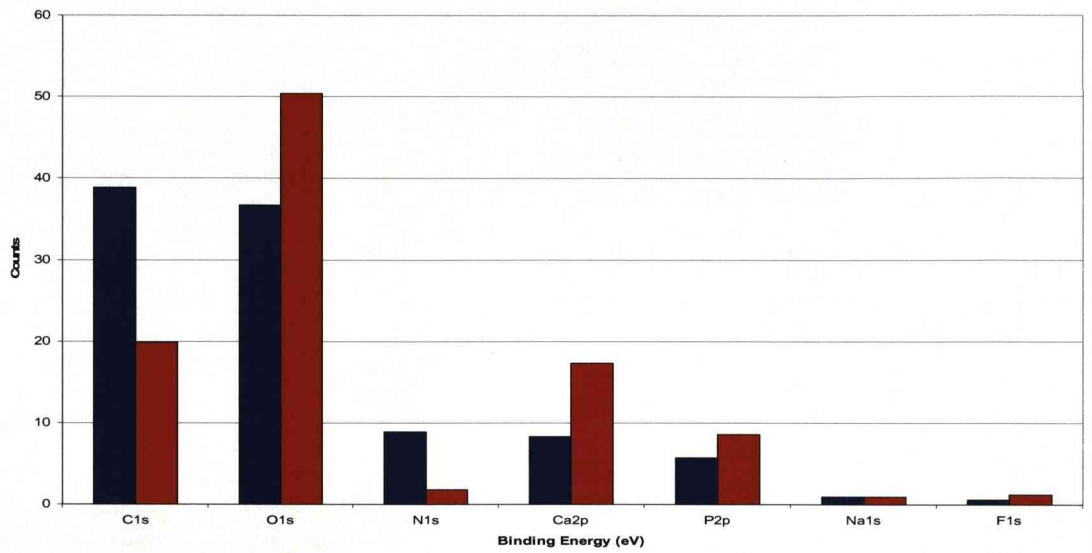


**Figure 5.50.** Graph showing the effect of argon ion sputtering upon acid challenged artificial saliva treated NaF coated non etched dentine on concentration [atomic %] before (blue) and after 10 mins argon ion sputtering (red).

When the ratio of inorganic and organic phase was compared, there was an increase in the inorganic phase for all the samples following argon ion sputtering (table 5.15). It would appear that although there is a decrease in the inorganic phase following acid challenge of the NaF and artificial saliva treated surface, following argon ion sputtering, the ratio increases, the increase being above that of the non NaF treated sample (treatment 8). This suggests that the NaF does offer some form of protection to the bulk of the dentine from acid challenge.

| Treatment | Concentration [Atomic %] | | Ratio |
|---|---|---|---|
| | C1s | Ca2p | C : Ca |
| Treatment 10 before $Ar^+$ | 38.9 | 8.3 | 1 : 0.21 |
| Treatment 10 after $Ar^+$ | 19.9 | 17.3 | 1 : 0.87 |
| Treatment 7 before $Ar^+$ | 36.3 | 10 | 1 : 0.28 |
| Treatment 7 after $Ar^+$ | 15.1 | 18.1 | 1 : 1.2 |
| Treatment 2 before $Ar^+$ | 26.6 | 14.1 | 1 : 0.53 |
| Treatment 2 after $Ar^+$ | 18.6 | 18.8 | 1 : 1.01 |
| Treatment 8 before $Ar^+$ | 40.6 | 8.7 | 1 : 0.21 |
| Treatment 8 after $Ar^+$ | 25.9 | 17.4 | 1 : 0.67 |
| Treatment 5 before $Ar^+$ | 29.2 | 13.1 | 1 : 0.45 |
| Treatment 5 after $Ar^+$ | 31.8 | 15.6 | 1 : 0.49 |

**Table 5.15**. The ratio of inorganic and organic phases of dentine following argon ion sputtering ($Ar^+$) of non etched dentine following: treatment 10 (NaF and artificial saliva then acid challenge ) treatment 7 (NaF and artificial saliva) , treatment 2 (NaF), treatment 5 (artificial saliva), treatment 8 (artificial saliva and acid challenge)

## 5.5 Discussion

The purpose of using XPS in this study was to assess the changes in the chemical composition of the treated dentine surfaces. XPS was proven useful in this respect due to the high resolution of the spectra produced and the ability to semi quantify the concentrations of element of interest. The addition of an argon ion gun to the XPS setup allowed assessment of below surface atomic layers. It was hoped this would enable an estimation of the penetration depth of the nanoparticulate silica into the dentinal tubules.

During the creation of the dentine discs from whole teeth, a smear layer (a layer of microcrystalline cutting debris) was produced (Pashley 1986). The presence of a smear layer can result in the occlusion of the dentinal tubules, therefore, the removal of the smear layer is paramount to studies of possible new occluding agents (Ghazali 2003). Several methods of removing the smear layer are commonly used. These include acid etching and sonication in $dH_2O$ (Suge, Ishikawa et al. 1995; Ten Bosch, De Vries et al. 1997). In this study, both methods were investigated, as acid etching has also been shown to increase dentine tubule diameter, which would increase the possibility of nanoparticulate penetration of the tubules.

The spectra observed for the non etched (sonicated) dentine sample was comparable to those reported in previous studies (Ruse and D.C. 1991; Ten Bosch, De Vries et al. 1997; Sennou, A.A. Lebugle et al. 1999). However, the presence of minor ions that are sometimes present in the dentine, such as magnesium sodium and fluoride, was not detected. This is not unusual, as the presence of ions such as fluoride and sodium is determined by the environment from which the tooth was removed. It can also be suggested that the teeth used in this study were obtained from an archival store and, as such, the length of time the teeth had remained in storage was unknown. Prolonged periods of time between extraction and testing may result in loss of minor ions from the dental structure.

In this study citric acid was used as the acidic agent due to its physiological relevance in the periodic acid challenge of the oral cavity. Citric acid is also often used as a demineralising agent, as many bonding agents used in periodontal therapies require the dentine surface to be demineralised (Labahn, Fahrenbach et al. 1992;

Kinney, Balooch et al. 1995). Citric acid has been shown to remove the smear layer following cavity preparation and demineralises the treated dentine surface, which is due to its ability to chelate calcium(Labahn, Fahrenbach et al. 1992; Hara, Ando et al. 2005). Therefore, the observed decreases in Ca2p and P2p concentrations, following citric acid etching, were as hypothesised. The observed elemental concentrations, following citric acid etching, were comparable to those obtained in previous studies following acid etching. The observed decreases in Ca2p and P2p indicate that etching resulted in the almost complete demineralisation of the dentine surface (Ruse and D.C. 1991) As evidenced by the increased C1s and N1s concentrations, removal of the apatite or mineralised phase results in exposure of the organic matrix. Unlike enamel, dentine erosion does not result in the creation of a lesion or pits, as the demineralised organic content of dentine is not lost by erosion progression (Marshall, Wu-Magidir et al. 1998; Sennou, A.A. Lebugle et al. 1999; Ganss, Klimek et al. 2004). Although dentine has demonstrated a higher rate of dissolution following acid erosion in comparison to enamel, it has been hypothesised that the presence of the organic matrix may reduce erosion progression (Sennou, A.A. Lebugle et al. 1999). It has previously been suggested that the demineralised organic matrix makes further demineralisation a diffusion controlled process(Hara, Ando et al. 2005).

Following argon ion sputtering, there was an increase in the mineralised phase of the dentine, which would suggest the demineralised zone had been removed. Previous studies have identified that exposure of dentine to a demineralising agent resulted in an outer layer of fully demineralised organic matrix, followed by a partially demineralised zone until the mineralised inner dentine is reached (Ganss, Klimek et al. 2004). Previous studies have estimated the depth of the demineralised zone following hydrochloric acid etching to be 1$\mu$m (Ruse and D.C. 1991). However, it has been previously demonstrated that citric acid affects the dentine to a greater depth than hydrochloric acid (Labahn, Fahrenbach et al. 1992). Therefore, it may be suggested that the sputter depth following 10 minutes of argon ion sputtering in the current study was greater than 1$\mu$m.

The presence of nanoparticulate silica on both the etched and non etched dentine surfaces was identified by the appearance of a Si2p peak and the enhancement of the

O1s peak. Further analysis of the spectra obtained suggested the presence of the nanoparticulate coating masked the dentine. This was evidenced by the decreases in concentrations of both organic and inorganic dentine associated elements. Previous studies using the QCM-D and hydraulic conductance (chapters 3 and 4) have suggested that the nanoparticles were able to penetrate the dentinal tubules leading to occlusion of patent tubules. An argon ion gun was used to remove surface layers to investigate the sub surface chemical composition. It was hoped this would offer an insight into the penetration depth of the different treatments. Following 10 minutes of argon ion sputtering of both the etched and non etched dentine samples treated with silica, there was a reduction in the Si2p peak intensity. However, a peak was still present, which was coupled with the re-emergence of some of the dentine associated peaks. This would suggest that not all the dentine associated nanoparticles had been removed from the surface, following argon ion sputtering, and would therefore suggest that those nanoparticles still present had penetrated and were associated with the dentinal tubules.

An attempt was made to continue argon ion sputtering in 5 and 10 minute increments until the silica signal was removed, as this could be used to estimate a penetration depth of the nanoparticles into the tubules. Following 160 minutes of argon ion sputtering, the silica signal was diminished but still apparent. However, the reliability of results obtained following sputtering times over 15 minutes is questionable. It was noted that argon ion bombardment for times over 15 minutes resulted in a change in the C1s peak shape. Examination of the C1s peak shape indicates the formation of graphite, which would suggest that argon ion sputtering for extended periods of time resulted in detrimental alterations to the surface structure and, therefore, chemistry had occurred. As such, spectra obtained following argon ion sputtering periods greater than 15 minutes were deemed inaccurate and untrustworthy. Previous studies have also demonstrated that argon ion bombardment can result in differential sputtering of dentine surfaces. It has been suggested that the two phases of dentine posses different sputter rates and, as such, a surface may become deficient in the more easily removed element or phase or become enriched in the more tenacious component (Miller, Bowles et al. 1994). Previous studies have suggested a more efficient removal of organic material in

comparison to the removal of crystalline material (Ten Bosch, De Vries et al. 1997). This would also question the reliability of the longer periods of argon ion sputtering.

Fluoride is a common component of oral care preparations, such as dentifrices and mouth rinses/washes. Fluoride has been shown to be effective in protecting teeth against decay (Sano, Nakashima et al. 2007). The principle of its protective effect is the precipitation of $CaF_2$ like materials on the tooth surface (Schlueter, Ganss et al. 2007). It is also widely observed that fluoride can aid remineralisation of demineralised, dentine structures, impeding erosion progression. It has been suggested that fluoride treatment results in the production of fluroapatite whereby fluoride ions are incorporated into the hydroxyapatite structure (ten Cate J.M. 1997). Research has demonstrated that a 100ppm fluoride mouth rinse contributed to increased fluoride incorporation into experimental root lesions which showed a thick outer layer of acid resistant mineral in-vivo (Teranaka and Koulourides, 1981) It has been speculated that the mode of action of fluoride in preventing erosion of dental surfaces is the creation of loosely bound $CaF_2$ like layer on the surface. This provides some additional mineral to be dissolved during an acid attack before the underlying mineralised tissue is attacked (Ganss, Kilmek et.al. 2001). Therefore, NaF was used in this study as a positive control. NaF is used in dentifrices as a carrier of fluoride ions (Arnold, Dorow et al. 2006). It was, therefore, unsurprising that, unlike nanoparticulate silica treatment, NaF treatment did not result in a masking of the underlying dentine.

It has been suggested that fluoride can re-harden eroded enamel surfaces and therefore may assist in strengthening hard tooth tissue against dental erosion (Ganss, Klimek et al. 2001). However, the results of this study would indicate that the protection offered by NaF treatment under the conditions described in this study was negligible. The increased consumption of acidic foods and drinks in the modern diet has contributed to the increased prevalence of dental erosion (Ganss, Klimek et al. 2001; Hara, Karlnsey et al. 2008). Therefore, the ability of an occluding agent to withstand acid challenge is vital for its longer term effect on preventing sensitivity.

As expected, acid challenge of the NaF treated surface did result in decreases in the inorganic dentine associated elements, exposing the collagen matrix of the organic

dentine phase, demonstrated by the increases in C1s and N1s concentrations. The protective effect of fluoride treatment from mineral loss during severe acid challenge has been widely debated, with only a small protective effect being reported (Van Rijkom et. al. 2003; Hughes, West, et. al. 2004). It can therefore be suggested, that NaF treatment was not able to offer protection from acid attack. Previous studies have demonstrated that titanium tetra fluoride treatment of mineralized dental surfaces was able to inhibit acid erosion to a greater extent than NaF (Exterkate and ten Cate 2007). It was assumed that this is due to the formation of a glaze like layer on the titanium tetra fluoride treated surfaces. It has been hypothesised that the glaze like layer is due to the titanium reacting with oxygen atoms in phosphate groups on the tooth surface to form stable titanium oxide (Schlueter, Ganss et al. 2007). It was hypothesised that, in a similar manner the creation of a nanoparticulate silica coating would act as a barrier to acid challenge protecting the dentine from acid erosion.

Acid challenge of the silica treated surfaces did result in a decrease in the Si2p concentrations, but the silica peak was still present. However, the concentrations of the dentine associated elements remained low. This would suggest that the nanoparticulate silica coating was able to withstand acid challenge but there was some loss of silica from the surface. It could be suggested that the citric acid challenge accelerates the dissolution of the nanoparticles adhered to the surface, resulting in the formation of a gel like coating. Fluctuations in pH of the colloidal silica sol can result in the coagulation of the nanoparticles (Iler 1979a; Bergna 1994). A further suggestion could be that acid challenge accelerates the dissolution of the nanoparticulate surface coating but not the removal of the coating. The protective effect of the nanoparticulate coating was also suggested by the continued presence of Ca2p and P2p peaks following argon ion sputtering of the non etched dentine, following silica treatment and acid challenge.

In the oral cavity, the creation of a salivary pellicle is of great physiological importance. It acts as a barrier, which is important in maintaining the integrity of the enamel surface by preventing demineralization and facilitating remineralisation (Hannig and Balz 2001; Hannig and Joiner 2006). Therefore, it is of importance that any coating created on the dentine surface is able to adsorb salivary components.

Treatment of both etched and non etched dentine with artificial saliva resulted in an increase in an inorganic phase of dentine, which would suggest the remineralisation of the etched dentine as well as the creation of a pellicle coating. The creation of the pellicle coating is suggested by the appearance of a characteristic C1s peak shape following artificial saliva treatment. However, despite the increased concentrations of Ca2p and P2p which would appear to indicate an increased mineral content, the remineralisation of the dentine cannot be stated as being achieved with any certainty. Remineralisation is the process of net mineral deposition within a carious tissue. Demineralisation of enamel leads to dissolution of hydroxyapatite and diffusion of calcium and phosphorous ions towards the enamel surface, saturation of calcium and phosphorous ions on the surface results in a re-precipitation of hydroxyapatite forming an initial superficial layer on the surface (Arnold, Dorow et al. 2006). Compared to enamel, the mechanism of dentine remineralisation is more complex (Preston, Smith et al. 2008). Unlike enamel, dentine is a tissue with an organic matrix of collagen and other proteins in which the crystalline apatite mineral is embedded (Vollenweider, Brunner et al. 2007). The apatite phase in mineralised dentine is, therefore, classified as intra-fibrillar. It has been suggested that remineralisation occurs from the re-growth of the remaining mineral crystals (Preston, Smith et al. 2008).. It has also been proposed that dentine remineralisation can be influenced by the presence of phospohoproteins since they have the ability to bind calcium and may, therefore, act as a template for remineralisation (Marsh 1989; Hara, Karlnsey et al. 2008). This may account for the decrease in the C1s concentration as the carbon rich matrix becomes coated in the newly acquired mineral phase. Although argon ion sputtering did result in an increase in the C1s peak of the etched dentine sample following artificial saliva treatment this was accompanied by an increase in the Ca2p peak intensity. However, comparison of the ratio of inorganic and organic phases of dentine would suggest that argon ion sputtering had little effect on the mineral content and, therefore, may suggest that remineralisation of the organic matrix had occurred. Therefore, the increases in the inorganic dentine phase observed were not just due to the creation of a pellicle layer and the adsorption of calcium and phosphorous containing compounds to the surface.

Fluoride has been shown to enhance the rate and efficacy of dentine remineralisation (Sano, Nakashima et al. 2007; Preston, Smith et al. 2008). It has been demonstrated

that fluoride ions act as a strong promoter of mineralization of demineralised dentine. Previous studies have also demonstrated enhanced calcium and phosphorous uptake following NaF treatment of dentine (Mellberg, Pertrou et al. 1991; Charvat, Soremark et al. 1995). This would explain the enhanced concentrations of Ca2p and P2p observed, following artificial saliva treatment of NaF coated etched dentine. Again accompanying these increases was a decrease in the C1s and N1s concentrations, which would suggest that the increased mineralised component of the dentine was masking the previously exposed organic matrix. Argon ion sputtering resulted in a further increase of the inorganic phase of dentine, which was accompanied by an increase in the F1s concentration. It could be suggested that the fluoride ions were able to penetrate the dentine surface and the demineralised organic matrix. The ability of fluoride to aid the remineralisation of dentine has previously been shown to be dependent on the presence of the demineralised organic matrix (Ganss, Klimek et al. 2004). As previously discussed, remineralisation of dentine is not solely the precipitation of apatite on the surface but the formation of intra-fibrillar apatite upon the exposed organic matrix. Otherwise the dentine will not regain its previous mechanical properties (Vollenweider, Brunner et al. 2007; Hara, Karlnsey et al. 2008; Tay and Pashley 2008).

Silicate ions have previously been shown to promote apatite induction by insoluble dentine matrix (Saito, Toyooka et al. 2003). This is not surprising, as silica is a common component of bioactive glasses. Bioactive glasses are thought to promote calcium phosphate formation and therefore mineralization for bone regeneration and tissue engineering. The use of bioactive glasses in dentine remineralisation has also been investigated (Forsback, Areva et al. 2004; Vollenweider, Brunner et al. 2007). It has been demonstrated that nanoparticulate bioactive glass can increase the dentine remineralisation rate (Vollenweider, Brunner et al. 2007). It has been previously suggested that silica can catalyse the formation of hydroxyapatite and can significantly shorten the induction period of the spontaneous precipitation of apatite (Skirtic, Antonucci et al. 2001). Therefore, it was hypothesised that the presence of the silica nanoparticles could aid remineralisation of the demineralised dentine. However, analysis of the spectra suggest that, although the presence of the silica coating does result in the adsorption of calcium and phosphorous, these increases were diminished in comparison to those obtained in the absence of a nanoparticulate

silica coating. A possible explanation is the masking of the underlying dentine by the presence of the coating. Therefore, it can be suggested the increased concentration of dentine associated elements was due to the creation of a pellicle layer upon the nanoparticulate silica coating. Previous work using the QCM-D was able to identify the efficient adsorption of artificial saliva compounds to the nanoparticulate silica coating. The appearance of the characteristic C1s peak shape following artificial saliva treatment of silica coated dentine would suggest that the silica coating did not alter pellicle formation. Pellicle formation is a highly selective process with only a fraction of the proteins available in saliva being found in the pellicle(Hannig and Joiner 2006).

It can be suggested that the presence of the nanoparticulate coating inhibited the remineralisation of the etched dentine as it acted as a barrier between the artificial saliva and the underlying dentine. A similar effect was noted following treatment of enamel with titanium fluoride derivatives, which, as previously discussed, are thought to protect dentine and enamel from acid challenge by the formation of a protective Titanium oxide layer. Titanium fluoride treatment was shown to inhibit remineralisation due to the formation of the protective glaze like precipitate layer that prevents penetration of the calcium and phosphorous ions from the bulk (Exterkate and ten Cate 2007). As discussed, unlike the remineralisation of the enamel, remineralisation of the dentine requires apatite formation on the organic matrix, not just on the surface of the dentine. Argon ion sputtering resulted in a decrease in the dentine associated elements and an increase in the concentration of silica. It would appear that artificial saliva production had resulted in the substantial adsorption of a pellicle layer masking the nanoparticulate silica. From this, it could be stated that the use of nanoparticulate silica as a remineralising treatment is undesirable.

The creation of an artificial saliva pellicle upon dental surfaces has been shown to aid the protection of the underlying mineralised dental surfaces from the regular and periodic acid challenge that is associated with ingestion of acidic foods and drinks (Hannig and Joiner 2006). Previous studies have predominantly focused on the ability of the pellicle to protect enamel against acid erosion. It was previously demonstrated that, like enamel, saliva treatment of dentine to create a pellicle layer

aided the protection of the dentine from acid erosion as evidenced by reduced mineral loss (Hall, Buchanan et al. 1999; Wetton, Hughes et al. 2006). It was therefore hypothesised that, following artificial saliva treatment of the dentine, there would be a reduced loss of inorganic elements from the treated dentine surfaces, enhancing the protective effect of the treatments.

Following acid challenge of the artificial saliva treated etched dentine surface there was an increase in the Ca2p concentration in comparison with the artificial saliva treated etched dentine surface. This was accompanied by a decrease in the C1s concentration. Analysis of the C1s peak shape suggested that acid challenge had resulted in the loss of the characteristic artificial saliva peak shape. It could be proposed that this is due to removal of the proteins of the acquired surface pellicle layer resulting in the exposure of the remineralized dentine below. However, when non etched dentine was considered, there was a decrease in the inorganic phase. This could be due to differences in the composition of the acquired pellicle on etched and non etched dentine, as the inorganic phase of dentine was still elevated in comparison to that of non etched dentine that had not undergone any artificial saliva treatment. It is possible that the composition of the acquired pellicle was different on the etched and non etched dentine, with the pellicle for the non etched dentine having a higher mineralised content.

Despite NaF treatment, there was a decrease in the inorganic phase of dentine following acid challenge in comparison to the NaF and artificial saliva treated etched dentine. However, following argon ion sputtering, there was an increase in the inorganic phase to the same level of the non acid challenged surface prior to argon sputtering. It could be suggested that the reduction in inorganic phase concentrations was due to the removal of calcium ions from the acquired pellicle, and not from the underlying dentine surface. The presence of calcium ions within the pellicle of the NaF treated dentine could be due to the reported ability of fluoride to enhance the rate and efficiency of the remineralisation process (Saito, Toyooka et al. 2003). Therefore, remineralisation of the dentine is accelerated and saturation of the organic matrix with calcium and phosphate ions could occur sooner. Which means that inorganic phase elements can become incorporated into the pellicle layer as proposed for non etched dentine. A similar pattern was noted for non etched dentine. This

could mean that treatment of the dentine with NaF in the presence of a pellicle coating did offer enhanced protection from acid challenge (Savarino, Breschi et al. 2004; Preston, Smith et al. 2008).

Acid challenge of silica and artificial saliva treated dentine surfaces did result in a decrease in the concentration of both Ca2p and P2p. However, following argon ion sputtering of the non etched dentine sample the Ca2p concentration increased considerably and silica was still present on the surface. It can be suggested that the presence of both nanoparticulate silica and an acquired pellicle layer did offer protection to the underlying dentine from acid challenge. The decreases in dentine associated elements observed are the removal of the elements of the acquired pellicle and not the demineralisation of the underlying dentine. This can be demonstrated by the continued presence of Si2p and the alteration of the characteristic artificial saliva C1s peak, following acid challenge. The increases in Ca2p and P2p following argon ion sputtering would indicate that the underlying dentine was unaffected by acid challenge, as previously observed in the absence of a pellicle layer. As such, nanoparticulate silica coating of dentine can be used as a method of protection from acid challenge but it would not be suitable as a remineralising agent.

Although XPS resulted in many insights into the abilities of the coatings to adhere to dentine, it was still not possible to definitively state that the different treatments were able to aid remineralisation of the dentine. Remineralisation requires not only increased mineral content but any resulting apatite material formed has to form a composite material within the collagen matrix of demineralised dentine or the mechanical stability of the material is not achieved (Vollenweider, Brunner et al. 2007). As the role of dentine within the oral cavity requires many important mechanical properties, it is paramount that a remineralising treatment restores these also. Therefore, further examination of the mechanical properties following treatment would be required.

## Chapter 6 Discussion

### 6.1 Introduction

The aim of this project was to investigate the use of nanoparticulate silica as an oral care treatment for dentine sensitivity. There were three objectives which this project attempted to explore:

1. The creation of the nanoparticulate coatings, the effect of altering the underlying polymer layer and the possibility of creating a commercially favourable "one-step" process.
2. The ability of the nanoparticulate coatings to reduce the permeability of dentine and therefore act as a desensitizing agent.
3. The ability of the coatings to aid remineralisation through the adsorption of salivary components and to withstand acid challenge.

In this chapter the results presented in previous chapters (chapters 2, 3, 4 and 5) will be used to discuss the aims of the overall project.

### 6.2 The creation of the nanoparticulate coatings

Previous research at the University of Liverpool into the creation of nanoparticulate coatings on surfaces used a simple two step dipping method to coat samples. Prior to addition of the nanoparticles a polymer binding layer was created to alter the surface charge and enhance the adsorption of the nanoparticles to the surface(Cousins, Doherty et al. 2004). This project assessed the necessity of the polymer binding layer for the creation of a uniform and continuous coating of nanoparticles.

It was apparent following analysis of the TEM images that in the absence of a polymer binding layer there was minimal adhesion of the silica nanoparticles to the carbon coated TEM grids. With large areas of sparse coverage and small clusters of particles adhered to the surface. The QCM-D also demonstrated the minimal adsorption of nanoparticles onto both gold and HA coated surfaces, in the absence of a polymer binding layer. Both QCM-D and TEM demonstrated an enhanced level of adsorption when the largest diameter 21nm (Ludox® TM-50) silica sol was used in comparison to the other silica

grades. It was surmised that this is due to the increased particle size which could result in an increased ability to form hydrogen bonds (Napper 1970). Therefore, it was concluded that on carbon, gold and HA surfaces there was a requirement for a polymer binding layer. It was however, demonstrated using the QCM-D that the nanoparticles were able to adsorb to the dentine surface. The presence of silica upon both acid etched and non etched dentine surfaces was confirmed using XPS. It was hypothesised that the silica nanoparticles were able to enter the dentinal tubules, becoming trapped, so were not removed following washing. Hydraulic conductance experiments demonstrated that there was a reduction in dentine permeability following treatment with the nanoparticulate silica sols. It could be suggested therefore that the nanoparticles were able to reduce the permeability of the dentine by entering and occluding the dentinal tubules. XPS analysis added further support to this theory as argon ion sputtering to remove the surface layers resulted in a reduction but not the removal of the silica signal.

In the presence of a polymer binding layer it was demonstrated that, a continuous nanoparticulate coating could be achieved on gold, HA and carbon surfaces. It was established using the QCM-D that the creation of a polymer layer prior to introduction of a silica sol to the surface, resulted in the increased adsorption of nanoparticles to the surface. The enhanced coverage, and the creation of a continuous coating of nanoparticles in the presence of a polymer binding layer, was confirmed with TEM.

### 6.2.1 Altering the underlying polymer

Three different polymers were tested in this project. Two Zetag™ polymers, with differing molecular weights were selected and a chemically different polymer UCARE™ polymer JR-125. One of the Zetag™ polymers, Zetag™ 7689 ($10^8$Da) was the polymer used in the original studies by Cousins et al (Cousins, Doherty et al. 2004). To establish if the molecular weight of the polymer would affect the coating a lower molecular weight Zetag™ polymer Zetag™ 7109 ($10^6$Da) was also tested. With the TEM it was established that differences in the molecular weight of the polymer resulted in discrepancies in the density of the coatings. It was noted that decreasing the molecular weight of the polymers resulted in a decrease in the variation in density of the

nanoparticulate coating. It was suggested that this may be due to the ability of the polymer to uncoil within solution. There are two mechanisms that may prevent a polymer from uncoiling; concentration and charge (Teraoka 2002). Zetag™ 7689 is only 80% cationic while the lower molecular weight polymer Zetag™ 7109 is 100% cationic. It was suggested that the combined effect of a higher molecular weight, and the enhanced possibility of coiling, the Zetag™ 7689 polymer was most probably adhering to the surface in a coiled manner. The coiling would result in the masking of binding sites for the nanoparticles and also in enhanced areas of density, which would explain, the observed areas of increased density and areas of minimal or no nanoparticulate coverage. An attempt was made to maximise the possibility of uncoiling by reducing the concentration of the polymer 10-fold. This resulted in the creation of a more continuous nanoparticulate coating, with minimal areas of enhanced density and no areas of non coating on the grid. When the lower molecular weight polymer Zetag™ 7109 was used a continuous coating of nanoparticles was still achieved. As such further experiments were based on the use of the lower molecular weight Zetag™ polymer 7109 and the use of Zetag™ 7689 was discontinued for the purpose of this project.

Comparison of the lower molecular weight Zetag™ 7109 with the chemically different UCARE™ polymer JR-125 established that there was little variation at either the higher and lower concentrations when analysed using the TEM. However, investigation of the creation of the coatings on gold surface using the QCM-D suggested that there were differences in the mechanisms of adsorption of the two polymers onto the gold surface. It was hypothesised that the Zetag™ polymer may be adhering in a coiled manner and then uncoiling once adsorbed to the surface. Although Zetag™ 7109 has a shorter chain length than the original Zetag™ 7689 polymer it still has a longer chain length than that of UCARE™ polymer JR-125. As such the increased polymer chain length will increase the possibility of inter chain interactions within the solution (Teraoka 2002). This could result in the adsorption of the polymer chains onto the surface in the coiled form. Adsorption may lead to a conformational change in the polymer due to the formation of new bonds. This could initiate the uncoiling of the polymer forming a

rigidly adsorbed layer and explain the dual phases of the observed binding curve obtained with QCM-D.

When the HA surface was tested the binding curve obtained from addition of Zetag™ 7109 closely resembled that of obtained when the UCARE™ polymer JR-125 was used. It was also apparent using QCM-D that there was an increase in the viscosity of the Zetag™ 7109 polymer on the HA surface. It was surmised that altering the surface chemistry increased the affinity of the Zetag™ polymer for the surface, and the polymer chains were adsorbing to the surface in the coiled form, with uncoiling hindered due to spatial constriction. This would also explain the enhanced viscosity of the polymer on the HA surface, as amongst the coiled polymer chains water and other solvents would become incorporated (Young 1981). Therefore, on the HA surface the Zetag™ 7109 polymer coating would still have water and solvent molecules incorporated. This hypothesis was also supported by the increased reduction in hydraulic conductance obtained when the Zetag™ polymer was used in comparison to UCARE™ polymer JR-125. This would suggest that the Zetag™ 7109 polymer was forming a denser coating, upon the dentine surface, than that of UCARE™ polymer JR-125.

### 6.2.2 The creation of a "one-step" process

As previously discussed the ease of use is paramount to any commercial products success. To simplify the coating procedure an attempt was made to create a "one-step" treatment, rather than the traditional two step coating, of creating a polymer binding layer prior to the addition of the nanoparticles. Two commercially available silica containing products, were investigated (Ludox® CL and Percoll™) both these products have had their surface charge altered rendering them positive. Although it was hypothesised they would therefore be able to adsorb to the surface without requiring a polymer binding layer TEM analysis deemed both unsuitable.

It was therefore attempted to alter the surface charge of the nanoparticles by directly adsorbing a poly cationic polymer onto the silica nanoparticles. TEM demonstrated that high shear mixing of the lowest molecular weight polymer (UCARE™ polymer JR-

125), and the 14nm diameter Ludox® HS-40 resulted in a dense coating, with many areas being too dense to visualise. However, there was a small area of monolayer coating, where individual nanoparticles with a hexagonal close packing arrangement could be observed. It was suggested that the highly organised packing arrangement was due to the creation of an individual polymer coating upon the individual nanoparticles. This would result in steric stabilisation of the nanoparticles and therefore the periodic and uniform separation of the nanoparticles. Interpenetration of the polymer chains surrounding the nanoparticles is thermodynamically unfavourable, and leads to repulsion of the particles hence the ordered spacing (Napper 1970; Shaw 1992).

Addition of a polymer to a nanoparticulate sol can also result in flocculation or aggregation of the nanoparticles (Napper 1970; Coradin and Lopez 2003). Flocculation may occur by two different mechanisms:

1. Particle bridging: where the polymer bridges more than one particle, which would lead to flocc formation,(Napper 1970).
2. Charge neutralisation: where polymer adsorption onto a particle surface can decrease interparticle electrostatic repulsion, inducing coagulation (Coradin and Lopez 2003).

It was suggested that the large areas of dense coating observed were related to the creation of aggregates of nanoparticulates within the solution, following addition of the polymer. It was attempted to break up any aggregates that may form during mixing using an ultrasonic probe. However, TEM analysis identified that the nanoparticles still adsorbed to the surface as distinct aggregates. Hydraulic conductance established that there was a reduction in permeability upon addition of the sonic mixed UCARE™ polymer JR-125 and HS-40. Although it appears the "one-step" treatment resulted in an enhanced reduction in permeability in comparison to that obtained for UCARE™ polymer JR-125 or Ludox® HS-40 alone, this was shown not to be statistically significant. It could therefore be suggested that the aggregates formed did not increase the density of the coating greatly and were minimal.

### 6.3 The ability of the nanoparticulates to reduce the permeability of the dentine

The ability of an agent or coating to reduce dentine permeability is a common and standard test of any potential desensitizing agent. It was identified that all three nanoparticulate silica sols were able to reduce the dentine permeability by a statistically significant amount. It can be suggested that the nanoparticles were able to reduce permeability by penetrating and occluding the dentinal tubules, and not the creation of a surface coating alone. As discussed in section 6.2 XPS and QCM-D analysis also suggested the nanoparticles were able to enter the dentinal tubules resulting in occlusion. Preliminary studies using AFM (data not shown) identified spheres of nanoparticulate size at the rim of the open dentine tubules, also supporting this hypothesis. However, AFM analysis of these samples is difficult due to the size of the nanoparticles and the requirement for the AFM tip to be in close proximity to the dentine tubules, which can lead to the tip being trapped in the tubule and breaking. However these results indicate that the nanoparticulate silica is able to penetrate the tubules as originally hypothesised.

Addition of a polymer layer to enhance the occlusion of the dentinal tubules, did result in an increased reduction in hydraulic conductance when the Zetag™ 7109 polymer was used, but not UCARE™ polymer JR-125. This could be due to the differences in the adsorption of the polymer to the surface as demonstrated with QCM-D. If as proposed the Zetag™ polymer does adsorb to the surface in a coiled manner the coating would be denser than that obtained from treatment with the UCARE™ polymer. It would, therefore, enhance the occluding abilities of the silica nanoparticles. However, statistical analysis demonstrated that there were no statistically significant differences in the occluding abilities of the two step polymer and nanoparticulate silica treatments, and the treatment of the dentine with the 21nm nanoparticulate silica sol alone. It can therefore, be suggested that the added complexity of creating a polymer binding layer prior to addition of the nanoparticulate silica, was not necessary.

## 6.4. The nanoparticulate treatments ability to withstand the oral environment and protect the dentine.

The ability of a nanoparticulate coating to withstand shear would affect its success as a coating agent. Within the oral environment the nanoparticulate coating would be subjected to regular increases in shear force, due to the flow of artificial saliva across the surface. Using the QCM-D the ability of the nanoparticulate coatings to withstand shear was investigated. It was shown that the nanoparticulate coatings created were able to withstand a continuous flow of $dH_2O$ for a period of 16 hours (overnight).

### 6.4.1 The ability of the nanoparticulate coating to protect the dentine from acid challenge

Within the oral cavity exposed dentine would be subjected to regular acid challenge associated with the ingestion of various food stuffs resulting in the decrease of the oral pH (Whelton 2004). Exposure of dentine to acidic conditions results in the demineralisation of the dentine (a loss of the inorganic phase) (Ruse, N.D.,1991). The mechanical properties of the dentine require the presence of both phases of dentine. The loss of the mineralised phase due to acid challenge can lead to the impairment of the functioning of the tooth, that may lead to further periodontal problems possibly leading to the loss of the tooth (Nanci 2003). XPS analysis was able to identify the continued presence of silica on the dentine surface despite a 10 minute citric acid challenge. It was theorised that acid challenge resulted in an acceleration of the dissolution of the nanoparticles adhered to the surface resulting in the formation of a gel like coating but not the removal of the coating. Unlike on the NaF treated samples following acid challenge, there were no decreases in the inorganic dentine phase peaks which would suggest acid demineralisation of the surface. It can therefore be surmised that the creation of a nanoparticulate coating does offer some protection of the underlying dentine from acid challenge and further demineralisation.

### 6.4.2 The adsorption of a pellicle layer onto the nanoparticulate coatings.

Previous studies have demonstrated that the presence of a salivary pellicle coating upon the dental surface can offer some protection from acid challenge by acting as a barrier

and can also facilitate the remineralisation of the surface (Hannig and Balz 2001; Hannig and Joiner 2006). As such the ability of the nanoparticulate coating to adsorb a salivary pellicle and withstand acid challenge may enhance the protection of the tooth and aid in the prevention of further exposure of the dentine. Using the QCM-D it was possible to monitor the adsorption of salivary components in-situ overnight. Protein adsorption is a complex process which can be influenced by the chemical and physical characteristics of the surface. It was possible using QCM-D to measure the effect of artificial saliva flow on, gold and HA surfaces as well as HA and gold surfaces subsequently coated in 0.03g/ Zetag™ 7109 and Ludox® TM-50. It was noted that there were several differences in the binding curves obtained on the different test surfaces. The differences in the binding curves would suggest differences in the composition and arrangement of the adsorbed salivary layer on the different surfaces. However, a stable and irreversibly adsorbed layer was created on all the test surfaces.

XPS was used to investigate the chemical components of the adsorbed layer. It could be demonstrated that there was a characteristic Carbon peak shape, following artificial saliva treatment of both the silica and all the non silica treated surfaces. It can be surmised that this was due to the specific adsorption of a salivary protein, which was not altered despite changes in the surface chemistry upon creation of a nanoparticulate coating. However, the differences in the binding curve observed using QCM-D suggests that there may be conformational constraints on the proteins when adsorbed onto the nanoparticulate coating. These conformational constraints may hinder the adsorption of secondary components of the salivary pellicle, masking or obscuring binding sites. This was demonstrated by the absence of a secondary binding curve on the nanoparticulate coated surfaces. This would therefore, alter the overall composition of the adsorbed salivary pellicle.

The remineralisation of dentine is a complex process. Unlike enamel, remineralisation of the dentine tissue requires that the mineral content is deposited within the intra fibrillar collagen matrix and not as a superficial layer deposited on the surface (Arnold, Dorow et al. 2006; Preston, Smith et al. 2008). Therefore, the true remineralisation of

the surface could not be alluded to in this project. However, increases in the mineral phase of dentine were used to suggest remineralisation may have occurred. XPS demonstrated that treatment of etched dentine with artificial saliva, resulted in an increase in the inorganic phase of dentine. However, the presence of a nanoparticulate coating diminished the increases in inorganic phase components following artificial saliva treatment. This may be due to the combined affect of the silica coating masking the underlying dentine, and the conformational changes in the primary adsorbed layer hindering the adsorption of the secondary phase components, as the QCM-D results suggested. It can therefore be suggested that, the creation of a nanoparticulate coating inhibited the remineralisation of the dentine. Although it still enabled the creation of a salivary pellicle it prevents the salivary components from contacting the dentine, and therefore initiating the creation of apatite within the collagen matrix, leading to the remineralisation of the dentine.

Further investigations will be required to fully understand the effect of the nanoparticulate coating upon remineralisation of the dentine and the creation of a salivary pellicle. Although the results from the XPS and QCM-D experiments presented in this project indicate that the presence of the nanoparticulate coating does not prevent the adsorption of salivary molecules to the surface. However, there may be some differences to the composition of the salivary pellicle and due to the creation of a protective coating on the surface it may hinder the remineralisation process. Although XPS analysis did suggest that some of the components remained the same in the appearance of a characteristic peaks shape XPS analysis was also unable to offer any further insight into how the composition of the salivary pellicle may be altered by the presence of a nanoparticulate coating.

## Chapter 7

## Conclusions and Future work

### 7.1 Conclusions

From the work presented in this study it could be concluded that:-

1. Nanoparticulate silica could significantly reduce the permeability of etched dentine.
2. In a 2 step coating process the molecular weight and the percentage charge of the binding polymer influences the uniformity of the coating.
3. On dentine surfaces the silica nanoparticles appear to bind in the absence of a polymer binding layer and penetrate the dentinal tubules
4. A two step polymer and nanoparticulate silica coating was able to withstand flow conditions overnight with no loss of mass from the surface.
5. The presence of a nanoparticulate coating did not prevent the adsorption or creation of a salivary pellicle.
6. A nanoparticulate coating on dentine is able to withstand a 1 % citric acid challenge

### 7.2 Novelty of the study

This study investigated the novel use of nanoparticulate silica as a coating for dentine sensitivity prevention. Although the use of particulate silica as a dental coating has previously been investigated the use of nanoparticulate sols of the dimensions used in this project had not previously been tested. The creation of a one step nanoparticulate coating through the shear mixing of a nanoparticulate sol and a polymer solution resulted in the creation of new coating.

However, the novelty of this project was also in the use of application with both XPS and QCM-D being utilised in a new manner. Although XPS has been used previously to investigate the effect of binding agents to dentine, it has not been used to investigate the effect of different coatings, acid challenge and the remineralisation of dentine. The majority of XPS studies focus on enamel surfaces with very few investigating dentine

possibly due to the porous nature of dentine which results in it being a less than ideal substrate for XPS investigations. QCM-D is commonly used for evaluating protein adsorption to surfaces. The use of the QCM=D to investigate the creation of a dentine surface and its ability to withstand a flow system offers a novel use. However, the use of the HA coated crystals also offers a new dimension of novelty. The HA coated crystals are a new product and from previous discussions with Q-sense I was the one of the first researchers in the UK to use them. The adhesion of a dentine disc to a gold QCM-D crystal surface also offers a new area of possibility to use the QCM-D with no published work relating to the use of the QCM-D in this manner.

### 7.3 Future Work

Following the investigations discussed in this thesis, a number of projects can be identified to investigate the use of nanoparticulate silica for oral care.

1. In this project the ability of the silica nanoparticles to penetrate the dentinal tubules has been suggested. Further work could assess the depth of penetration and therefore the longevity of any desensitizing effect that may be elicited by the treatment. Two techniques have been identified to do this using fractured dentine discs:
    a. environmental SEM. An environmental SEM should not require the coating of the substrates which has hindered the use of SEM for analysis of the nanoparticulate coatings in the past.
    b. NanoSIMS
2. The ability of the nanoparticulate silica coatings to influence remineralisation requires further work. The ability to aid the remineralisation of demineralised dentine would offer a great advantage to the consumer. A more detailed analysis is required. This could be achieved using micro/nano hardness testing of both dentine and enamel. It would also be possible using micro/nano hardness testing to assess the protective capabilities of the nanoparticulate silica against acid challenge.

3. Investigate the effect of different acids on the protective effect of NaF and Nanoparticulate silica treatments, as an acid that demineralises the dentine in a pH dependent manner unlike citric acid which acts as a calcium chelater may indicate different responses. It may also be of interest to investigate the effect of different concentrations of acid and different time periods of acid challenge.
4. Investigate the antimicrobial (anti-plaque) effect of the nanoparticulate coating when the underlying substrate is enamel or HA.

**Chapter 8 References**

Absi, E. G., Addy, M., Adams, D. (1987). Dentine hypersensitivity A study of the patency of dentinal tubules in sensitive and non-sensitive cervical dentine. Journal of Clinical Periodontology 14(5): p. 280-284.

Addy, M. (1990). Etiology and Clinical Implications of Dentine Hypersensitivity. The Dental Clinics of North America 34(3): p.503-514.

Addy, M. and Urquhart, E. (1992). Dentine hypersensitivity: its prevalence, aetiology and clinical management. Dental Update 19(10): p. 407-412.

Amelincx, S., Van Dyck, D., et al. (1997). Applications on Materials Science, Solid-state Physics and Chemistry. Methods I, VCH Verlagsgesellschaft mbH.

Andersson, M., Andersson, J., et al. (2005). Quartz Crystal microbalance with dissipation monitoring (QCM-D) for real time measurements of blood coagulation density and immune complement activation on artificial surfaces. Biosensors and Bioelectronics 21(1): p.79-86.

Arnold, W. H., Dorow, A., et al. (2006). Effect of fluoride toothpaste on enamel demineralization. BMC Oral Health 6(8).

Atashbar, M. Z., Bejcek, B., et al. (2005). QCM biosensors with ultra thin polymer films. Sensors and Actuators B 107(2): p. 945-951.

Baldan, A. (2002). Progress in Ostwald ripening theories and their applications to nickel-based superalloy. Journal of Materials Science 37(11): p. 2171-2202.

Banfield, N. and Addy M. (2004). Dentine hypersensitivity: development and evaluation of a model in situ to study tubule patency Journal of Clinical Periodontology 31(5): p. 325-335.

Bartold, P. M. (2006). Dentine Hypersensitivity: a review. Australian Dental Journal 51(3): p. 212-218.

Beamson, G., Briggs, D., et al. (1990). Performance and application of the scienta ESCA300 spectrometer. Surface and Interface Analysis 15(9): p. 541-549.

Berglin, M., Olsson, A., et al. (2008). The Interaction Between Model Biomaterial Coatings and Nylon Microparticles as Measured with a Quartz Crystal Microbalance with Dissipation Monitoring. Macromolecular Bioscience 8(1).

Bergna, H. E. (1994). The colloid Chemistry of Silica Chapter 1, Colloid Chemistry and Silica an Overview Advances in Chemistry Series. Bergna, H. E. American Chemical Society. 234: p. 1-50.

Berkovitz, B. K. B., Holland, G. R. et al. (1992). A Colour Atlas and Textbook of Oral Anatomy Histology and Embryology, Wolfe.

Berkovitz, B. K. B., Holland, G. R. et al. (2005). Oral Anatomy, Histology and Embryology, Mosby.

Blake, G. C. (1968). The peritubular translucent zones in human dentine. British Dental Journal 104: p. 57-59.

Brannstrom, M. (1966). Sensitivity of dentine. Oral Surgery, Oral Medicine and Oral Pathology 21: p. 517-526.

Brannstrom, M. and Astrom A. (1972). The hydrodynamics of the dentine; its possible relationship to dental pain. The International Dental Journal 22(2): p. 219-227.

Brannstrom, M. and Johnson, G. B. (1978). The Sensory mechanism in human dentine as
revealed by evaporation and mechanical removal of dentine. Journal of Dental Research 57: p. 49-53.

Briggs, D. and Riviere, J. C. (1983). Chapter 3 Spectral Interpretation. Practical Surface Analysis by Auger and x-ray Photoelectron Spectroscopy. eds. Briggs, D. and Seah, M. P. John Wiley and Sons: 87-139.

Carlson, T. A. (1975). Photoelectron and Auger Spectroscopy Plenium Press.

Charvat, J., Soremark, R., et al. (1995). Titaniumtetrafluoride for treatment of hypersensitive dentine. Swedish Dental Journal 19(1-2): p. 41-46.

Cherng, A. M., Chow, L. C., et al. (2004). Reduction in Dentin permeability using mildly supersaturated calcium phosphate solutions Archives of Oral Biology 49(2): p. 91=98.

Chescoe, D. and Goodhew, P. J. (1990). The Operation of Transmission and Scanning Electron Microscopes., Oxford University Press.

Chitpan, M., Wang, X., et al. (2007). Monitoring the Binding Processes of Black Tea Thearubigin to the Bovine Serum Albumin Surface using Quartz Crystal Microbalance with Dissipation Monitoring. Journal of Agriculture and Food Chemistry 55(25): p. 10110-10116.

Churchley, D., Rees, G. R., et al. (2007). Fluoropolymers as low surface - energy tooth coatings for oral care. International Journal of Pharmaceutics.

Coffey, C. T., Ingram, M. J. et al. (1970). Analysis of human dentinal fluid. Oral Surgery, Oral Medicine and Oral Pathology 30: p. 835-837.

Collaert, B. and Fischer, C. (1991). Dentine Hypersensitivity: a review. Endodontics and Dental Traumatology 7: p. 145-152.

Coradin, T. and Lopez, P. J. (2003). Biogenic Silica Patterning: Simple Chemistry or Subtle Biology? CemBioChem 3: p. 1-9.

Cousins, B. G. (2005). The Effect of a Nanoparticulate Silica coating on Cellular Response. Department of Clinical Sciences. Liverpool, University of Liverpool. Doctor in Philosophy: 232.

Cousins, B. G., Allison, H. E. et al. (2007). Effects of a nanoparticulate silica substrate on cell attachment of Candida Albicans. Journal of Applied Microbiology 102(3): p. 757-65.

Cousins, B. G., Doherty, P. J., et al. (2004). The effect of silica nanoparticulate coatings on cellular response Journal of Materials Science: Materials in Medicine 15(4): p. 355-359.

Couve, E. (1986). Ultrastructural changes during the life cycle of human odontoblasts. Archives in Oral Biology 31(10): p.634-651.

de Assis, C. A., Antoniazzi, R. P. et al. (2006). Efficacy of Gluma Desensitizer on dentin hypersensitivity in periodontally treated patients Brazilian Oral Research 20(3): p. 252-256.

Deschaume, O., Shafran, K. L., et al. (2006). Interactions of Bovine Serum Albumin with Aluminum Polyoxocations and Aluminum Hydroxide. Langmuir 22(24): p. 10078-10088.

Dowell, P. and Addy, M. (1983). Dentine hypersensitivity - A review Aetiology, symptoms and theories of pain production Journal of Clinical Periodontology 10(4): p. 341-350.

Duran, I., Sengun, A. et al. (2005). In vitro dentine permeability evaluation of HEMA-based (desensitizing) products using split-chamber model following in vivo application in the dog Journal of Oral Rehabilitation 32(1): p. 34-38.

Exterkate, R. A. M. and ten Cate, J. M. (2007). Effects of new titanium fluoride derivatives on enamel de- and remineralisation. European Journal of Oral Sciences 115(2): p. 143- 147.

Feiler, A. A., Sahloholm, A., et al. (2007). Adsorption and viscoelastic properties of fractionated mucin (BSM) and bovine serum albumin (BSA) studied with quartz crystal microbalance (QCM-D). Journal of Colloid and Interface Science 315(2): p. 475-481.

Fischer, C., Fischer, R.E. et al. (1992). Prevalence and distribution of cervical dentine hypersensitivity in a population in Rio de Janeiro. Brazilian Journal of Dentistry 20: p. 272-276.

Flynn, J., Galloway, R. et al. (1985). The incidence of hypersensitive teeth in the west of Scotland. Journal of Dentistry 13: p. 230-236.

Fogel, R., Mashazi, P., et al. (2007). Critical assessment of the Quartz Crystal Microbalance with Dissipation as an analytical tool for biosensor development and fundamental studies: Metallophthalocyanine-glucose oxidase biocomposite sensors. Biosensors and Bioelectronics 23(1): p. 95-101.

Forsback, A. P., Areva, S., et al. (2004). Mineralization of dentin induced by treatment with bioactive glass S53P4 in vitro. Acta Odontologica Scandinavica 63(1): p. 14-20.

Galli, C., Collaud Coen, M., et al. (2002). Creation of nanostructures to study the topographical dependency of protein adsorption. Colloids and Surfaces B: Biointerfaces 26(3): p. 255-267.

Ganss, C., Klimek, J., et al. (2001). Effectiveness of two fluoridation measures on erosion progression in human enamel and dentine in vitro. Caries Research 35(5): p. 325-330.

Garberoglio, R. and Brannstrom, M. (1976). Scanning electron microscopic investigation of human dentinal tubules. Archives in Oral Biology 21: p.355-362.

Garvey, M. J. (2004). Personal communications and discussions with. J. M. Convery. Liverpool.

Ghazali, F. B. C. (2003). Permeability of dentine. Malaysian Journal of Medical Science 10(1): p. 27=36.

Gillam, D. G., Bullman, J.S. et al. (1996). Efficacy of a potassium nitrate mouthwash in alleviating cervical dentine sensitivity (CDS). Journal of Clinical Periodontology

Gillam, D. G., Mordan, N. J., et al. (1997). The Dentin disc surface: A plausable model for dentin physiology and dentin sensitivity evaluation. Advances in Dental Research 11(4): p.487-501.

Goodhew, P. J., Humphreys, J., et al. (2001). Electron Microscopy and Analysis. London, Taylor and Francis.

Graf, H. and Glasse, R. (1977). Morbidity, prevalence and intra oral distribution of hypersensitive teeth. Journal of Dental Research 56(Special issue A): 162 abstract 479.

Gregoire, G., Guignes, P., et al. (2005). Effect of self-etching adhesives on dentin permeability in a fluid flow model. The Journal of Prosthetic Dentistry 93(1): p. 56-63.

Gwinnett, A. J. (1984). Smear Layer: Morphological considerations. Operative Dentistry 3(Supplement ): p. 3-12.

Hall, A. F., Buchanan, C. A., et al. (1999). The effect of saliva on enamel and dentine erosion. Journal of Dentistry 27(5): p. 333-339.

Hannig, M. and Balz, M. (2001). Protective Properties of Salivary pellicles from two different intra oral sites on enamel erosion Caries Research 35(2): p. 142-148.

Hannig, M. and Joiner, A. (2006). Chapter 2 The structure, function and properties of the aquired pellicle. The Teeth and Their environment. ed. Duckworth, R. M.. 19: p. 29-64.

Hara, A. T., Ando, M., et al. (2005). Influence of the organic matrix on root dentine erosion by citric acid. Caries Research 39(2): p. 134-138.

Hara, A. T., Karlnsey, R. L., et al. (2008). Dentine remineralisation by simulated saliva formulations with different Ca and Pi contents. Caries Research 42(1): p. 51-56.

Helms, C. R. (1988). Chapter 3 Physical structure and Chemical nature of the Si-SiO2 Interfacial region. The Si-SiO2 System. P. Balk, Elsevier: p. 77-128.

Hercules, D. (2004). Electron Spectroscopy : Applications for Chemical Analysis. Journal of Chemical Education 81(12): p. 1751-1766.

Hildebrand, C., Fried, K., et al. (1995). Teeth and Tooth Nerves. Progress in Neurobiology 45(3): p. 165-222.

Hoffman, S. (1983). Chapter 4 Depth Profiling. Practical Surface Analysis by Auger and X-ray Spectroscopy. Briggs, D. and Seah, M. H. John Wiley and Sons: p. 141- 179.

Hofman, S. (1986). Practical Surface Analysis: state of the art and Recent Developments in AES, XPS, ISS and SIMS. Surface and Interface Analysis 9(1): p. 3-20.

Holand, G. R., Narhi, M. N. et al. (1997). Guidelines for the design and conduct of clinical trials on dentine hypersensitivity. Journal of Clinical Periodontology 11: p. 808-813.

Hsiao, Y. H., Ogawa, T., et al. (1994). A new oxalate treatment for dentine tubule occlusion. Archives in Oral Biology 39(supplement): p. 135S.

Hughes, J.A., West, N.X. and Addy, M. (2004). The protective effect of fluoride treatments against enamel erosion in-vitro. Journal of Oral Rehabilitation 31: 357-363.

Iler, R. K. (1979a). Chapter 1 the occurrence, Dissolution, and deposition of Silica. The Chemistry of Silica. ed. R. K. Iler, John Wiley and Sons. 1: p. 3-115.

Iler, R. K. (1979b). Chapter 3 Polymerisation of Silica. The Chemistry of Silica. ed. R. K. Iler, John Wiley and Sons: p. 174-311.

Iler, R. K. (1979c). Chapter 4 Colloidal Silica Concentrated Sols. The Chemistry of Silica. ed. R. K. Iler, John Wiley and Sons: p. 312-461.

Iler, R. K. (1979e). Chapter 7 Silica in Biology. The Chemistry of Silica. ed. R. K. Iler, John Wiley and Sons: p. 730-780.

Irwin, C. R. and Mc Cusker, P. (1997). Prevelence of dentine hypersensitivity in a general dental population Journal of the Irish Dental Association 43: p. 7-9.

Jackson, R. J. (2000). Potential treatment modalities for dentine hypersensitivity home use products. Tooth wear and sensitivity. eds. M. Addy, G. Embery, M. Edgar and R. Orchardson. London, Dunitz: p. 327-338.

Jacobsen, P. L. and Bruce, G. (2001). Clinical Dentin Hypersensitivity: understanding the causes and prescribing a treatment. The Journal of Contempary Dental Practice 2(1): p. 1-8.

Jenkins, R. (1986). An introduction to X-ray spectrometry John Wiley and sons.

Kimura, Y., Wilder-Smity, P., et al. (2000). Treatment of dentine hypersensitivity by lasers: a review. Journal of Clinical Periodontology 27: p.715-721.

Kinney, J. H., Balooch, M., et al. (1995). Mineral distribution and dimensional changes in human dentin during demineralization. Journal of Dental Research 74(5): p. 1179-1184.

Labahn, R., Fahrenbach, W. H., et al. (1992). Root Dentin Morphology After Different modes of citric acid and Tetracycline hydrochloride conditioning. Journal of Periodontology 63(4): p. 303-309.

Lambert, J. B., McLauglin, C. D., et al. (1999). X-ray Photoelectron Spectroscopy and Archaeology: XPS offers unique advantages for analyzing a wie range of artifacts. Analytical Chemistry News and Features 71(17): p. 614A-620A.

Lan, W. H. and Liu, H.-C. (1995). Sealing of human dentinal tubules by Nd:YAG laser. Journal of Clinical Laser Medicine and Surgery 13: p. 329-333.

Lan, W. H. and Liu, H.-C. (1996). Treatment of Dentin hypersensitivity by Nd:YAG laser. Journal of Clinical Laser Medicine and Surgery 14: p. 89-92.

Ling, T. Y. Y., Gillam, D. G., et al. (1997). An investigation of potential desensitizing agents in the dentine disc model: a scanning electron microscopy study The Journal of Oral Rehabilitation 24(3): 191-203.
Liu, M., Chan, C., et al. (2007). Filling in dentinal tubules. Nanotechnology 18(47): 475104.

Lord, M. S., Cousins, B. G., et al. (2006). The effect of silica nanoparticulate coatings on serum protein adsorption and cellular response. Biomaterials 27: p. 4856-862.

Mac Carthy, D. (2004). Dentine hypersensitivity: a review of the literature. Journal of the Irish Dental Association 50(1): p. 36-41.

Macdonald, R. (1983). Chapter 1 Silicon in Igneous and Metamorphic Rocks. Silicon Geochemistry and Biogeochemistry. ed. Aston, S. R. Academic Press. 1: p. 1-37.

Marsh, M. E. (1989). Binding of calcium and phosphate ions to dentin phosphophoryn. Biochemistry 28(1): p. 346-352.

Marshall, G. W., Wu-Magidir, I. C., et al. (1998). Effects of citric acid concentration on dentin demineralization dehydration and rehydration: Atomic force Microscopy study. Journal of Biomedical Materials Research 42(4): p. 500-507.

Marx, K. A. (2003). Quartz Crystal Microbalance: A useful tool for studying thin polymer films and complex Biomolecular systems at the solution-surface interface. Biomacromolecules 4(5): 1099-1120.

McArthur, S. L. (2006). Applications of XPS in bioengineering. Surface and Interface Analysis 38(11): p. 1380-1385.

Mellberg, J. R., Pertrou, I. D., et al. (1991). Evaluation of the Effects of a Pyrophosphate-Fluoride Anti calculus Dentifrice on remineralisation and Fluoride uptake in situ. Caries Research 25(1): p. 65-69.

Miller, R. G., Bowles, C. Q., et al. (1994). The effects of ion sputtering on dentin and its relation to depth profiling. Journal of Dental Research 73(8): p. 1457-1461.

Mjor, I. A. (1985). Dentine - predentine complex and its permeability, pathology and treatment overview. Journal of Dental Research 64(Special issue): p. 621-627.

Mjor, I. A. and Nordahl, I. (1996). The Dentistry and Branching of Dentinal Tubules in Human Teeth. Archives in Oral Biology 41(5): p. 401-412.

Mongiorgi, R. and Prati, C. (1994). Mineralogical and crystallographical study of g-calcium oxalate on dentine surfaces in-vitro. Archives in Oral Biology 19(Supplement): p. 152S.

Monkawa, A., Ikoma, T., et al. (2006). Fabrication of hydroxyapatite ultra thin layer on gold surface and its application for quartz crystal microbalance technique. Biomaterials 27(33): p. 5748-5754.
Morrison, S. R. (1990). The Chemical Physics of Surfaces, Plenium Press.

Moulder, J. F.,. Stickle, W. F, et al. (1992). Handbook of X-ray photoelectron Spectroscopy : A reference book of standard spectra for identification and interpretation of XPS data, Perkin Elmer Co.

Mumford, J. M. and A. V. Newton (1969). Transduction of hydrostativ pressure to electric potential in human dentin. Journal of Dental Research 48: p. 226.

Munke, C. (2005). Alignment procedures for the use of the FEI 120KV Tecnai G2 Spirit BioTWIN. University of Liverpool.

Nanci, A. (2003a). Dentin-Pulp Complex. Ten Cate's Oral Histology, Development, Structure and Function. ed. Nanci, A. St Louis: p.192-239.

Nanci, A. (2003b). Enamel :Composition, Formation and structure. Ten Cate's Oral Histology Development, Structure adn Function. Nanci, A.. St Louis, Mosby: p. 145-191.

Napper, D. H. (1970). Colloid Stability Industrial Engineering and Chemistry Product Research and Development 9(4): p. 467-477.

Orchardson, R. and Cadden, S.W. (2001). An update on the physiology of the dentine-pulp complex. Dental Update 28: p. 200-209.

Orchardson, R. and Gillam, D. G. (2006). Managing dentin hypersensitivity. Journal of the American Dental Association 137(7): p. 990-998.

Pamir, T., Ozyazici, M., et al. (2005). The efficacy of three desensitizing agents in treatment of dentine hypersensitivity Journal of Clinical Pharmacy and Therapeutics 30(1): p. 73-76.

Pashley, D. H. (1986). Dentin Permeability, Dentin Sensitivity, and treatment through tubule occlusion. Journal of Endodontics 12(10): p. 465-474.

Pashley, D. H. (1996). Dynamics of the Pulpo-Dentin complex. Critical Reviews in Oral Biology and Medicine 7(2): p. 104-133.

Pashley, D. H. (2002). Pulpodentin Complex. Seltzer and Bender's Dental Pulp. eds. Hargreaves, K. M. and. Goodis, H. E Quintessence Publishing Co, Inc: p. 63-94.

Pereira, J. C., Segala, A.D., et al. (2005). Effect of desensitizing agents on the hydraulic conductance of human dentin subjected to different surface pre-treatments adn in vitro study. Dental Materials 21(2): p. 129-138.

Pertoft, H. (2000). Fractionation of cells and subcellular particles with Percoll. Journal of Biochemical and Biophysical Methods 44(1): p. 1-30.
Pietruska, M., Paniczko, A., et al. (2006). Efficacy of local treatment with chlorhexidine gluconate drugs on the clinical status of periodontium in chronic periodontitis patients. Advances in Medical Science 51(Suppl 1): p. 162-165.

Polito, P. and Antila, R. (1968). Acetylcholinesterase and noradrenaline in the nerves of mammalian dental pulps. Acta Odontologica Scandinavica 26: P. 641.

Preston, K. P., Smith, P. W., et al. (2008). The influence of varying fluoride concentrations on in vitro remineralisation of artificial dentinal lesions with differing lesion morphologies. Archives in Oral Biology 53(1): p. 20-26.

Prutton, M. (1998). Introduction to Surface Physics, Oxford Science Publications.

Rapp, R., Avery, J.K.,et al. (1959). A study of the Distribution of Nerves in Human Teeth. Journal of the Canadian Dental Association 23: P. 447.

Raven, P. H. and Johnson, G.B. (1999). Part VIII Viruses and simple Organisms Chapter 31 Protists. Biology. eds Raven, P.H. and Johnson, G.B. WCB McGraw - Hill. 1: p. 615.

Roach, P., D. Farrar, et al. (2006). Surface Tailoring for controlled Protein adsorption: Effect of Topography at the nanometre scale and chemistry. Journal of the American Chemical Society 128(12): p. 3939-3945.

Roach, P., Eglin, D., et al. (2007). Modern Biomaterials : a review - bulk properties and implications of surface modifications. Journal of Materials Science: Materials in Medicine 18(7): p. 1263-1277.

Roach, P., Farrar, D., et al. (2005). Interpretation of Protein Adsorption: Surface - Induced Conformational Changes. Journal of the American Chemical Society 127(22): p. 8168-8173.

Roach, P., Shirtckiffe, N. J., et al. (2006). Quantification of surface-bound proteins by fluorometric assay: comparison with Quartz Crystal Microbalance and Amido Black Assay. Journal of Physical Chemistry B 110(41): 20572 -20579

Rodahl, M., F. Hook, et al. (1995). Quartz Crystal Microbalance setup for frequency and Q-factor measurements in gaseous and liquid environments. Review of Scientific Instruments 66(7): p. 3924-3930.

Ruse, N. D. (1991). Adhesion to bovine dentin- surface characterization. Journal of Dental Research 70(6): p. 1002-1008.

Saito, T., Toyooka, H., et al. (2003). In vitro study of remineralisation of dentin: effects of ions on mineral induction by decalcified dentin matrix. Caries Research 37(6): p. 445-449.
Sano, H., Nakashima, S., et al. (2007). Effect of a xylitol and fluoride containing toothpaste on the remineralisation of human enamel in vitro. Journal of Oral Science 49(1): p. 67-73.

Savarino, L., Breschi, L., et al. (2004). Ability of restorative and fluoride releasing materials to prevent marginal dentine demineralization. Biomaterials 25(6): p. 1011-1017.

Schenkels, L. C. P. M.,. Veerman, E. C. I., et al. (1995). Biochemical Composition of Human Saliva in relation to other mucosal fluids. Critical Reviews in Oral Biology and Medicine 6(2): p. 161-175.

Schlueter, N., Ganss, C., et al. (2007). Effect of titanium tetrafluoride and sodium fluoride on erosion progression in enamel and dentine in vitro. Caries Research 41(2): p. 141-145.

Seltzer, S. (1971). Hypothetic mechanisms for dentine sensitivity. Oral Surgery, Oral Medicine and Oral Pathology 31(3): p. 388-399.

Sennou, H. E., Lebugle, A.A., et al. (1999). X-ray photoelectron spectroscopy study of the dentin-glass ionomer cement interface. Dental Materials 15(4): p. 229-237.

Shaw, D. J. (1992). Introduction to Colloid and Surface Chemistry, Buterworth Heinenmann.

Skirtic, D., Antonucci, J. M., et al. (2001). Silica and zirconia- hybridized amorphous calcium phosphate: Effect on transformation to hydroxyapatite. Journal of Biomaterial Materials Research Part A 59(4): p. 597-604.

Spencer, C. P. (1983). Chapter 4 Marine Biochemistry of Silicon. Silicon Geochemistry and Biogeochemistry. Aston, S. R. Academic Press. 1: p. 101-142.

Stadler, H., Mondon, M., et al. (2003). Protein Adsorption on surfaces: dynamic contact-angle (DCA) and quartz-crystal microbalance (QCM) measurements. 375: 53-61.

Stryer, L. (1999). Biochemistry, W.H. Freeman and Company

Suge, T., Ishikawa, K., et al. (1995). Effects of fluoride on the calcium phosphate precipitation method for dentinal tubule occlusion. Journal of Dental Research 74(4): p.1079-1085.

Tay, F. R. and Pashley, D. H. (2008). Guided tissue remineralisation of partially demineralised human dentine Biomaterials 29(8): p. 1127-1137.

Ten Bosch, J. J., De Vries, J., et al. (1997). X-ray-induced photoelectron spectroscopy of dentin as a function of duration of Ar(+)-ion etching Advances in Dental Research 11(4): p. 395-402.

Ten Cate, A. R. and Nanci A. (2003). Structure of the Oral Tissue. Ten Cate's Ora Histology Development, Structure and Function. Nanci, A. St Louis, Mosby: p. 1-16.

Ten Cate, A. R. and Shelton, L. (1966). Cholinesterase activity in human teeth. Archives in Oral Biology 11: p. 423.

ten Cate, B. (2004). The role of saliva in mineral equilibria - caries, erosion and calculus formation. Saliva and Oral Health. Edgar, M., Dawes, C., and O'Mullane, D. British Dental Journal. 1: p. 120-135.

Ten Cate, J.M. (1997). Review of fluoride with special emphasis on calcium fluoride mechanisms in caries prevention . European Journal of Oral Sciences. 105: 461-465.

Teranaka, T. and Koulourides, T. (1987). Effect of a 100ppm fluoride mouth rinse on experimental root caries in humans. Caries Research 21: 326-332.

Teraoka, I. (2002). Polymer Solutions An Introduction to Physical Properties, John Wiley and Sons, INC.

Van Rijkom, H., Ruben, J., Vieira, A., Huysmans, M.C., Truin, G.J. and Mulder, J. (2003) Erosion inhibiting effect of sodium fluoride and titanium tetra fluoride treatment in-vitro. Euopean Journal of Oral Science 111:253-257.

Voinova, M. V., Rodahl, M., et al. (1999). Viscoelastic Acoustic Response of Layered Polymer Films at Fluid-Solid Interfaces: Continuum Mechanics Approach. Physica Scripta 59(5): p. 391-396.

Vollenweider, M., Brunner, T. J., et al. (2007). Remineralisation of human dentin using ultra fine bioactive glass particles. Acta Biomaterialia 3(6): p. 936-943.

Wagberg, L., Pettersson, G., et al. (2004). Adsorption of bi layers and multi layers of cationic and anionic co-polymers of acrylamide on silicon oxide. Journal of Colloid and Interface Science 274(2): p. 480-488.

Wakabayashi, H., Hamba, M., et al. (1993). Effect of irradiation by semiconductor laser on responses evoked in trigeminal radial neurons by tooth pulp stimulation. Lasers in Surgery and Medicine 13: p. 605-610.

Welle, A., Chiumiento, A., et al. (2007). Competitive protein adsorption on micro patterned polymeric biomaterials, and viscoelastic properties of tailor made extracellular matrices. Biomolecular Engineering 24(1): p. 87-91.

Wetton, S., Hughes, J., et al. (2006). Exposure time of enamel and dentine to saliva for protection against erosion: a study in vitro. Caries Research 40(3): p. 213-217.

Whelton, H. (2004). Introduction: the anatomy and physiology of salivary glands. Saliva and Oral Health Edgar, M., Dawes, C. and O'Mullane, D. British Dental Journal. 1: p. 1-13.

Winter, H. F., Bishop, J. G., et al. (1963). Transmembrane potentials of Odontoblasts. Journal of Dental Research 42(2): p. 594-598.

Young, R. J. (1981). Introduction to Polymers, Chapman and Hall.

Zappa, U. (1994). Self-applied treatments in the management of dentine hypersensitivity. Archives in Oral Biology 39(supplement): p. 107S-112S.

Zhang, Y., Agee, K., et al. (1998). The effects of Pain-Free® desensitizer on dentine permeability and tubule occlusion overtime, in vitro Journal of Clinical Periodontology 25(11): p. 884-891.